UNIVERSITÀ
DEGLI STUDI
DI PADOVA

Head Office: Università degli Studi di Padova
Department of Industrial Engineering

Ph.D. COURSE IN: Industrial Engineering
CURRICULUM: Electrical Energy Engineering
SERIES: XXX

Model Predictive Control: An Effective Control Approach for High Performance Induction Machine Drives

Coordinator of PhD Course: Prof. Paolo Colombo
Coordinator of Cirruculum: Prof. Roberto Turri
Supervisor: Prof. Silverio Bolognani

Ph.D. student: Mahmoud Mohamed

Preface

ABSTRACT

Induction machine drives with various configurations are getting a lot of attention in several industrial applications. Due to this increasing demand in industrial applications, the significance of developing effective control approaches for obtaining a high dynamic performance from the induction machine drives became essential. Up to the present time, the control of induction machine drives using power converters has been based on the principle of mean value, using pulse width modulation with linear controllers in a cascaded structure. Recent research works have demonstrated that it is possible to use Predictive Control to control induction machine drives with the use of power converters, without using modulators and linear controllers. This new approach will have a strong impact on control in power electronics in coming decades. The advantages of Predictive Control are noticed through the ability to consider a multi-objective case within the model, easy inclusion of non-linearities within the model, simple treatment of system constraints, easy of digital implementation, and flexibility of including modifications and extension of control horizons according to the required applications. Upon this, the research presented in this thesis concerns with developing different control topologies for various configurations of induction machine drives based on finite control set model predictive control (FCS-MPC) principle, which actuates directly the switch states of the voltage source inverter (VSI). In addition, for enhancing the robustness of the induction machine drives, different sensorless approaches are utilized and tested for validations.

The first topology of induction machine drives that has been studied is the induction motor (IM) drive. An effective model predictive direct torque control (MP DTC) approach is used to control the torque and stator flux of the motor through the utilization of an effective cost function, through which the understanding and comparing implementation variants and studying convergence and stability issues can be easily investigated. The speed sample effect on the control variants and overall performance of the proposed MP DTC is analyzed, which enables the understanding of the real base principle of DTC, as well as why and when it works well. Two different sensorless procedures for estimating the speed and rotor position are used by the proposed MP DTC approach; the first utilizes a model reference adaptive system (MRAS) observer, while the other exploits the prediction step during the implementation of proposed MP DTC to get the speed information through performing a linear extrapolation of the speed values starting from the last two estimated samples. Extensive simulation and experimental tests have been carried out to validate the effectiveness of both sensorless approaches in achieving precise tracking of speed commands for a wide range of variations. For enhancing the robustness of proposed MP DTC, the stator flux as a control variable is replaced with controlling the flow of the reactive power through the induction motor drive. As the reactive power is a measured quantity compared with the estimated value of stator flux, thus, the sensitivity of the control against parameters variation is limited, and this confirmed through the obtained results from both simulation and experimental tests. In addition, an effective alternative approach to the MP DTC is presented, which based on controlling the instantaneous values of the active and reactive powers of the IM drive based on model predictive principle, instead of controlling the torque and flux as in MP DTC. This technique has the advantage that all controlled variables are became measured quantities (active and reactive powers), thus the estimation problems that commonly present in classic DTC schemes are effectively limited. For the last two control approaches (MP DTC $^{\text{reactive power control}}$, and MP IPC$^{\text{active and reactive power control}}$), the sensorless that utilizes the predictive feature is also adopted. Obtained results via simulation and experiments confirm the feasibility of the two alternatives control procedures in obtaining a robust dynamic response of IM drive.

To limit the accompanied ripple contents in the controlled values of electromagnetic torque and stator flux of induction motor, an effective ripple reduction technique has been presented. The technique is based on the derivation of the optimal value for the weighting factor (w_f) used in the cost function. A detailed mathematical derivation of the optimal value of w_f is introduced based on the analysis of torque and flux ripples behaviors. The proposed ripple reduction technique has been validated via simulation utilizing Matlab/Simulink software,

and experimentally tested using a fast control prototyping dSpace 1104 board. In addition, the prediction step based sensorless approach is adopted during implementation. The performance of the IM drive using the proposed approach is compared with the results obtained from MP DTC approach that uses an arbitrary value of w_f. The comparison confirms the validity of the proposed ripple reduction procedure in reducing the ripple contents in the controlled variables while preserving the permissible computation burdens during the implementation.

The FCS-MPC principle is also utilized to control the current of induction motor as an alternative to classic field oriented control (FOC), the proposed model predictive current control (MPCC) approach belongs to the class of the hysteresis predictive control (for limiting the switching frequency) as the MPCC is triggered by the exceeding of the error of a given threshold. In addition, a sensorless drive is achieved by including an effective Luenberger observer (LO) for precise estimation of rotor flux vector together with stator current, speed and load torque. The stator currents are estimated to eliminate the accompanied noise in their values when they are directly measured, thus the currents noise during prediction is limited. An effective pole placement procedure for the selection of observer gains has been adopted. The procedure is based on shifting the poles of the observer to the left of the motor poles in the complex (s-plane) with low imaginary part, so that the stability of the observer is enhanced for wide speed range. The feasibility of the sensorless MPCC for IM drive is confirmed through the obtained simulation and experimental results.

The second topology of induction machine drives that has been studied is the doubly fed induction motor (DFIM) drive. An effective model predictive direct torque control (MP DTC) algorithm is developed for controlling the torque and rotor flux of DFIM drive. In addition, an effective sensorless approach is presented, which estimates the speed and rotor position in an explicit way without the need for involving the flux in the estimation process, thus the effect of parameters variation on the overall performance of the sensorless observer is effectively limited, this has been approved through the obtained results that are performed for a wide speed range from sub-synchronous to super-synchronous speed operation. During the operation, the stator resistance and magnetizing inductance values are changed from their original values to study the variation effect on the observer performance. Matlab/Simulink software and a prototyping dSpace 1104 control board are used to validate the effectiveness of proposed sensorless MP DTC approach through simulation and experiments, respectively. The results proof the robustness of the proposed sensorless approach and its ability to achieve precise estimation of the speed and rotor position.

The third topology of induction machine drives that has been studied is the doubly fed induction generator (DFIG). A detailed analytical derivation for the proposed model predictive direct power control (MP DPC) approach for DFIG is presented, which as a sequence considered as a transposed control approach from the MP DTC used before for doubly fed induction motor (DFIM). A sensorless approach based on model reference adaptive system (MRAS) observer is adopted for estimating the speed and rotor position. Both simulation using Matlab/Simulink software and experimental test using a prototyping dSpace 1104 control board have tested the dynamic performance of the drive. Obtained results affirm the feasibility of the proposed MP DPC approach in achieving a decoupled control of active and reactive powers for DFIG.

In summary, it can be said that the proposed model predictive control approaches have proved their ability in achieving high dynamic performance for different topologies of induction machine drives. In addition, the proposed sensorless techniques have confirmed their effectiveness for a wide range of speed variations. All of this are approved and validated through extensive simulation and experimental tests.

SOMMARIO

Gli azionamenti con machine ad induzione (macchine asincrone nelle loro varie configurazioni), stanno riacquistando molta attenzione in diverse applicazioni industriali. A causa di questo crescente interesse applicativo, è diventato di essenziale importanza lo sviluppo di efficaci tecniche di controllo per ottenere dagli azionamenti in questione elevate prestazioni dinamiche. Fino ad oggi, il controllo degli azionamenti con macchina a induzione alimentati da convertitori di potenza è basato sul "principio del valore medio" delle grandezze in commutazione, utilizzando la modulazione di larghezza di impulsi con controllori lineari in una struttura a cascata. Recenti ricerche hanno dimostrato che è possibile utilizzare il Controllo Predittivo per controllare gli azionamenti con macchina a induzione, con l'utilizzo di convertitori di potenza senza utilizzare modulatori e controllori lineari. Questo nuovo approccio avrà un forte impatto sul controllo dell'elettronica di potenza nei prossimi decenni. I vantaggi del Controllo Predittivo derivano dalla possibilità di perseguire problemi multi-obiettivo, di includere facile le non linearità all'interno del modello, di trattare in modo semplice i vincoli di sistema, nonché dalla facilità di implementazione digitale e dalla flessibilità di includere modifiche ed estensioni al controllo secondo le applicazioni richieste. Inlinea con tutto ciò, la ricerca presentata in questa tesi riguarda lo sviluppo di diverse topologie di controllo per varie configurazioni di azionamenti con macchine a induzione, basate sul principio di Controllo Predittivo a modello con insieme finito degli stati di controllo (Finite Control Set Model Predictive Control - FCS-MPC), che definisce direttamente l'assetto dell'inverter di tensione (VSI). Inoltre, per aumentare la robustezza degli azionamenti, vengono proposti e sperimentati diversi approcci senza sensori elettromeccanici (sensorless).

La prima topologia studiata di azionamenti con macchina a induzione (IM) è l'azionamento con motore a gabbia. Il controllo diretto di coppia (DTC) è aggiornato in termini di controllo predittivo a modello (MP DTC) e usato per controllare la coppia e il flusso statorico attraverso l'utilizzo di una efficace funzione di costo attraverso la quale è anche possibile facilmente comprendere e confrontare le varianti di implementazione e studiare i problemi di convergenza e di stabilità. Viene analizzato l'effetto della velocità sulle diverse versioni di controllo e sulle prestazioni complessive del MP DTC proposto; ciò consente di comprendere appieno il principio del DTC, nonché perché e quando esso funzioni bene. Vengono utilizzate due diverse procedure di stima della posizione e della velocità del rotore nel MP DTC proposto; il primo utilizza uno stimatore adattivo con modello di riferimento (MRAS), mentre l'altro sfrutta la stessa fase di predizione del MP DTC proposto per ottenere le informazioni sulla velocità effettuando infine un'estrapolazione lineare dei valori di velocità a partire dagli ultimi due campioni stimati. Sono state eseguite numerose prove in simulazione e sperimentali per convalidare l'efficacia di entrambi gli approcci sensorless nell'ottenere un preciso inseguimento del comando di velocità per una vasta gamma di situazioni. Per migliorare la robustezza del MP DTC proposto rispetto alle variazioni parametriche, il controllo del flusso dello statore viene sostituito con quello della potenza reattiva assorbita dal motore ad induzione; di conseguenza la sensibilità del controllo alle variazioni dei parametri è limitata e ciò è confermato attraverso i risultati ottenuti sia dalla simulazione che dalle prove sperimentali. Inoltre, viene presentato un ulteriore efficace approccio alternativo per il MP DTC, basato sul principio del controllo predittivo a modello dei valori istantanei delle potenze attive e reattive dell'azionamento, invece di controllare la coppia e il flusso come nell'usuale MP DTC. Questa variante ha il vantaggio che tutte le variabili controllate sono divenute quantità misurate (potenze attive e reattive) e quindi i problemi di stima comunemente presenti nei classici schemi DTC sono efficacemente limitati. Per gli ultimi due approcci di controllo (controllo di coppia e di potenza reattiva e controllo di potenza attiva e reattiva) viene anche adottato la stima della velocità rotorica che sfrutta la funzione predittiva del controllo. I risultati ottenuti attraverso la simulazione e la sperimentazione confermano la fattibilità delle due procedure alternative di controllo per ottenere una risposta dinamica robusta dell'azionamento con IM.

Per limitare il ripple che accompagna gli andamenti controllati della coppia e del flusso statorico del motore, è stata presentata una tecnica efficace di riduzione della sua ampiezza. La tecnica è basata sull'impiego di un valore ottimale per il fattore di ponderazione w_f utilizzato nella funzione di costo per sommare i due contributi che la definiscono. Viene introdotta una derivazione matematica dettagliata del valore ottimale di w_f attraverso l'analisi dei comportamenti dell'ondulazione di coppia e del flusso. La tecnica di riduzione del ripple proposta è stata verificata tramite la simulazione usando il software Matlab/Simulink e sperimentalmente utilizzando la scheda di rapida prototipazione del controllo dSpace 1104. Ancora, l'implementazione adotta l'approccio sensorless basato sulla fase di predizione. Le prestazioni dell'azionamento con IM utilizzando quest'ultimo approccio proposto sono confrontate con i risultati ottenuti con l'approccio MP DTC che utilizza invece un valore arbitrario di w_f. Il confronto conferma la validità della procedura di riduzione del ripple nelle variabili controllate mantenendo nel contempo gli oneri di calcolo entro i limiti consentiti per l'implementazione.

Il principio FCS-MPC è anche utilizzato per controllare la corrente del motore di induzione come alternativa al controllo classico ad orientamento di campo (Field Oriented Control -FOC). L'approccio proposto di controllo di corrente di tipo predittivo (Model Predictive Current Control - MPCC) appartiene alla classe del controllo predittivo ad isteresi (per limitare il frequenza di commutazione) in quanto il MPCC viene attivato dal raggiungimento dell'errore di corrente di una determinata soglia. In questo caso, la caratteristica sensorless dell'azionamento è ottenuta includendo un efficace osservatore Luenberger (LO) per una precisa stima del vettore del flusso del rotore insieme alla coppia di carico e alla velocità. È stata adottata una efficace procedura di allocazione dei poli per la selezione dei guadagni dell'osservatore; la procedura si basa sul posizionamento dei poli dell'osservatore a sinistra di quelli del motore nel complesso (piano di s) con una ridotta parte immaginaria, in modo che la stabilità dell'osservatore sia migliorata in un'ampia gamma di velocità. La fattibilità dell'azionamento sensorless con MPCC è ancora confermata attraverso la simulazione e i risultati sperimentali.

La seconda topologia degli azionamenti con macchina a induzione che è stata studiata è l'azionamento con motore ad anelli con rotore alimentato da invertitore e statore da rete (Doubly Fed Induction Motor DFIM). È stato sviluppato un efficace algoritmo predittivo a modello (MP DTC) per il controllo dinamico della coppia e del flusso di rotore dell'azionamento DFIM. Inoltre, viene presentato un approccio efficace di soluzione sensorless che valuta la velocità e la posizione del rotore in modo esplicito senza la necessità di coinvolgere la stima del flusso nel processo di predizione; di conseguenza l'effetto delle variazioni dei parametri sulle prestazioni complessive dell'osservatore di posizione e velocità è sensibilmente limitato. Questo è stato provato attraverso i risultati ottenuti con test eseguiti in un'ampia gamma di velocità, dal sub-sincronismo a velocità super-sincrona. Durante l'operazione, la resistenza dello statore e i valori di induttanza di magnetizzazione sono stati modificati rispetto ai valori reali per studiare l'effetto di variazioni parametriche sulle prestazioni dell'osservatore. Anche in questo caso, il software Matlab/Simulink e una scheda di controllo dSpace 1104 sono stati utilizzati per convalidare l'efficacia dell'approccio sensorless del MP DTC per l'azionamento. I risultati dimostrano la robustezza del controllo sensorless proposto e la sua capacità di ottenere una precisa stima della posizione e della velocità del rotore.

La terza topologia di azionamenti con macchina a induzione che è stata studiata è quella del generatore ad induzione con rotore avvolto (DFIG) e invertitore sul rotore. Viene presentata una derivazione analitica dettagliata del controllo predittivo diretto di potenza (MP DPC) per DFIG, che trasferisce ed estende l'approccio di controllo del MP DTC citato prima per il motore a induzione a doppia alimentazione (DFIM). Una soluzione sensorless ancora basata sull'osservatore adattivo a modello di riferimento (MRAS) è adottato per stimare la velocità e la posizione del rotore. Sia le simulazioni usando il software Matlab/Simulink che i test sperimentali utilizzando la scheda dSpace 1104 hanno mostrato le elevate prestazioni dinamiche dell'azionamento. I risultati ottenuti confermano la fattibilità del metodo MP DPC proposto per ottenere un controllo disaccoppiato di potenze attive e reattive per DFIG.

In sintesi, si può dire che l'utilizzo proposto del controllo predittivo a modello ha dimostrato la sua capacità di ottenere elevate prestazioni dinamiche per le diverse topologie degli azionamenti con macchina ad induzione considerati. Inoltre, le tecniche sensorless proposte hanno confermato la loro efficacia per una vasta gamma di velocità. Tutto questo è stato verificato e validato attraverso una vasta attività analisi simulativa e di sperimentazione in laboratorio.

ACKNOWLEDGEMENT

All deepest thanks are due to God, the merciful and the compassionate for the uncountable gifts given to me. Thanks to God, who has given me my family: they are the light in my life. To my father whose soul will be always with me, to my lovely mother whose prayers, cooperation at all stages of this work and against all odds, have been simply overwhelming. To my wife Sara: who means the world to me, to my kids Rodyna, Yousef, and Yaseen: who are the light of my eyes.

I would like to express my great thanks to Prof. Silverio Bolognani for his discussions and encouragement. I would like to express my deepest thanks to him for his kind supervision, generous advice, clarifying suggestions and support during each step of this work. Thanks a lot to Prof. Nicola Bianchi for his encouragement.

A special thank goes to Mr. Mosè Castiello for his support: I value his technical assistance very much. Many thanks to all the friends I have met during the last years in the Electrical Drives Laboratory (EDLAB). In addition, I sincerely appreciate the friendship and help of my PhD fellows Davide da ru', Yawei wang, Virginia manzolini, Cristian babetto, Giacomo bacco, and Francesco Toso.

The authors would like to thank Fondazione Cassa di Risparmio di Padova e Rovigo that funded the three-year PhD scholarship to Mahmoud Mohamed

Mahmoud, 2017

CONTENTS

LIST OF FIGURES

LIST OF TABLES

ACRONYMS

FOC	Field oriented control
DTC	Direct torque control
IM	Induction motor
DC	Direct current
AC	Alternating current
PWM	Pulse width modulation
MRAS	Model reference adaptive system
Im	Imaginary part
Re	Real part
ISR	Interrupt service routine
DSP	Digital signal processor
HW	Hardware
VSI	Voltage source inverter
ZOH	Zero order hold
S/H	Sampling and holding
PI	Proportional integrator
MPC	Model predictive control
MP DTC	Model predictive direct torque control
MP IPC	Model predictive instantaneous power control
MPCC	Model predictive current control
CCS-MPC	Continuous control set- Model predictive control
FCS-MPC	Finite control set- Model predictive control
DSC	Direct self-control
GPC	Generalized predictive control
DMC	Dynamic matrix control
LQR	Linear quadratic regulator
DMTC	Direct mean torque control
DSPC	Direct speed control
MAC	Model algorithmic control
EHAC	Extended horizon adaptive control
EPSAC	Extended predictive self-adaptive control
RHC	Receding horizon control
SVM	Space vector modulation
LO	Luenberger observer
DFIM	Doubly fed induction motor
DFIG	Doubly fed induction generator
DPC	Direct power control
PLL	Phase locked loop

NOMENCLATURE

m	Electromagnetic torque
M_n	Rated torque
$\bar{\psi}_s$	Stator flux vector
$\psi_{\alpha s}, \psi_{\beta s}$	Stator flux components in αβ stationary frame
$\bar{\psi}_s^r$	stator flux vector in rotor frame
$\bar{\psi}_r$	Rotor flux vector
$\psi_{\alpha r}, \psi_{\beta r}$	Rotor flux components in αβ stationary frame
ψ_{dr}, ψ_{qr}	Rotor flux components in dq reference frame
$\bar{\psi}_{rs} = \bar{\psi}_{rs}^s$	Rotor flux vector referred to stator side
$\bar{\psi}_r^r$	Rotor flux vector in rotor frame
Ψ_n	Rated flux of the machine
w_f	Weighting factor
E_{max}	Maximum error limit
Λ	Cost function (convergence condition)
$\bar{e}$	Error vector
$\bar{u}_s$	Stator voltage vector
$u_{\alpha s}, u_{\beta s}$	Stator voltage components in αβ stationary frame
u_{ds}, u_{qs}	Stator voltage components in dq reference frame
$\bar{u}_{rs}^s$	Rotor voltage vector referred to stator side
$\bar{u}_r^r$	Rotor voltage vector in rotor frame
$\bar{\imath}_s$	Stator current vector
$\bar{\imath}_s^s$	Stator current vector in stationary frame
$\bar{\imath}_s^r$	Stator current vector in rotor frame
$i_{\alpha s}, i_{\beta s}$	Stator current components in αβ stationary frame
i_{ds}, i_{qs}	Stator current components in dq reference frame
I_{sn}	Nominal value of stator current
$\bar{\imath}_r$	Rotor current vector
$\bar{\imath}_{rs}$	Rotor current vector referred to stator side
$\bar{\imath}_r^r$	Rotor current vector in rotor frame
R_s	Stator resistance
R_r	Rotor resistance
R_{rs}	Rotor resistance referred to stator side
L_s	Stator self-inductance
L_r	Rotor self-inductance
L_M	Mutual inductance
L_t	Transient inductance
L_{ls}	Stator leakage inductance
L_{lr}	Rotor leakage inductance
p	Pole pairs
ω_m	Mechanical angular speed
ω_{me}	Electromechanical angular speed
θ_{me}	Rotor position
i	Voltage index
k_P, k_I	Proportional and integral gains of PI controller of MRAS observer for IM

k_{PP}, k_{II}	Proportional and integral gains of PI controller of MRAS observer for DFIG
N_{com}	Number of commutations
F_{sw}	Switching frequency
α	Acceleration
σ	Total leakage factor
P_s	Stator active power
Q_s	Stator reactive power
P_{shaft}	Shaft mechanical power of IM
P_{sn}	Rated active power
Q_{sn}	Rated reactive power
S_n	Rated apparent power
f_s	Stator supply frequency
ω_s	Stator angular frequency
θ_s	Stator flux angle in stationary frame
$\Omega_{s,rated}$	Rated angular frequency
$\Omega_{sl,n}$	Rated angular slip
$\bar{i}_m$	Magnetizing current vector
$\bar{\psi}_m$	Magnetizing airgap flux
ψ_{pm} , ψ_{qm}	Magnetizing airgap flux components in the synchronously rotating (p-q) frame
i_{ps} , i_{qs}	Stator current components in the synchronously rotating (p-q) frame
$\bar{u}_{emf}$	Back emf voltage vector
ω_e	Supplied electrical angular frequency (=angular velocity of the stator magnetizing flux)
ω_{slip}	Angular slip
T_r	Rotor time constant
m_{ripple}	Torque ripple
D_m	Torque deviation
S	Ascending torque slope (torque derivative)
T_s	Sampling time
$\bar{u}_{s,opt}$	Optimal stator voltage vector
w_{opt}	Optimal weighting factor
G	Luenberger observer gains matrix
λ	Correction element for Luenberger observer
$\hat{m}_{load}$	Estimated load torque
J	Moment of inertia
$\hat{\theta}_r$	Estimated rotor flux angle
θ_1	Angle of rotor current vector $\bar{i}_r$ with respect to α_s-axis of stator reference frame
θ_2	Angle of rotor current vector $\bar{i}_r$ with respect to α_r-axis of rotor reference frame
μ	Angle of stator magnetizing flux with respect to α_s-axis of stator reference frame
ΔR_s	Variation of stator resistance
ΔL_M	Variation of magnetizing inductance
φ	Angle between stator and rotor fluxes space vector
ω_r	Angular speed of stator flux vector in rotor reference frame
U_{dc}	DC link voltage

SUBSCRIPTS

ω	Speed dependent terms
u	Voltage dependent terms
r, s	Rotor/stator reference
*	Denote the reference value
^	Denote the estimated value
~	Denote the predicted value
0	Denote the initial value

Chapter 1

Introduction

At present time, the Induction Machine (IM), also known as Asynchronous Machine, has been widely used in industrial applications, such as heavy lifting, wind turbine, marine propulsion, hydroelectric power stations, railway traction and electrical vehicle. Since the first induction motor invented in 1880s; to date, more than 90% of industrial drive applications are using induction machine. However, excluding applications which do not require the control system, most of these motors are not controlled precisely due to various reasons. One main reason in using uncontrolled IM is due to the level of difficulty in controlling it, for example, because of the non-linearity and complexity of the dynamic model. On the other hand, some industrial applications require certain control aspects , that must be fulfilled by the controlled drive. The IM can be utilized with different configurations working as a motor or as a generator, and to achieve the best dynamic performance from these different configurations, the proposed control approaches can be profitably adopted. Within the contents of this thesis , different topologies of induction machine (IM) are studied and controlled with effective control procedures, so that a detailed survey about this machine has been carried out and discussed.

1.1 Historical Background

The understanding of the historical background of induction machine control is essential and helpful; moreover, the contributions of this thesis can also be extended and applied in different fields. In the past few decades, for the general objectives; such as improved performance, high-energy efficiency and increased safety levels, researchers have been investigated on the IM control from different perspectives. One of the approaches is from hardware point of view, such as improving the semiconductor switches; multi-level inverters and additional phases of motor winding. Another approach is the control theory development, due to the digital control platforms that are well developed and extensively applied in the power electronics applications. These digital control platforms provide powerful computational capacity for implementing more complex control methodologies. The modern control engineering had significantly developed since the early 20th century, due to the advance of technology. Initially, the control engineering arose when engineers attempted to ensure the productivity in the manufacturing industries by gathering the plant information to plan operations [1]. Meanwhile, the feedback control is developed and analyzed for automatic control systems [2].

Afterwards, the control theory is developed and applied in many different fields, such as process control, chemical control and power electronics. In the early days, the induction motor speed was adjusted by using the silicon controlled rectifier back in 1960s [3], after that, the voltage-frequency v/f control was investigated and

even today still commonly used for applications with low performance requirements. The high performance control of induction motor drive was not found until the Field Oriented Control (FOC) become the industry standard for AC motor drive, since it transforms the AC motor dynamics close to a DC motor.

Figure 1.1 illustrates the categories of popular control theories for induction motor drive. Among them, FOC and Direct Torque Control (DTC) are more like methodology than theory. To differ with new control algorithms, FOC is placed under PI-based control. However, various control strategies are still using the same structure of FOC technique by applying different control algorithms, since R. H. Park [4] published the concept of rotating reference frame in 1929, in which the idea of FOC was developed based on the electromagnetic torque proportional to the cross product of stator current and rotor flux ($\bar{\imath}_s \times \bar{\psi}_r$) , which decoupled the control of torque and filed excitation, similar to a DC motor. After that, the Indirect FOC was presented by Hasse in 1968 [5] and the concept of Direct FOC was developed by Blaschke a couple of years later [6], both of the orientations are aligned with the rotor flux vector. Alternatively, the DTC employs hysteresis control directly with stator flux and torque references based on a look-up table, which was presented by Noguchi [7], later the similar method of Direct Self Control (DSC) was developed by Depenbrock [8].

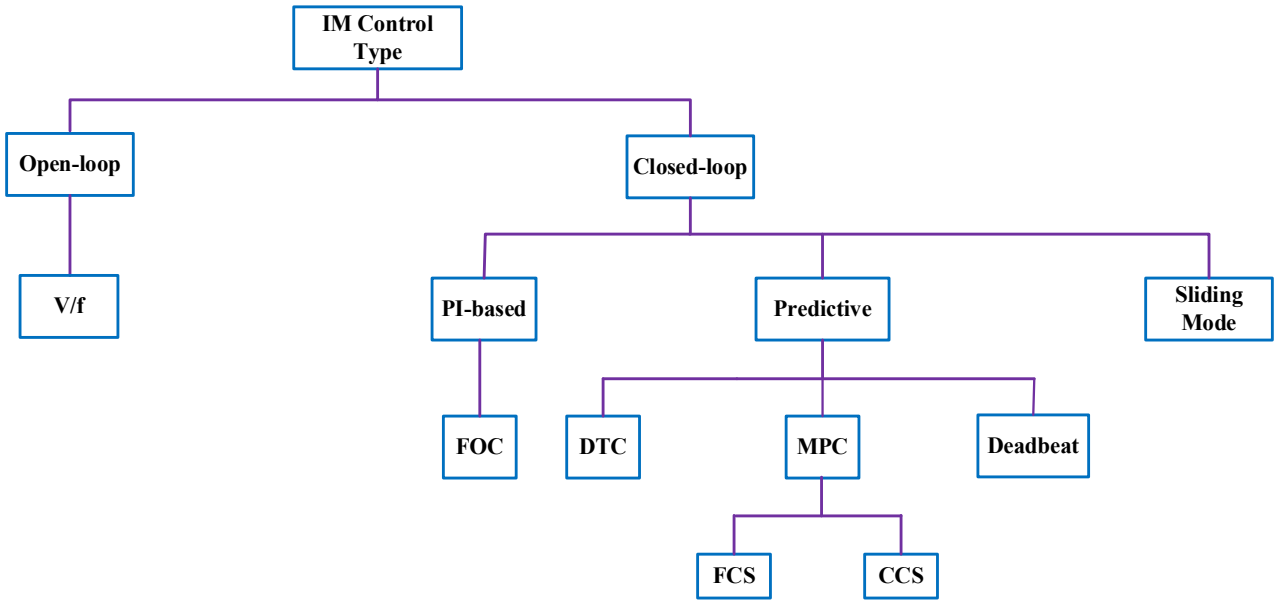

Figure 1.1: Induction motor control techniques

Unlike the synchronous motors, which have identical position of flux and rotor shaft during operations, the induction motor has slip difference between the electromagnetic flux and the actual rotor shaft position. The estimation of flux position is essential for d-q rotating frame transformation. In the concept of FOC, the Indirect FOC does not require the magnitude information of the rotor flux as a feedback signal, the d-axis current is defined based on the open-loop model and the rotor flux position is simply estimated from the reference values of currents and the real-time rotor shaft position. On the other hand, the idea of Direct FOC is investigated with the existence of rotor flux measurement in the initial contribution [6], which is not effective for most applications; hence, various types of flux observers were developed for accommodating such situation. The study of flux observer is another aspect of induction motor control; the goal is to estimate the information of flux vector of motor based on the available measurements, such as current, voltage and speed.

Direct FOC normally requires rotor flux observer, moreover, DTC generally needs the observer of stator flux. Once the flux information is observed, a torque estimation could be straightforward. The categories of observer could be divided into closed-loop and open-loop. A well-known closed-loop observer is the Luenberger observer [9], which is employed in Chapter 5 of this thesis. Other types of closed-loop observers, such as Gopinahth's type observer [10] and Kalman Filter observer [11], have been developed at the research level. On the other hand, the open-loop observers are developed directly from the motor model without the measurements of error feedback, for example, the Voltage or Stator Model, Current or Rotor Model, Voltage-Current and Speed Model, and Voltage-Speed Model. The open-loop observers are normally employed in the research field for speed sensor-less control, which tends to observe the motor shaft speed and position, in order to accomplish for the applications where the speed and position sensors are undesired, due to cost, cabling, robustness and construction. Many contributions of speed sensor-less control were published for induction motor application [12, 13, 14].

In order to give a focused view on the sensorless topics and its implementation on different types of induction machine, the current thesis introduces and implements different sensorless techniques for the purpose of estimation of the rotational speed and rotor position for various topologies of IM drives. In this thesis, the major scope is focused on the high performance control of different topologies of IM drives, especially optimal control utilizing Model Predictive Control technique.

1.2 Thesis Objectives

In view of the foregoing brief discussion, the objectives of the thesis are summarized as follows:

- Replacing the classical control techniques used for induction machine drives such as FOC and DTC, with efficient Model Predictive Controllers, through which high dynamic performance can be achieved. Due to its merits that will be reported in literature review; Finite Control Set Model Predictive Control (FCS MPC) approach is utilized in this thesis for controlling different induction machine configurations such as three-phase induction motor (IM), doubly fed induction motor (DFIM), and doubly fed induction generator (DFIG). The last two configurations (DFIM and DFIG) are chosen to be studied beside the induction motor drive due to their multiple advantages, such as the capability of handling bulk of power with less rated power converters in the rotor circuit, and the ability of integration with renewable energy sources such as wind energy systems.

- Enhancing the robustness of the controlled induction machine drives through the utilization of different sensorless schemes for estimating mechanical speed and rotor position needed for implementing the proposed control algorithms.

- Simplifying the digital implementation procedure for the proposed control algorithms and reducing the ripple contents in the controlled variables and thus improving the dynamic performance of the controlled drive.

- Investigating and analyzing the effect of some control variants on the overall performance of proposed control procedures (torque control, current control, power control), such as the effect of speed on the control algorithm. Also, studying the impact of the weighting factor (w_f) on the combination of the controlled variables in the cost function, and developing a way for the optimal selection of w_f. This makes easy the understanding of the real base principle of proposed control approaches, as well as why and when they work well.

1.3 Thesis Outlines

The current thesis is organized in eight chapters as follows:

Chapter 1 gives an overview about the historical background of using induction machine drives and the different control techniques used for them. In addition, it presents the motivations, objectives and outlines of the thesis.

Chapter 2 presents a review of model predictive control approach, which has been selected as the main control principle, based on which different control algorithms are developed in this thesis. The chapter analyses the different types of MPC approaches clarifying the points of strength and weakness in each one, and identifying the selected approach in the current thesis.

Chapter 3 presents an assessment of the proposed model predictive direct torque control approach for induction motor drive. It also introduces a detailed description about the procedure of implementation and its requirements. The chapter presents two different sensorless approaches for enhancing the dynamic performance of IM drive; one utilizes model reference adaptive system (MRAS) observer, while the other utilizes the predictive feature of proposed MP DTC. In addition to that, the chapter presents two other control techniques, which are based on the same control principle (model predictive) and can be used as alternatives to MP DTC approach. The first one replaces the torque as a control variable with controlling the reactive power flow, while the other replaces the control of torque and flux with the control of instantaneous active and reactive powers flow inside the IM drive and it is called instantaneous power control (IPC).

Chapter 4 introduces an effective ripple reduction procedure to be utilized by the proposed MP DTC introduced in chapter 3; this is to reduce effectively the ripple contents in the controlled flux and torque variables. The procedure is based on the optimum calculation of the weighting factor w_f value instead of imposing an offline arbitrary value like that one adopted in most of previous researches about MP DTC for IM drives. The proposed MP DTC in this chapter utilizes also the second sensorless solution introduced in chapter 3 that obtains the speed from the difference between the discrete samples of the stator current (exploitation of predictive step).

Chapter 5 presents an effective current control approach for IM drive based on model prediction, which is considered an alternative to classic PI control used in conventional field oriented control (FOC) drives, thus avoiding the shortages of this previous control technique. The chapter introduces also an effective sensorless scheme based on Luenberger observer (LO) with an improved method for calculating the observer's gains to achieve high stability of the observer for wide speed ranges.

Chapter 6 introduces an effective model predictive direct torque control technique (MP DTC) for a doubly fed induction machine (DFIM) working in motoring mode, this type of operation mode is not frequently presented even though it has high demands in some industrial application like marine propulsion and railway tractions. The chapter presents a detailed analysis of the DFIM model and the implementation procedure of the proposed MP DTC; in addition, an effective sensorless approach is used, which extracts the speed and rotor position in an explicit way without the need for involving the flux in the estimation process, thus the effect of parameters variation on the overall performance of the sensorless observer is effectively limited, the chapter investigates the effect of parameters variation on the observer's response, and as expected theoretically, the drive exhibits a robust dynamic performance.

Chapter 7 presents and analyzes the second topology of the doubly fed induction machine (DFIM), working as a generator (DFIG). The chapter introduces a detailed description of the process for transposing from model predictive direct torque control (MP DTC) for $DFIM_{motor}$ introduced in chapter 6 to model predictive direct

power control (MP DPC) for $DFIG_{generator}$. A sensorless approach, which utilizes a model reference adaptive system (MRAS) observer, is adopted for estimating the speed and rotor position.

Chapter 8 summarizes the main contributions and outputs of the work performed in the thesis along with recommendations for future work, and finally the publications from the thesis research work are listed.

Chapter 2

Literature review

2.1 Model Predictive Control (Effective control solution for electrical drives)

In recent years, Model Predictive Control (MPC), with its advantage in multi-variable constraint control system, had been widely used in industry for last few decades [15]. The initial idea of MPC was published in 1980s, on Model predictive heuristic control [16] and Dynamic Matrix Control (DMC) [17]. Following the same track, the Generalized Predictive Control (GPC) was presented in 1987 [18, 19]. The objectives of DMC and GPC are different due to the concentration on different applications, DMC was focused on multivariable constrained control for oil and chemical applications, on the other hand, the GPC was attempted to invent a new adaptive control. In the earlier years, the method of Linear Quadratic Regulator (LQR) had been extensively studied for optimal control without constraints [20], where the optimal control sequence was generated using the state feedback law and the feedback gain matrix was calculated using an algebraic Riccati equation. In order to reduce the on-line computational load, a receding horizon implementation was formulated in [21]. The implementation of MPC for electrical machine drives and power converters was started almost after presenting the base principles of the control method by few years as reported in [22, 23].

The main difference between the MPC formulation used for controlling the AC drives and the well-known feedback control schemes with Pl controllers is the pre-calculation of the behavior of this controlled system and the consideration of this behavior in the control signal before a difference between the real value and the reference value really occurs, whereas the feedback control only reacts and tries to correct a control difference when it has already appeared.

All predictive control schemes for electrical drives can be classified according to two criteria: The depth of the pre calculation, the so-called prediction horizon, and the way the control action is generated. Whereas some predictive controllers take into account the discrete characteristic of an inverter and calculate directly the specific switching states and it is identified as finite control set (FCS), others derive a control variable with a continuous value identified as continuous control set (CCS), which has to pass a modulator afterwards.

The two configuration of model predictive control can be shown via Figure 2.1, where u(k) refers to the controlled variable and s(k) refers to the switching action, while d(k) denotes to the duty ratio.

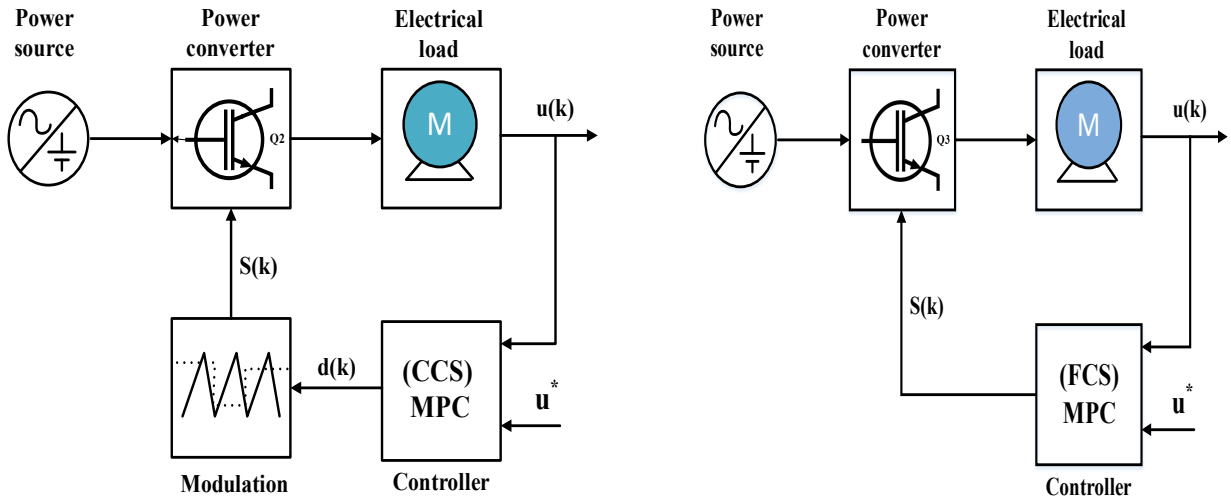

(a) MPC with continuous control set (b) MPC with finite control set

Figure 2.1: Model predictive control configurations

Table 2.1 shows some examples of the different families of model predictive control.

TABLE 2.1
Different families of MPC

		Type of control	
		With modulator (CCS)	**Direct (FCS)**
Predictio n horizon	1	Direct Control of IM Currents	Direct Torque Control
		Direct Flux Control	Direct Self Control
			Direct Speed Control
	>1	Generalized Predictive Control	Direct Model Predictive Control

The methodology of all the controllers belonging to the MPC family is characterized by the following strategy, represented in Figure 2.2:

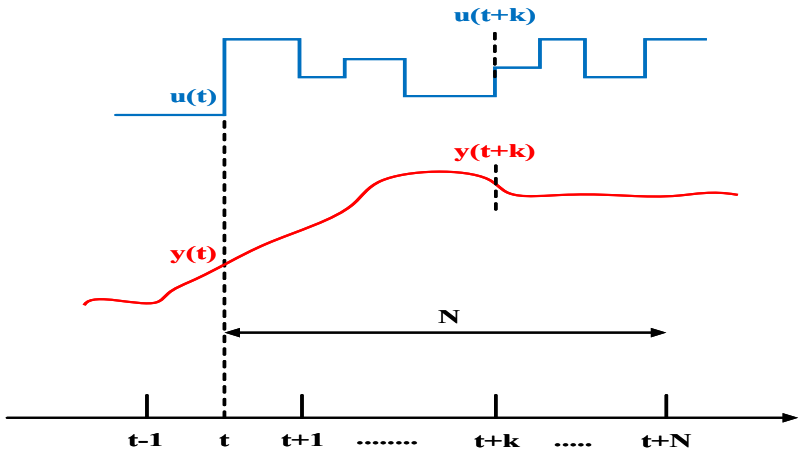

Figure 2.2: MPC strategy

1. The future outputs for a determined horizon N, called the prediction horizon, are predicted at each instant t using the process model. These predicted outputs y(t + k) for k = 1 .... N depend on the known values up to instant t (past inputs and outputs) and on the future control signals u(t+k), k = 0 ..... N −1, which are those to be sent to the system and calculated.
2. The set of future control signals is calculated by optimizing a determined criterion to keep the process as close as possible to the reference trajectory R(t + k) (which can be the set point itself or a close approximation of it). This criterion usually takes the form of a quadratic function of the errors between the predicted output signal and the predicted reference trajectory [24]. The control effort is included in the objective function in most cases. An explicit solution can be obtained if the criterion is quadratic, the model is linear, and there are no constraints; otherwise an iterative optimization method has to be used. Some assumptions about the structure of the future control law are also made in some cases, such as that it will be constant from a given instant.
3. The control signal u(t) is sent to the process whilst the next control signals calculated are rejected, because at the next sampling instant y(t + 1) is already known and step 1 is repeated with this new value and all the sequences are brought up to date. Thus the u(t + 1) is calculated using the receding horizon concept.

Due to its various merits, the finite control set FCS-MPC is utilized as the common control technique based on which different configurations of asynchronous machine drives are controlled, this will be illustrated in details in the following chapters.

It is worth to mention that the tree family of predictive controllers contains other different algorithms corresponding with model predictive control (MPC) topology, which can be reviewed in the following sub-sections.

2.1.1 Classification of predictive control schemes based on operational principle

Considering the functional principles of the different predictive control algorithms, it can be seen that these can be classified into three main groups. A decision can be made between hysteresis-based, trajectory-based and model- based strategies. Indeed, these families are not clearly separated from each other and sometimes the transition between them is rather floating. In the following subsections the three strategies are explained.

2.1.1.1 Hystersis- based predictive controllers

The basic principle of hysteresis-based control strategies is to keep the value of the controlled variable within a tolerance band or a tolerance area, the so-called hysteresis. The simplest form of such a controller is the well-known hysteresis or bang-bang controller. Although in literature bang-bang controllers are not considered to be predictive controllers, however, clearly show their typical behavior.

An improved form of a multidimensional bang-bang controller is the predictive current control scheme proposed by Holtz and Stadtfeld [22]. Using this controller, the switching instants are determined by the limits of the tolerance band.

Figure 2.3 shows the functional principle; in this case a circular hysteresis boundary is chosen, whose position in the stator coordinate system is given by the stator current reference vector $i^*_{s,k}$. If the actual value of the stator current $\bar{i}_{s,k}$ reaches the border of the hysteresis area, the next switching state of the inverter is selected via prediction and optimization: At first, the future trajectories of the stator current vector are precalculated for all possible switching states and the time instant k at which the actual current will leave the tolerance band is determined. The basis for these calculations are the well-known mathematical differential equations of electric

machines. Besides, it shall be noted that the circular tolerance region itself moves along with the stator current space vector within the complex plane. This movement is indicated with the dotted circle in Figure 2.3.

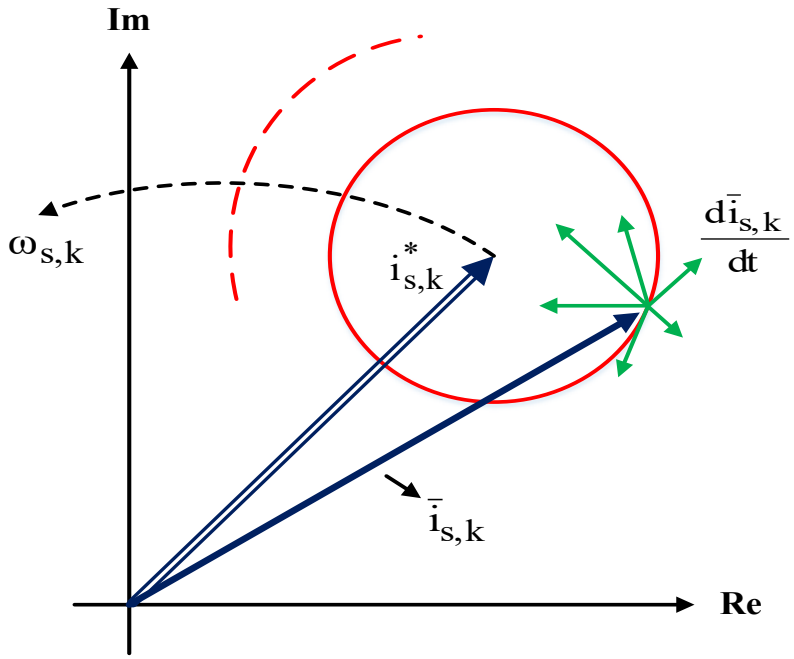

Figure 2.3: Hysteresis- based predictive controller

The optimal switching state vector, which possesses the longest stay-time within the hysteresis, is selected. With this optimization criterion, the switching frequency of the inverter is minimized; of course, other optimization criteria are also possible, e.g. minimum current distortion or minimum torque ripple.

Hysteresis-based strategies have the advantage that precise knowledge of the system to be controlled is not required. Even with possible model divergences, the control error can be kept within the specified limit band by the hysteresis controller. To achieve this, it must always be ensured that the hysteresis controller reacts very quickly if the actual value has gone outside of the hysteresis band. This is a major problem if the hysteresis-based predictive controller is implemented in a digital processor, as the detection of the reference signal crossing the hysteresis band will be done only during the next sampling instant and the selected action is applied in the second next interval. It may happen that the error has, at this time, already grown to a large value.

2.1.1.2 Trajectory- based predictive controllers

Trajectory-based control methods are based on the principle to force the system onto precalculated system trajectories. Once the system has been pushed onto one of these trajectories, it remains there because of its own properties until a change is enforced from outside.

The first trajectory-based predictive control scheme has been published in 1984 by Kennel [25], at that time, however, being a control strategy for a line-commutated thyristor converter. Sometime later, well-known control schemes like Direct Self Control (DSC) by Depenbrock [26] or Direct Mean Torque Control (DMTC) by Flach [27] for the control of induction machines were published. Some more schemes, like Sliding Mode Control [28]

or Direct Torque Control (DTC) [29, 30] are a combination of hysteresis based and trajectory-based schemes, whereas Direct Speed Control (DSPC) by Mutschler [31] can be regarded as a pure trajectory-based control scheme even if some hysteresis based aspects are included in it. In the following, DSPC will be explained as an example of trajectory-based predictive control.

Similar to the schemes of Depenbrock [26] and Takahashi/Noguchi [30] the switching states of the inverter are classified into the groups “torque increasing”, “slowly torque decreasing” and “quickly torque-decreasing”. For short time intervals, the inertia of the system as well as the derivatives of the load torque and the machine torque can be assumed to be constant values. Then the system behavior can be represented by a set of parabolas in the speed error/acceleration plane as shown in Figure 2.4. These parabolas are also natural trajectories of the system.

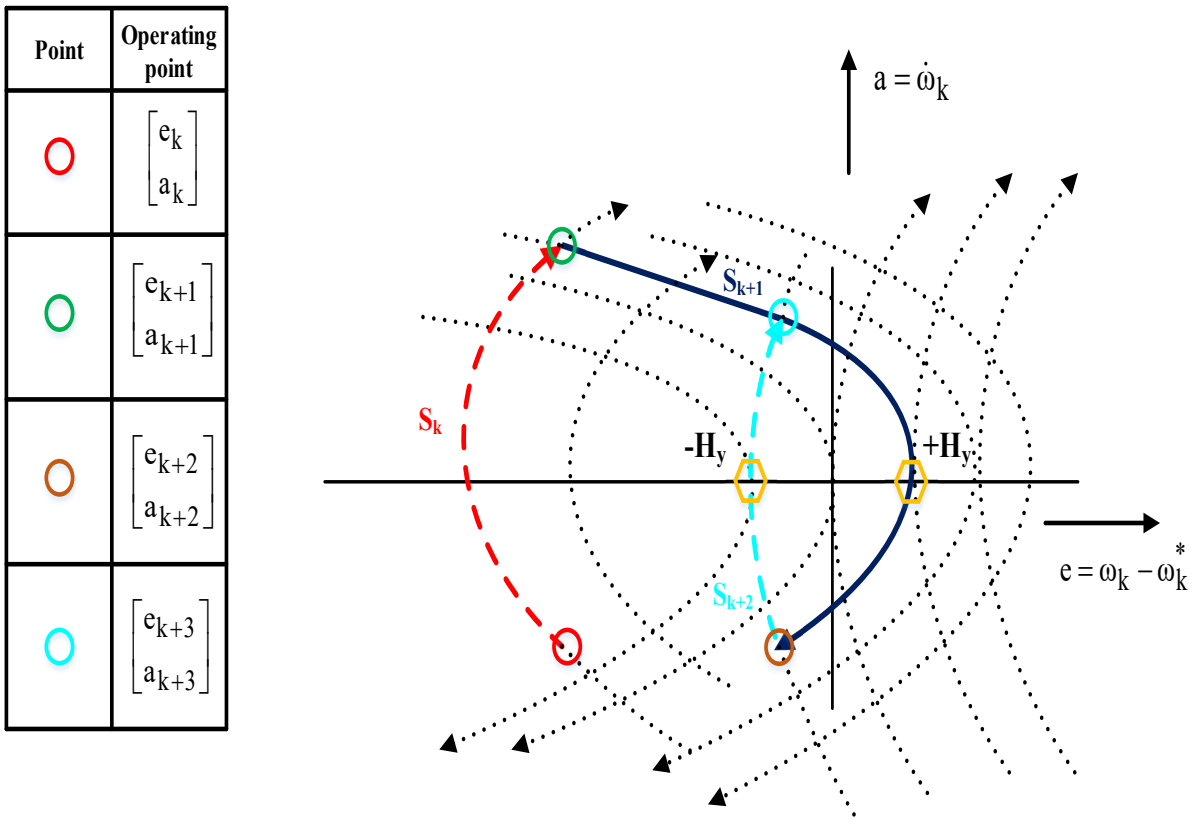

Figure 2.4: Trajectory- based predictive controller

As proposed in the DSPC scheme according to Mutschler [31], the initial system state is assumed to be at the point $[e_k \quad a_k]^T$. The desired operating point is always the origin of the coordinate system, i. e. there is no control error (e= 0) and the acceleration is zero (a= 0). The system cannot be held in this condition for long time since this would require an infinite switching frequency. Hence, a kind of hysteresis band between $-H_y$ and $+H_y$ is defined; this is described above as the hysteresis-based aspect inside DSPC. In this way, the maximum switching frequency can be reduced to an acceptable value. Apart from that, this strategy is purely a trajectory-

based scheme. To reach the predefined hysteresis area, at first, a torque increasing switching state is chosen. Now the system state moves along the dotted parabola (trajectory) until $[e_{k+1} \quad a_{k+1}]^T$ is reached. In this point, the trajectory of the switching state S_k crosses another parabola for a torque-decreasing switching state S_{k+1}, which will pass through the point $+H_y$.

The intersection point between S_k and S_{k+1} in $[e_{k+1} \quad a_{k+1}]^T$ has been determined as the optimum switching instant in advance. Hence, at the correct time instant, switching can take place without any delay and therefore the desired state point $+H_y$ can be reached as fast as possible. Exactly in the precalculated time instant, the inverter is commutated into switching state S_{k+1}. The system state now moves along the new parabola until the point $[e_{k+2} \quad a_{k+2}]^T$ is reached. At this point a torque-increasing switching state S_{k+2} is chosen; the system state now moves along the corresponding trajectory through $-H_y$ until it reaches the parabola of the switching state S_{k+1}, again at the point $[e_{k+3} \quad a_{k+3}]^T$. In steady state operation, the system state keeps moving along the path and the speed error e is kept within the predefined tolerance band $-H_y$ to $+H_y$.

Trajectory-based predictive control is based on a very precise prediction of the future control system behavior. Hence, in contrast to hysteresis controllers, controllers of this type require an exact model of the system to be controlled. Because of the quite complex pre-calculation of the system trajectories, these methods are better suited for implementations in the form of digital controllers on microprocessors.

2.1.1.3 Model- based predictive controllers

The principle of model-based predictive control abbreviated MPC was introduced for industrial control applications in the 1970s after first ideas of this strategy have already been published in the 1960s. Subsequently, MPC gained importance mainly in the field of chemical industry and later on, it gained more regard in the academic area. MPC does not denote a special control algorithm, but rather a whole family of controller types. Common characteristic of all these controllers is the principle to determine an optimum value for the actuating variable by using an explicit model of the system to be controlled and by minimizing a cost function.

For a first introduction into the subject of MPC, there exist several papers from technical journals that give an introduction or also a survey about the different model-based control schemes. The article from Morari/Lee [15] is recommended here, in which an overview about past, present and future improvement possibilities of MPC are presented. To present the ideas of MPC in an easily understandable manner, the article mainly avoids mathematical equations. For control engineers interested in the mathematical background of MPC, the detailed tutorial by Rawlings [32] is a good reference.

To the family of model-based predictive control belong, among other methods, schemes like Dynamic Matrix Control (DMC), Model Algorithmic Control (MAC), Extended Horizon Adaptive Control (EHAC) and Extended Predictive Self-Adaptive Control (EPSAC) [33]. In contrast to these control strategies, Internal Model Control does not belong to the MPC class, even though its name suggests this and even if some authors see this in such a way, e. g. Garcia, Prett and Morari [34]. Seborg, on the other hand, classifies it correctly, not as a predictive, but as an “alternative scheme” [35]. A detailed comparison of different MPC strategies had been presented by de Keyser et al. [36] and Garcia et al. [34].

Control structures belonging to the family of model-based predictive control have totally different structures than the predictive controllers commonly used in drive technology. Of course, these controllers possess a similar structure, as they also use an explicit and separately identifiable model of the controlled system for the pre-calculation of the system behavior and therefore also for the selection of optimum values for the actuating variables.

2.1.1.3.a Principle of operation of Model- based predictive controllers

The principle of operation of MPC controller can be explained with the help of the structure shown in Figure 2.5. Its central part is the model, which is used to predict the future behavior of the system to be controlled. The prediction consists of two components:

The free response shows the expected behavior of the system output y(t+j) assuming future values of the actuating variables being equal to zero.

The forced response forms the additional component of the system response based on the precalculated set of future actuating values u(t+j).

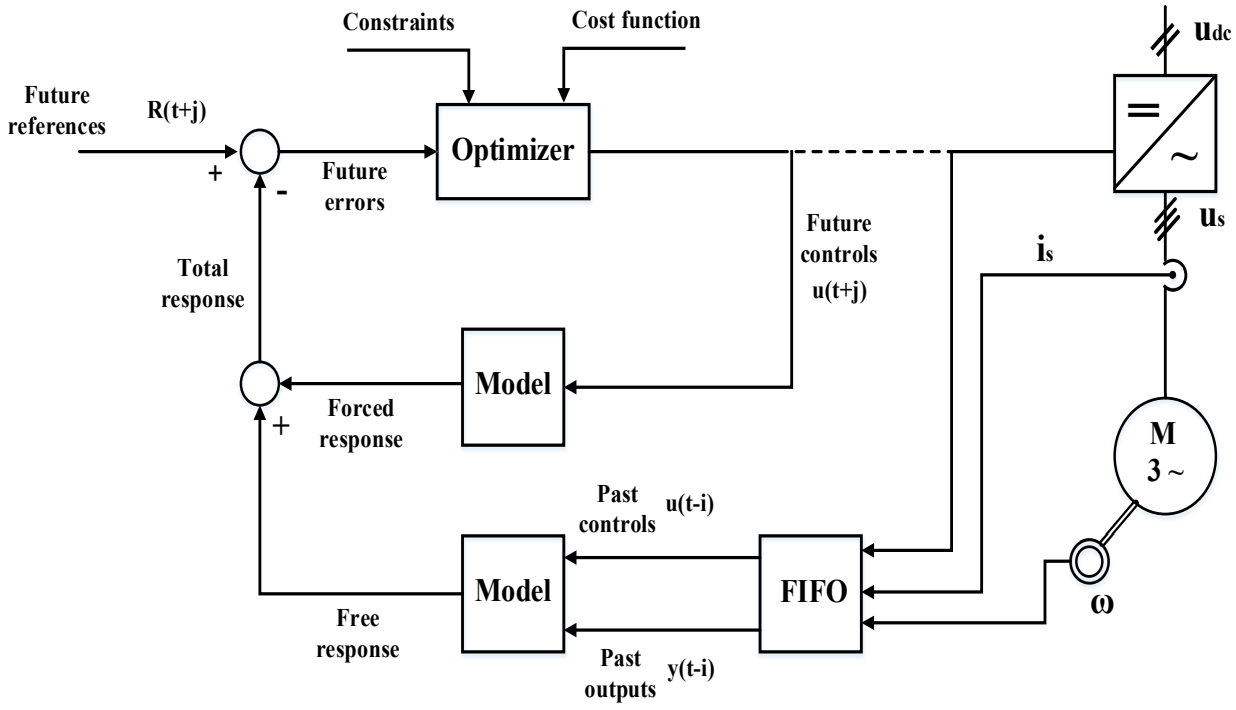

Figure 2.5: Typical structure of MPC controller

For linear systems, the entire future system behavior, the total response, can be determined as the sum of the free and forced response using the superposition principle. This sum is pre-calculated up to the prediction horizon N_p. According to the prediction horizon, a set of future reference values the system output should be equal too, does also exist. The difference between future reference and precalculated actual values delivers the future control error.

An optimization algorithm determines a set of optimum future actuating values u(t+j) from the expected error, taking system restrictions (constraints) and the cost function into account. A simple open-loop control scheme would only apply this pre-calculated future sequence of values for the actuating variables to the system. By using past values of the output and of the actuating variables up to the past horizon, this method changes into closed-loop control.

Only the first element of the calculated state vector u(t) is applied to the system and afterwards the whole procedure of prediction, optimization and controlling is again repeated for each sampling cycle. Hence, the prediction horizon is shifted forward; this principle is called Receding Horizon Control (RHC).

The functional principle of model-based predictive control based on Receding Horizon Control represents a kind of "natural" predictive control, as it is very close to human behavior. For example when driving a car, the driver does not look immediately in front of his car, but he looks far ahead and changes the actuating variables, e. g. the position of the steering wheel, gas pedal and brake before he approaches for instance a red traffic light or a curve. Besides, he pre-calculates the behavior of the car for a certain distance in front of him up to a finite horizon taking future values of the actuating variables into account; he optimizes the amount of acceleration or braking according to his optimization criteria for this distance and acts accordingly. Like in real MPC, different optimization criteria are possible, leading to different results. If the driver desires the shortest possible duration of his trip, he will accelerate and brake more rapidly than if a reduction of fuel consumption is an optimization criterion.

Due to the pre-calculation of the system behavior up to the prediction horizon, MPC inevitably leads to a high calculation demand. The calculation complexity can be significantly reduced with the introduction of a so-called control horizon N_u. After N_u steps, it is assumed that the steady state is reached and so the controller output remains constant. Figure 2.6 illustrates this situation.

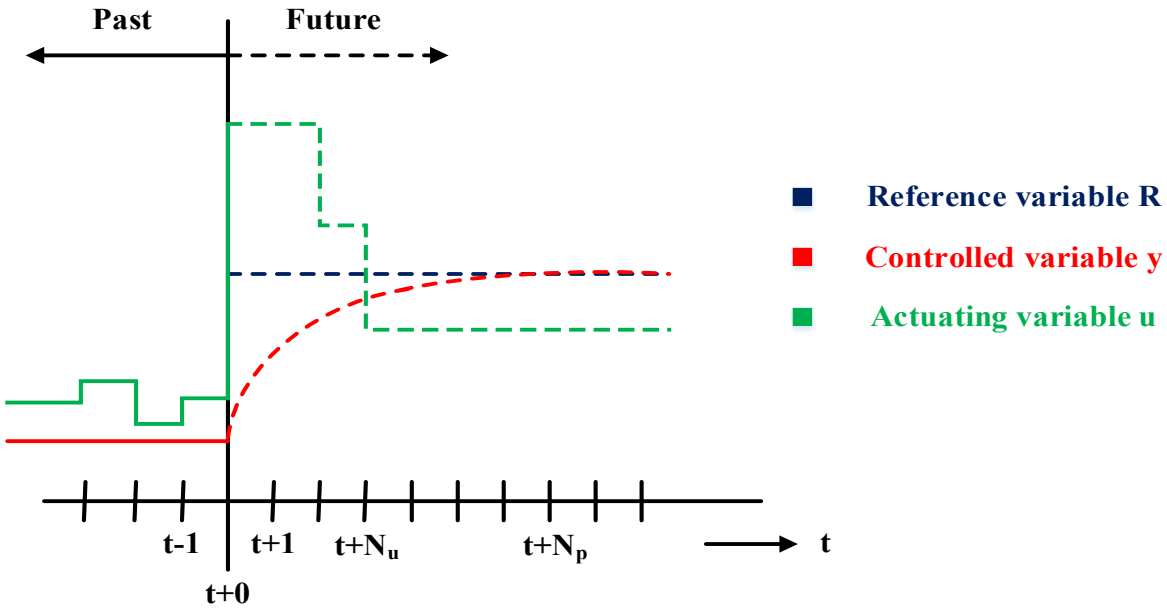

Figure 2.6: Definition of the control and prediction horizon

In spite of this modification in the control scheme, still a higher mathematical effort is necessary for model-based control of a system compared to other control algorithms. Hence, main areas of applications for MPC algorithms are, among others, the chemical and process industry [34, 37], since the processes to be controlled there are very well suited for MPC. The time constants of the whole system are rather large (in the range of minutes or even higher). Hence, calculation time is not a problem in this case. In the area of electrical drives, however, much higher sampling rates are needed. Several proposals to overcome this problem have been made [38, 39] and the research field is still opened to realize improved results with electrical drives applications.

2.2 Past, Present, and Future Challenges of MPC for Power Converters and Machine Drives

MPC has been a good solution for industrial applications for decades [40, 41]. However, once the simplicity and good performance of the MPC controller in the power electronics field has been demonstrated, the question to be answered is, why is it not already extensively used in the industry?

As a major challenge, the MPC needs an accurate model of the system, and this is not usually a simple task in highly dynamic systems. However, in recent years, the modeling of complex electrical systems has been greatly improved, and this challenge can be solved. Although more research is necessary, it is now possible to find applications of MPC to power converters where Luenberger and extended-state observers are used to avoid the effects of system parameter uncertainties [42, 43, and 44].

A drawback of the MPC strategies is the exponential increase of the computational burden if the prediction horizon, N, is longer than one and, in the case of FCS-MPC, if the number of switching states to be studied, i , is high. This fact was critical in the past, but nowadays, the high-speed microprocessors can carry out complex iterative calculations and the FCS-MPC methods can be executed with sampling times around several decades of microseconds [45].

Additionally, MPC techniques such as generalized predictive control (GPC) can deal with long prediction horizons without significantly increasing the computational burden [46]. In addition, some authors have developed FCS-MPC techniques that evaluate a reduced set of switching states in cases where the possible switching states are high. For instance, in [47], a three-phase CHB multilevel converter has been considered with N =1. This converter has 125 possible voltage vectors, but the proposed method just calculates the cost function for the seven vectors located around the last voltage vector applied to the converter. Despite this, finding computationally efficient MPC control algorithms is an open issue.

Usually considered an advantage, the FCS-MPC method avoids using a modulation stage. However, this usually leads to spread harmonic spectra of the output waveforms. This can be solved by either considering it in the cost function [39] or using a modulation stage and applying the FCS-MPC considering all the possible combinations of the switching states of the converter [48].

Other MPC concerns are the design of an efficient cost function and the tuning of the weighting factors. In this case, it can be affirmed that a systematic way to design the cost function with the best weighting factors tuning is still missing. However, some works have introduced a first approach to solve the problem, facilitating the electrical engineers' design work [49].

Finally, it should be noted that there is a lack of analytical tools to evaluate the performance of MPC for power converters and drives without having to carry out extensive simulations or experiments. Therefore, it is expected that another area of future research would be the development of such tools.

Upon the above-mentioned review, the present research work is dealing with presenting solutions to some issues related to MPC strategy when controlling electrical machine drives as reported earlier. The present research work is focusing on the utilization of FCS-MPC as a control strategy for different topologies of asynchronous (induction) machine drives (induction motor (IM), doubly fed induction motor (DFIM) and doubly fed induction generator (DFIG)). In addition, different sensorless techniques have been presented to increase the robustness of proposed control procedures. Moreover, an analytical investigation is introduced to evaluate the performance of proposed MPC procedures respecting to different control variables, such as the effect of the speed sample during the implementation, and the effect of the weighting factor on the controlled variables.

Chapter 3

Assessment of Model Predictive Direct Torque Control for Induction Motor Drives

3.1 Introduction

In recent years, an intensive research has been developed in order to find simpler control schemes for induction motors that meet the most demanding requirements, such as low torque ripple, low harmonic distortion or quick dynamic response. Today Field Oriented Control (FOC) [50] and Direct Torque Control (DTC) [8, 51] are considered the most important techniques to achieve high performance AC motor drives. Direct Torque Control is intended as the control technique for three-phase voltage source inverter-fed induction motor drive that defines the output voltage vector of the inverter ”directly” on the basis of the torque and flux errors without the interposition of current control loops [52]. DTC belongs also to the class of the Predictive Control, as the choice of the inverter voltage vector, to be applied to the motor in the next control cycle, is based on a prediction of the error derivatives caused by the future voltage vectors deliverable by the inverter, among which the more appropriate is selected [53, 54]. DTC has two variants referred as Finite Control Set, if the selection of the voltage vector is performed among the base six active inverter spatial vectors (U1⋯⋯U6) and two null spatial vectors (U0 and U7), (without the interposition of a PWM voltage control action), and Convex Control Set if voltage vectors of any phase angle are available combining two or more base inverter voltage vector thanks to a PWM voltage control. Several papers have been written about DTC for Induction motors [55, 56, 57]. Apart from a few of them, which have given fundamental contributions to the subject, the most of the others are devoted to different alternative implementations, aimed to solve specific problems, and supported by intuition or ingenuity of the proposer rather than by a solid mathematical derivation. This makes difficult the understanding of the real base principle of DTC, as well as why and when it works well.

For this purpose, this chapter is dedicated for introducing an effective formulation of the DTC based on model prediction, which gives a way for understanding and comparing implementation variants and for studying convergence and stability issues in a systematic manner. In addition, the proposed model predictive DTC formulation is utilized to regulate the reactive power instead of the flux as a control variable. This proposal is presented due to the independency of reactive power on machine parameters as it is a measurable quantity and consequently better drive performance can be achieved. Moreover, the model predictive topology is extended to control the instantaneous active and reactive power flow through the machine, this control topology is termed as instantaneous power control (IPC) and it combines both the merits of FOC and DTC while avoiding their shortages such as using PWM for voltage control and using PI controllers in addition to the presence of co-ordinate transformation. Two sensorless techniques are proposed for enhancing the drive performance; one of them is based on MRAS observer, while the other is developed through utilizing the predictive nature of proposed DTC control approach.

3.2 Theoretical approach to proposed DTC formulation

The Direct Torque Control (DTC) proposed here is a discrete time technique based on the control of the torque m and the stator flux vector module $|\bar{\psi}_s|$ of the machine instead of the currents as in a conventional FOC technique. To explain DTC it is convenient to introduce a new complex variable $\bar{\zeta}$, defined as:

$$\bar{\zeta} = \frac{m}{M_n} + jw_f \frac{|\bar{\psi}_s|}{\Psi_n} \tag{3.1}$$

where M_n and Ψ_n are the torque and flux nominal values, while w_f is an iterative weighting factor . The two components of $\bar{\zeta}$ are normalized because torque and flux have different orders of magnitude and different units.

For a reference vector $\bar{\zeta}^*_k = m^*_k/M_n + j\,|\psi^*_{s,k}|/\Psi_n$ given at the sampling time kT_s, it is possible to define, in the same sampling time, the error $\bar{e}_k$ as:

$$\bar{e}_k = \bar{\zeta}^*_k - \bar{\zeta}_k = \frac{m^*_k - m_k}{M_n} + jw_f \frac{|\psi^*_{s,k}| - |\bar{\psi}_{s,k}|}{\Psi_n} = e_{m,k} + jw_f\, e_{|\bar{\psi}_s|,k} \tag{3.2}$$

The target of the control is to maintain at any sampling time the vector $\bar{\zeta}_k$ as close to the reference $\bar{\zeta}^*_k$ as possible that is $|\bar{e}_k|$ very close to zero, by applying a proper voltage vector to the machine. In other words, the following inequality must be satisfied:

$$|\bar{e}_k| = \sqrt{(e_{m,k})^2 + w_f^2 \left(e_{|\bar{\psi}_s|,k}\right)^2} \le E_{max} \tag{3.3}$$

At any sampling time kT_s, where E_{max} is a prefixed value greater than zero introduced in order to limit switching frequency . When $|\bar{e}_k|$ reaches or excides the limit E_{max} an action has to be taken to reduce it with the aim of satisfy (3.3) again by $|\bar{e}_{k+1}|$, deciding the voltage vector to be applied to the machine, in order to bring back the working point inside the limit circle. In the case of Finite Control Set approach, the possible voltage vectors are chosen among the six inverter spatial vectors (U1⋯U6) and the two null spatial vectors (U0 and U7). The main structure of the control algorithm will be deeply described in the next sections. Figure 3.1 reports the vectors $\bar{e}$ in the (m-$|\psi_s|$) plane after two different actions.

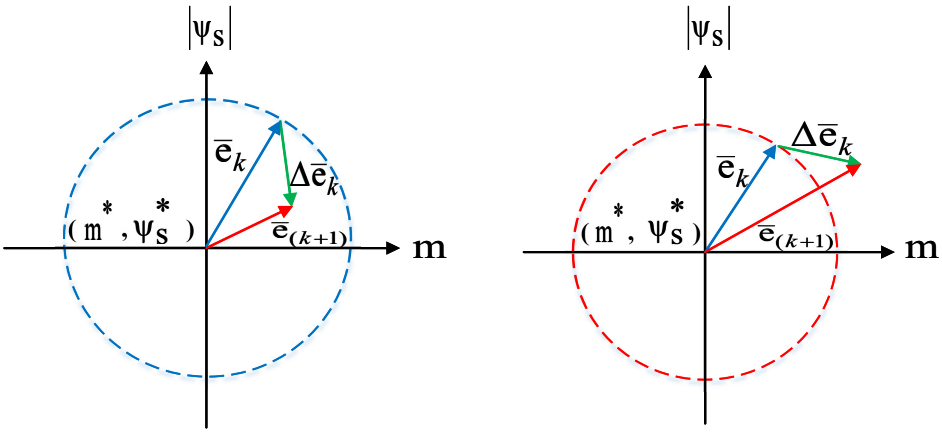

a. Correct response **b. Incorrect response**

Figure 3.1: Conditions for the existence of DTC in the error plane.

Inequality (3.3) is satisfied if the working point $(m,|\psi_s|)$ is inside the circle of radius E_{max} center in $(m^*,|\psi_s^*|)$. In the case of Figure 3.1(a) the action taken at time kT_s (at which (3.3) is just lost) is correct as the inequality is satisfied at time $(k+1)T_s$. The action shown in Figure 3.1(b) is wrong as the working point at $(k+1)T_s$ is outside the limit circle and then $|\bar{e}_{k+1}| > E_{max}$. One can realize that when the error goes outside the limit, the way to reduce it is to choose a voltage vector causing a negative derivative of the error vector module:

$$\frac{d|\bar{e}|}{dt} = \frac{d\sqrt{e_m^2 + w_f^2\, e_{|\bar{\psi}_s|}^2}}{dt} = \frac{e_m \frac{de_m}{dt} + w_f\, e_{|\bar{\psi}_s|} \frac{de_{|\bar{\psi}_s|}}{dt}}{|\bar{e}|} \leq 0 \tag{3.4}$$

Then convergence conditions, equivalent to (3.4) and referred to sampling time kT_s are one of the following:

$$\Lambda_k = e_{m,k}\left(\frac{de_m}{dt}\right)_k + w_f e_{|\bar{\psi}_s|,k}\left(\frac{de_{|\bar{\psi}_s|}}{dt}\right)_k \leq 0 \tag{3.5}$$

$$\Lambda_k = -e_{m,k}\left(\frac{d(m/M_n)}{dt}\right)_k - w_f e_{|\bar{\psi}_s|}\left(\frac{d(|\bar{\psi}_s|/\Psi_n)}{dt}\right)_k \leq 0$$

The second equality being valid if m^* and $|\psi_s^*|$ are constant. Prediction nature of DTC is evident from the last equations as the control is decided by the future (of course predicted) error derivatives. As explained later, the control algorithm chooses the spatial vector that produces torque and flux transients that reduce |e|. More than one voltage vector may satisfy the convergence condition.

Different implementation variants have been proposed in the last decades for choosing the optimal vector in order also to meet additional specifications as minimizing switching frequency, losses and so on, through look-up-tables or other implementation techniques; condition (3.4) or (3.5) anyway has to be satisfied for guaranteeing the right performance of the control.

3.3 IM electromechanical model

In order to apply the control principle introduced above, an appropriate IM discrete model can be carried out, a detailed mathematical derivation for the equivalent circuit is presented in appendix A . Assuming the four parameter equivalent circuit of Figure 3.2, in which all quantities are space vectors in the stationary α-β reference frame and rotor quantities and parameters are referred to stator.

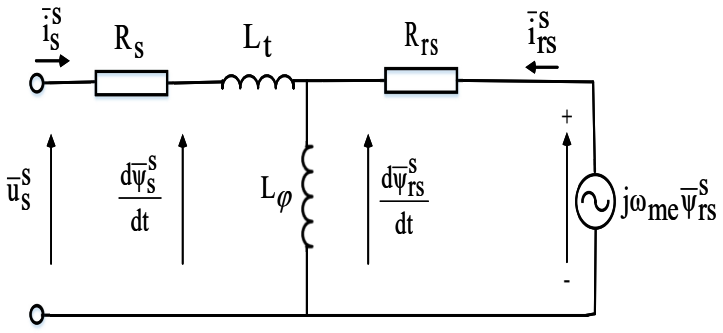

Figure 3.2: Space vector equivalent circuit of IM in stationary reference frame

From Figure 3.2, the following voltage balance can be written

$$\left(\frac{d\bar{\psi}_s}{dt}\right)_k = \bar{u}_{s,k} - R_s\bar{i}_{s,k} \tag{3.6}$$

$$\left(\frac{d\bar{\psi}_{rs}}{dt}\right)_k = -R_{rs}\bar{i}_{rs,k} + j\omega_{me,k}\bar{\psi}_{rs,k} \tag{3.7}$$

where $\omega_{me,k}= p\omega_{m,k}$. In addition: $R_{rs}=R_r(L_M/L_r)^2$; $L_\varphi= L_M^2/L_r$; $L_t=L_s- L_M^2/L_r$, and $\bar{\imath}_{rs,k} = \bar{\imath}_{r,k}\, L_r/L_M$; $\bar{\psi}_{rs,k} = \bar{\psi}_{r,k}\, L_M/L_r$.

Flux-current relationships are expressed by

$$\bar{\psi}_{s,k} = (L_t + L_\varphi)\bar{i}_{s,k} + L_\varphi\, \bar{i}_{rs,k} \tag{3.8}$$

$$\bar{\psi}_{rs,k} = L_\varphi\, (\bar{i}_{s,k} + \bar{i}_{rs,k}) \tag{3.9}$$

After some manipulations (3.7) can be replaced with the following equation

$$\left(\frac{d\bar{i}_s}{dt}\right)_k = \frac{1}{L_t}\left[\bar{u}_{s,k} - \left(R_s + R_{rs}\frac{L_t+L_\varphi}{L_\varphi}\right)\bar{i}_{s,k} + \frac{R_{rs}}{L_\varphi}\bar{\psi}_{s,k} - j\omega_{me,k}(\bar{\psi}_{s,k} - L_t\bar{i}_{s,k})\right] \tag{3.10}$$

Equations (3.6) and (3.10) constitute the state model that describes the electrical dynamics of the motor.
It is worth noticing that derivative of the stator current is composed by two contributions, the first of which

$$\left(\frac{d\bar{i}_s}{dt}\right)_k^{(u)} = \frac{1}{L_t}\left[\bar{u}_{s,k} - \left(R_s + R_{rs}\frac{L_t+L_\varphi}{L_\varphi}\right)\bar{i}_{s,k} + \frac{R_{rs}}{L_\varphi}\bar{\psi}_{s,k}\right] \tag{3.11}$$

depends on the applied voltage at interval k-th but it is independent of the speed, while the second one

$$\left(\frac{d\bar{i}_s}{dt}\right)_k^{(\omega)} = -\frac{1}{L_t}\left[j\omega_{me,k}(\bar{\psi}_{s,k} - L_t\bar{i}_{s,k})\right] \tag{3.12}$$

contains the k-th sample of speed but not the voltage.

Motor torque can be then expressed by

$$m_k = 1.5\, p\, \mathrm{Im}(\breve{\psi}_{s,k}\, \bar{i}_{s,k}) \tag{3.13}$$

where accent ˘ is for complex conjugate. From (3.13) the derivative for the torque results as

$$\left(\frac{dm}{dt}\right)_k = 1.5\, p\, \mathrm{Im}\left(\frac{d\breve{\psi}_{s,k}}{dt}\bar{i}_{s,k} + \breve{\psi}_{s,k}\frac{d\bar{i}_{s,k}}{dt}\right) \tag{3.14}$$

where derivatives in (3.14) are given by (3.6) and (3.10) in term of spatial voltage vector.

Similarly, from (3.6) the derivative for the flux module can be expressed in terms of spatial voltage vectors by:

$$\left(\frac{d|\psi_s|}{dt}\right)_k = \frac{1}{|\bar{\psi}_{s,k}|}(\psi_{\alpha s,k}u_{\alpha s,k} + \psi_{\beta s,k}u_{\beta s,k} - R_s(\psi_{\alpha s,k}i_{\alpha s,k} + \psi_{\beta s,k}i_{\beta s,k})) \tag{3.15}$$

Now all derivatives components for torque and flux following all possible spatial inverter voltage vectors can be estimated and then implemented in terms of the convergence condition (3.5).

3.4 Digital Implementation

The digital implementation of the proposed control has to consider its discrete time behavior so that while the system is running subjected to certain variables (current, voltages …), then the control algorithm performs its calculations. Therefore, results of any calculation can be used not before the next control cycle. In addition, the predictive feature of the control can allow future sampled values to be predicted every time they are required in performing the numerical computation of the currents and/or voltages that will affect the system in the next sampling time. To explain better the approach, let us suppose that the drive is running in interval k-th from sampling time kT_s to time $(k+1)T_s$, supplied by voltage $\bar{u}_{s,k}$. The algorithm is divided in two steps.

3.4.1 Prediction step

The predicted values at instant (k+1) of the motor stator flux and current can be derived by applying (3.6) and (3.10) resulting in:

$$\tilde{\bar{\psi}}_{s,k+1} = \bar{\psi}_{s,k} + T_s\left(\frac{d\bar{\psi}_s}{dt}\right)_k \tag{3.16}$$

$$\tilde{\bar{i}}_{s,k+1} = \bar{i}_{s,k} + T_s\left(\frac{d\bar{i}_s}{dt}\right)_k$$

where accent ~ is for predicted values.
Using (3.13), the torque at instant (k+1) is also predicted, and then the errors is calculated by (3.2) and eventually (3.3) can be applied.

3.4.2 Voltage selection step

If the predicted error $|\tilde{e}_{k+1}|$ is greater than E_{max}, then the control will have to identify a new spatial vector $\bar{u}_{s,k+1}$ that will reduce the error in the next step. To define that, the algorithm predicts the value of Λ_{k+1} by means of (3.5) (where the derivatives are obtained applying (3.6), (3.10), (3.14) and (3.15) in (k+1)) for each of the base spatial vectors provided by the inverter:

$$\tilde{\Lambda}^i_{k+1} = \left[\tilde{e}_{m,k+1}\left(\frac{d\tilde{e}_m}{dt}\right)_{k+1} + w_f\tilde{e}_{|\bar{\psi}_s|_{k+1}}\left(\frac{d\tilde{e}_{|\bar{\psi}_s|}}{dt}\right)_{k+1}\right]^i \tag{3.17}$$

being i=0,…,7 the voltage vector index (i=0 and 7 return the null voltage vectors).

Among all the voltage vectors, the control will choose the one that minimizes the value of $\tilde{\Lambda}^i_{k+1}$, i.e. determines its higher negative value, and it will apply it to the machine in the next step.
The implementation described here follows step by step the procedure described in Sect. 3.2.

3.5 Sensorless technique (first solution)

As described above, the drive control uses information on the motor speed. In this Section the attempt of replacing the speed measurement by a speed estimate or by removing the speed need, and thus realizing a sensorless drive, is discussed. One can easily realize that speed is used for both the feedback of the speed loop and the DTC algorithm. The two scopes have different requirements of precision and dynamics and then the speed estimate could be done with different approaches. The first approach to be used is based on MRAS observer , and then the two scopes are analysed as follows:

3.5.1 Speed loop

For the speed loop, an MRAS observer is proposed. In an MRAS, rotor flux vector is estimated in a reference model, which is independent of speed, and then compared with the one estimated by using an adaptive model, which uses speed as a parameter. The reference $^{(1)}$ and adaptive $^{(2)}$ model are obtained by rearranging the equations in Sect 3.3. An error derived from the difference between the two estimated vectors is used to feed a PI controller as shown in Figure 3.3.

The output of the controller is used to tune the adaptive model. The tuning signal actuates the rotor speed, which makes the error signal zero [58]. The adaptation mechanism of MRAS could be a simple gain or a PI controller as used here:

$$\tilde{\omega}_{me} = k_P \varepsilon + k_I \int \varepsilon dt \tag{3.18}$$

where input ε of the PI controller is:

$$\varepsilon = \psi_{\beta r}^{(1)} \psi_{\alpha r}^{(2)} - \psi_{\alpha r}^{(1)} \psi_{\beta r}^{(2)} \tag{3.19}$$

Equation for the Reference model is expressed as follows:

$$\frac{d\bar{\psi}_r^{(1)}}{dt} = \frac{L_r}{L_M}\left[\bar{u}_s - (R_s \bar{i}_s + \sigma L_s \frac{d\bar{i}_s}{dt})\right] \tag{3.20}$$

while that describing the Adaptive model is

$$\frac{d\bar{\psi}_r^{(2)}}{dt} = -\frac{R_r}{L_r}\bar{\psi}_r^{(2)} + j\omega_{me,k}\bar{\psi}_r^{(2)} + \frac{L_M R_r}{L_r}\bar{i}_s \tag{3.21}$$

The approach here described for the speed estimation is well known together with its limits and merits.

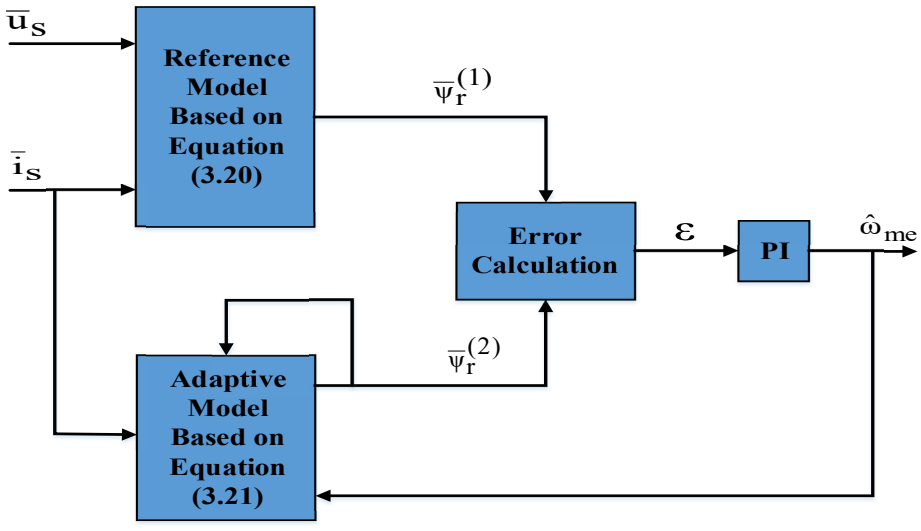

Figure 3.3: Block diagram of MRAS observer

3.5.2 DTC algorithm

The proposed Direct Torque Control uses, in principle, speed information for both the Prediction step and the Voltage selection step. Hereafter the two steps are discussed from this point of view.

3.5.2.1 Prediction step

Speed sample $\omega_{me,k}$ is required for stator current prediction as the derivative (3.10) contains a part dependent on the speed (see (3.12)). On the contrary, no speed information is involved in the flux prediction.
As a first solution speed estimation carried out by the MRAS algorithm for closing the speed loop can be exploited for the prediction step too and simulation and experimental results presented in Figures 3.5, 3.6, 3.7, 3.8, 3.12, 3.13, 3.14 and 3.15 refer to this solution. However, an alternative speed estimation technique can be used as a second solution via exploiting the prediction step of the DTC algorithm and such an approach is described in Sect. 3.8.

3.5.2.2 Voltage selection step

The DTC control strategy does not have to compute a precise voltage vector but only to select the vector among the base voltage vector at the output of the inverter that satisfies at the best the convergence condition (3.5). Speed does not affect flux dynamics while it appear in the torque derivative that can be rewritten as

$$\left(\frac{dm}{dt}\right)_{k+1} = 1.5\ p\ \mathrm{Im}\left\{\left[\left(\frac{d\breve{\bar{\psi}}_s}{dt}\right)_{k+1}\bar{i}_{s,k+1} + \breve{\bar{\psi}}_{s,k+1}\left(\frac{d\bar{i}_s}{dt}\right)^{(u)}_{k+1}\right] + \left[\breve{\bar{\psi}}_{s,k+1}\left(\frac{d\bar{i}_s}{dt}\right)^{(\omega)}_{k+1}\right]\right\} \tag{3.22}$$

which contains a first term (in the first [ ] bracket) depending on the applied voltage at interval (k+1)-th (and then depending on voltage vector index i=0..7) but it is independent of the speed in $(k+1)T_s$, while the second one depends on the (k+1)-th sample of speed but not on the voltage.

The second term constitutes a bias in the computation of $\tilde{\Lambda}^i_{k+1}$ from (3.17), common and constant for each voltage vector index and then the speed does not affect the voltage selection based on the minimization of $\tilde{\Lambda}^i_{k+1}$ and can be omitted. This is analytically proved as follows:
The torque and flux derivatives can be written as

$$\left(\frac{dm}{dt}\right)_{k+1} = 1.5\ p\ \mathrm{Im}\left[\left(\frac{d\breve{\bar{\psi}}_s}{dt}\right)_{k+1}\bar{i}_{s,k+1} + \breve{\bar{\psi}}_{s,k+1}\left(\frac{d\bar{i}_s}{dt}\right)_{k+1}\right] \quad \text{, and}$$

$$\left(\frac{d\bar{\psi}_s}{dt}\right)_{k+1} = \frac{1}{|\bar{\psi}_{s,k+1}|}\ \mathrm{Re}\left[\left(\frac{d\bar{\psi}_s}{dt}\right)_{k+1}\breve{\bar{\psi}}_{s,k+1}\right] \tag{3.23}$$

The convergence condition given by (3.5) can be rewritten as

$$\Lambda'_{k+1} = (m^* - m_{k+1})\left(\frac{dm'}{dt}\right)_{k+1} + \rho(\psi^* - |\bar{\psi}_s|_{k+1})\left(\frac{d\bar{\psi}_s}{dt}\right)_{k+1} > 0 \tag{3.24}$$

where $\rho = \frac{w_f}{(1.5\ p)^2}\frac{M_n^2}{\Psi_n^2}$, and

$$\left(\frac{dm'}{dt}\right)_{k+1} = \mathrm{Im}\left[(\breve{u}_{s,k+1} - R_s\breve{i}_{s,k+1})\bar{i}_{s,k+1} + \breve{\bar{\psi}}_{s,k+1}\left(\frac{d\bar{i}_s}{dt}\right)_{k+1}\right]$$

$$\left(\frac{dm'}{dt}\right)_{k+1} = \mathrm{Im}\left[\breve{u}_{s,k+1}\bar{i}_{s,k+1} + \breve{\bar{\psi}}_{s,k+1}\left(\frac{d\bar{i}_s}{dt}\right)_{k+1}\right] \tag{3.25}$$

The current derivative is given by (3.10), then after substitution and abbreviations the torque derivative can be written as

$$\frac{dm'}{dt} = \mathrm{Im}\left[\bar{u}_{s,k+1}\left(\frac{\breve{\psi}_{s,k+1}}{L_t} - \breve{\imath}_{s,k+1}\right)\right] + \mathrm{Im}\left[-\frac{R}{L_t}\breve{\psi}_{s,k+1}\bar{\imath}_{s,k+1} + j\omega_{me,k+1}\bar{\psi}_{s,k+1}\left(\frac{\breve{\psi}_{s,k+1}}{L_t} - \breve{\imath}_{s,k+1}\right)\right] \quad (3.26)$$

From (3.26), we get two terms,

$$A(\bar{u}_s) = \mathrm{Im}\left[\bar{u}_{s,k+1}\left(\frac{\breve{\psi}_{s,k+1}}{L_t} - \breve{\imath}_{s,k+1}\right)\right], \text{ and}$$

$$B = \omega_{me,k+1}\frac{\bar{\psi}^2{}_{s,k+1}}{L_t} - \mathrm{Im}\left[\frac{R}{L_t}\breve{\psi}_{s,k+1}\bar{\imath}_{s,k+1} + j\omega_{me,k+1}\bar{\psi}_{s,k+1}\breve{\imath}_{s,k+1}\right] \quad (3.27)$$

Where $R = R_s + R_{rs}\frac{L_t + L_\varphi}{L_\varphi}$.

From (3.23), the flux derivative can be rewritten as

$$\left(\frac{d\bar{\psi}_s}{dt}\right)_{k+1} = \frac{1}{|\bar{\psi}_{s,k+1}|}\,\mathrm{Re}\left[\left(\bar{u}_{s,k+1} - R_s\bar{\imath}_{s,k+1}\right)\breve{\psi}_{s,k+1}\right] \quad (3.28)$$

From (3.28), we get another two terms,

$$C(\bar{u}_s) = \mathrm{Re}\left[\bar{u}_{s,k+1}\breve{\psi}_{s,k+1}\right], \text{ and } D = -\mathrm{Re}\left[R_s\bar{\imath}_{s,k+1}\breve{\psi}_{s,k+1}\right] \quad (3.29)$$

From (3.24), (3.27) and (3.29), the convergence condition can be summarized as follows,

$$e_{m,k+1}A(\bar{u}_s) + \frac{\rho e_{|\bar{\psi}_s|,k+1}}{|\bar{\psi}_{s,k+1}|}C(\bar{u}_s) > -\left(e_{m,k+1}B + \frac{\rho e_{|\bar{\psi}_s|,k+1}}{|\bar{\psi}_{s,k+1}|}D\right) \quad (3.30)$$

So if more than one voltage vector $\bar{u}_s$ satisfies (3.30), then $\bar{u}_{s,optimal}$ is the first vector that produces the maximum value of the convergence condition. Maximum does not depend on ω_{me} and only slightly on $\bar{\imath}_s$.

The overall proposed control scheme is therefore that shown in Figure 3.4. The three phase two level Voltage Source Inverter (VSI) is represented by a Zero-Order Hold (ZOH) block that is used for converting the discrete time signals to continuous time signals needed by the drive. A sample and hold (S/H) block is referring to the sampling (capturing) of a continuously varying signal (i.e. stator current) and holds (freeze) its value at a constant level for a specified minimum period in order to achieve an accurate measurement. Speed loop and prediction block are both utilizing the estimated speed; torque reference is obtained through a speed controller (PI), while flux reference is imposed as a constant value.

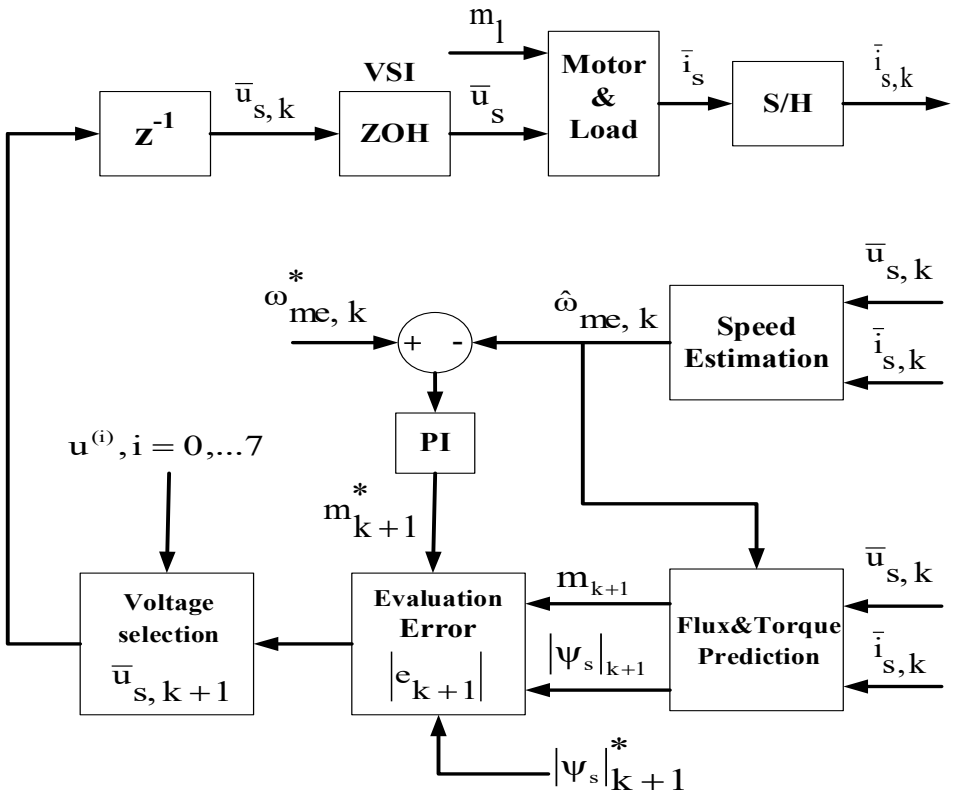

Figure 3.4: Proposed DTC scheme

3.6 Simulation verification

Matlab/Simulink environment is used firstly to validate the proposed MP DTC approach, the tests are carried out for both high speed and low speed ranges to investigate the performance of the drive at different operating conditions as follows:

3.6.1 High speed range

The dynamic performance of the drive is tested for a given speed commands of (1400→1800 RPM) at times of (0.05→2 sec), the predefined absolute value of error limit E_{max} is maintained at 0.1, a load torque of 3.0 Nm is applied at time of t=1 sec. The reference value of stator flux is kept at 0.5 Vs, as can be shown from Figure 3.5; the results confirm the effectiveness of the proposed control system. In addition, the MRAS sensorless technique exhibits an appropriate performance; this can be clearly viewed through the speed profile change and rotor position figures. The response of the control is illustrated clearly through Figure 3.6 that presents the waveforms of error, cost function voltage index and rotor position. The last three figures report that when the absolute value of the estimated error $|\bar{e}|$ exceeds maximum value E_{max} (used for limiting switching frequency), instantaneously ; the control estimates the value of cost function, determines its minimum value and switches to the voltage index responsible for that. The parameters of the machine and control data specifications are given in appendix B.

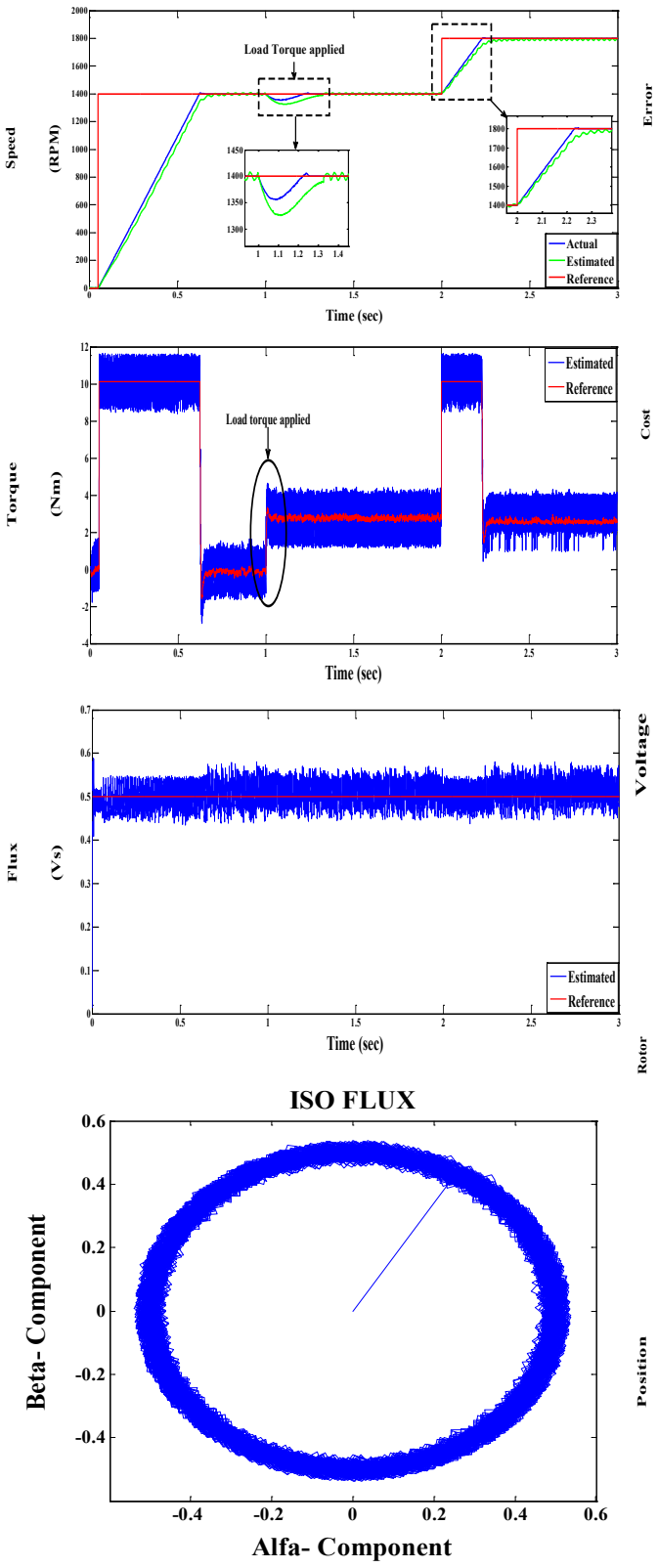

Figure 3.5: Simulation results at high speed

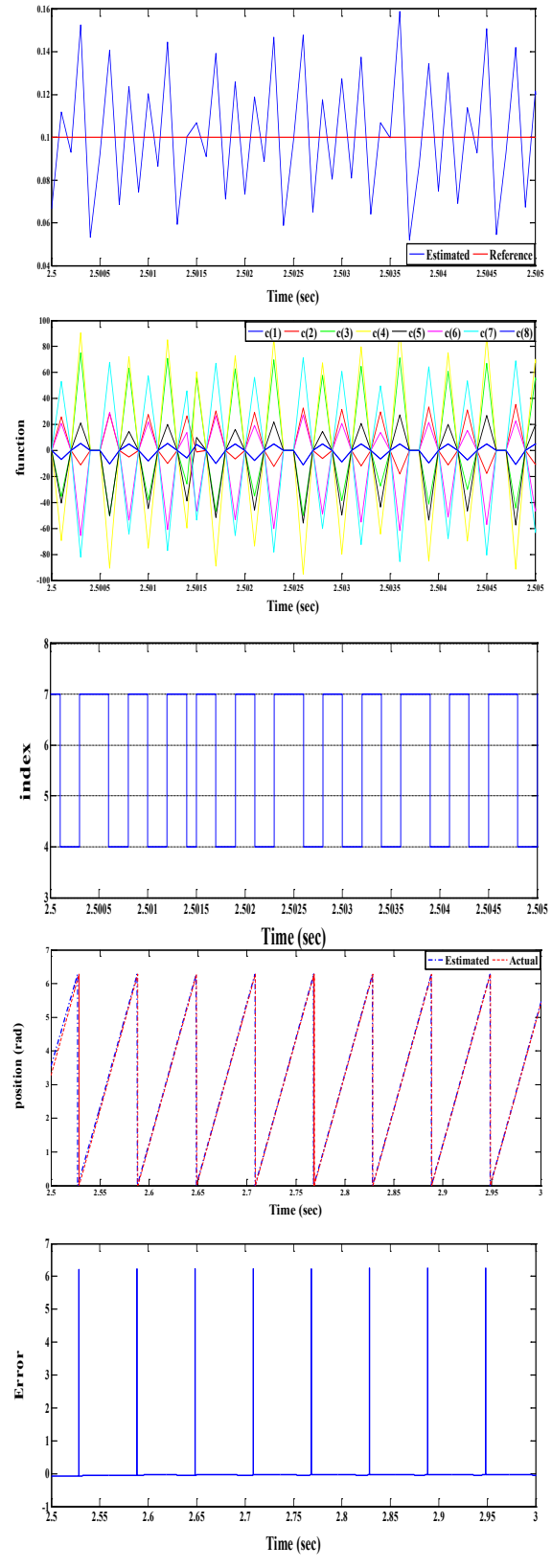

Figure 3.6: Control response

3.6.2 Low speed range

The drive performance is verified at low speed range, the speed command profile is defined as (800 → 50 RPM), at times of (0.05 →1 sec). A load torque of two Nm is applied at starting. The flux reference is held to 0.3 Vs, while the maximum error value E_{max} is kept at 0.1. Shown results in Figures 3.7 and 3.8 assure the validity of proposed control procedure even at very low speed ranges, this is clarified via fast and precise transient dynamic response for the changes in speed profile.

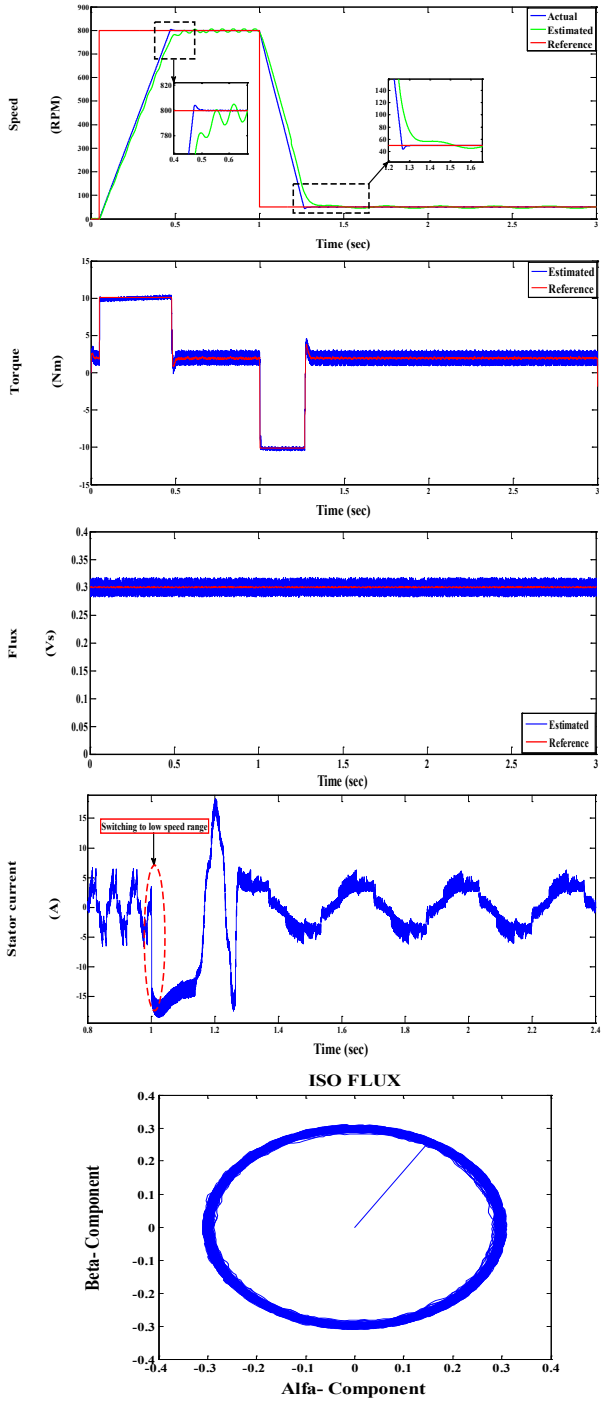

Figure 3.7: Simulation results at low speed

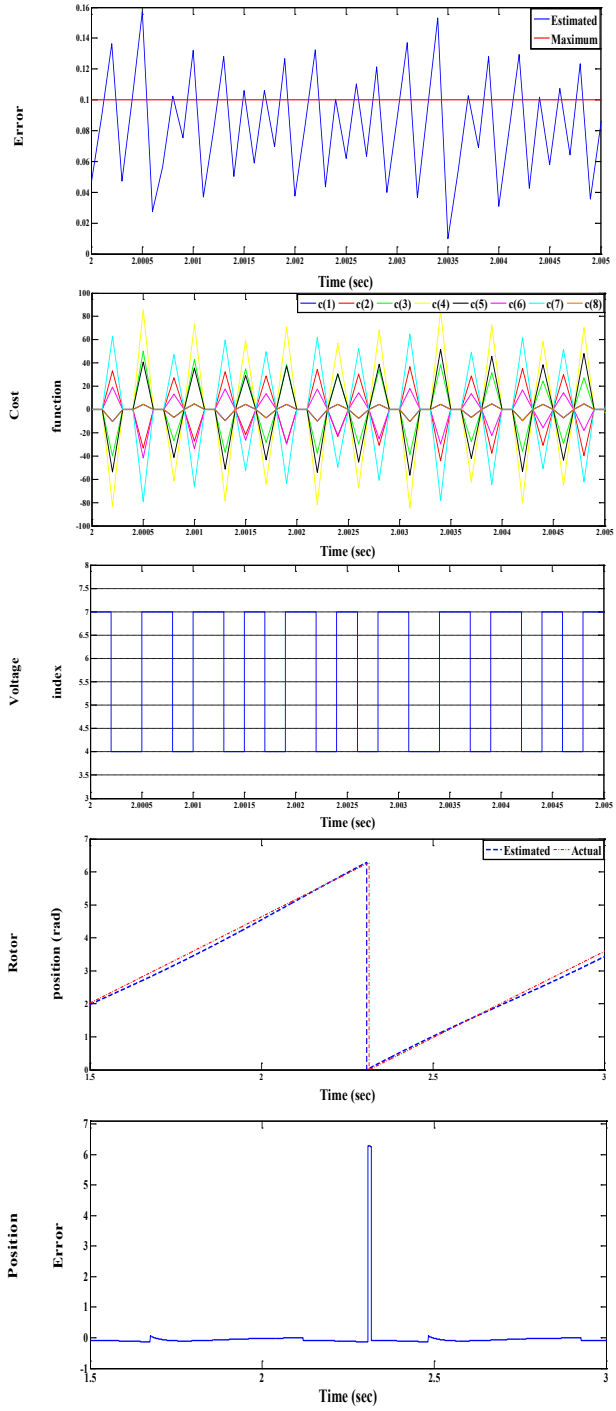

Figure 3.8: Behavior of control

3.7 Experimental validation

The drive of Figure 3.4 has been tested experimentally using dSpace 1104 fast control prototyping board that provides to the inverter the six commands for the six switches opening and closing. Overview of the test bench is illustrated through Figure 3.9.

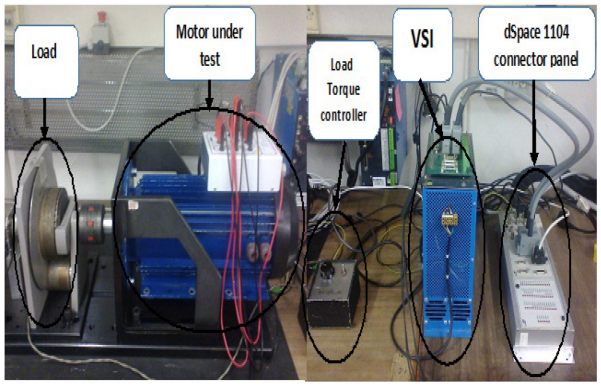

Figure 3.9: Test bench overview

The command updating sequence used for the dSpace board is illustrated through Figure 3.10, which can be described in details as follows:

The new duty cycle values are calculated inside the interrupt service routine on the master PPC (ISR–PPC). The interrupt service routine is triggered by the PWM interrupt (ST1PWM signal). The PPC transfers the values to the slave DSP, which stores them in global variables [59]. In the middle of the switching period, an interrupt is triggered on the slave DSP that starts a routine (ISR-DSP) for copying the calculated values from the global variables to the compare registers of the PWM unit. The duty cycle is updated with the values from the compare register, if the Timer has reached the next zero point. Then, the duty cycle is updated for the next PWM period if the new values are stored on the slave DSP before the slave DSP interrupt has been triggered. Otherwise, the duty cycles are updated with a second next PWM period. This fact is important in the specific laboratory HW used for the experimental validation, because the DTC control code required a lot of computation time and then the new values of duty cycles are updated after two PWM periods. Consequently, the control, described in Sect. 3.4, has to be modified. The flux and current predictions of one-step are not enough, but they must be extended to the next step predicting the values $\bar{\imath}_{s,k+2}$, $\bar{\psi}_{s,k+2}$ and, from them, all the other quantities (2-step prediction block). Finally, the error $\bar{e}_{(k+2)}$ is predicted and, accordingly, $\bar{u}_{s,k+2}$ is selected.

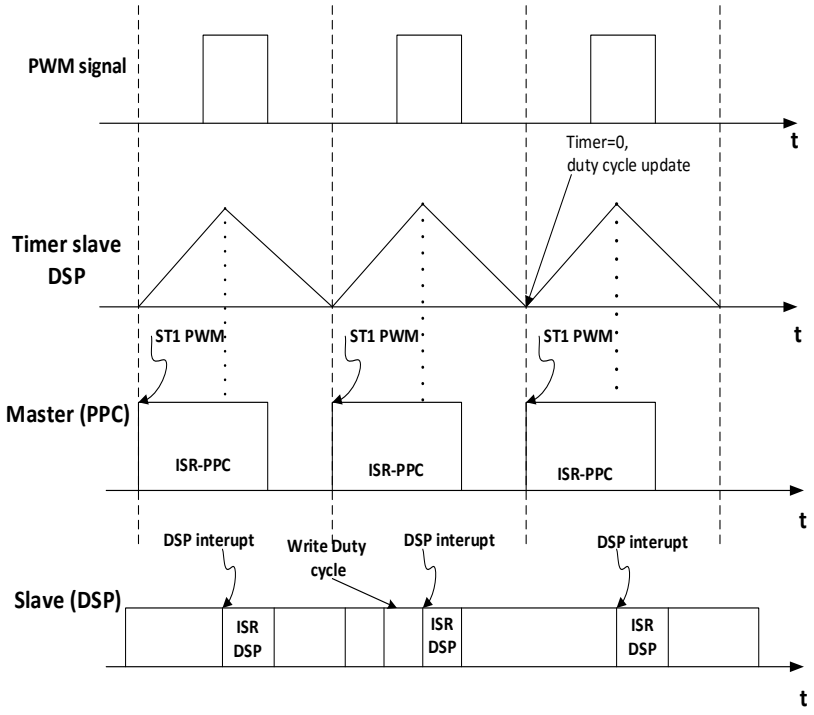

Figure 3.10: PWM duty cycles updating procedure

3.7.1 Tests with PWM vectors graph

Figure 3.11 shows the switch state graph that can be adopted, in addition to the usage of E_{max}, for limiting the frequency of the inverter switch commutation [60]. Table 3.1 reports the comparison of some key control performance figures for different implementation variants: with 2-step prediction combined with or without switch state graph. Comparison is expressed in term of average error at the switching instant and number of commutation (N_{com}) of a–phase during 1 sec. It can be deduced that 2–step prediction reduce the amplitude of the exceeded average error, while the use of the switch state graph decreases the number of commutation (as expected) but increases the average error impeding some time the selection of the best voltage vector.

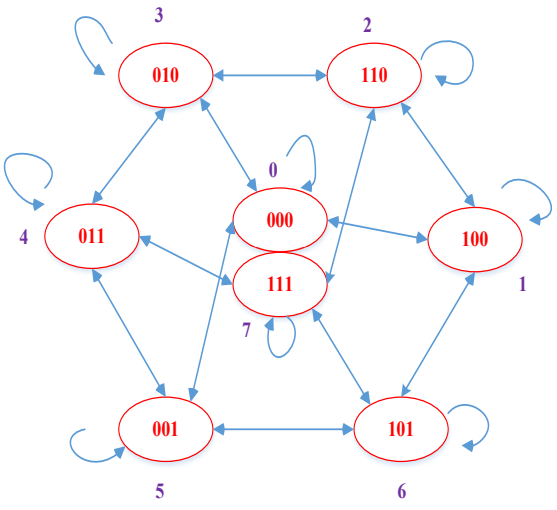

Figure 3.11: Switch state graph

TABLE 3.1
Performance comparison among different control procedures: with and without switch state graph

Range	With prediction, without graph			With prediction, with graph		
	Error	N_{com}	F_{sw}	Error	N_{com}	F_{sw}
High speed	0.1104	3014	502 Hz	0.1315	2654	442 Hz
Low speed	0.08803	3727	621 Hz	0.0983	2213	369 Hz

3.7.2 Results for high speed range

The drive performance is experimentally tested for a given speed profile of (1400→ 1800 RPM) at times of (0→ 3 sec), flux reference value is held to 0.5 Vs, while a load torque of 1.5 Nm is applied at t=0.5 sec. The maximum value of permissible error is kept at 0.1 , Figure 3.12 shows the dynamic behavior of the drive from which the effectiveness of proposed controller is confirmed, while Figure 3.13 gives a concentrated analysis for the action taken by the control system , the results assure also the proper performance for sensorless MRAS technique.

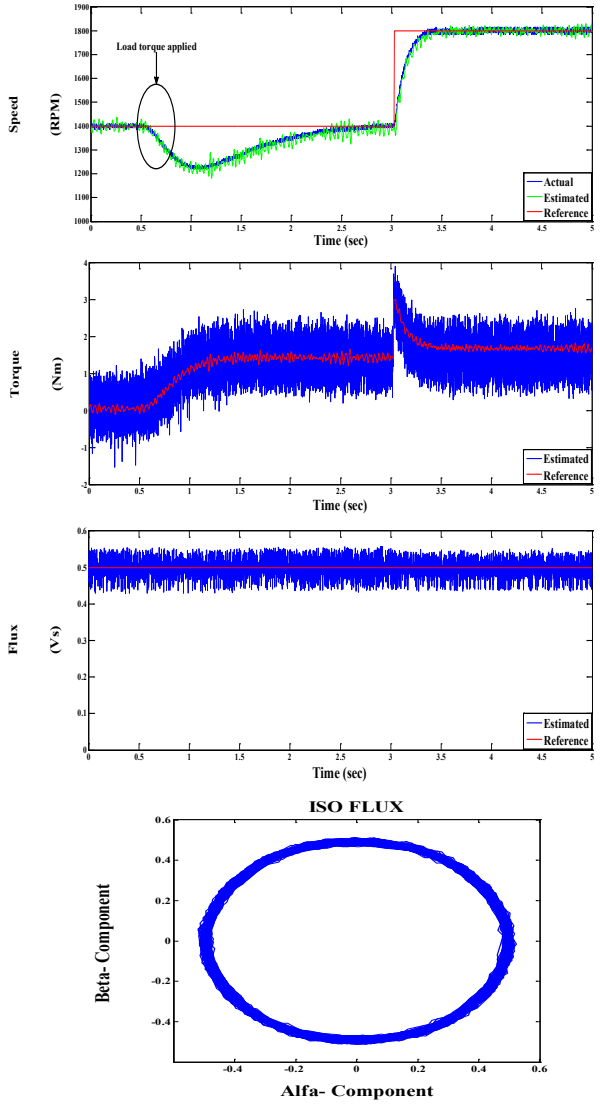

Figure 3.12: Experimental results at high speed

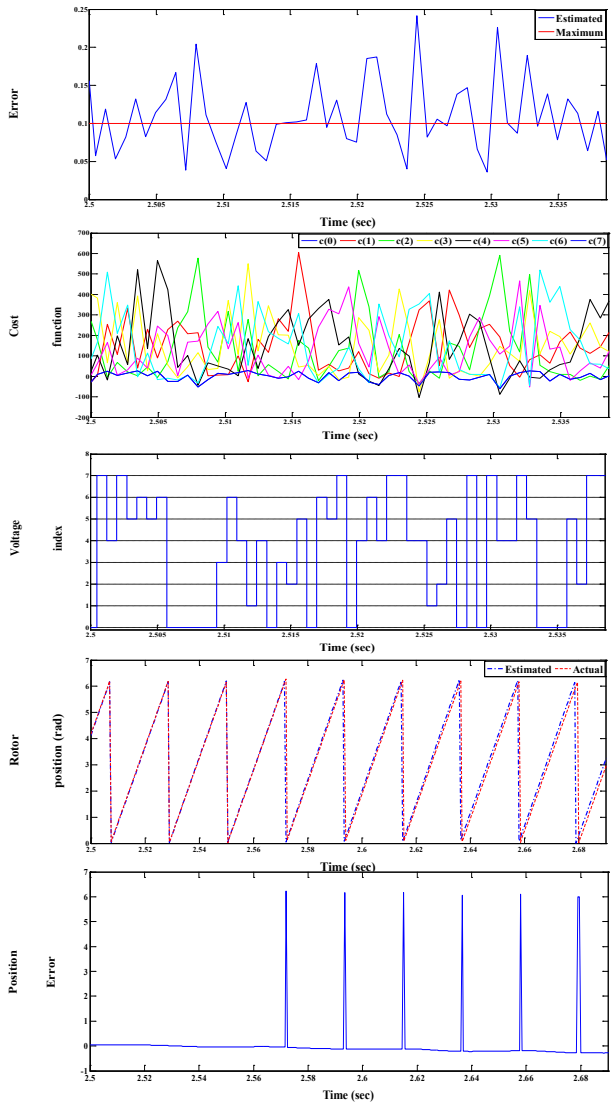

Figure 3.13: Control response

3.7.3 Results for low speed range

To confirm the viability of proposed sensorless control system, the drive performance is tested for low speed range, in which the drive is driven at speed profile of (800 → 50 RPM), at times of (zero → 0.5 sec). A load torque of two Nm is applied at starting, a flux reference of a value of 0.3 Vs is applied, and the error limit is set to 0.1. It can be shown that the sensorless algorithm presents proper behavior at very low speed range; this can be noticed from the speed and rotor position profiles. Figures 3.14 and 3.15 show the dynamic response for the drive and control response, respectively.

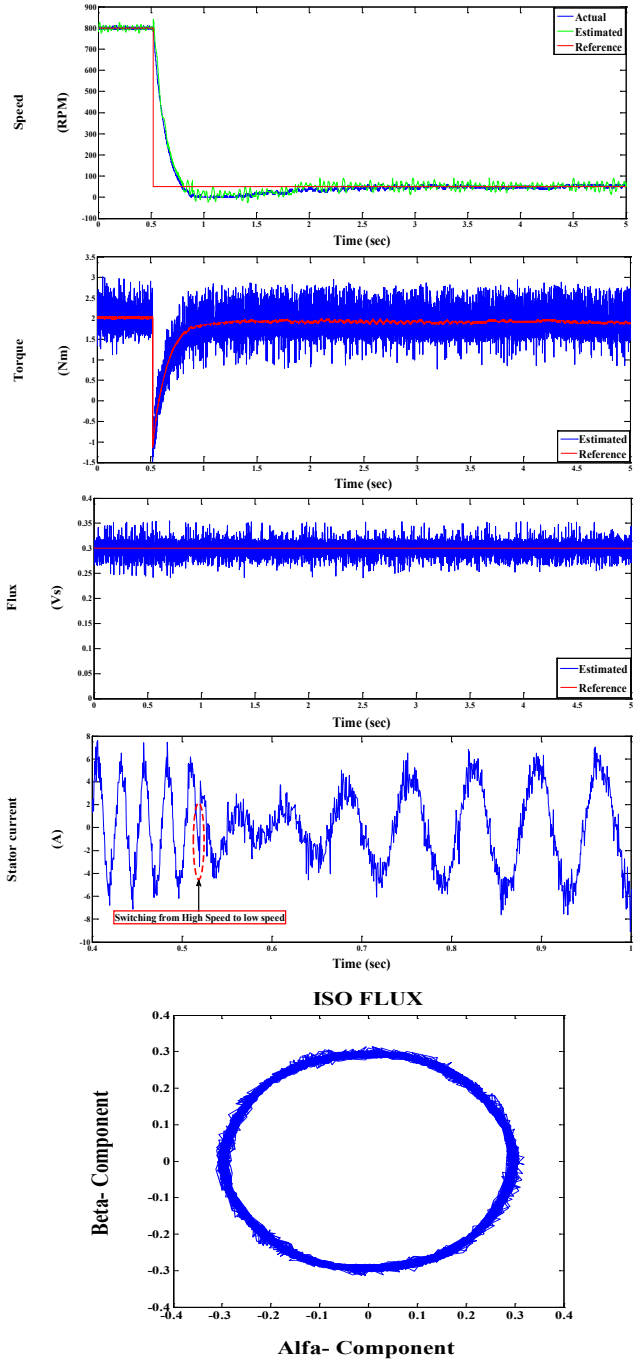

Figure 3.14: Experimental results at low speed

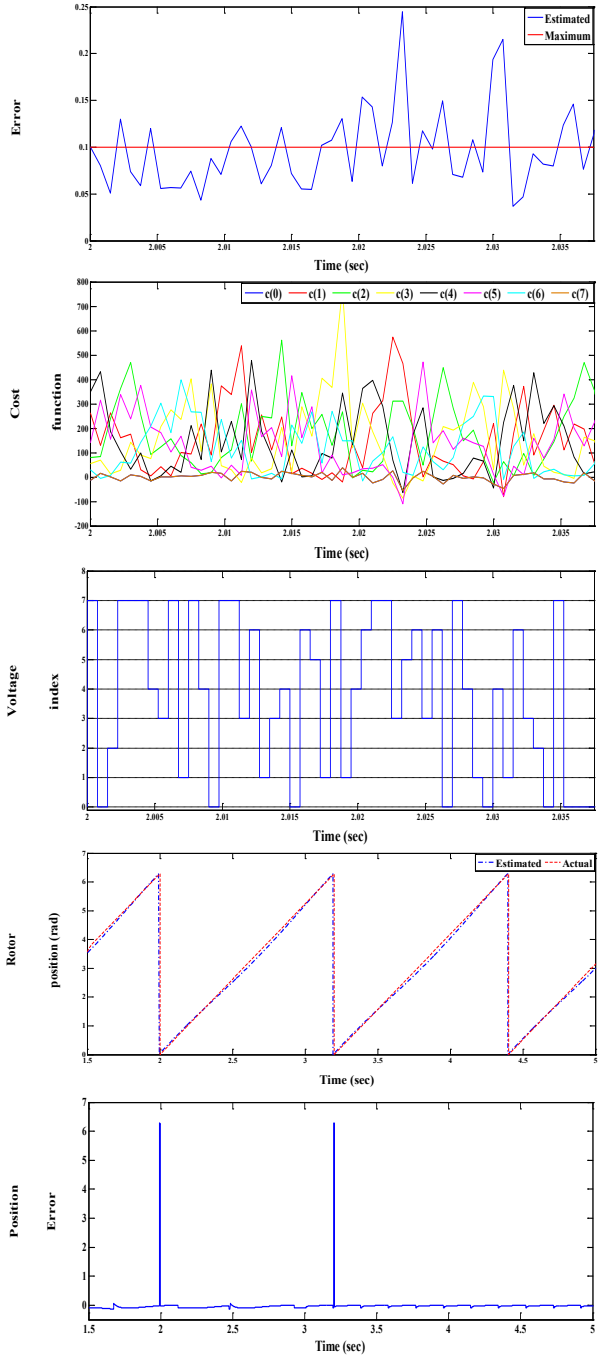

Figure 3.15: Analysis of control action

3.8 Sensorless technique (second solution)

As an alternative solution for speed estimation, the predictive nature of proposed MP DTC algorithm can be utilized to achieve this task. To explain this procedure, let's suppose that the drive is running in the sampling interval between kT_s and $(k+1)T_s$ (the current interval), let us consider the sampling interval between $(k-1)T_s$ and kT_s (the last completed interval). Both instants $(k-1)T_s$ and kT_s belong to the past as shown in Figure 3.16.

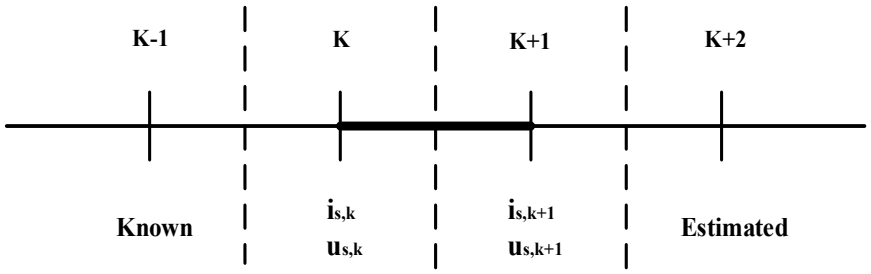

Figure 3.16: Control algorithm sampling intervals

The current in kT_s follows the

$$\bar{\imath}_{s,k} = \bar{\imath}_{s,k-1} + T_s\left(\frac{d\bar{\imath}_s}{dt}\right)_{k-1} = \bar{\imath}_{s,k-1} + T_s\left(\frac{d\bar{\imath}_s}{dt}\right)_{k-1}^{(u)} + T_s\left(\frac{d\bar{\imath}_s}{dt}\right)_{k-1}^{(\omega)} \tag{3.31}$$

where

$$\left(\frac{d\bar{\imath}_s}{dt}\right)_{k-1}^{(u)} = \frac{1}{L_t}\left[\bar{u}_{s,k-1} - \left(R_s + R_{rs}\frac{L_t+L_\varphi}{L_\varphi}\right)\bar{\imath}_{s,k-1} + \frac{R_{rs}}{L_\varphi}\bar{\psi}_{s,k-1}\right] \tag{3.32}$$

and

$$\left(\frac{d\bar{\imath}_s}{dt}\right)_{k-1}^{(\omega)} = -\frac{1}{L_t}\left[j\omega_{me,k-1}(\bar{\psi}_{s,k-1} - L_t\bar{\imath}_{s,k-1})\right] \tag{3.33}$$

Just after kT_s we have the availability of the measured $\bar{\imath}_{s,k}$ and $\bar{\imath}_{s,k-1}$. Therefore we can write:

$$\bar{\imath}_{s,k} - \bar{\imath}_{s,k-1} - T_s\left(\frac{d\bar{\imath}_s}{dt}\right)_{k-1}^{(u)} = T_s\left(\frac{d\bar{\imath}_s}{dt}\right)_{k-1}^{(\omega)} \tag{3.34}$$

and then, from (3.32)

$$\omega_{me,k-1} = jL_t\frac{\bar{\imath}_{s,k} - \bar{\imath}_{s,k-1} - T_s\left(\frac{d\bar{\imath}_s}{dt}\right)_{k-1}^{(u)}}{T_s(\bar{\psi}_{s,k-1} - L_t\bar{\imath}_{s,k-1})} \tag{3.35}$$

that should result in a real number. The latter can be computed better by

$$\omega_{me,k-1} = -L_t\,\mathrm{Im}\left[\frac{\left(\bar{\imath}_{s,k} - \bar{\imath}_{s,k-1} - T_s\left(\frac{d\bar{\imath}_s}{dt}\right)_{k-1}^{(u)}\right)\mathrm{conj}(\bar{\psi}_{s,k-1} - L_t\bar{\imath}_{s,k-1})}{T_s(\bar{\psi}_{s,k-1} - L_t\bar{\imath}_{s,k-1})\,\mathrm{conj}(\bar{\psi}_{s,k-1} - L_t\bar{\imath}_{s,k-1})}\right] \tag{3.36}$$

All quantities in (3.35) and (3.36) are measured or are computed starting from measurements at previous sampling instant (k-1), and thus no predicted quantity is used during the estimation process.
For the elaboration to be performed in interval k (in order to predict quantities in k+1) we need $\omega_{me,k}$ which is not yet available. The latter can be estimated by assuming the same acceleration in intervals (k-2) and (k-1) equal to

$$\alpha = (\omega_{me,k-1} - \omega_{me,k-2})/T_s \tag{3.37}$$

Then,
$$\omega_{me,k} = \omega_{me,k-1} + \alpha\, T_s = 2\omega_{me,k-1} - \omega_{me,k-2} \tag{3.38}$$

It is worth to notice that (3.38) is nothing but a linear extrapolation of the speed values starting from the last two estimated samples; thus $\omega_{me,k}$ can be acquired.

The proposed predictive scheme can be developed assuming torque and rotor flux as references [61]. In this way, the highest pullout torque is obtained and it is possible to combine the advantages of rotor flux orientation and stator flux control. The strategy adopted needs neither the rotor resistance of the machine nor the coordinate transformation based on the rotor flux position, leading to a high performance drive using a simple control scheme. From the IM equations in Sect. 3.3, the following expressions of the electromagnetic torque can be found at steady state as a function of either the rotor flux or the stator flux:

$$m_k = 1.5\, p\omega_{me,k} \frac{\bar{\psi}_{r,k}^2}{R_r} \tag{3.39}$$

$$m_k = 1.5\, p \left(\frac{L_M}{L_S}\right)^2 \omega_{me,k} R_r \frac{\bar{\psi}_{s,k}^2}{R_r^2 + \omega_{me,k}^2 (\sigma L_r)^2} \tag{3.40}$$

Note that (3.39) is valid also during transients. By (3.39)–(3.40), the torque characteristic of an IM under constant rotor flux operation increases linearly with $\omega_{me,k}$, and the maximum torque is constrained by the maximum current allowable for the inverter. On the contrary, the torque characteristic under constant stator flux operation exhibits a maximum value at an angular slip speed which depends on the machine parameters. the IM equations, written in a reference frame synchronous with the rotor flux and aligned with the d-axis, the space vector of the stator flux can be expressed as given in [62] by

$$m_k = \frac{L_s}{L_M}\left[(1 + s\sigma T_r)\bar{\psi}_{r,k} + j\frac{\sigma L_r}{\bar{\psi}_{r,k}}\frac{m_k}{1.5\, p}\right] \tag{3.41}$$

Its amplitude furnishes the reference for the stator flux amplitude needed by a DTC scheme, as a function of the rotor flux and torque references. Under constant rotor flux operation, it becomes

$$|\psi_{s,k}|^* = \sqrt{\left(\frac{L_s}{L_M}|\psi_{r,k}|^*\right)^2 + (\sigma L_s)^2 \left(\frac{L_r}{L_M}\frac{m_k^*}{1.5\, p|\psi_{r,k}|^*}\right)^2} \tag{3.42}$$

The IM drive is tested using (3.42) , acquired results prove the effectiveness of the proposed sensorless solution in obtaining a robust speed estimation. Through results (simulation and experimental), it can be noticed that the stator flux command variation is tracking the the change in torque command to achieve a robust operation of the DTC control system.The flowchart that explains the execution procedure for selecting the voltage vectors based on proposed technique is viewed through Figure 3.17.

Figures 3.18, 3.19 presents the simulation results, through which it can be noticed that the proposed sensorless procedure exhibits good performance for a wide speed range that is given as (1200 → 600 → 50 RPM) at times of (0.05 → 1 → 2 sec), the reference value of rotor flux is set to 0.3Vs, a load torque of two Nm

is applied at starting. The maximum error limit is taken as 0.1. It is noticed the variation in the estimated value for stator flux follows the variation in the reference torque. Also the stator flux locus shows the increase in flux magnitude required to maintain the rotor flux magnitude fixed to the commanded value.

Figures 3.20, 3.21 view the experimental results obtained for a speed profile change of (1200 → 600 → 50 RPM) at times of (0 → 1 → 3 sec), a load torque of two Nm is applied to the motor at starting, the reference of the rotor flux is the same use din simulation test, and the maximum error value is set also to the same one in simualtion (0.1). Experimental results assure the validity and feasibility of proposed sensorless control approach for a wide variation in speed commands.

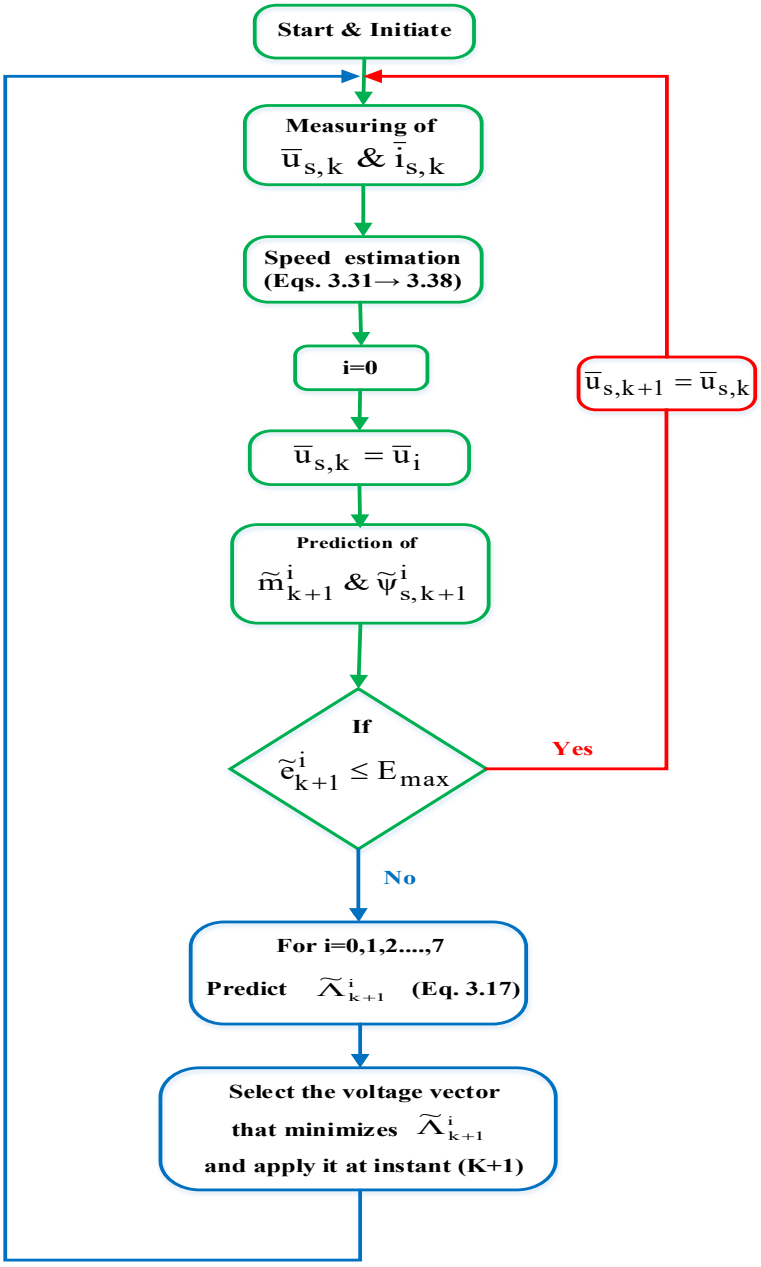

Figure 3.17: Voltage vector selection procedure

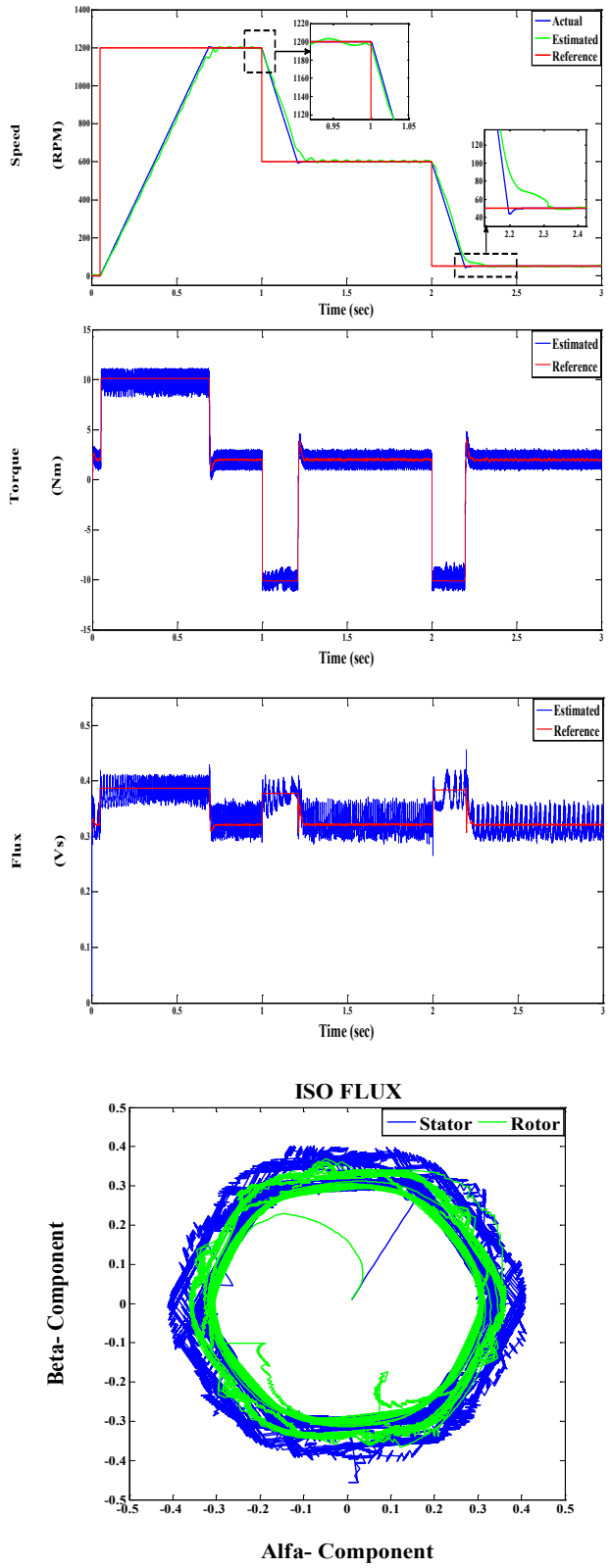

Figure 3.18: Simulation results for proposed procedure

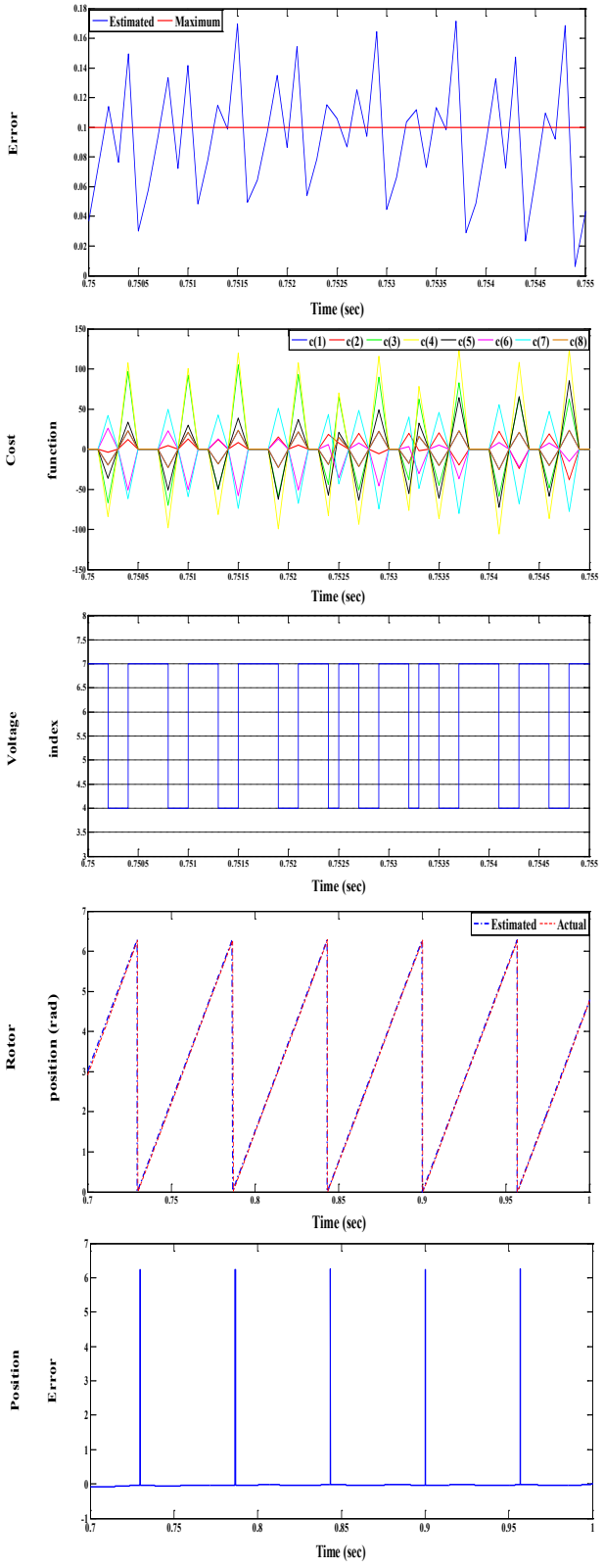

Figure 3.19: Control behavior analysis

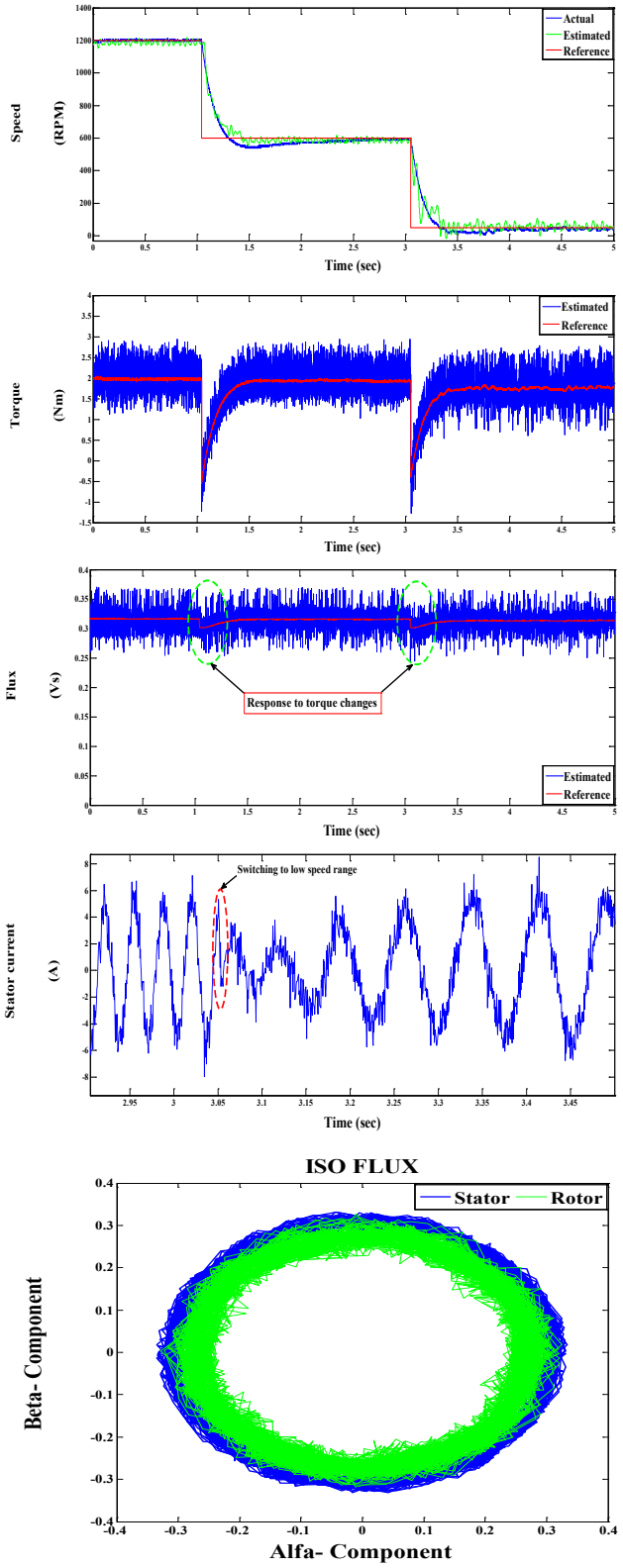

Figure 3.20: Experimental results for drive performance

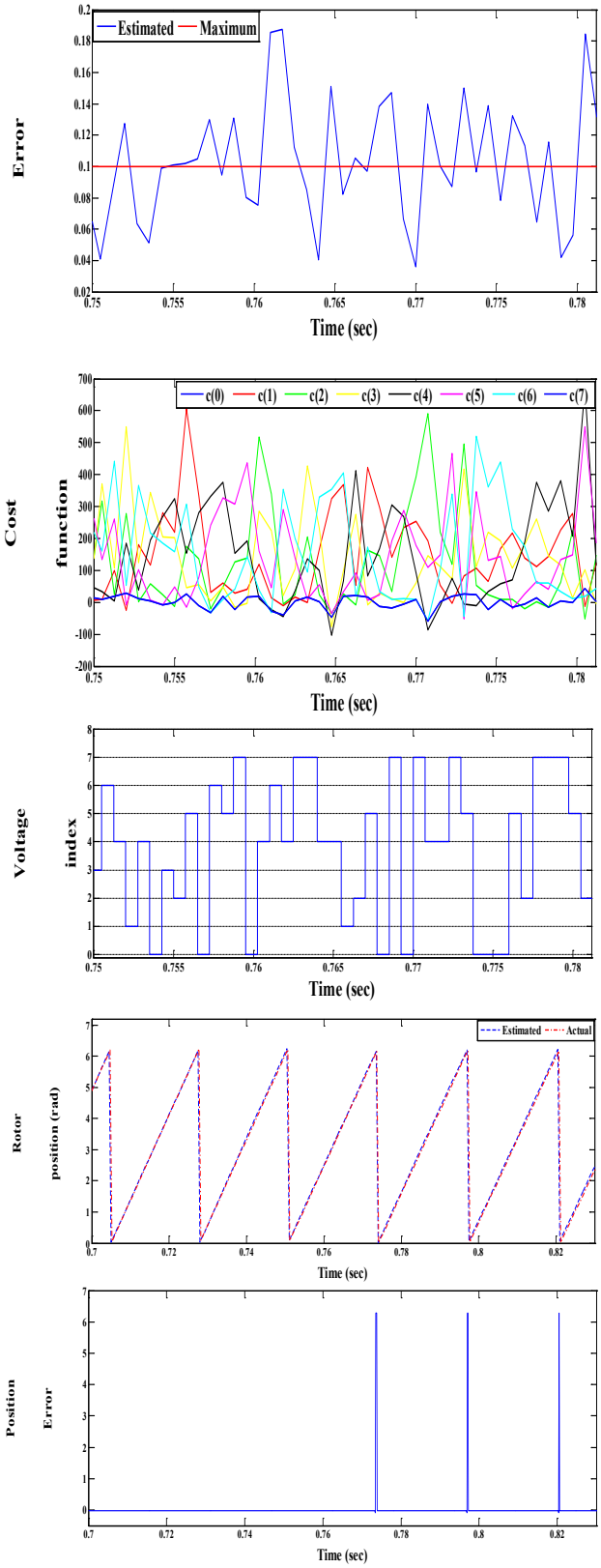

Figure 3.21: Control response

3.9 Utilization of reactive power as a control variable

The formulation of MP DTC given by (3.17) is reformed to utilize torque and reactive power flow through the IM as control variables. It utilizes and manages the reactive power (which provides the magnetic flux) of the machine rather than using the flux as a target value as managed in Sect. 3.2. The contributions of this technique are confirmed via simple implementation, robustness and limited dependency on knowledge of motor parameters, this due to the fact that reactive power is acquired directly through the measured variables (voltages and currents) without complicated post processing.

Figure 3.22 shows a basic layout of the proposed MP DTC scheme for the IM drive, the scheme is mostly the same as shown in Figure 3.4 except utilizing the reactive power instead of stator flux. The sensorless approach that is presented in Sect. 3.8 is used in this scheme for estimating the speed and rotor position.

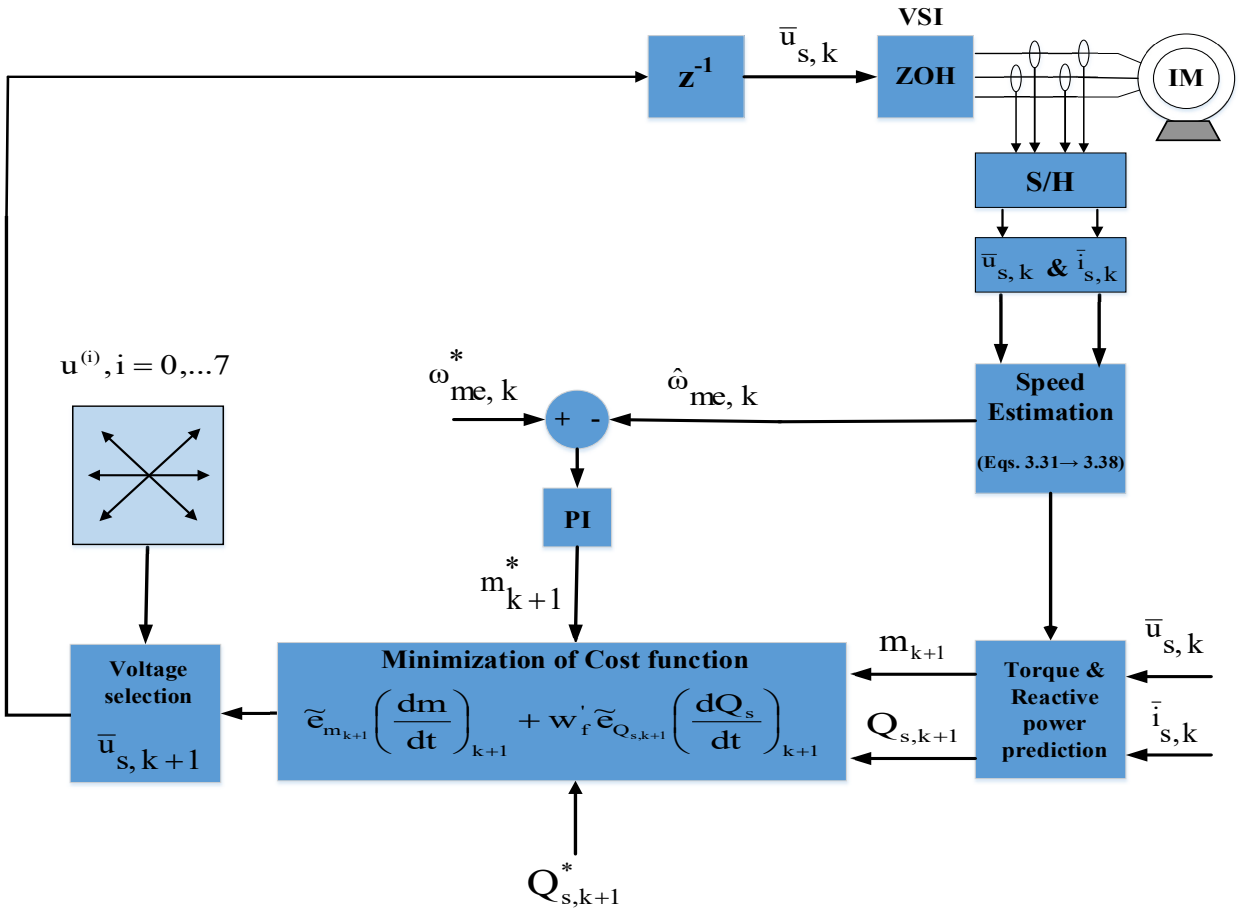

Figure 3.22: Complete system configuration for proposed MP DTC scheme

Torque reference is obtained through a speed controller (PI), while reactive power reference is given by the rated reactive power multiplied to the ratio of the actual angular frequency to the rated angular frequency. The weighting factor w'_f used in the cost function is selected offline in an arbitrary way.

3.9.1 Implementation procedure

The same procedure presented in Sect. 3.4 is used to implement the proposed scheme as follows:

3.9.1.1 Prediction step

The predicted value at instant (k+1) T_s of the motor torque can be derived using the relationships given in (3.13) and (3.14) as

$$\tilde{m}_{k+1} = m_k + T_s \left(\frac{dm}{dt}\right)_k \tag{3.44}$$

The reactive power of the motor can be expressed at instant kT_s by

$$Q_{s,k} = 1.5\ p\ \mathrm{Im}\left(\check{\imath}_{s,k}\ \bar{u}_{s,k}\right) \tag{3.45}$$

From (3.45) the derivative of reactive power can be computed by

$$\left(\frac{dQ}{dt}\right)_{s,k} = 1.5p\mathrm{Im}\left(\frac{d\check{\imath}_{s,k}}{dt}\bar{u}_{s,k} + \check{\imath}_{s,k}\frac{d\bar{u}_{s,k}}{dt}\right) \tag{3.46}$$

where current derivative in (3.46) is given by (3.6) and the voltage derivative is calculated by

$$\frac{d\bar{u}_{s,k}}{dt} = \frac{\bar{u}_{s,k} - \bar{u}_{s,k-1}}{T_s} \tag{3.47}$$

From (3.45 and 3.46) the predicted value of reactive power at instant $(k+1)T_s$ can be calculated by

$$\tilde{Q}_{s,k+1} = Q_{s,k} + T_s \left(\frac{dQ_s}{dt}\right)_k \tag{3.48}$$

3.9.1.2 Voltage selection step

In this stage, the control procedure predict the value of cost function at instant $(k+1)T_s$ using (3.49) which is calculated in terms of (3.14, 3.44, 3.46 and 3.48) which already given as functions of all spatial voltage vectors supplied by the inverter as following:

$$\tilde{\Lambda}^{i}_{k+1} = \left[\tilde{e}_{m,k+1}\left(\frac{d\tilde{e}_m}{dt}\right)_{k+1} + w'_f\tilde{e}_{Q_{s,k+1}}\left(\frac{d\tilde{e}_{Q_s}}{dt}\right)_{k+1}\right]^{i} \tag{3.49}$$

If the predicted error $|\bar{e}_{k+1}|$ crossovers the error limit Emax, then the control will choose, a suitable voltage vector $\bar{u}_{s,k+1}$ that will minimizes the value $\tilde{\Lambda}^{i}_{k+1}$ and consequently results in receding the error in the next step, this vector will be applied to the stator terminals in the next control cycle.
The reference value of the reactive power $Q^{*}_{s,k+1}$ is given by

$$Q^{*}_{s,k+1} = Q_{s,n}\frac{\omega_{s,k+1}}{\Omega_{s,rated}} \tag{3.50}$$

where
$$\omega_{s,k+1} = 2\pi f_s = \omega_{me,k+1} + \frac{\Omega_{sl,n}}{M_n}\, m_{k+1} \tag{3.51}$$

and $Q_{s,n}$, $\left(\Omega_{s,rated} = 2\pi f_{rated}\right)$, $\Omega_{sl,n}$ are the rated reactive power, rated angular frequency and rated angular slip, respectively.
The procedure of optimal voltage vectors selection is the same as viewed in Figure 3.17, except that the reactive power replaced the stator flux. It is worth to notice that the voltage selection is still does not depend on the speed sample and this can be verified analytically through the following relationships.
Speed contributes in the torque derivative calculation that can be rewritten as

$$\left(\frac{dm}{dt}\right)_{k+1} = 1.5\ p\ Im\left\{\left[\left(\frac{d\breve{\psi}_s}{dt}\right)_{k+1}\bar{\imath}_{s,k+1} + \breve{\psi}_{s,k+1}\left(\frac{d\bar{\imath}_s}{dt}\right)^{(u)}_{k+1}\right] + \left[\breve{\psi}_{s,k+1}\left(\frac{d\bar{\imath}_s}{dt}\right)^{(\omega)}_{k+1}\right]\right\} \tag{3.52}$$

which contains a first term (in the first [ ] bracket) depending on the applied voltage at instant (k+1)-th but it is independent of the speed in $(k+1)T_s$, while the second bracket relies on the (k+1)-th sample of speed but not on the voltage.

The two terms of torque derivative can be expressed by

$$A(\bar{u}_s) = 1.5\ p\ Im\left\{\left(\breve{u}_{s,k+1}\bar{\imath}_{s,k+1}\right) + \frac{1}{L_t}\left(\bar{u}_{s,k+1}\breve{\psi}_{s,k+1} - R\breve{\psi}_{s,k+1}\bar{\imath}_{s,k+1}\right)\right\} \tag{3.53.a}$$

and
$$B = 1.5\ p\ Im\left\{j\omega_{me,k+1}\breve{\psi}_{s,k+1}\bar{\imath}_{s,k+1}\right\} \tag{3.53.b}$$

In the same manner the reactive power derivative can be given by

$$\left(\frac{dQ}{dt}\right)_{s,k+1} = 1.5\ p\ Im\left\{\left[\bar{u}_{s,k+1}\left(\frac{d\breve{\imath}_s}{dt}\right)^{(u)}_{k+1}\right] + \left[\bar{u}_{s,k+1}\left(\frac{d\breve{\imath}_s}{dt}\right)^{(\omega)}_{k+1}\right] + \breve{\imath}_{s,k+1}\left(\frac{d\bar{u}_s}{dt}\right)_{k+1}\right\} \tag{3.54}$$

Utilizing (3.10), the reactive power derivative yields to

$$\begin{aligned}\left(\frac{dQ}{dt}\right)_{s,k+1} = \\ 1.5\ p\ Im\left\{\frac{1}{L_t}\left[-R\bar{u}_{s,k+1}\breve{\imath}_{s,k+1} + \frac{R_{rs}}{L_\varphi}\bar{u}_{s,k+1}\breve{\psi}_{s,k+1} - \right.\right. \\ \left.\left. j\omega_{me,k+1}\bar{u}_{s,k+1}\left(\breve{\psi}_{s,k+1} - L_t\breve{\imath}_{s,k+1}\right)\right] + \breve{\imath}_{s,k+1}\left(\frac{d\bar{u}_s}{dt}\right)_{k+1}\right\}\end{aligned} \tag{3.55}$$

From (3.55), we get another two terms

$$C(\bar{u}_s) = 1.5\ p\ Im\left\{\frac{1}{L_t}\left[-R\bar{u}_{s,k+1}\breve{\imath}_{s,k+1} + \frac{R_{rs}}{L_\varphi}\bar{u}_{s,k+1}\breve{\psi}_{s,k+1}\right] + \breve{\imath}_{s,k+1}\left(\frac{d\bar{u}_s}{dt}\right)_{k+1}\right\} \tag{3.56.a}$$

and $$D = 1.5\ p\ \mathrm{Im}\left\{\frac{1}{L_t}\left[-j\omega_{me,k+1}\bar{u}_{s,k+1}(\breve{\psi}_{s,k+1}-L_t\check{\imath}_{s,k+1})\right]\right\} \quad (3.56.b)$$

From (3.53.a, 3.53.b, 3.56.a and 3.56.b) and by substituting the parts of torque and reactive power derivatives in (3.49), the convergence condition (cost function) yields to the following inequality,

$$e_{m,k+1}A(\bar{u}_s) + e_{Q_{s,k+1}}C(\bar{u}_s) > -(e_{m,k+1}B+e_{Q_{s,k+1}}D) \quad (3.57)$$

Therefore, if more than one voltage vector $\bar{u}_s$ satisfies (3.57), then $\bar{u}_{s,optimal}$ is the first voltage vector that meets at the largest extend the convergence condition maximizing the left term in (3.57). Since A and C do not depend on speed, it results that optimal voltage vector does not depend on ω_{me} (and only slightly on $\bar{\imath}_s$). Then the speed does not affect the voltage selection based on the minimization of $\tilde{\Lambda}^i_{k+1}$ and can be omitted.

3.9.2 Simulation validation

Matlab Simulation is primary used to validate and test the proposed MP DTC scheme illustrated through Figure 3.22. The test is carried out for a given speed profile change of (1200→ 50 RPM) at times of (0.05 2 sec). A load torque of two Nm is applied at starting. The reference value of reactive power is set as specified in (3.50). The predefined maximum error limit E_{max} is set to 0.1. As can be viewed through Figure 3.23, the drive dynamic performance exhibits fast and precise transient response, in addition the sensorless technique afford its effectiveness for a wide speed variations down to very low speed range (2 % of rated speed). I t can be noticed also that the flux variations follow the change in the estimated value of reactive power of the machine. From Figure 3.24, the control response can be observed through the vectors switching according to the instantaneous variation in the absolute estimated error. In addition, the actual and estimated rotor position confirm the validity of sensorless procedure presented in Sect. 3.8. Moreover, the ISO flux gives an information about the instantaneous variation of stator flux following the reactive power change.

3.9.3 Experimental validation

The layout for the test bench viewed in Figure 3.9 is used to verify the feasibility of proposed MP DTC scheme. The test is carried out for a speed commands of (1200→ 50 RPM) at times of (0 → 1 sec), a load torque of 2 Nm is applied at starting. The reactive power commands are set according to (3.50). The maximum error limit is held to 0.1. Through Figure 3.25 it can be noticed that the proposed control procedure is feasible and presents enhanced dynamic response , this can be shown through the estimated and actual speed profile , torque, reactive power variation and flux which tracks the reactive power change. Figure 3.26 views the action taken by the control system , and gives informations about the rotor position that confirm the validity of sensorless approach, and finaly the iso flux assure that the flux inside the machine follows the change in the controleed reactive power.

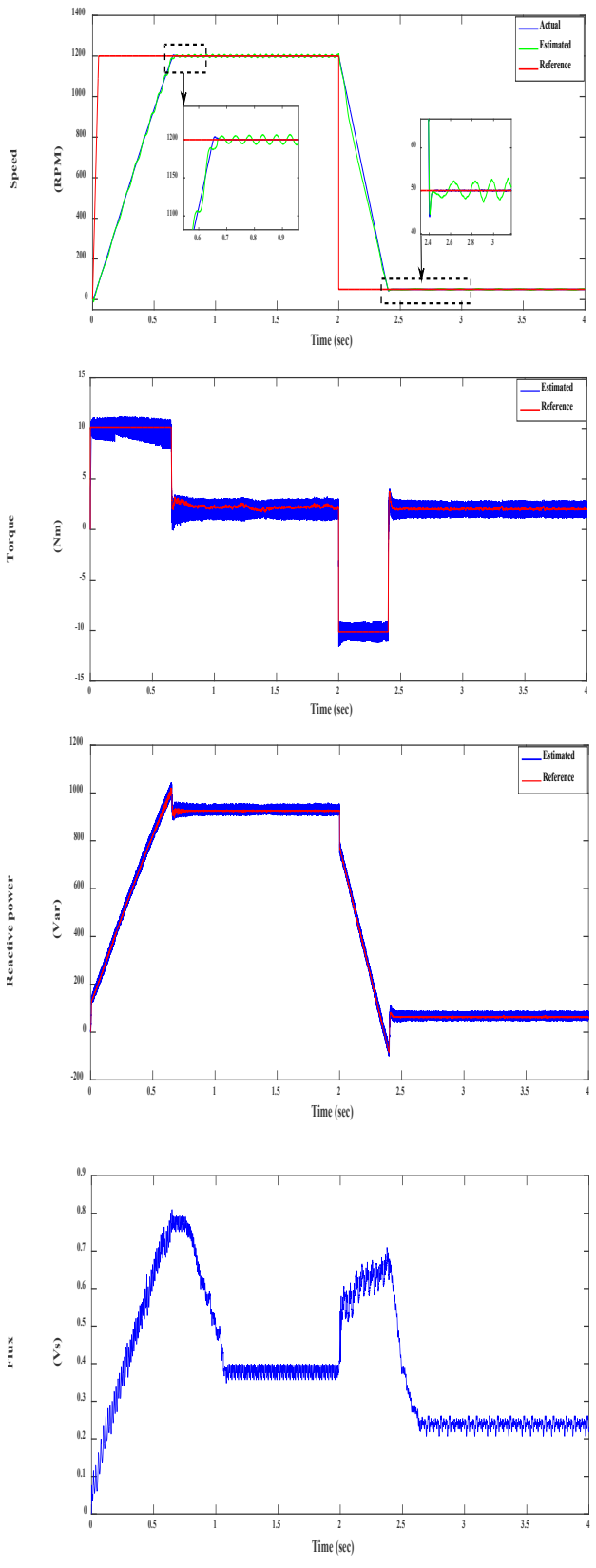

Figure 3.23: IM dynamic performance

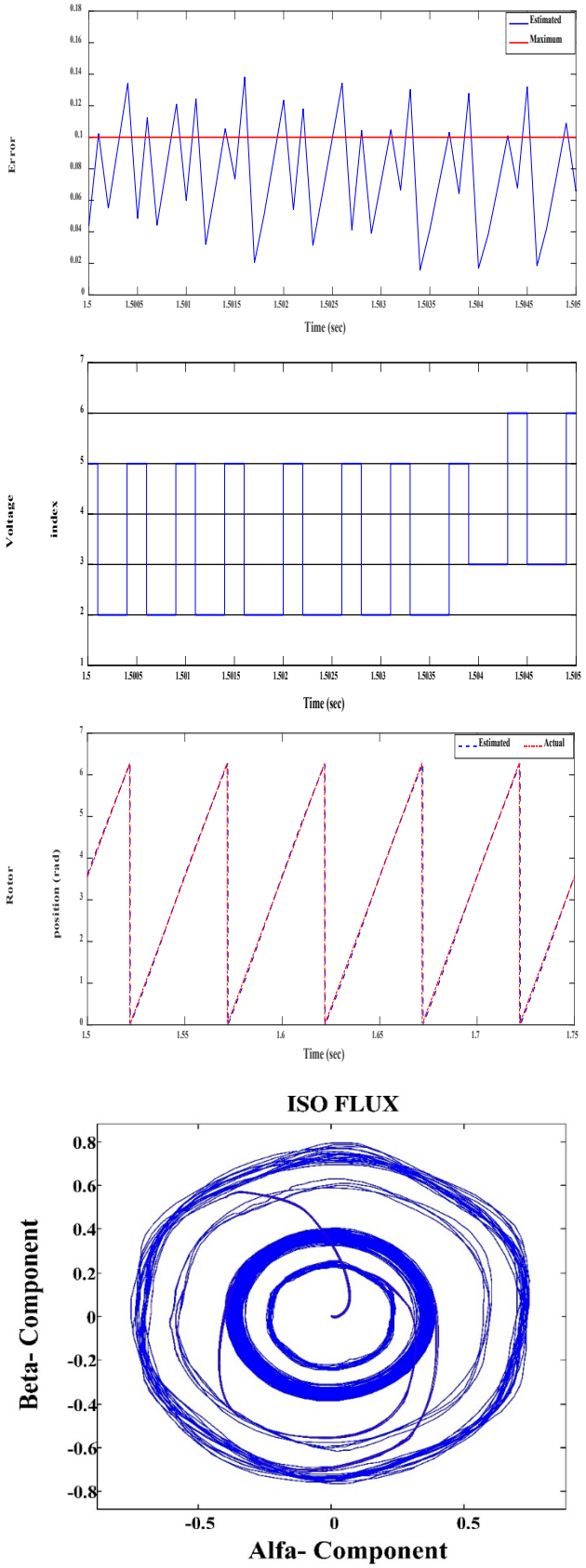

Figure 3.24: Control response, rotor position and ISO flux

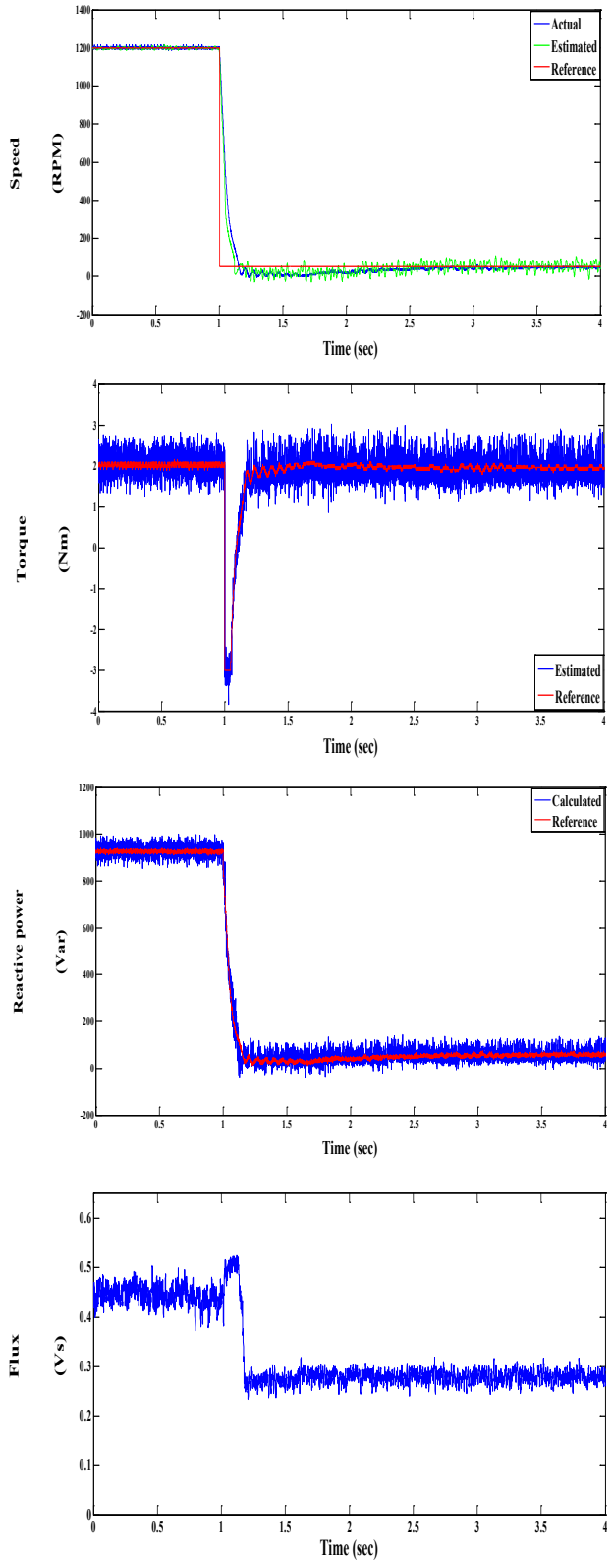

Figure 3.25: IM dynamic performance

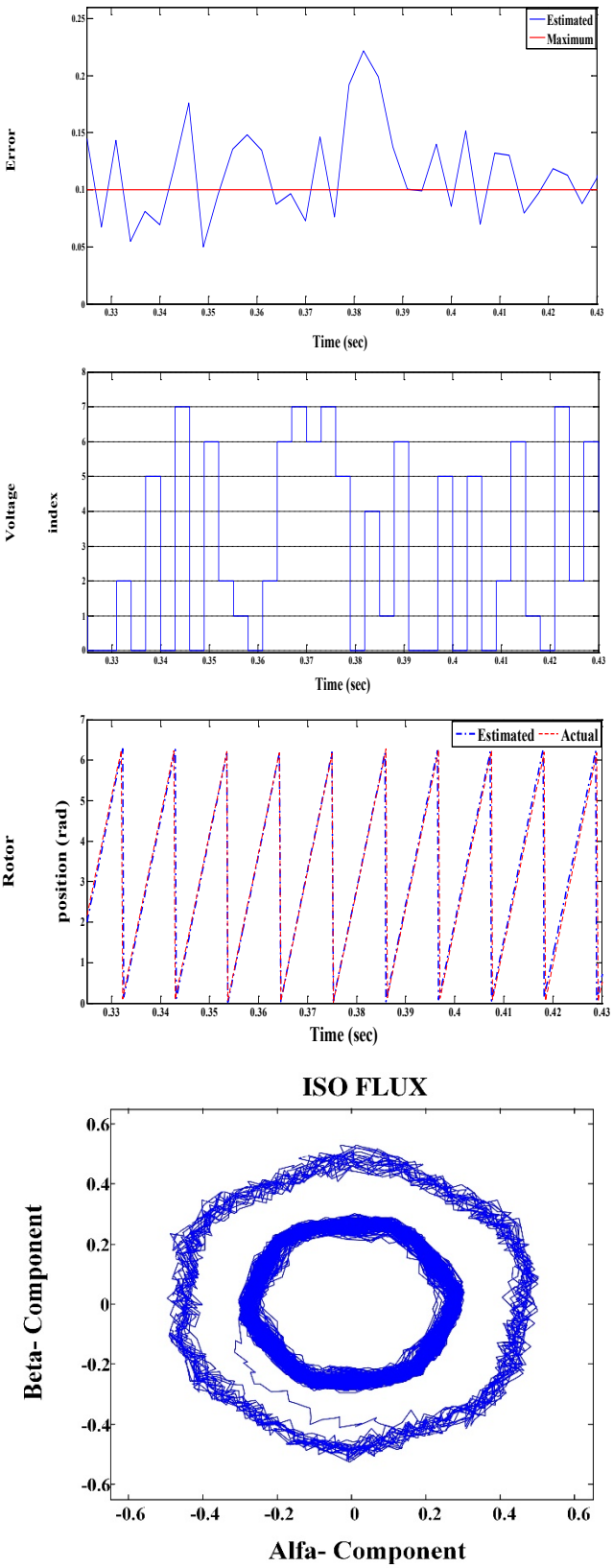

Figure 3.26: Control response, rotor position and ISO flux

3.10 Model predictive instantaneous power control for IM drive

The first model predictive control topology presented in Sect. 3.2 aimed to utilize the torque and stator flux as control variables, while the topology introduced in Sect. 3.9 pertained to utilize the reactive power as an alternative control variable for the stator flux while keeping the torque as a second control variable. It can be noticed that the torque itself is still estimated in terms of the measured currents and estimated stator flux as given by (3.13) and this is quite accepted solution compared with using torque meter, but to increase the robustness of the system instead of still controlling the torque besides regulating the reactive power as introduced in Sect. 3.9, the torque can be replaced with the active power as a control variable. Thus, now the IM drive is under what is called instantaneous power control (IPC), in which the active and reactive powers replace the torque and flux as control variables.

The concept of power control was applied to reactive power compensator applications since many years [63], but the application to electrical machine is still limited, some studies concerned with studying this control procedure and applying it to AC machines as reported in [64] and [65]. The instantaneous power control method (IPC) introduced in these previous studies combines the features of both classic DTC and FOC techniques. Consequently, it still requires the usage of co-ordinate transformation and PI controllers. This in addition to the need for using a PWM for voltage control purposes.

In order to avoid these gaps, an effective formulation for IPC based on model prediction is introduced and analyzed in this section. The proposed MP IPC combine all the merits from FOC and DTC while overcoming their shortages, this is clear from the absence of co-ordinate transformation, less dependency on machine parameters and avoiding the usage of PWM. In addition, to enhance the control robustness, the sensorless technique introduced in Sect. 3.8 is utilized. It is worth to mention that, IPC procedure appears to be suitable for medium performance drives systems, which do not require operating at very low or zero speed.

3.10.1 Theoretical approach to proposed MP IPC

The proposed MP IPC algorithm consists of two main stages- the first is concerned with the derivation of power reference commands, while the second is dedicated for the utilization of model prediction. Both stages are treated and analyzed in the following subsections.

In principle, the complex apparent power of the machine represented in space vector notation can be given by:

$$S_k = 1.5\left(\bar{u}_{s,k}\check{I}_{s,k}\right) \tag{3.58}$$

From (3.58), the instantaneous active and reactive powers are calculated as follows:

$$P_{s,k} = 1.5\mathrm{Re}\left(\bar{u}_{s,k}\check{I}_{s,k}\right) \tag{3.59}$$

$$Q_{s,k} = 1.5\mathrm{Im}\left(\bar{u}_{s,k}\check{I}_{s,k}\right) \tag{3.60}$$

The instantaneous active power $P_{s,k}$ includes the power consumed in the slip- dependent rotor resistance of the machine (R_r/slip) (this is true if the losses in iron and losses due to stator resistance are ignored), plus the

power related to magnetic energy variation. While, the instantaneous reactive power denotes to the instantaneous rate of change in flux vector's magnitude and its acceleration, as discussed later.

If $P_{s,k}$ is controlled, and the flux in the machine is kept constant, then this approximately controls the developed torque of the machine as

$$P_{s,k} = m_k \omega_{m,k} \tag{3.61}$$

where $\omega_{m,k} = \left(\frac{\omega_{me,k}}{p}\right)$ is the mechanical angular speed. Similarly, the reactive power controls the flux in the machine.

3.10.1.1 Power reference generation stage

The simplest reference to be derived is the active power one $P^*_{s,k}$, since this reference is directly related to the desired torque developed by the machine.

It is clear that $P^*_{s,k}$ can be calculated by

$$P^*_{s,k} = m^*_k \omega_{m,k} \tag{3.62}$$

where m^*_k is the reference torque.

Equation (3.62) works to some extent, but it can generates values of active power which may be insufficient to develop and generate the reference torque m^*_k. This is due to that not all input active power to the machine participates in generating the output power. This is because of losing some power in stator resistance and iron losses in addition to the power dissipated in the rotor resistance, which in terms depends on the slip of the machine.

If it is assumed that the power lost in stator resistance and that goes as iron losses can be neglected, the power loss due to rotor resistance cannot be avoided.

The power flow inside the machine can be represented as shown in Figure 3.27 through which it can be noticed that the input active power is splitted into two parts, the first dissipates into the rotor resistance while the second is consumed as mechanical output power.

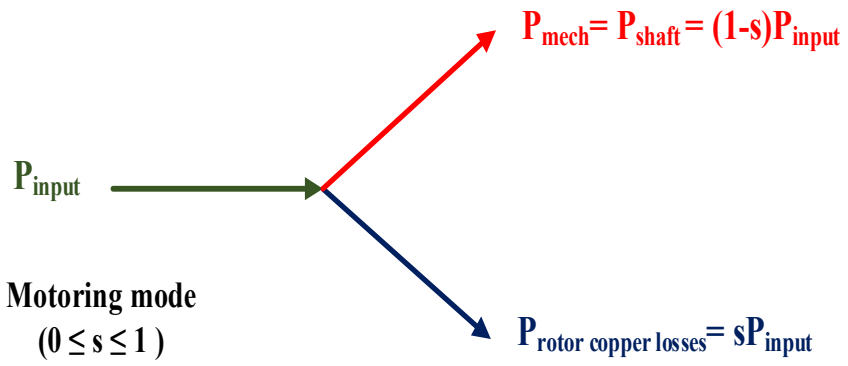

Figure 3.27: Power flow inside induction motor

Thus, to make the output mechanical power equal to the desired shaft power, the part of power lost in the rotor resistance should be compensated, and to do this the machine slip should be identified.

According to above hypothesis and assuming that the slip is known, the active power reference to be utilized can be represented by:

$$P^*_{s,k} = \frac{P_{shaft}}{1-slip} = \frac{m^*_k \omega_{m,k}}{1-slip} \tag{3.63}$$

where P_{shaft} is the desired shaft mechanical power.

To develop a formulation for the slip to be used for the compensation purpose, the derivation of reactive power reference value is utilized. Figure 3.28 shows the space vector diagram of voltages, currents and fluxes for the induction machine.

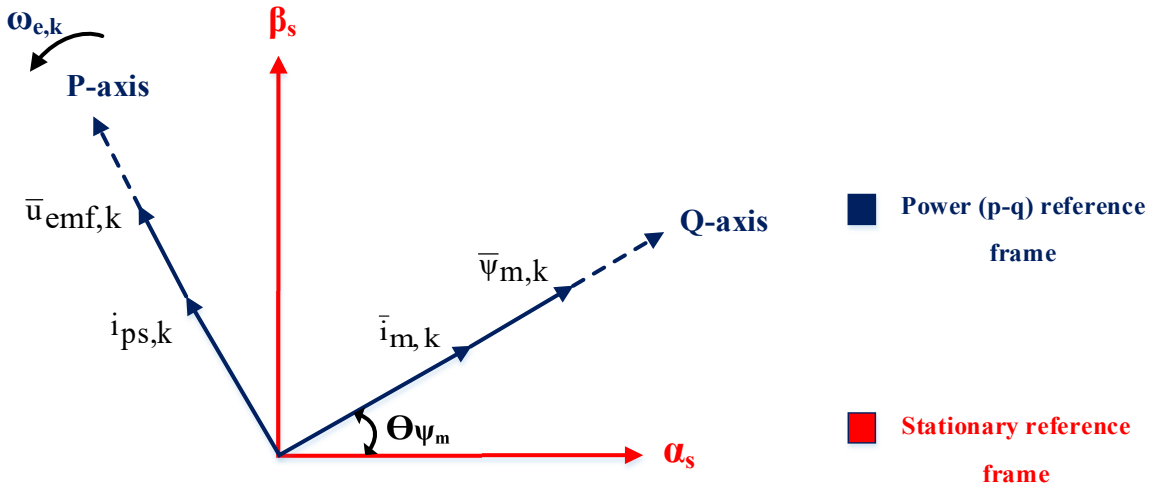

Figure 3.28: Space vector representation for IPC

From Figure 3.28, it can be noticed that the reactive power $Q_{s,k}$ can be given via the multiplication of the back emf voltage $\bar{u}_{emf,k}$ in one axis of the machine and the magnetizing current $\bar{\imath}_{m,k}$ in the other axis, thus

$$\left|Q_{s,k}\right| = 1.5\bar{\imath}_{m,k}\bar{u}_{emf,k} = 1.5\bar{\imath}_{m,k}\omega_{e,k}\bar{\psi}_{m,k} \tag{3.64}$$

where $\omega_{e,k} = \omega_{me,k} + \omega_{slip,k}$ is the applied electrical frequency and $\bar{\psi}_{m,k}$ is the magnetizing airgap flux.

From (3.64), the reference angular slip $\omega^*_{slip,k}$ can be calculated by

$$\omega^*_{slip,k} = \frac{-|Q^*_{s,k}|}{1.5\bar{\imath}^*_{m,k}\bar{\psi}^*_{m,k}} - \omega_{me,k} \tag{3.65}$$

It is worth to notice that the relation between the magnetizing flux and magnetizing current can be given by

$$\bar{\psi}_{m,k} = L_M * \bar{i}_{m,k} \tag{3.66}$$

The negative sign in (3.65) results from the sign of $Q^*_{s,k}$ that will be derived later.
From (3.65) and (3.66), the slip can be computed by

$$slip = \frac{\omega_{slip,k}}{\omega_{me,k}+\omega_{slip,k}} = 1 + \frac{\omega_{me,k}}{Q^*_{s,k} L_M (\bar{\psi}^*_{m,k})^2} \tag{3.67}$$

Then, from (3.67) and substituting in (3.63), the reference of active power can be derived as:

$$P^*_{s,k} = -\frac{m^*_k \omega_{m,k} Q^*_{s,k} L_M}{\omega_{me,k} (\bar{\psi}^*_{m,k})^2} = -\frac{L_M Q^*_{s,k} m^*_k}{p (\bar{\psi}^*_{m,k})^2} \tag{3.68}$$

From (3.64), it can be noticed that the reactive power is dependent on the angular slip frequency $\omega_{slip,k}$ of the machine which in turn is related to the developed torque of the machine.

The developed torque can be given after applying field oriented control principle as:

$$m_k = 1.5p \frac{L_M}{L_r} (\bar{\psi}_{m,k} \cong \psi_{qm,k}) i_{ps,k} \tag{3.69}$$

where ($\psi_{pm,k}$ and $\psi_{qm,k}$) and ($i_{ps,k}$ and $i_{qs,k}$) are the magnetizing airgap flux and stator current components in the synchronously rotating (p-q) frame as illustrated in Figure 3.28.

Using the same FOC principle, the angular slip frequency can be given by

$$\omega_{slip,k} = \frac{i_{ps,k} L_M}{T_r |\bar{\psi}_{m,k} \cong \psi_{qm,k}|} \tag{3.70}$$

where $T_r = L_r / R_r$ is the rotor time constant.
From (3.69) the p component of stator current is given as:

$$i_{ps,k} = \frac{m_k}{1.5p \frac{L_M}{L_r} |\bar{\psi}_{m,k} \cong \psi_{qm,k}|} \tag{3.71}$$

From (3.71) and by substituting in (3.70) and assuming that the rotor leakage inductance is very small compared with the rotor inductance ($L_r \cong L_M$), this results

$$\omega_{slip,k} = \frac{m_k L_M}{1.5p |\bar{\psi}_{m,k} \cong \psi_{qm,k}|^2 T_r} \tag{3.72}$$

Then, by substituting from (3.72) into (3.64), the reactive power reference to be used is given by

$$Q^*_{s,k} = -\left[\frac{|\bar{\psi}_{m,k} \cong \psi_{qm,k}|^2}{L_M} \omega_{me,k} + \frac{m^*_k}{1.5pT_r} \right] \tag{3.73}$$

It is worth to notice that the negative sign (-) in (3.73) is used to give the right sign for inductive reactive power, as the induction machine is considered as inductive load. It should be noted also that changing the sign in (3.73) to be negative in contrast to the reference value for reactive power that is previously used in Sect. 3.9 and represented by (3.50), does not change the fact that the reactive power is the provider of the flux inside the machine.

3.10.1.2 Power prediction stage

From (3.59) and (3.60), the derivatives of active and reactive powers can be computed as:

$$\frac{dP_{s,k}}{dt} = 1.5\mathrm{Re}\left[\bar{u}_{s,k}\frac{d\check{\imath}_{s,k}}{dt} + \check{\imath}_{s,k}\frac{d\bar{u}_{s,k}}{dt}\right] \tag{3.74}$$

$$\frac{dQ_{s,k}}{dt} = 1.5\mathrm{Im}\left[\bar{u}_{s,k}\frac{d\check{\imath}_{s,k}}{dt} + \check{\imath}_{s,k}\frac{d\bar{u}_{s,k}}{dt}\right] \tag{3.75}$$

The derivatives for the stator current and stator voltage are previously defined by (3.10) and (3.47), respectively.

Consequently, from (3.59), (3.60), (3.74) and (3.75), the values of active and reactive powers can be predicted at instant $(k+1)T_s$ as follows:

$$P_{s,k+1} = P_{s,k} + \frac{dP_{s,k}}{dt} \tag{3.76}$$

$$Q_{s,k+1} = Q_{s,k} + \frac{dQ_{s,k}}{dt} \tag{3.77}$$

3.10.2 Implementation procedure

After the derivation of active and reactive powers reference values using (3.68) and (3.73), and after the calculation of the predicted values using (3.76) and (3.77), the next step is to utilize a cost function that will guide the control system to select the most suitable voltage vector to be applied to the motor's terminals, in the case that the absolute value of estimated error exceeds its maximum limit as can be seen in Figure 3.29 that illustrates the action taken be control for two different cases according to the instantaneous value of the absolute error.

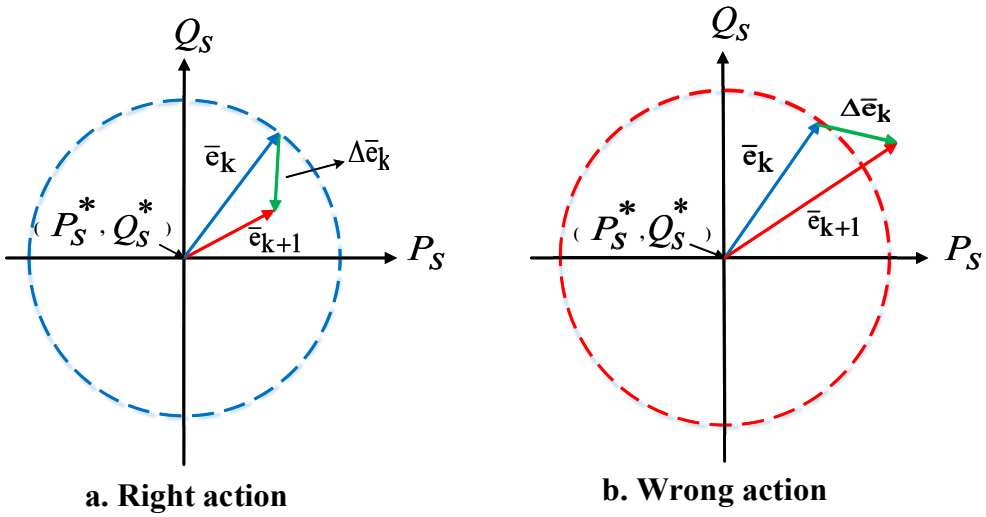

Figure 3.29: Conditions for the existence of IPC in the error plane

The error vector can be represented at instant kT_s as:

$$\bar{e}_k = \frac{P^*_{s,k} - P_{s,k}}{S_n} + jw''_f \frac{Q^*_{s,k} - Q_{s,k}}{S_n} = e_{P_{s,k}} + jw''_f e_{Q_{s,k}} \tag{3.78}$$

where S_n is the rated apparent power of the induction machine.

In the same manner introduced in previous sections, the target of the control is to maintain at any sampling time the vector $|\bar{e}_k|$ very close to zero, by applying a proper voltage vector to the machine. In other words, the following inequality must be satisfied:

$$|\bar{e}_k| = \sqrt{\left(e_{P_{s,k}}\right)^2 + \left(w''_f\right)^2 \left(e_{Q_{s,k}}\right)^2} \leq E_{max} \tag{3.79}$$

From (3.79) it can be noticed that, when the error exceeds E_{max} the proper way to bring it agin below, is to select the voltage vector which causes negative variation to the error, and to check this, (3.79) is derived respecting to the time and from the results of derivation a convergence condition which will be responsible for selecting these optimal voltage vectors, is derived at instant $(k+1)T_s$ as follows:

$$\widetilde{\Lambda}^i_{k+1} = \left[\tilde{e}_{P_{s,k+1}} \left(\frac{\widetilde{de_{P_s}}}{dt}\right)_{k+1} + w''_f \tilde{e}_{Q_{s,k+1}} \left(\frac{\widetilde{de_{Q_s}}}{dt}\right)_{k+1}\right]^i < 0 \tag{3.80}$$

where w''_f is a weighting factor used to give a weight for the reactive power respecting to the active power, but it is not crucial to have an exact value for w''_f as both values of active and reactive powers are normalized with the

same value of nominal apparent power S_n, and thus the value of w_f'' is determined by iteration until we reach to a weight balance between the values of the controlled active and reactive powers. This process can be achieved via simple iterations without the need for adopting any procedure for selecting w_f''.

It is worth to notice that all terms used by (3.80) are obtained previously via (3.76), (3.77), (3.74) and (3.75). Thus, the control now can perform its task in the selection of optimal voltage vectors to be applied according to the instantaneous error between the reference and predicted values of active and reactive powers.

It should be noticed that the formulation of convergence condition given by (3.80) is still assure that the voltage selection step is independent of speed change effect and this can be easily proved if we make the same analysis introduced previously in Sects. 3.5.2.1 and 3.9.1.2.

The complete system configuration for the proposed MP IPC is shown via Figure 3.30 through which it can be noticed that there is no existence for PWM used regularly with FOC. The sensorless procedure introduced in Sect. 3.8 is utilized to provide the speed information required in the prediction stage.

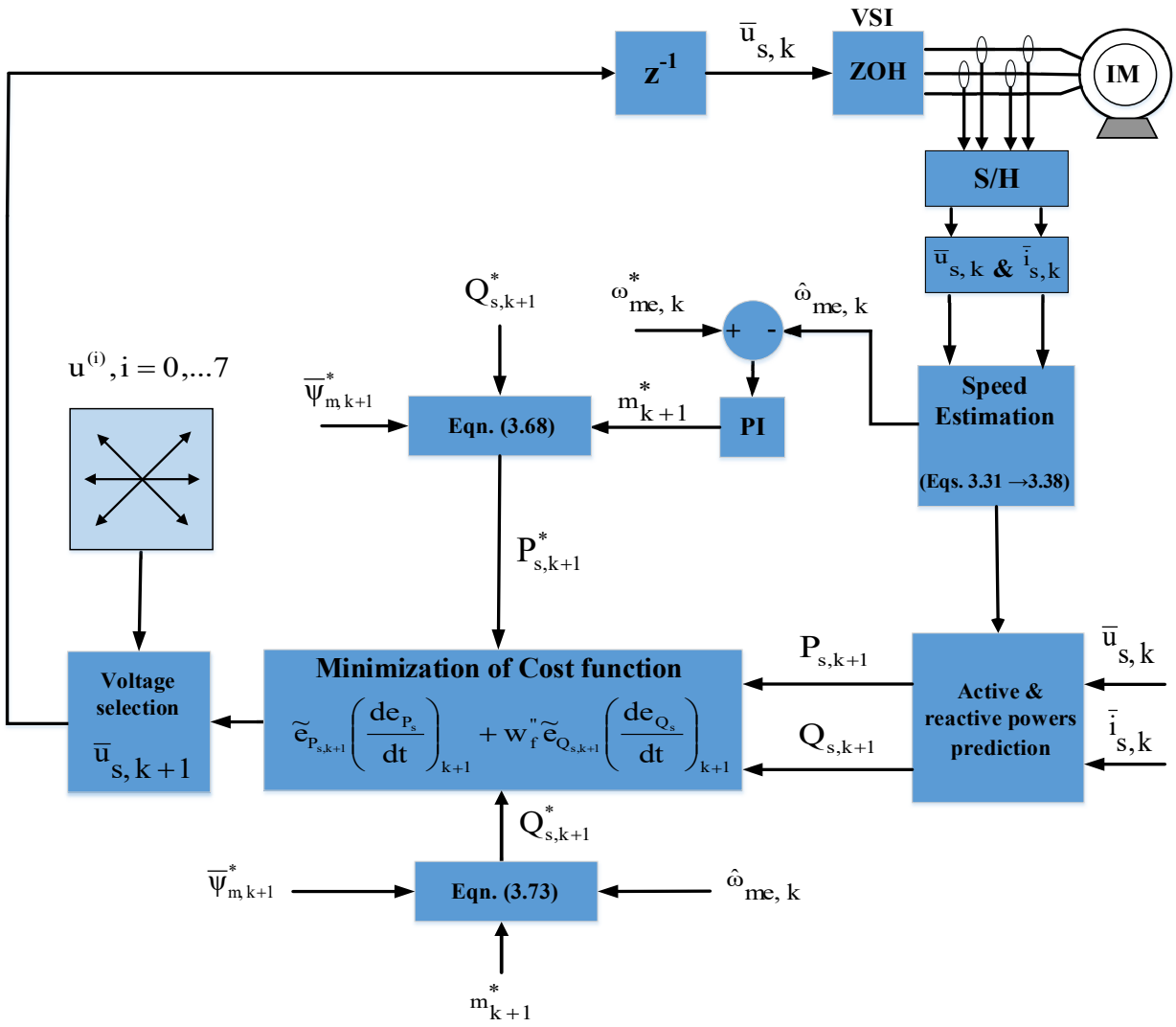

Figure 3.30: Overall scheme layout for proposed MP IPC technique

3.10.3 Simulation validation

Matlab/Simulink software is used firstly to validate the effectiveness of proposed MP IPC, the tests are carried out for a speed range of (0→ 1200→ 1600→ 600 RPM) at times of (0 → 0.5→ 1.5→ 3 sec), aload torque of 2 Nm is applied at starting. The reference value for the magnetizing flux $\bar{\psi}^{*}_{m,k}$ is kept at 0.5 Vs, while the maximum error limit is held to 0.06. Obtained results confirm the feasibility of the control procedure this can be noticed via Figure 3.31 which illustrates the dynamic performance of the IM drive, the actual and estimated speed are precisely matched which assure again the validity of sensorless procedure, while the flux profile showing the correct decoupling of two components of magnetizing flux with definite tracking of the refrence value, in addition, bothe active and reactive powers are following precisely their imposed refrence values. Figure 3.32 gives a detailed overview on the control response for each instant of variation in the absolute value of estimated error. It shows also the rotor position profile from which the effectiveness of the sensorless approach is also proofed.

3.10.4 Experimental validation

A dSpace1104 control prototyping board is used to implement experimentally the proposed MP IPC procedure, the overall layout for the test bench used is the same shown in Figure 3.9. The tests are carried out for a speed profile change of (1200→ 1600→ 600 RPM) at times of (0→ 1→ 2.5 sec), the reference value for the magnetizing flux is kept at 0.5 Vs, while a two Nm load torque is applied at starting. The value of E_{max} is held to 0.06 as the same used in simulation test. It is worth to notice that the value of E_{max} is choicable one, but it is preferable to be used for limiting the switching frequency, and here the value is selected taking into consideration that the values of the estimated active and reactive powers will be higher than that if the torque and flux are selected as control variables, thus a lower error limit is predefined. The results assure the high dynamic performance for IM drive. Through Figure 3.33 the speed , torque, flux, active and reactive power can be shown, it is observed that the sensorless technique exhibits proper tracking for the speed change, while an accurate decoupling for the magnetizing flux components is achieved. Also, the estimated values for the active and reactive power follow accurately their references. Figure 3.34 gives an information about the absolute error behaviour and its corresponding voltage index change, in addition the rotor position waveform views a definite matching between the actual and estimated signals.

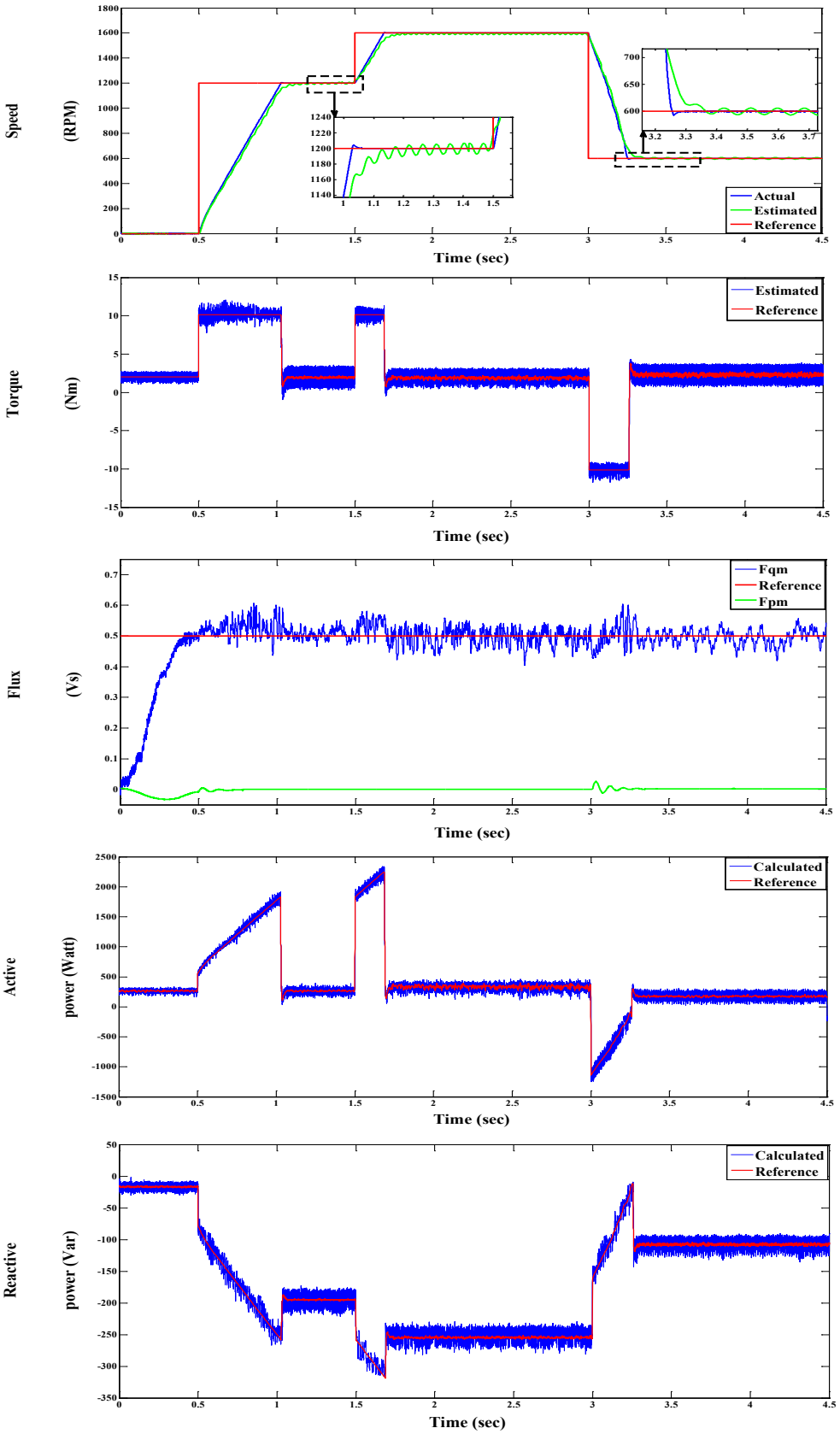

Figure 3.31: Dynamic performance for IM drive (simulation)

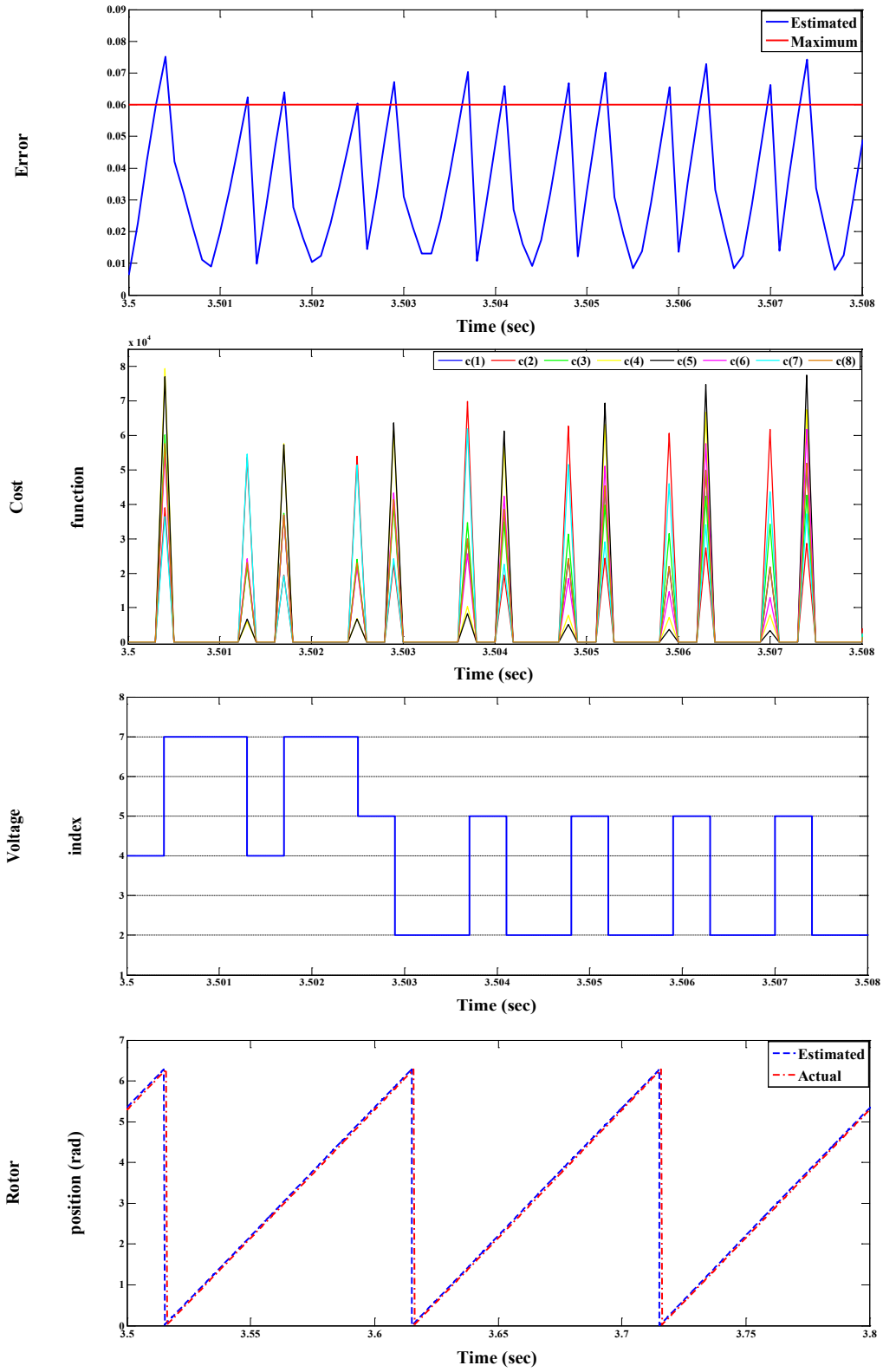

Figure 3.32: Control response and rotor position (simulation)

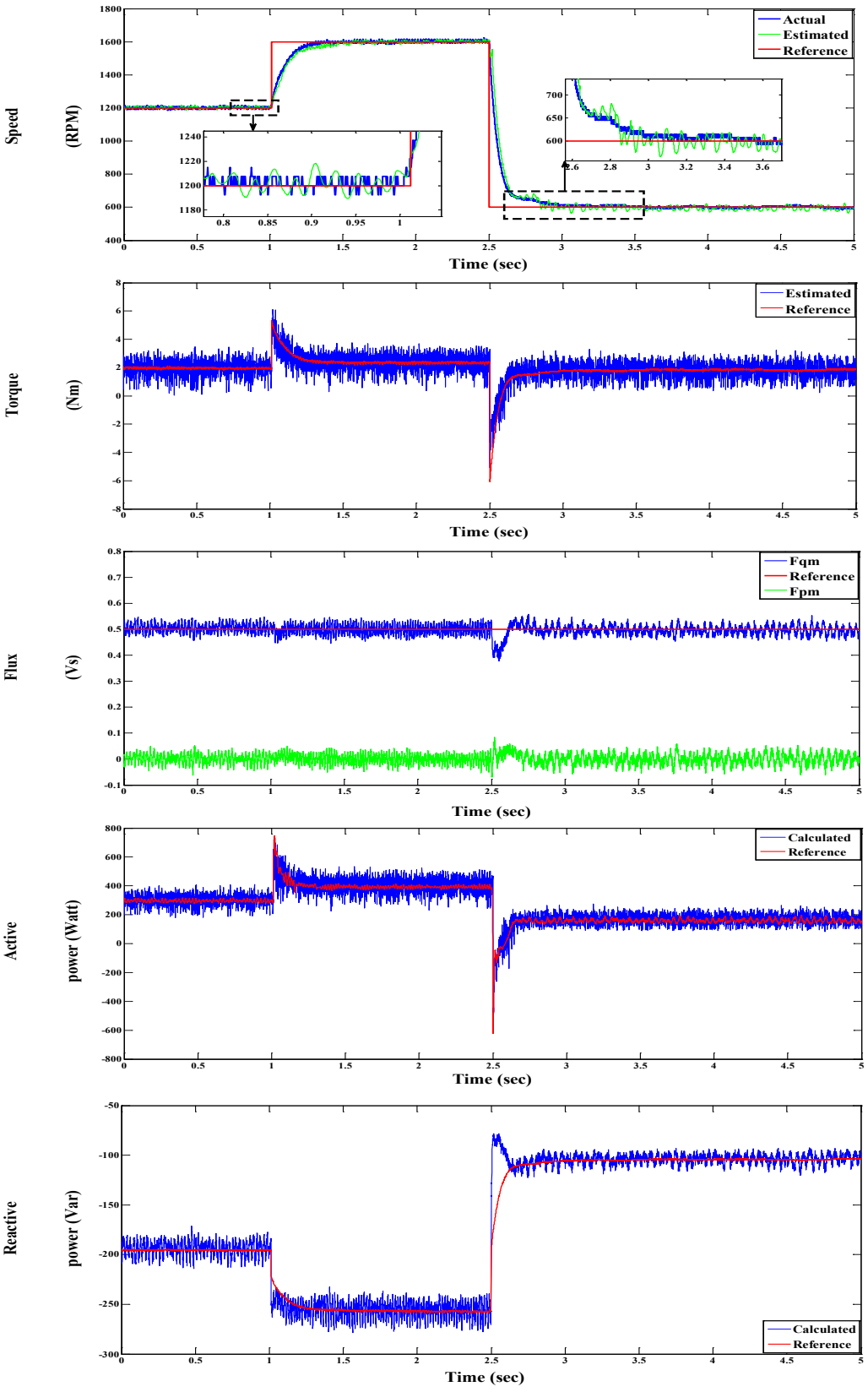

Figure 3.33: Dynamic behavior for IM drive (experimental)

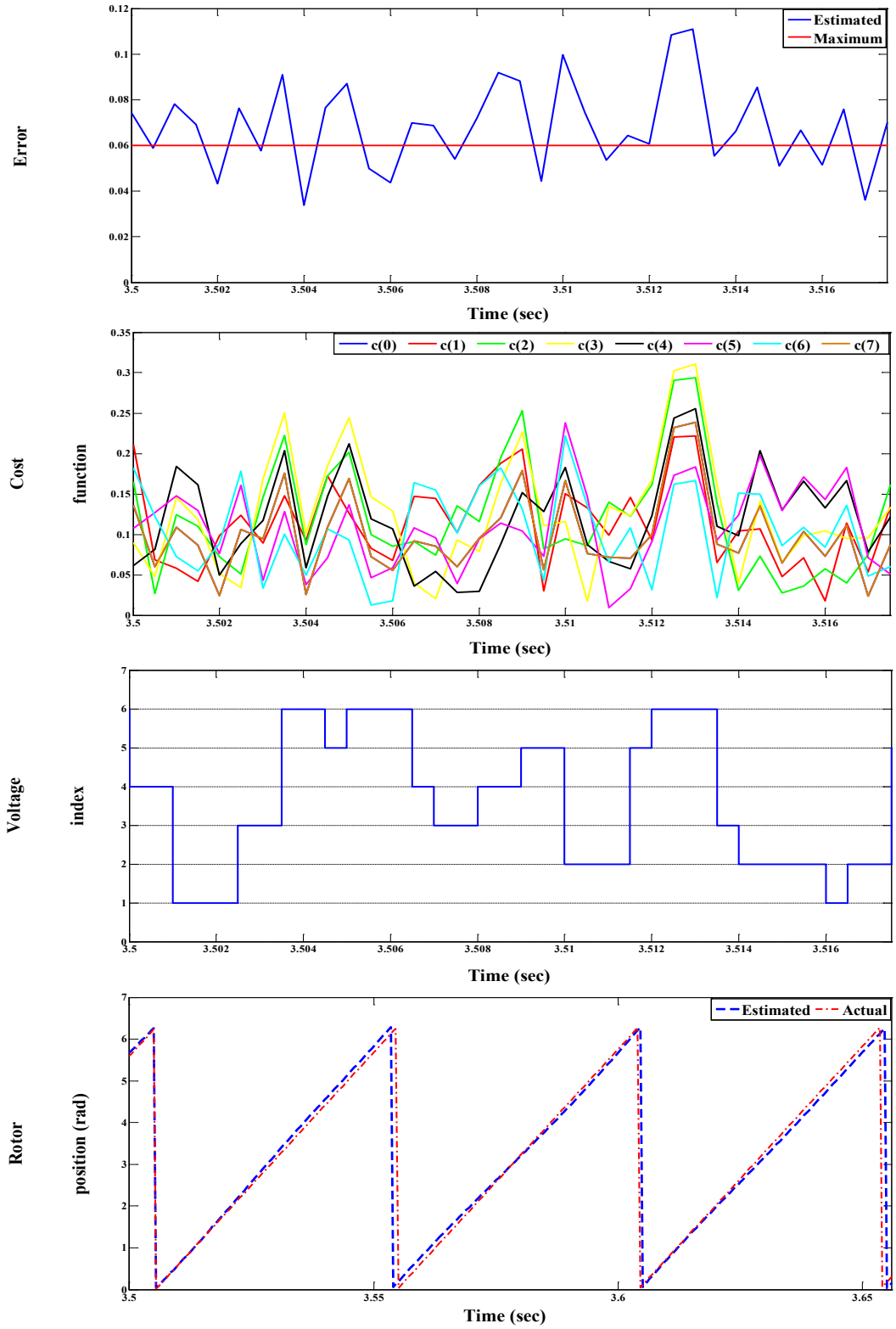

Figure 3.34: Control action and rotor position (experimental)

Chapter 4

Effective Ripple Reduction Procedure for the Proposed MP DTC for IM drives

4.1 Introduction

DTC hysteresis based controller has some disadvantages, such as: variable switching frequency and dependency on the hysteresis band and motor speed, this is in addition to remarkable torque pulsations (ripples). These torque ripples can be minimized by shortening the sampling period, which causes high switching frequency, and consequently responsible for high switching losses. As a result, some studies focused recently on using combined DTC and space vector modulation [66, 67] and predictive torque control (PTC) and other intelligent control methods for torque ripple reduction of induction motor drives as in [68].

Different control variables, objectives and bounds can be comprised in a single cost function with the finite control set model predictive control and concurrently be controlled with the basis of preference control factor is defined as ‘’weighting factor’’ [69, 70, 71, and 72]. If the variables are with the same nature then no need to set the weighting factor but when the control variables are with various type (unequal magnitude value and diverse measuring unit) in a single cost function, then selecting the most suitable value of weighting factor become a problem and deteriorates the dynamic performance of the system extensively.

Up till now, no mathematical methods or control design techniques to adapt the weighting factor for equally important terms and at present they are evaluated with the iterative estimation method [73]. This procedure is used regularly to modify the weighting factor. However, with this method, the weighting factor can be regulated and better dynamic behavior can be obtained but this is still based on approximation. So, this weighting factor should be optimized to get the best dynamic performance of the control system.

As a solution for this issue, this chapter proposes an effective analytical method for evaluating the optimum value of weighting factor to be used in predictive control algorithm to reduce the torque ripple as well as flux control of the IM drive fed by a three phase two level VSI. Moreover, the senesorless approach that is used in previous chapter and explained in Sect. 3.8 is utilized to achieve high dynamic performance for the IM drive.

4.2 Optimum Weighting Factor Selection Methodology

Torque ripples of the induction motor can be given by:

$$m_{ripple}^2 = \frac{1}{T_s}\int_0^{T_s}(D_m + St)^2 dt \tag{4.1}$$

where, m_{ripple} is the torque ripple , D_m is the torque deviation equal to $(m_k - m_k^*)$ and S is the ascending torque slope (Torque derivative), which can be calculated at instant k as follows:

$$S_k = -\left(\frac{R_s}{\sigma L_s} + \frac{R_r}{\sigma L_r}\right) m_k - Kp\omega_{me,k}\left(\psi_{\alpha s,k}\psi_{\alpha r,k} + \psi_{\beta s,k}\psi_{\beta r,k}\right) + K\left(u_{\beta s,k}\psi_{\alpha r,k} - u_{\alpha s,k}\psi_{\beta r,k}\right) \quad (4.2)$$

where $K = \frac{3p}{2}\frac{L_m}{\sigma L_s L_r}$.

The torque ripples given by (4.1) can be represented in a simplified way as follows:

$$m_{ripple}^2 = \frac{1}{T_s}\int_0^{T_s}\left(D_m^2 + S_k^2 t^2 + 2D_m S_k t\right)dt \quad (4.3)$$

To get the optimum value of weighting factor, we have to derivate (4.3) with respect to weighting factor and set the derivative to zero. It is worth to notice that only the torque slope S_k is related to the weighting factor because only S_k is related to the optimum selected voltage vectors $\left(u_{\alpha s,opt}, u_{\beta s,opt}\right)$, which come from a cost function. As a result,

$$m_{ripple}^2 = m_{ripple}^2(S_k),\ S_k = S_k(\bar{u}_{s,opt}) \text{ , and } \bar{u}_{s,opt} = \bar{u}_{s,opt}(w_{opt}) \quad (4.4)$$

Therefore,
$$m_{ripple}^2 = m_{ripple}^2(w_{opt}) \quad (4.5)$$

Equation (4.3) gives the relation between the torque slope and torque ripple, whereas (4.2) represents the relation between the torque slope and the optimum selected voltage vectors from a cost function which in terms depends on the weighting factor. The relation between the last and the selected optimum voltages can be summarized as follows:

After substitution of w_f with w_{opt} , then the cost function used in model predictive control algorithm in chapter 3, and represented by (3.5) can be expressed as follows:

$$\tilde{\Lambda}_k^i = \left[\tilde{e}_{m,k}\left(\frac{d\tilde{e}_m}{dt}\right)_k + w_{opt}\tilde{e}_{|\psi_s|,k}\left(\frac{d\tilde{e}_{|\psi_s|}}{dt}\right)_k\right]^i \quad (4.6)$$

Applying the Taylor expansion around the reference values in (4.6) to express the model predictive variables in a linear manner as follows:

$$m_k = m_k^* + K\left(\psi_{\alpha r,k}\Delta\psi_{\beta s,k} + \psi_{\beta s,k}\Delta\psi_{\alpha r,k} - \psi_{\alpha s,k}\Delta\psi_{\beta r,k} - \psi_{\beta r,k}\Delta\psi_{\alpha s,k}\right) \quad (4.7)$$

$$\left|\bar{\psi}_{s,k}\right| = \left|\psi_{s,k}^*\right| + \psi_{\alpha s,k}\Delta\psi_{\alpha s,k} + \psi_{\beta s,k}\Delta\psi_{\beta s,k} \quad (4.8)$$

Torque and flux deviations are related to stator and rotor fluxes as follows:

$$Y(t_k) = \Gamma . X(t_k) \quad (4.9.a)$$

where,
$$Y(t_k) = \begin{vmatrix} m_k - m_k^* \\ \left|\bar{\psi}_{s,k}\right| - \left|\psi_k^*\right| \end{vmatrix} = \begin{vmatrix} \tilde{e}_{m,k} \\ \tilde{e}_{|\bar{\psi}_s|,k} \end{vmatrix} \quad (4.9.b)$$

and,
$$\Gamma = \begin{vmatrix} -K\psi_{\beta r,k} & K\psi_{\alpha r,k} & K\psi_{\beta s,k} & -K\psi_{\alpha s,k} \\ \psi_{\alpha s,k} & \psi_{\beta s,k} & 0 & 0 \end{vmatrix} \quad (4.9.c)$$

and, $$X(t_k) = \left[\Delta\psi_{\alpha s,k}, \Delta\psi_{\beta s,k}, \Delta\psi_{\alpha r,k}, \Delta\psi_{\beta r,k}\right]^T \quad (4.9.d)$$

The appropriate input voltage vector satisfies the following set of equations:

$$\frac{\delta}{\delta\Delta u_{\alpha s,k}}\tilde{\Lambda}_k^i = 0.0 \text{ , and } \frac{\delta}{\delta\Delta u_{\beta s,k}}\tilde{\Lambda}_k^i = 0.0 \quad (4.10)$$

From (4.6), (4.9.a) and (4.10), the following voltage displacement can be obtained

$$\Delta u_{\alpha s,k} = u_{\alpha s,k} - u_{\alpha s,k}^0 = \rho_1 + \frac{\Upsilon_1}{w_{opt}} \quad (4.11.a)$$

$$\Delta u_{\beta s,k} = u_{\beta s,k} - u_{\beta s,k}^0 = \rho_2 + \frac{\Upsilon_2}{w_{opt}} \quad (4.11.b)$$

where ^{0} subscript refers to the initial value for a given variable, and

$$\rho_1 = \frac{-h_1(g_{11}g_{22}^2 - g_{12}g_{21}g_{22})}{(g_{11}g_{22}+g_{12}g_{21})^2}, \rho_2 = \frac{-h_1(g_{12}g_{21}^2 - g_{11}g_{21}g_{22})}{(g_{11}g_{22}+g_{12}g_{21})^2} \quad (4.12.a)$$

$$\Upsilon_1 = \frac{-h_2(g_{21}g_{12}^2 - g_{11}g_{22}g_{12})}{(g_{11}g_{22}+g_{12}g_{21})^2}, \Upsilon_2 = \frac{-h_2(g_{22}g_{11}^2 - g_{11}g_{12}g_{21})}{(g_{11}g_{22}+g_{12}g_{21})^2} \quad (4.12.b)$$

and, $$\begin{bmatrix} g_{11} & g_{12} \\ g_{21} & g_{22} \end{bmatrix} = \begin{bmatrix} -KT_s\psi_{\beta r,k} & KT_s\psi_{\alpha r,k} \\ T_s\psi_{\alpha s,k} & T_s\psi_{\beta s,k} \end{bmatrix} \quad (4.12.c)$$

and, $$\begin{bmatrix} h_1 \\ h_2 \end{bmatrix} = \Gamma.Z.X(t_k) \quad (4.12.d)$$

and, $$Z = T_s\begin{bmatrix} \frac{1}{T_s} + Q_{11} & Q_{12} & Q_{13} & Q_{14} \\ Q_{21} & \frac{1}{T_s} + Q_{22} & Q_{23} & Q_{24} \\ Q_{31} & Q_{32} & \frac{1}{T_s} + Q_{32} & Q_{34} \\ Q_{41} & Q_{42} & Q_{43} & \frac{1}{T_s} + Q_{43} \end{bmatrix} \quad (4.12.e)$$

and, $$Q_{11} = Q_{22} = -\frac{R_s}{\sigma L_s}, \quad Q_{13} = Q_{24} = \frac{R_s(1-\sigma)}{\sigma L_m}, \quad Q_{31} = Q_{42} = \frac{R_r(1-\sigma)}{\sigma L_m}, \quad Q_{34} = -Q_{43} = -\omega_{me,k},$$

$$Q_{33} = Q_{44} = \frac{-R_r}{\sigma L_r}, \quad Q_{12} = Q_{21} = Q_{41} = Q_{14} = Q_{23} = Q_{32} = 0 \quad (4.12.f)$$

The above-mentioned equations give the relationship between the stator voltage vectors and weighting factor as specified in (4.11.a) and (4.11.b).

To find the optimum-weighting factor in the predefined cost function, we have to derivate the torque ripples given in (4.3) with respect to w_{opt} and equalize it by zero as follows:

$$\frac{dm_{ripple}^2}{dW_{opt}} = \frac{d}{dw_{opt}}\left(D_m^2 + \frac{1}{3}S_k^2T_s^2 + D_mS_kT_s\right) = 0 \quad (4.13)$$

Therefore, $$\frac{dS_k}{dw_{opt}} = 0 \quad (4.14.a)$$

and, $$\left(\frac{2}{3}S_kT_s^2 + D_mT_s\right) = 0 \quad (4.14.b)$$

From (4.14.b), we get

$$S_k = -\frac{3D_m}{2T_s} \tag{4.15}$$

From (4.2) and (4.14.a) the following equality can be obtained;

$$\psi_{\alpha r,k}\frac{du_{\beta s,k}}{dw_{opt}} = \psi_{\beta r,k}\frac{du_{\alpha s,k}}{dw_{opt}} \tag{4.16}$$

The derivatives in (4.16) can be obtained as following:

$$\frac{du_{\alpha s,k}}{dw_{opt}} = \frac{d}{dw_{opt}}\left(u^0_{\alpha s,k} + \Delta u_{\alpha s,k}\right) = \frac{d}{dw_{opt}}\left(\Delta u_{\alpha s,k}\right) = \frac{-\Upsilon_1}{w^2_{opt}} \tag{4.17.a}$$

$$\frac{du_{\beta s,k}}{dw_{opt}} = \frac{d}{dw_{opt}}\left(u^0_{u_{\beta s,k}} + \Delta u_{u_{\beta s,k}}\right) = \frac{d}{dw_{opt}}\left(\Delta u_{u_{\beta s,k}}\right) = \frac{-\Upsilon_2}{w^2_{opt}} \tag{4.17.b}$$

Consequently, (4.14.a) is not suitable for estimating the optimum value of weighting factor, because of each cancel from both sides of (4.16).
So, from (4.14.b) and (4.15) we get the criterion for the optimum selection of weighting factor.

Therefore, $$-\frac{3D_m}{2T_s} = K * \left[-\frac{1}{K}\left(\frac{R_s}{\sigma L_s} + \frac{R_r}{\sigma L_r}\right) m_k - p\omega_{me,k}\left(\psi_{\alpha s,k}\psi_{\alpha r,k} + \psi_{\beta s,k}\psi_{\beta r,k}\right) + \mu\right] \tag{4.18}$$

where, $\mu = \left(u_{\beta s,k}\psi_{\alpha r,k} - u_{\alpha s,k}\psi_{\beta r,k}\right)$.

The above equations are concluded to give the optimum value of the weighting factor used in (3.17) instead of w_f as following:

$$w_{opt} = \frac{\Upsilon_2\psi_{\alpha r,k} - \Upsilon_1\psi_{\beta r,k}}{\mu + \psi_{\beta r,k}(\rho_1 + u_{\alpha s,k-1}) - \psi_{\alpha r,k}(\rho_2 + u_{\beta s,k-1})} \tag{4.19}$$

The proposed model predictive DTC scheme and its algorithm with weighting factor optimization are shown in Figures 4.1 and 4.2, respectively. Proposed control procedure fulfils the following six steps:

- **Step 1**: Measuring of input stator voltage $\bar{u}_{s,k}$ and current $\bar{i}_{s,k}$, and estimation of speed sample $\omega_{me,k}$ by using the procedure previously presented in Sect. 3.8 , which utilizes the predictive nature of proposed DTC approach.
- **Step 2**: Estimation of the present torque and flux values by means of voltage model observer.
- **Step 3**: Calculation of the optimized weighting factor.
- **Step 4**: Prediction of the torque and stator flux for all possible voltage vectors (i=0…..7).
- **Step 5**: Checking the predicted values of torque and flux in the cost function given by (4.6).
- **Step 6**: The switching states correspond to the minimum value of cost function are selected in the next sampling time interval to actuate the inverter.

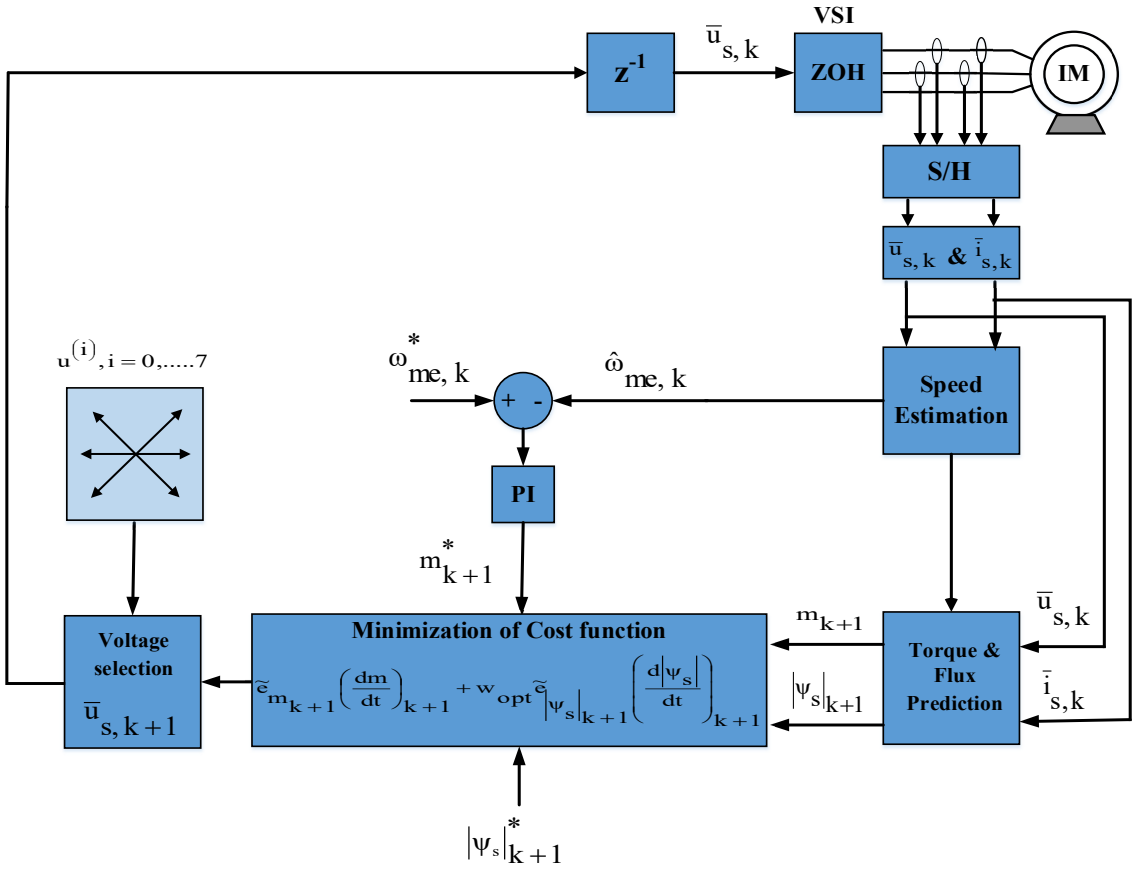

Figure 4.1: Proposed Model Predictive DTC scheme

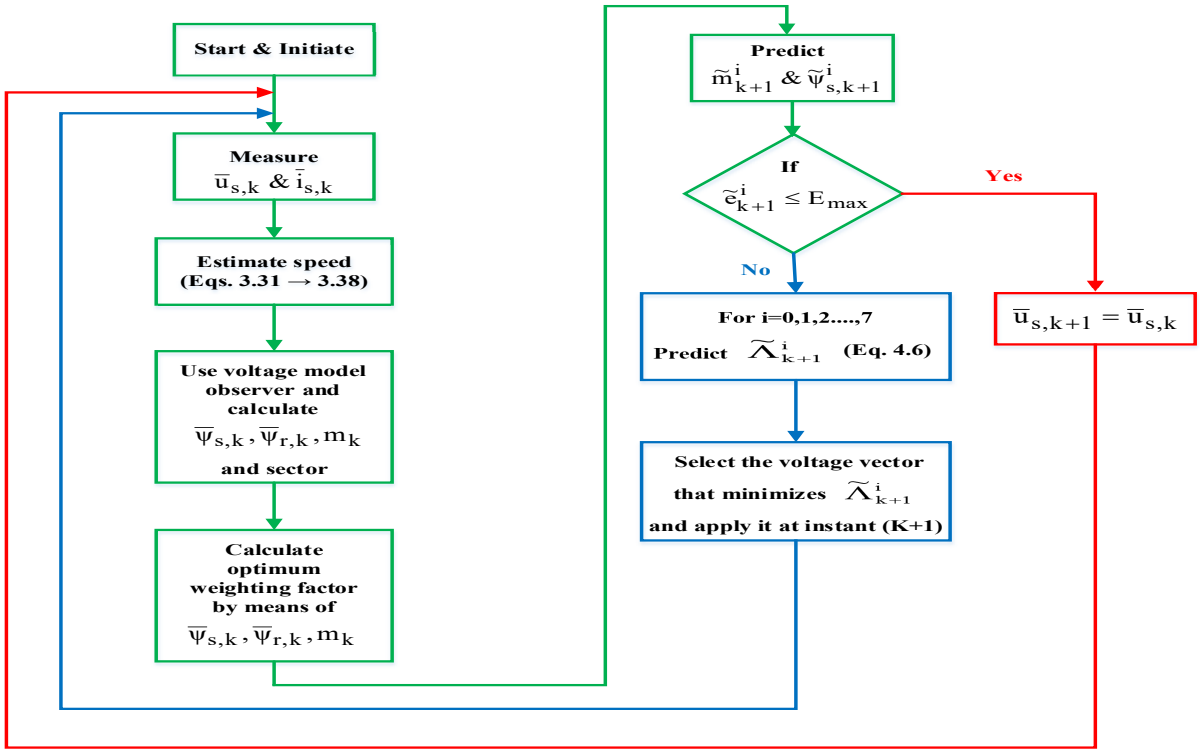

Figure 4.2: Flow diagram for proposed DTC approach

4.3 Simulation results

The simulation is used firstly for validating the proposed ripple reduction algorithm, the tests are carried out for two cases, the first uses the iterative way to select the weighting factor utilized by the cost function, while the other case pertains to the usage of optimum weighting factor calculation procedure. Both cases has the same test conditions with a speed profile of (1600 → 50 RPM), at times of (0.05 → 2 sec). The reference value of stator flux is set to 0.4 Vs, while the maximum limit for absolute error is kept at 0.1. A load torque of two Nm is applied since starting. The results can be summarized as:

4.3.1 Simulation results with arbitrary weighting factor

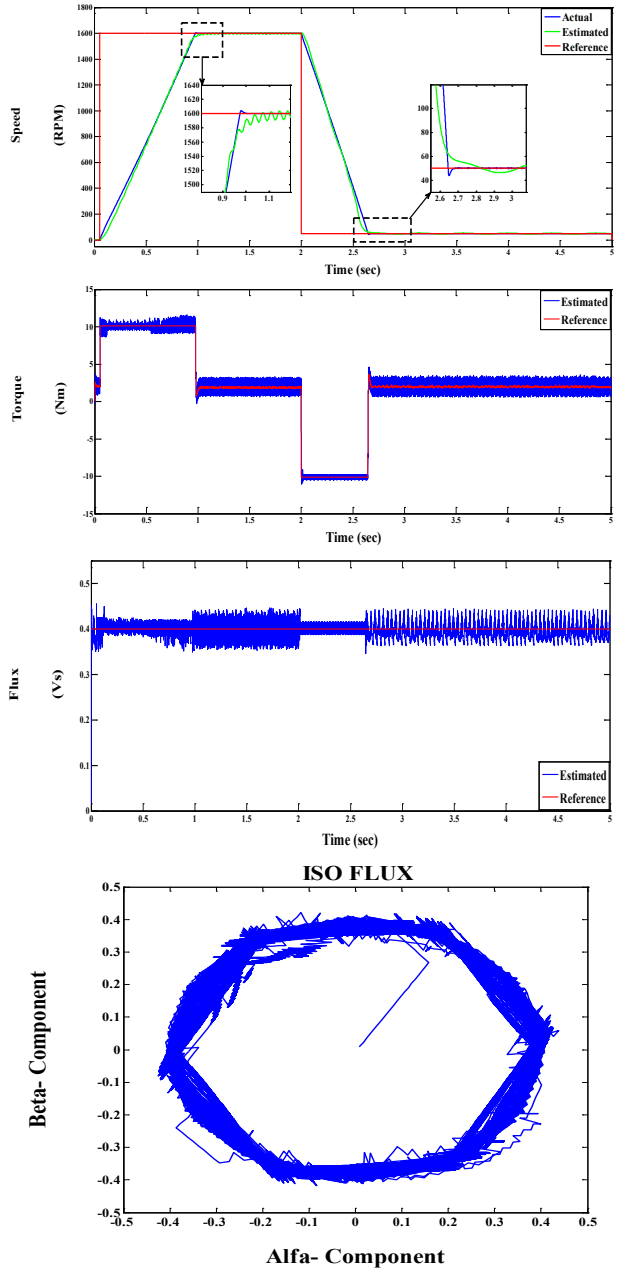

Figure 4.3: Dynamic response of IM drive

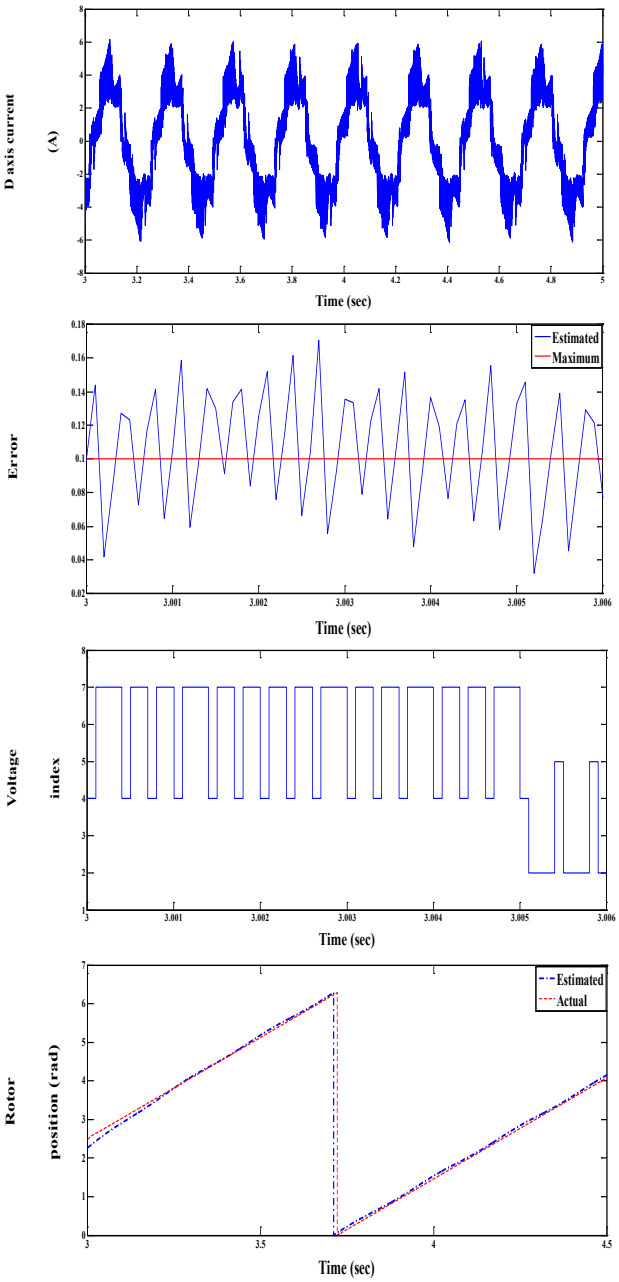

Figure 4.4: Current , control response and position

The drive performance for the proposed sensorless DTC algorithm which is presented in chapter 3, and which utilized a cost function with an arbitrary weighting factor, is shown in Figure 4.3, it is noticed that the drive has fast dynamic response for the change in speed commands from high speed to very low speed range. The sensorless speed and rotor position estimation mechanism also proved its validity at low frequency operating horizons this can be shown via Figure 4.4. On the other hand, it is noticed that there are remarkable ripples contents in the estimated values of torque, flux and current, which affect negatively the drive performance.

4.3.2 Simulation results with optimum weighting factor

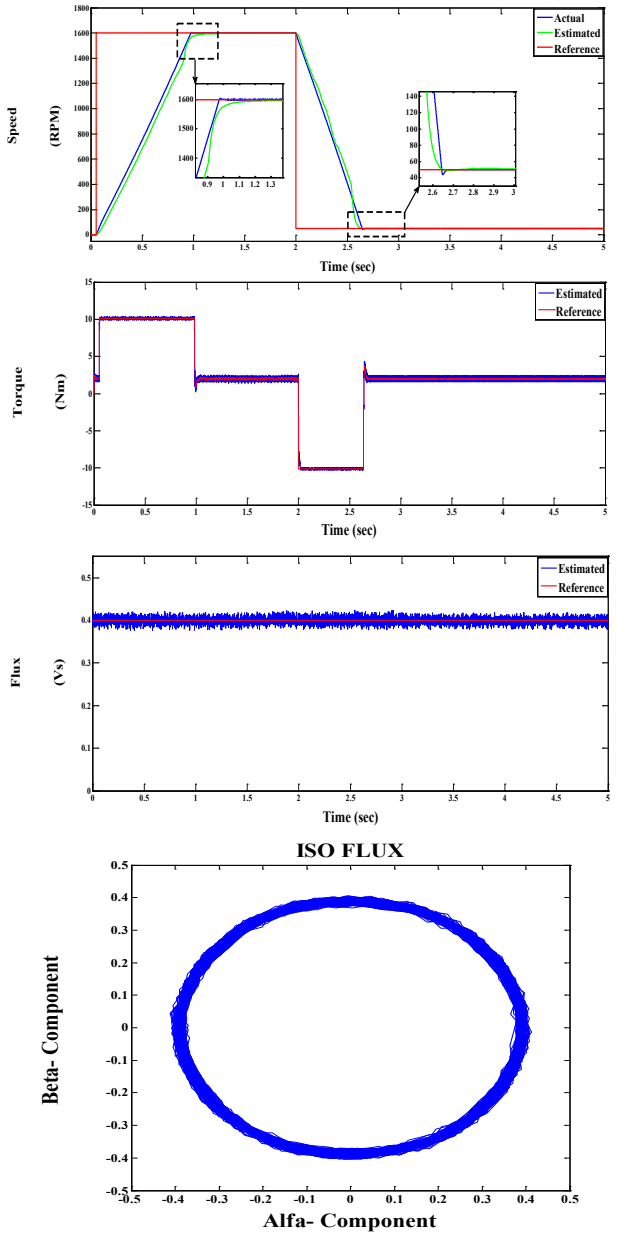

Figure 4.5: Dynamic response of IM drive

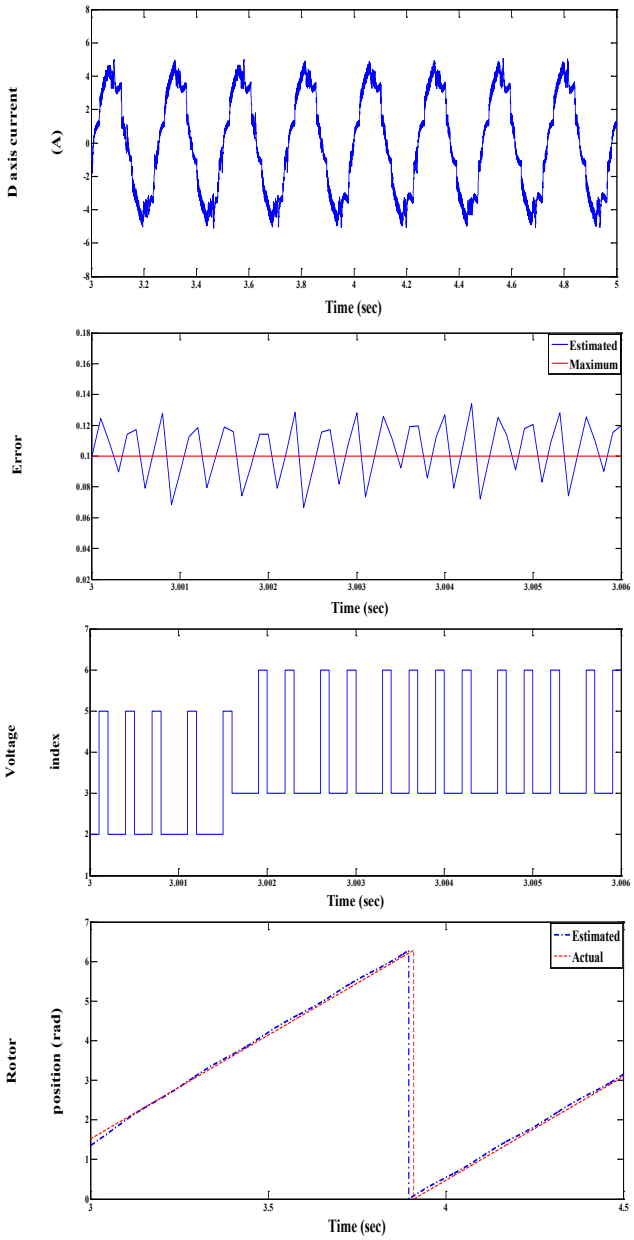

Figure 4.6: Current , control response and position

Figures 4.5 and 4.6 illustrate the dynamic performance of IM drive and control action in case of applying the procedure of optimum weighting factor. It is noticed that the ripple contents in the torque and flux are effectively reduced, and consequently the ripples in the stator currents. The sensorless technique confirm its ability with precise estimation for speed and rotor position. A comparison between the estimated motor variables (torque and flux) in both cases (with and without optimum weighting factor) can be shown through Figure 4.7, through which the effectiveness of proposed ripple reduction can be obviously confirmed.

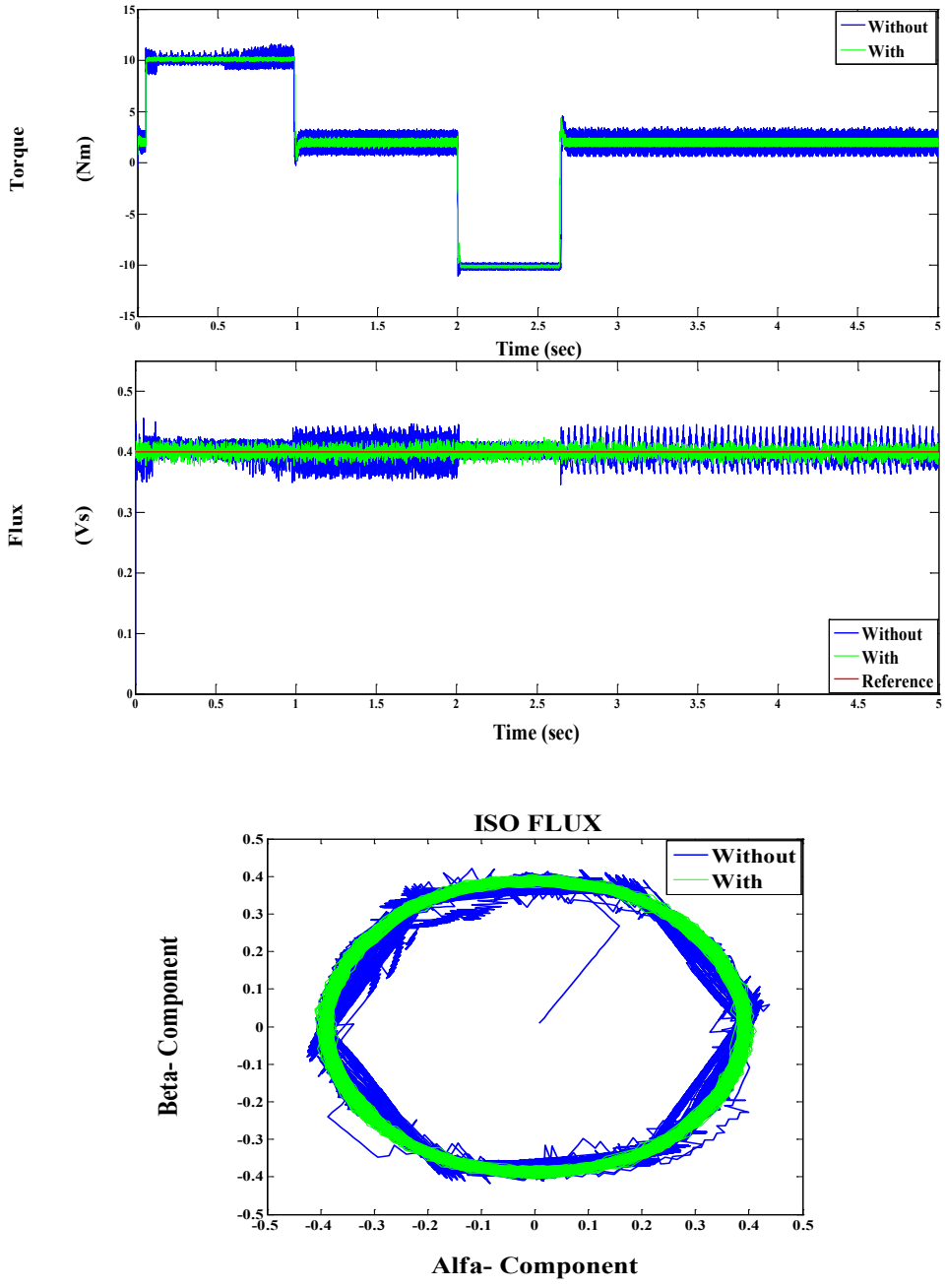

Figure 4.7: Comparison between estimated variables in two cases with and without w_{opt} (simulation validation)

Figure 4.8 illustrates the detailed variation of the weighting factor with respect to variation of the stator flux, the obtained results reports that when the estimated flux deviates from the reference value 0.4, the weighting factor increases to amend flux response, and when the estimated value of the flux approaches to the reference the weighting factor decreases.

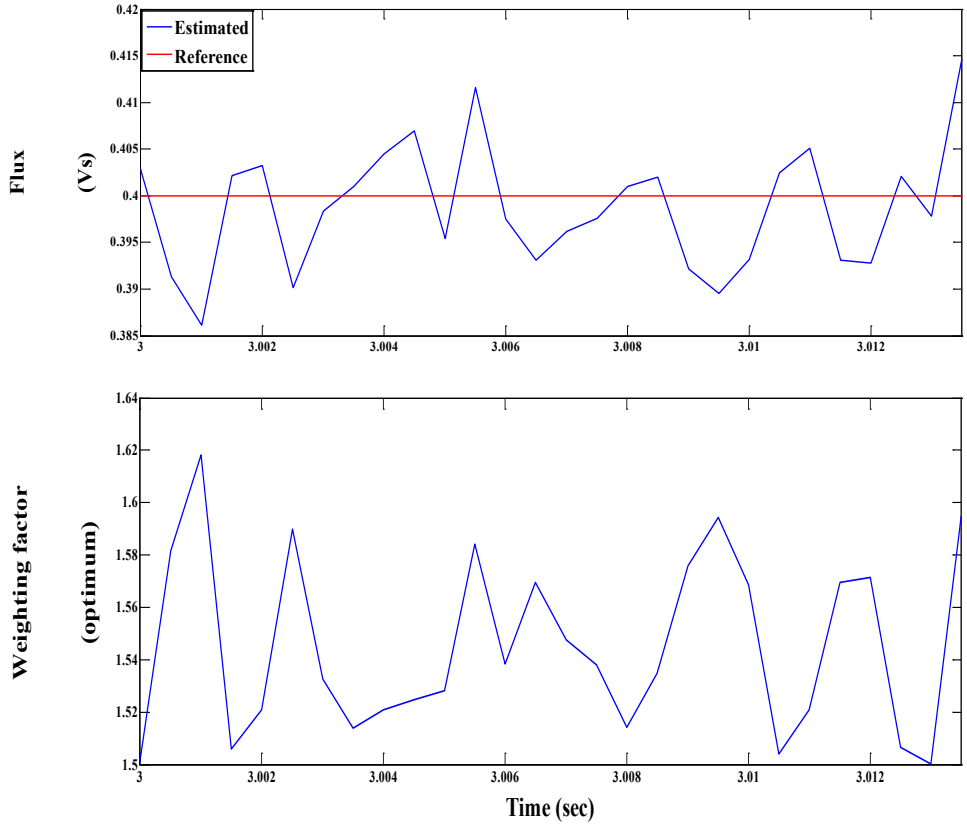

Figure 4.8: Optimum weighting factor variation with change of flux level (simulation)

4.4 Experimental validation

The proposed sensorless DTC schemes (with and without optimum weighting factor) are verified experimentally utilizing a dSpace 1104 prototyping control board. The same test bench shown in Figure 3.9 is used to perform the tests. The tests are carried out for the same given commands in simulation tests. A speed command profile of (1600 → 50 RPM) are imposed to the drive at times of (0 → 1 sec). A load torque of two Nm is applied to the motor at starting, a flux reference value of 0.4 Vs is selected. The maximum error limit E_{max} is set to 0.1. Obtained results shown in Figure 4.9 present the dynamic response of the drive when using an arbitrary value of weighting factor while Figure 4.10 gives a concentrated view on the action taken by the controller at each sampling interval. It can be noticed that the drive ehibits high performance and the snesorless procedure assured its feasibility for wide speed range. On the other hand the ripple contents in the estimated values are to some extent noticeable, this can be viewed through the torque , flux and current values.

4.4.1 Experimental results with arbitrary weighting factor

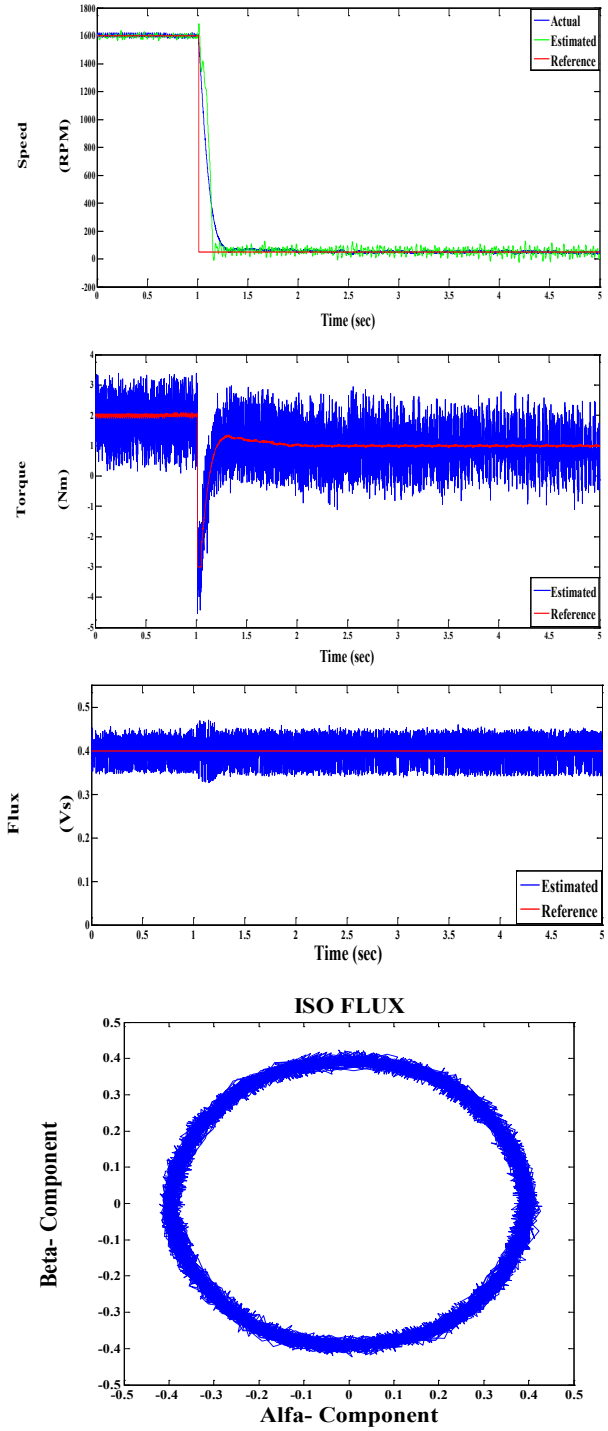

Figure 4.9: Dynamic performance of IM drive

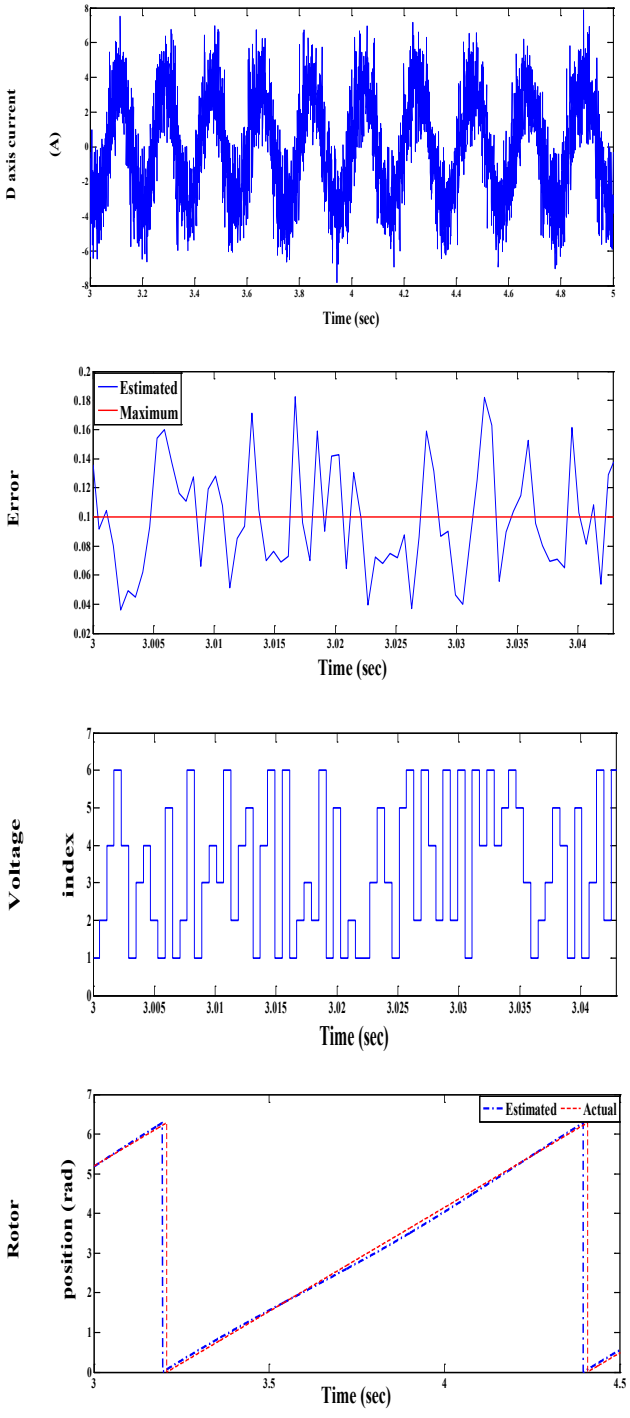

Figure 4.10: Current, control action and rotor position

4.4.2 Experimental results with optimum weighting factor

The following results viewed through Figures 4.11 and 4.12 are showing the dynamic response and detailed control action of the sensorless drive after implementing the optimum weighting factor calculation procedure, the experimental results assure the feasibility of proposed scheme, this can be clearly observed in the estimated values of torque, flux and current. In addition to that the sensorless technique intoduces high precision in the estimation of speed and rotor position even at very low speed range. The tests are carried out for the same test conditions in Sect. 4.4.1.

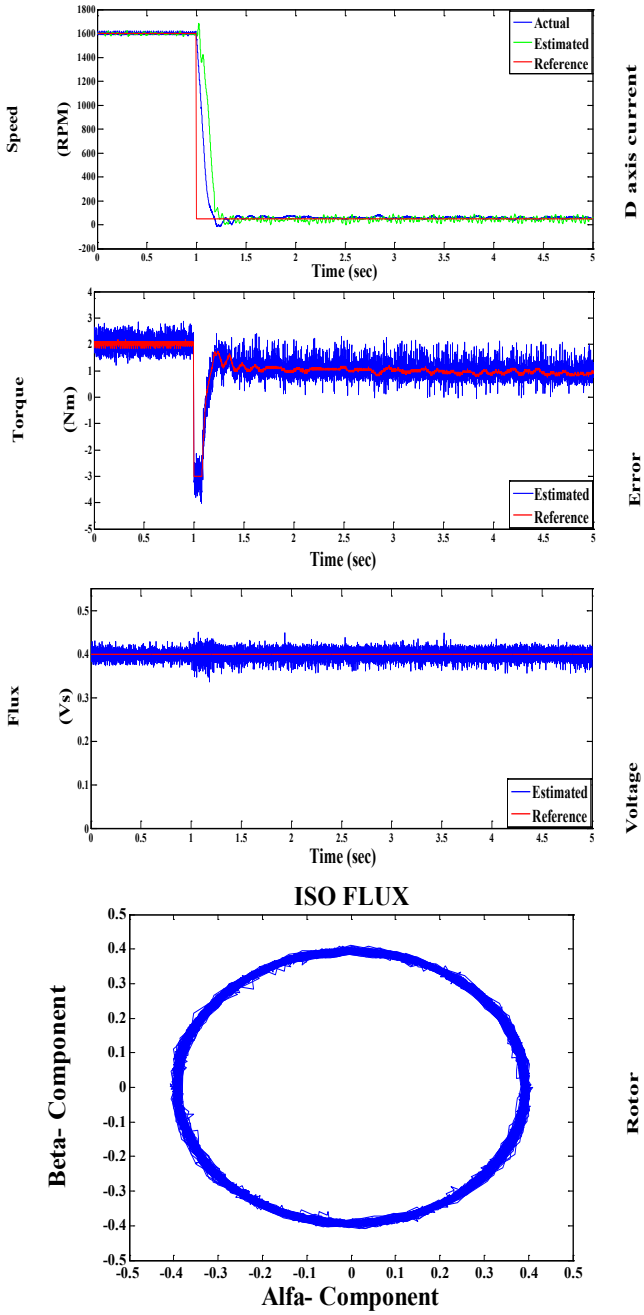

Figure 4.11: Dynamic performance of IM drive

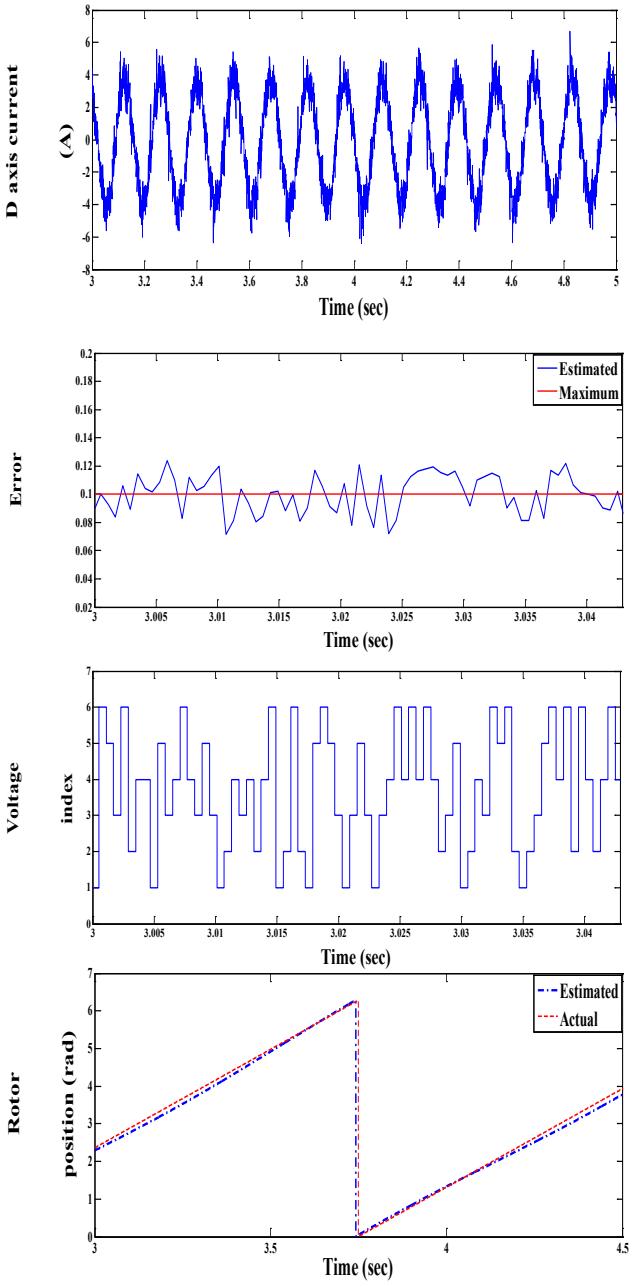

Figure 4.12: Current, control response and position

A full comparison between the estimated control variables in both cases are viewed in Figure 4.13, that clearly confirm the viability of the proposed ripple reduction procedure.

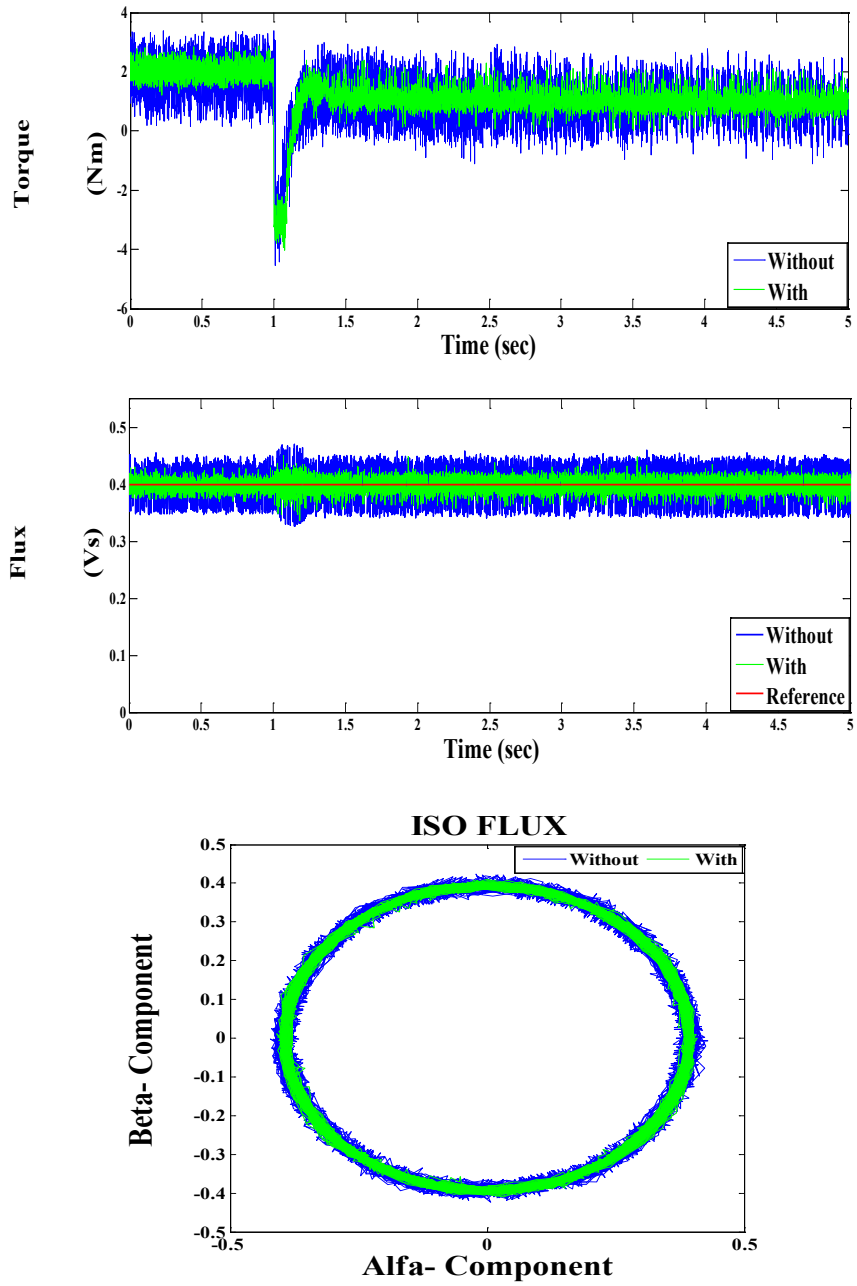

Figure 4.13: Comparison between estimated variables in two cases with and without w_{opt} (experimental validation)

The variation of the weighting factor respecting to the actual change in estimated flux values is shown through Figure 4.14. Experimental results assure the obtained simulation results viewed in Figure 4.8.

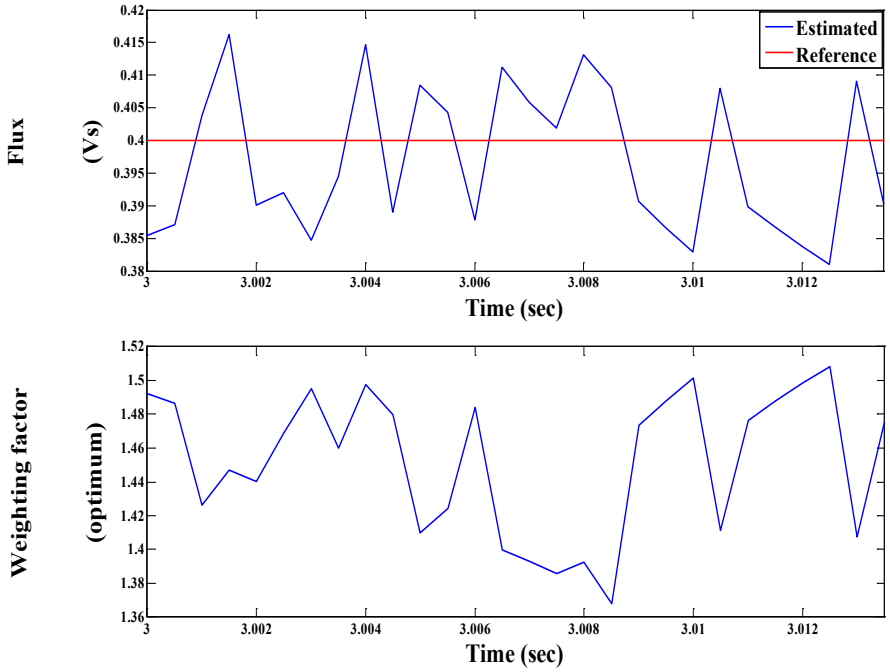

Figure 4.14: Optimum weighting factor variation with change of flux level (experimental)

The performance of the two procedures used for selecting the weighting factor can be analytically addressed as shown in Table 4.1 in terms of the average error as an indication for the ripple contents that are computed for both simulation and experimental tests. Obtained values confirm the validity of proposed selection procedure for w_{opt} in reducing the ripple contents in the controlled variables.

TABLE 4.1

Comparison of average errors for the two selection procedures of weighting factor w_f

	Simulation		**Experimental**	
	With arbitrary W_f	**With optimal W_{opt}**	**With arbitrary W_f**	**With optimal W_{opt}**
Average error $\|e_k\|$	0.1464	0.1054	0.1485	0.1043

In general, it can be stated that the derived value of w_{opt} can be also obtained with different formulations considering different control variables. For example; by considering the torque and rotor flux as references instead of torque and stator flux. This last configuration is presented in Sect. 3.8 and led to an improvement in the dynamic performance of IM drive. But on the other hand, the cost function that will have to be used in the case of designing the value of w_{opt} considering torque and rotor flux as control variables, should extend its terms to contain a part that deals with the current as a protection as in this case the torque characteristic of IM increases linearly with $\omega_{me,k}$; in addition to that the value of the w_{opt} is updated for each state change of the inverter switches and thus by this extra term in the cost function the computation time will increase which is considered not recommended during the real time implementation. That's why the ripple reduction procedure presented in this chapter is adopted as it combines simplicity in calculation and saving in computational time.

Chapter 5

Enhanced Model Predictive Current Control for Sensorless IM Drives

5.1 Introduction

General goals of the control schemes for AC drives are focused on achieving a fast and precise dynamic response with a minimum deviation from the desired quantities. Some of these schemes are concerned with regulating directly the torque and flux of the machine as reported in [74, 75, 76], while others are pertained to current regulation as [77, 78, 79, and 80].

The target from the current control is to track precisely the current references and to respond quickly to their variations in a very short time. There are various categories proposed for current controllers such as PI current control, hysteresis current control and predictive current control [81, 82, 83]. Model predictive control (MPC) is now getting a great attention for controlling the electrical drives and power converters alternative to classic PI in field orientation control (FOC) or vector control. This is obvious from its simple structure, ease of implementation, flexibility of adding nonlinearities and constraints to the system under control by MPC [84].

Generally, the model predictive control (MPC) has two types of implementation: continuous control-set (CCS-MPC) and finite control-set (FCS-MPC) [85]. The latter one is used extensively and exhibits good performance, as, especially, it takes the discrete nature of the inverter into account. One of the application of FCS-MPC for induction motor control is the model predictive current control (MPCC) [86]. The MPCC eliminates the usage of PI current controllers used by classic control schemes; in the same time, it presents less current ripples and reduction in the computation time if it is compared with predictive torque control method. Various studies dealt with the principle of predictive current control for induction motor (IM) drive [87, 88]. Some of them add some valuable contributions, but they did not explain the real base operation of the MPCC principle, when and why it works properly.

For this purpose, (i) an effective new formulation for the model predictive current control is introduced in this chapter. The new proposal gives a way in a systematic manner to investigate and understand the operation principle of MPCC also in terms of convergence and stability. The proposed scheme belongs to the class of (ii) the hysteresis predictive control (for limiting the switching frequency) as the MPCC is triggered by the exceeding of the error of a given threshold. In addition, (iii) a sensorless drives is achieved by including an effective Luenberger observer for precise estimation of rotor flux vector together with speed and load torque. At last the control scheme implements (iv) a field oriented control (FOC) for achieving the best dynamic behavior of the IM drive.

5.2 Proposed MPCC Approach

The aim of the control is to maintain at each sampling instant the predicted values of stator current components [$i_{ds,k}$ (flux component), $i_{qs,k}$ (torque component)] as near as possible to their corresponding references. For achieving this, the currents are measured, and the speed and angular position are estimated together with the rotor flux vector, the procedure of estimation will be given Sect. 5.6. The references of the current components are generated based on the principle of field-oriented control, in which the d-q coordinate frame is aligned with the rotor flux vector, and from the IM mathematical model given in Sect. 3.3 , the following relationships are obtained:

The IM torque can be given by

$$m_k = 1.5\, p\, \mathrm{Im}\left(\breve{\psi}_{s,k}\, \bar{\imath}_{s,k}\right) = 1.5\, p \frac{L_M}{L_r}\, \mathrm{Im}\left(\breve{\psi}_{r,k}\, \bar{\imath}_{s,k}\right) \tag{5.1}$$

The relation between the rotor flux and stator current can be given by

$$\bar{\psi}_{r,k} = L_r \bar{\imath}_{r,k} + L_M \bar{\imath}_{s,k} \tag{5.2}$$

Based on FOC basics,

$$\psi_{dr,k} = \psi_{r,k} \quad , \quad \psi_{qr,k} = 0.0 \tag{5.3}$$

, and

$$m_k = 1.5\, p \frac{L_M}{L_r}\, \psi_{r,k} i_{qs,k} \tag{5.4}$$

Assuming that the change in the rotor flux during steady state operation is very slow, then from the rotor voltage equation in d-q reference frame results:

$$0.0 = R_r i_{dr,k} + \left(\frac{d\psi_{dr,k}}{dt} \cong 0.0\right) \tag{5.5}$$

Thereafter from (5.2), (5.3), (5.4) and (5.5), the reference values of stator current components are calculated by

$$i^*_{ds,k} = \frac{\left|\bar{\psi}^*_{r,k}\right|}{L_M} \tag{5.6}$$

$$i^*_{qs,k} = \frac{2}{3p} \frac{L_r}{L_M} \frac{m^*_k}{\left|\bar{\psi}^*_{r,k}\right|} \tag{5.7}$$

The values obtained by (5.6) and (5.7) are then transformed to the (α-β) quantities $i^*_{\alpha s,k}$, $i^*_{\beta s,k}$ to be utilized by the MPCC. For given stator current component commands, at instant kT_s, the error vector at the same instant can be given as:

$$\bar{e}_k = \frac{i^*_{\alpha s,k} - i_{\alpha s,k}}{I_{sn}} + j \frac{i^*_{\beta s,k} - i_{\beta s,k}}{I_{sn}} = e_{i_{\alpha s,k}} + j e_{i_{\beta s,k}} \tag{5.8}$$

where I_{sn} denotes nominal value of stator current. The control target is to make $\bar{e}_k$ very near to zero, and this can be achieved through the appropriate choice of the inverter voltages to be applied to the motor in the next control cycle. Based upon that, the control has to fulfill the condition:

$$|\bar{e}_k| = \sqrt{\left(e_{i_{\alpha s,k}}\right)^2 + \left(e_{i_{\beta s,k}}\right)^2} \leq E_{max} \tag{5.9}$$

where E_{max} is designed for limiting the switching frequency.

When the actual error amplitude $|\bar{e}_k|$ oversteps E_{max} then the MPCC is started for predicting among the eight possible inverter voltage vectors the one that causes a predicted negative error variation, and then it applies it in the next control cycle. Based on this hypothesis, the cost function that will be used by MPCC to select the appropriate voltage vector can be written in one of the following two forms obtained by derivation of (5.9):

$$\Lambda_k = e_{i_{\alpha s,k}}\left(\frac{de_{i_{\alpha s}}}{dt}\right)_k + e_{i_{\beta s,k}}\left(\frac{de_{i_{\beta s}}}{dt}\right)_k < 0 \tag{5.10}$$

$$\Lambda_k = e_{i_{\alpha s,k}}\left(-\frac{di_{\alpha s}}{dt}\right)_k + e_{i_{\beta s,k}}\left(-\frac{di_{\beta s}}{dt}\right)_k < 0 \tag{5.11}$$

In this paper, the second formulation is used. The derivatives of stator current components are obtained by:

$$\left(\frac{di_{\alpha s}}{dt}\right)_k = \frac{1}{L_t}\left[u_{\alpha s,k} - Ri_{\alpha s,k} + \frac{R_{rs}}{L_\varphi}\psi_{\alpha s,k} + \omega_{me,k}(\psi_{\beta s,k} - L_t i_{\beta s,k})\right] \tag{5.12}$$

$$\left(\frac{di_{\beta s}}{dt}\right)_k = \frac{1}{L_t}\left[u_{\beta s,k} - Ri_{\beta s,k} + \frac{R_{rs}}{L_\varphi}\psi_{\beta s,k} - \omega_{me,k}(\psi_{\alpha s,k} - L_t i_{\alpha s,k})\right] \tag{5.13}$$

where $R = \left(R_s + R_{rs}\frac{L_t + L_\varphi}{L_\varphi}\right)$.

Now all terms of cost function (5.11) are available as functions of stator voltage vectors. Then the control can predict the value of (5.11) at instant $(k+1)T_s$, and select the voltage vector that minimize this value and apply it to the motor terminals.

5.3 Operation methodology for Proposed MPCC

To describe the sequence of operations for the proposed MPCC, the process is separated into two phases as follows.

5.3.1 Current Prediction phase

The stator current components are evaluated at instant (k+1) using (5.12) and (5.13) as:

$$\tilde{i}_{\alpha s,k+1} = i_{\alpha s,k} + T_s\left(\frac{di_{\alpha s}}{dt}\right)_k \tag{5.14}$$

$$\tilde{i}_{\beta s,k+1} = i_{\beta s,k} + T_s\left(\frac{di_{\beta s}}{dt}\right)_k \tag{5.15}$$

where accent ~ refers to the predicted values at instant (k+1). Subsequently, the current errors are estimated through (5.8) and condition (5.9) can be then verified.

5.3.2 Optimum voltage selection phase

The selection of an appropriate voltage vector to be applied to the motor terminals is based on the minimization of the cost function given by (5.11). The control predicts its value at instant (k+1) using the predicted values of current errors and derivatives as follows:

$$\tilde{\Lambda}^{i}_{k+1} = \left[e_{i_{\alpha s,k+1}} \left(-\frac{di_{\alpha s}}{dt} \right)_{k+1} + e_{i_{\beta s,k+1}} \left(-\frac{di_{\beta s}}{dt} \right)_{k+1} \right]^{i} \tag{5.16}$$

where derivatives are given by (5.12) and (5.13) as functions of the (k+1) step voltages. Stator fluxes in (k+1) is obtained in a manner like (5.14) and (5.15) utilizing (3.6) and (3.15).

Then at any instant in which the predicted value of the error $|e_{k+1}|$ oversteps the predetermined maximum value of the error E_{max}, the control searches among the eight possible voltage vectors (i=0….7), for the voltage vector that minimizes the value of cost function in (5.16), and will apply this vector to the stator in the next control cycle.

5.4 Sensorless technique

A Luenberger observer (LO) estimates not only the rotor flux vector and mechanical speed but it is also utilized to estimate the stator current and load torque to achieve better dynamic estimation response. Basic equations that describe the operation of the observer are derived from the machine model expressed in stationary reference frame as follows:

$$\left(\frac{d\hat{i}_s}{dt} \right)_k = -R\hat{i}_{s,k} + \frac{L_M}{\sigma L_s L_r} \left(\frac{1}{T_r} - j\hat{\omega}_{me,k} \right) \hat{\psi}_{r,k} + \frac{1}{\sigma L_s} \bar{u}_{s,k} + G\left(\bar{i}_{s,k} - \hat{i}_{s,k} \right) \tag{5.17}$$

$$\left(\frac{d\hat{\psi}_r}{dt} \right)_k = -\frac{L_M}{T_r} \hat{i}_{s,k} - \left(\frac{1}{T_r} - j\hat{\omega}_{me,k} \right) \hat{\psi}_{r,k} \tag{5.18}$$

where $\hat{i}_{s,k}$, $\hat{\psi}_{r,k}$ are the estimated stator current and rotor flux respectively, while G is the matrix of observer gains.

5.4.1 Design of gains

Traditional way to choose the observer's gains is to adjust the observer's poles to be proportional to the IM ones, but this can result in poles with a large imaginary part value, which may negatively affect the stability of the system especially in the high-speed ranges. In addition, the observer's gains have always speed dependent terms that negatively influence the speed estimation process [89], in which the gains matrix is defined as follows:

$$G = \begin{bmatrix} g1 & g2 & g3 & g4 \\ -g2 & g1 & -g4 & g3 \end{bmatrix}^{T} \tag{5.19}$$

The Eigen values of the observer gains calculated by the traditional way are expressed by

$$g1 = \frac{-(k-1)}{(L_s L_r - L_M^2)}(R_s L_r + R_r L_s) \tag{5.20}$$

$$g2 = (k-1)\hat{\omega}_{me} \tag{5.21}$$

$$g3 = (k-1)\frac{(R_r L_s - kR_s L_r)}{L_M} \tag{5.22}$$

$$g4 = \frac{-(k-1)(L_s L_r - L_M^2)\hat{\omega}_{me}}{L_M} \tag{5.23}$$

As can be noticed from (5.21) and (5.23), the observer gains are functions of motor parameters and speed, which negatively affect the stability of the observer, for example at high speed, with large imaginary part, the observer poles will exceeds the stability limit. In addition, at high speed with large imaginary part of the poles, the speed will increase and corrupted with high level of noise, and for avoiding that, the maximum gains value must be limited, and thus maximum attainable speed will be restricted.

At low speed, the observer poles corresponding to slower poles (the poles which are closed to imaginary axis of the complex s-plane), will move slowly causing a sluggish observer response.

Thus, to solve these problems, an effective pole placement method, which gives better performance especially at high-speed via shifting the observer's poles to the left of the motor's poles, with small change in imaginary part of the poles, is used here. The gains are calculated according to the following criteria:

The observer is a closed -loop system, which can be described in a state space form by the following equations:

$$\left(\frac{d\hat{i}_s}{dt}\right)_k = -(A_{11} + G)\hat{i}_{s,k} + A_{12}\hat{\psi}_{r,k} + B_1\bar{u}_{s,k} - G\bar{i}_{s,k} \tag{5.24}$$

$$\left(\frac{d\hat{\psi}_r}{dt}\right)_k = -A_{21}\hat{i}_{s,k} + A_{22}\hat{\psi}_{r,k} \tag{5.25}$$

where

$$A_{11} = -\left[\frac{R_s}{\sigma L_s} + \frac{(1-\sigma)}{\sigma T_r}\right] * I = a_{r11} * I \tag{5.26}$$

$$A_{12} = \frac{L_M}{\sigma L_s L_r}\left[\frac{1}{T_r} * I - \omega_{me} * \dot{I}\right] = a_{r12} * I + a_{i12} * \dot{I} \tag{5.27}$$

$$A_{21} = \frac{L_M}{T_r} * I = a_{r21} * I \tag{5.28}$$

$$A_{22} = \frac{-1}{T_r} * I + \omega_{me} * \dot{I} = a_{r22} * I + a_{i22} * \dot{I} \tag{5.29}$$

, and

$$I = \begin{bmatrix} 1 & 0 \\ 0 & 1 \end{bmatrix}, \dot{I} = \begin{bmatrix} 0 & -1 \\ 1 & 0 \end{bmatrix} \tag{5.30}$$

From (5.24), the observer gains matrix can be expressed by

$$A_{11} + G = \begin{bmatrix} a_{r11} + g1 & -g2 \\ g2 & a_{r11} + g1 \end{bmatrix} \tag{5.31}$$

The relation (5.31) has the following characteristic equations:

$$s^2 - 2(a_{r11} + g1)s + (a_{r11} + g1)^2 + g_2^2 = 0.0 \tag{5.32}$$

$$s^2 + 2\xi\omega_n s + \omega_n^2 = 0.0 \tag{5.33}$$

From (5.32) and (5.33), the natural frequency ω_n and damping coefficient ξ are calculated as follows:

$$\omega_n = \sqrt{g_2^2 + (a_{r11} + g_1)^2} \quad \text{, and} \quad \xi = -\frac{(a_{r11}+g_1)}{\sqrt{g_2^2+(a_{r11}+g_1)^2}} \tag{5.34}$$

From (5.34), it can be realized that the observer gains have a direct effect on observer responses. Thus, through proper selection of these gains, we can arrange the Eigen values of the observer in such a way that the system dynamic response becomes stable and insensitive to motor speed.

From (5.32), the observer poles are computed as follows:

$$s_1 = (a_{r11} + g1) + jg2 \quad \text{, and} \quad s_2 = (a_{r11} + g1) - jg2 \tag{5.35}$$

In practice, the Eigen values of the observer are designed and selected based on the following principles:

- Eigen values have negative real parts to ensure the system stability.
- They are located farther into the left of the complex (s-plane) compared to the Eigen values of the observed system, so that the state of the observer converges rapidly.
- (g1) is negative in order to increase the observer stability. In other words, the real part of the observer poles should be shifted to the left in the complex (s-plane).
- Selecting of g1 and g2 so that $|g2/(a_{r11} + g1)|$ is small, in order to ensure high damping response of the observer.
- The observer gains are always small in order to enhance observer robustness to noise.
- The observer poles should not be placed far to the left from imaginary (jω) axis, because if this happened, the elements of observer gains matrix will become large, and large gains values will make the controller output become large.

Thus, according to these criteria for the pole placement, the gains g1 and g2 are computed as follows:

$$g1 = -k\left[\frac{R_s}{\sigma L_s} + \frac{(1-\sigma)}{\sigma T_r}\right] \quad \text{, and} \quad g2 = k_p \tag{5.36}$$

where k is an arbitrary positive constant, and k_p is an arbitrary value ($\geq$ -1).

In digital simulation and experimentation, the acceptable values for k and k_p were found by trial-and-error to be 0.5.

The Luenberger observer estimates the speed utilizing the Lyapunov's stability criterion, which can be given in the form of

$$\left(\frac{d\hat{\omega}_{me}}{dt}\right)_k = K_1\lambda \tag{5.37}$$

where K_1 is a positive constant, and $\lambda = \left(\bar{\imath}_{s,k} - \hat{\imath}_{s,k}\right) \otimes \hat{\psi}_{r,k}$ is the correction element.

The estimation of speed is required in the prediction stage of stator current components and for closing the speed loop. To improve the speed estimation process, the load torque is also observed and utilized by the speed observer as following.

$$\left(\frac{d\hat{\omega}_{me}}{dt}\right)_k = \frac{p}{J}(\hat{m}_k - \hat{m}_{load}) + K_1\lambda \tag{5.38}$$

$$\left(\frac{d\hat{m}_{load}}{dt}\right)_k = -K_2\lambda \tag{5.39}$$

where $\hat{m}_k$ is the motor torque obtained from observed currents and fluxes according to (5.1), $\hat{m}_{load}$ is the estimated load torque, J is the moment of inertia, and K_2 is a positive constant.

To show the effectiveness of proposed gains calculation procedure, a root locus comparison between traditional gains and new gains is shown in Figure 5.1. It can be noticed that at high speed range, the imaginary term of the proposed observer poles (Figure 5.1.b) are lower than its value that is obtained from traditional gains (Figure 5.1.a), with benefits in the estimation response.

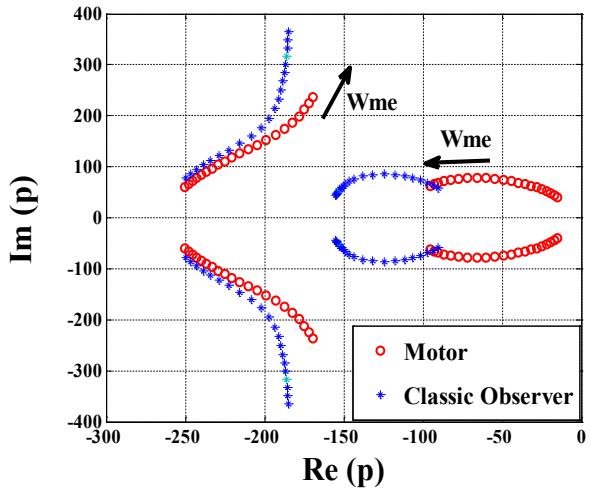

Figure 5.1.a: Classic Luenberger observer

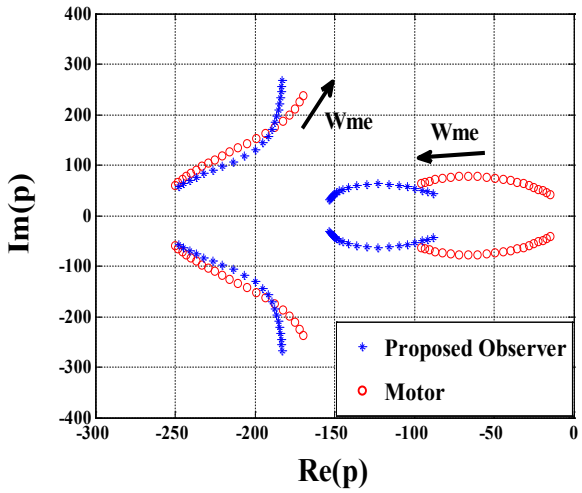

Figure 5.1.b: Proposed Luenberger observer

Figure 5.1: Poles position for different speed values

The overall layout of proposed MPCC drive is shown in Figure 5.2. No existence for PWM voltage control is observed in this configuration. Reference values for stator current components are obtained as described in Sect. 5.2 based on field orientation principle in d-q reference frame, and then transformed to α-β reference frame by using the estimated rotor flux angle $\hat{\theta}_{r,k}$ obtained from Luenberger observer as follows:

$$\hat{\theta}_{r,k} = \text{atan}\,\frac{\text{Im}\left(\hat{\psi}_{r,k}\right)}{\text{Re}\left(\hat{\psi}_{r,k}\right)} \tag{5.40}$$

Figure 5.3 shows the sequence of implementation procedure for the proposed topology and how the voltage vectors are selected. The proposed MPCC enables to investigate the speed effects on overall dynamic performance during different implementation stages (prediction and voltage selection), and this can be an addition which was not presented for predictive current control for induction motor before. To explain clearly, the speed role and estimation suitability are discussed in each stage as follows.

5.4.1.1 Speed role during prediction phase

From (5.12) and (5.13), it is noticed that both derivatives of stator current components include a part dependent on the speed and consequently (5.14) and (5.15) needs the speed to perform the prediction. Prediction step goal is deciding whether the predicted next error amplitude exceed error limit or not. Accuracy of the prediction is important but not crucial and therefore speed prediction by the previous proposed method is appropriated.

5.4.1.2 Speed role during voltage selection phase

According to the proposed procedure, the selection of optimum voltage is based on the minimization of the cost function given in (5.16). It can be reformed after separating the parts in the current derivatives that depend on the speed (apex$^{(\omega)}$) to the other one which are free of speed sample but depend on applied voltages (apex$^{(u)}$) as:

$$\tilde{\Lambda}^{i}_{k+1} = \left[e_{i_{\alpha s,k+1}} \left[\left(\frac{di_{\alpha s}}{dt}\right)^{u} + \left(\frac{di_{\alpha s}}{dt}\right)^{\omega} \right]_{k+1} + e_{i_{\beta s,k+1}} \left[\left(\frac{di_{\beta s}}{dt}\right)^{u} + \left(\frac{di_{\beta s}}{dt}\right)^{\omega} \right]_{k+1} \right]^{i} > 0.0 \tag{5.41}$$

where

$$\left(\frac{di_{\alpha s}}{dt}\right)^{u}_{k+1} = \frac{1}{L_t}\left[u_{\alpha s,k+1} - R i_{\alpha s,k+1} + \frac{R_{rs}}{L_\varphi} \psi_{\alpha s,k+1} \right] \tag{5.42}$$

$$\left(\frac{di_{\alpha s}}{dt}\right)^{\omega}_{k+1} = \frac{1}{L_t}\left[\omega_{me,k+1} (\psi_{\beta s,k+1} - L_t i_{\beta s,k+1}) \right] \tag{5.43}$$

$$\left(\frac{di_{\beta s}}{dt}\right)^{u}_{k+1} = \frac{1}{L_t}\left[u_{\beta s,k+1} - R i_{\beta s,k+1} + \frac{R_{rs}}{L_\varphi} \psi_{\beta s,k+1} \right] \tag{5.44}$$

$$\left(\frac{di_{\beta s}}{dt}\right)^{\omega}_{k+1} = \frac{1}{L_t}\left[-\omega_{me,k+1} (\psi_{\alpha s,k+1} - L_t i_{\alpha s,k+1}) \right] \tag{5.45}$$

After substitution of these terms in the cost function, the form of (5.41) will tend to be as follows:

$$e_{i_{\alpha s,k+1}}\left(\frac{di_{\alpha s}}{dt}\right)^{u}_{k+1}+e_{i_{\beta s,k+1}}\left(\frac{di_{\beta s}}{dt}\right)^{u}_{k+1} > -\left[e_{i_{\alpha s,k+1}}\left(\frac{di_{\alpha s}}{dt}\right)^{\omega}_{k+1}+e_{i_{\beta s,k+1}}\left(\frac{di_{\beta s}}{dt}\right)^{\omega}_{k+1}\right] \tag{5.46}$$

From (5.46), it can be deduced that this condition can be achieved via more than one voltage vector, but the optimum voltage vector that will be selected is that one which minimizes (5.16) or maximize the left side of (5.46). Maximization of the left side does not depend on the speed but only on the applied voltage vector at this instant, and thus the speed has no effect on the voltage selection procedure. This is the reason why in a classical implementation a unique and fixed look-up-table is used.

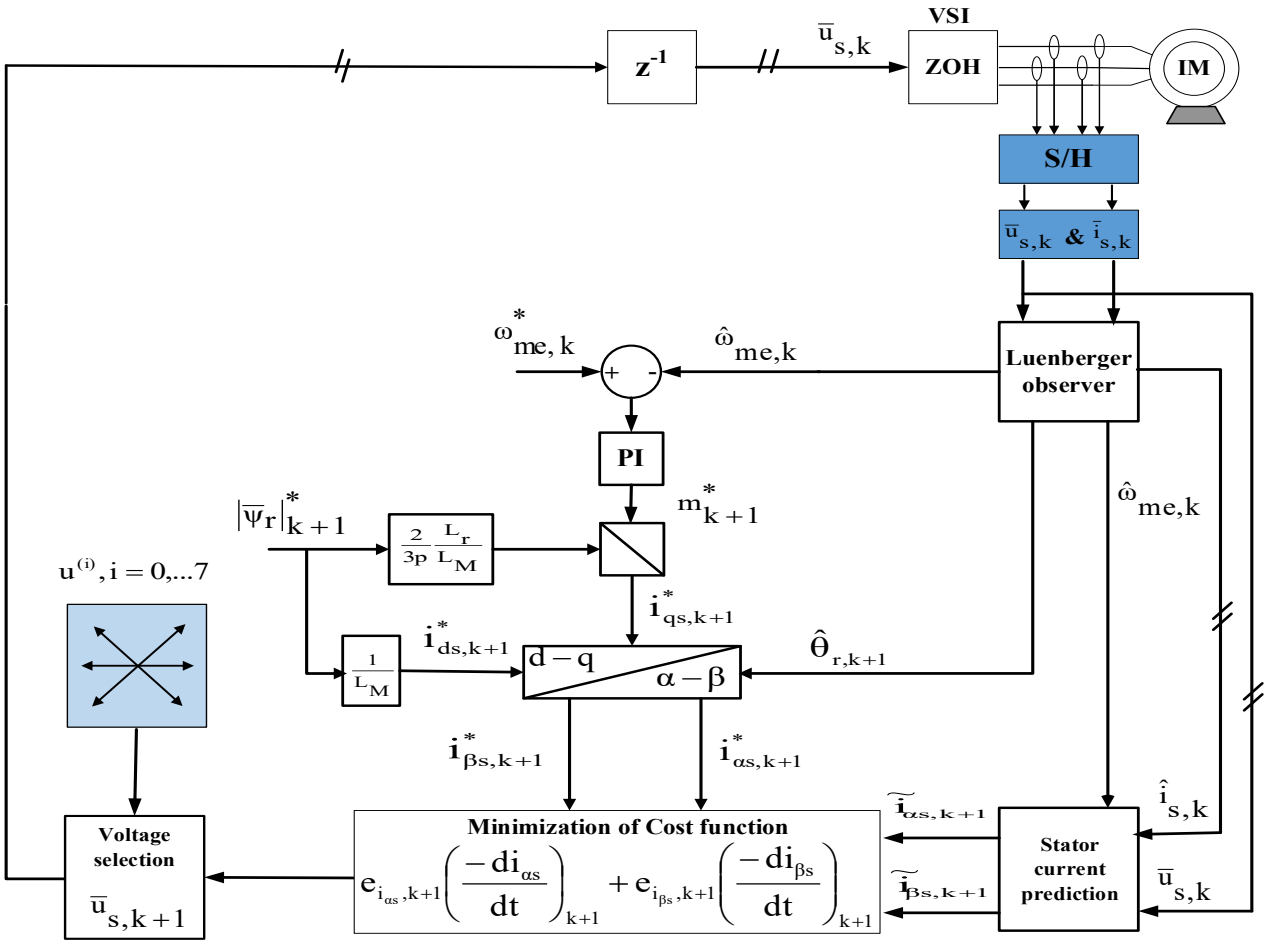

Figure 5.2: System layout for proposed MPCC algorithm

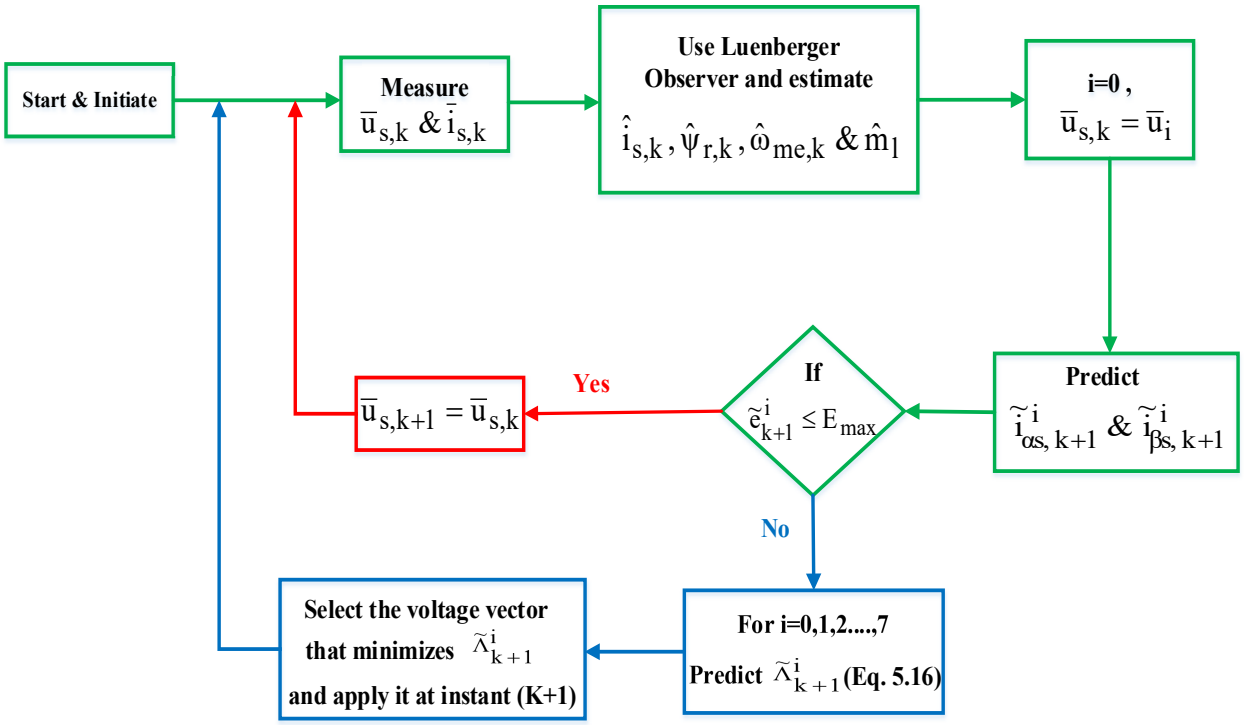

Figure 5.3: Sequence of implementation

From Figure 5.3, it can be noticed that the proposed control procedure fulfils the following four steps:

- **Step 1**: Measuring of input stator voltage $\bar{u}_{s,k}$ and current $\bar{\imath}_{s,k}$, and estimation of speed sample $\hat{\omega}_{me,k}$, rotor flux $\hat{\psi}_{r,k}$, stator current $\hat{\imath}_{s,k}$ and load torque $\hat{m}_l$.
- **Step 2**: Prediction of the stator current (α-β) components for all possible voltage vectors (i=0…..7).
- **Step 3**: Checking the predicted values of stator current components in the cost function given by (5.16).
- **Step 4**: The switching states correspond to the minimum value of cost function are selected in the next sampling time interval to actuate the voltage source inverter.

5.5 Simualtion results

The Matlab/Simulink siftware is firstly used to validate the effectiveness of proposed sensorless MPCC scheme, a speed profile change of (1000 → 800 → 400 → 30 → 400 → 800 → 1000 RPM) at times of (0.0 → 2 → 4 → 6 → 8 → 10 → 12 sec) is applied to the drive. A load torque of 1.5 Nm is applied to the motor at t=3 sec and removed at t=11 sec. The reference value of rotor flux is set to 0.4 Vs. The preset mximum allowable absolute error is tkaen as 0.1. Figure 5.4 illustrate the dynamic behavior of the drive, while Figure 5.5 views the current profiles and control action.

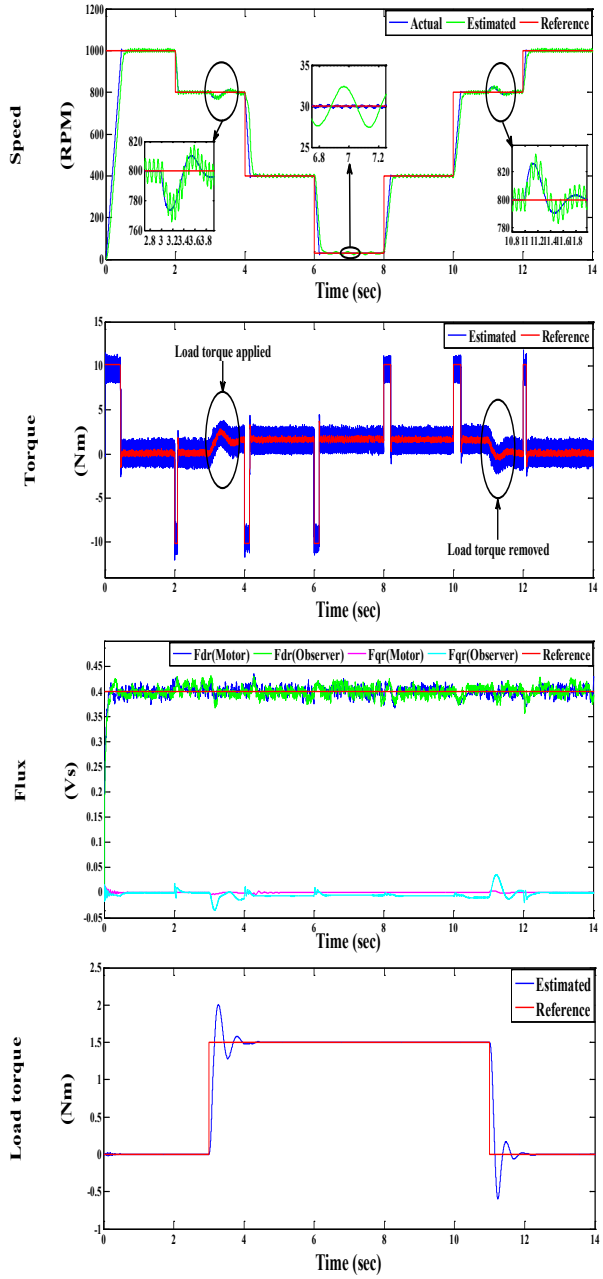

Figure 5.4: IM drive dynamic performance

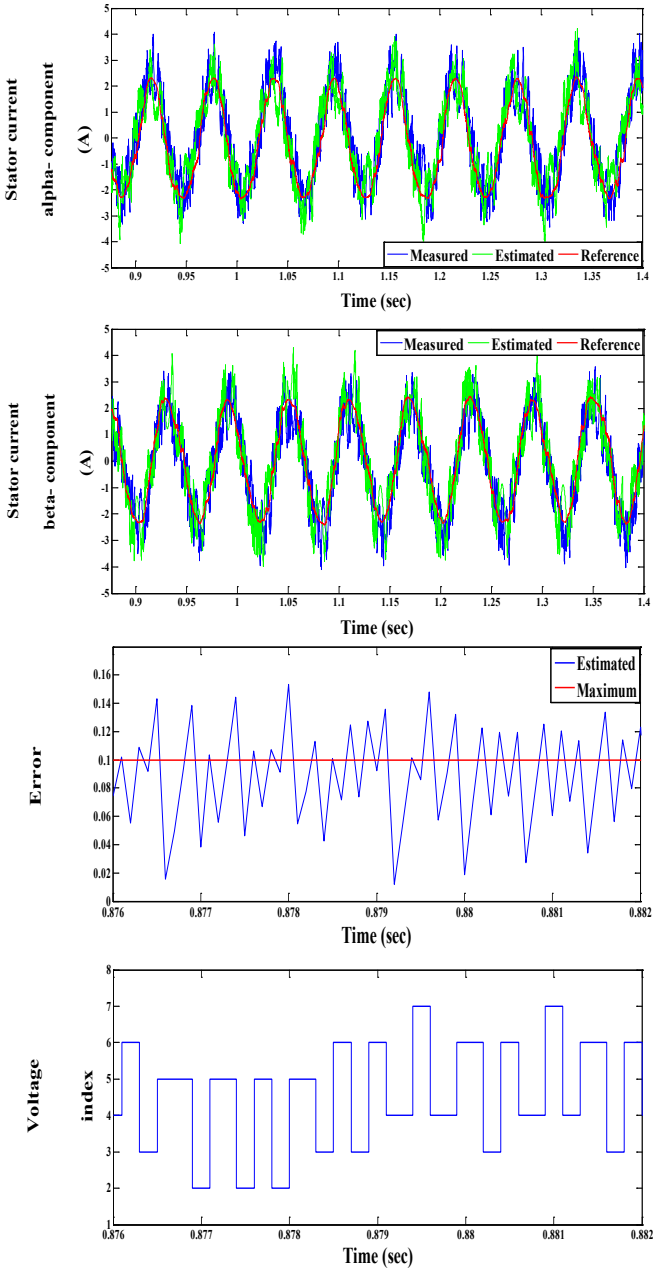

Figure 5.5: Current profiles and control response

As can be noticed from Figure 5.4, that the Luenberger based sensorless technique exhibits an appropriate performance in estimating the speed even at very low speed range (30 RPM). In addition to the speed, the rotor flux components and load torque are also precisely estimated. From Figure 5.5 it can be reported that the proposed Luenberger observer managed in tracking the actual stator current profiles, which consequently improve the overall estimation procedure. The control response can be also observed in the last figure that shows the transition from a voltage index to another at each instant happens that the predicted error exceeds its maximum limit E_{max}. Figure 5.6 illustrates a high matching between the actual and estimate rotor position that confirm the effectiveness of the proposed sensorless approach.

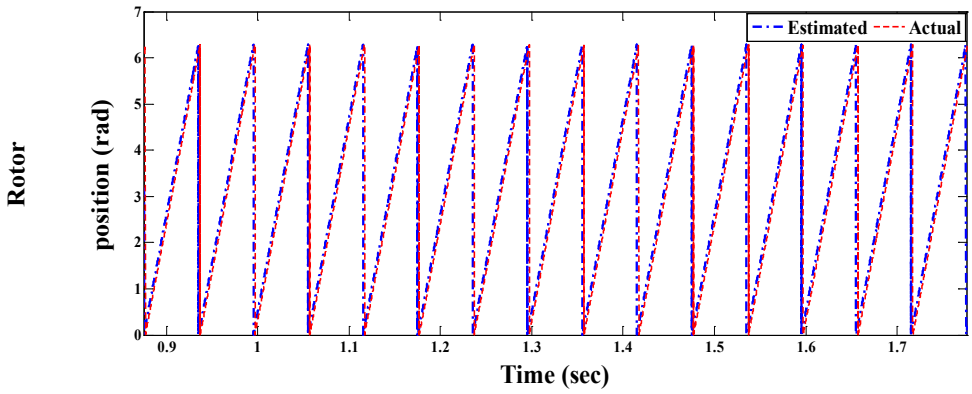

Figure 5.6: Rotor position (simulation)

5.6 Experimental validation

A dSpace 1104 control board is utilized to validate experimentally the effectiveness of the proposed sensorless MPCC. The machine under test is a two poles induction motor with wound rotor topology, the stator terminals are connected to the output of the inverter while the rotor terminals are short-circuited. Overview of the utilized test bench is shown in Figure 5.7. The data specifications for IM drive are given in appendix B.

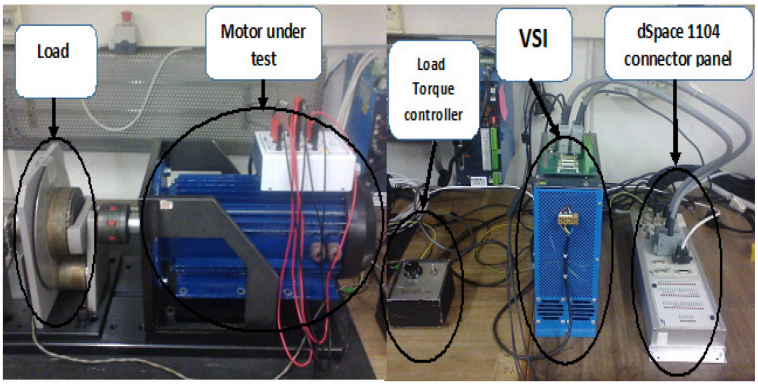

Figure 5.7: Experimental test bench

Obtained experimental results are illustrated in Figures 5.8 and 5.9, the same speed command levels are given for times of (0 → 2→ 6→ 8→ 10→ 12→ 16 sec) , while the load torque is applied and removed at (t=4 sec & t=14 sec), respectively. The rotor flux reference value and error limit E_{max} are the same used in simulation tests. The results confirm the effectiveness of proposed sensorless MPCC scheme that exhibits high dynamic performance for a variety of working speed ranges even at very low one.

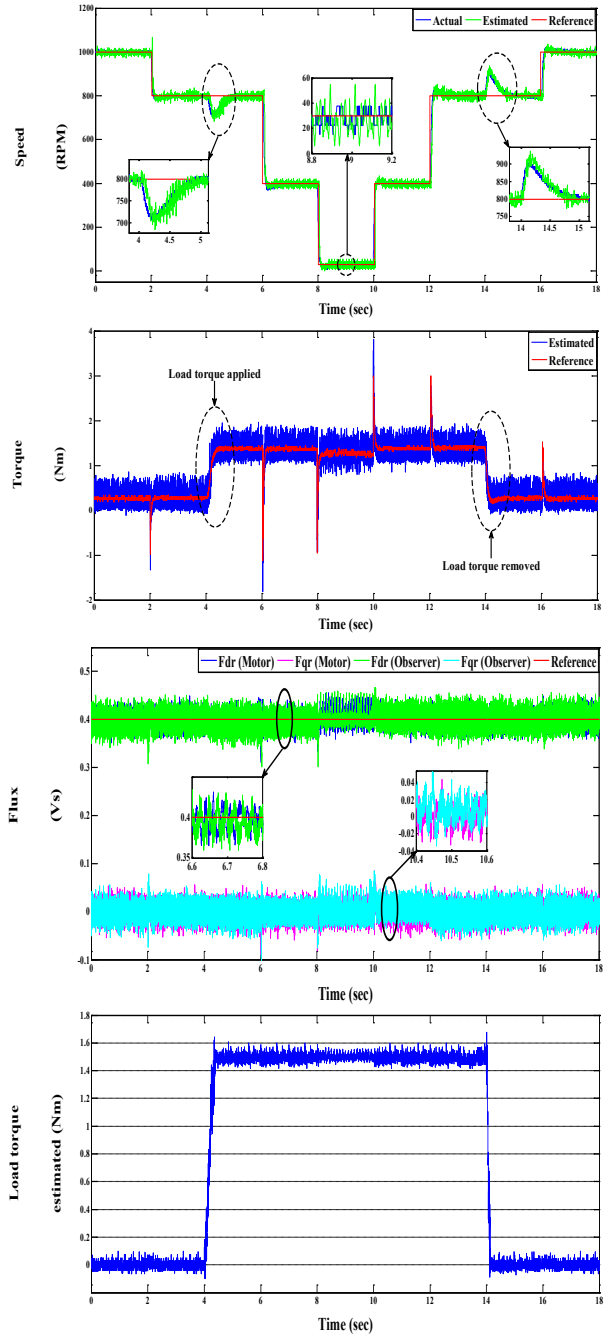

Figure 5.8: Dynamic performance of IM drive

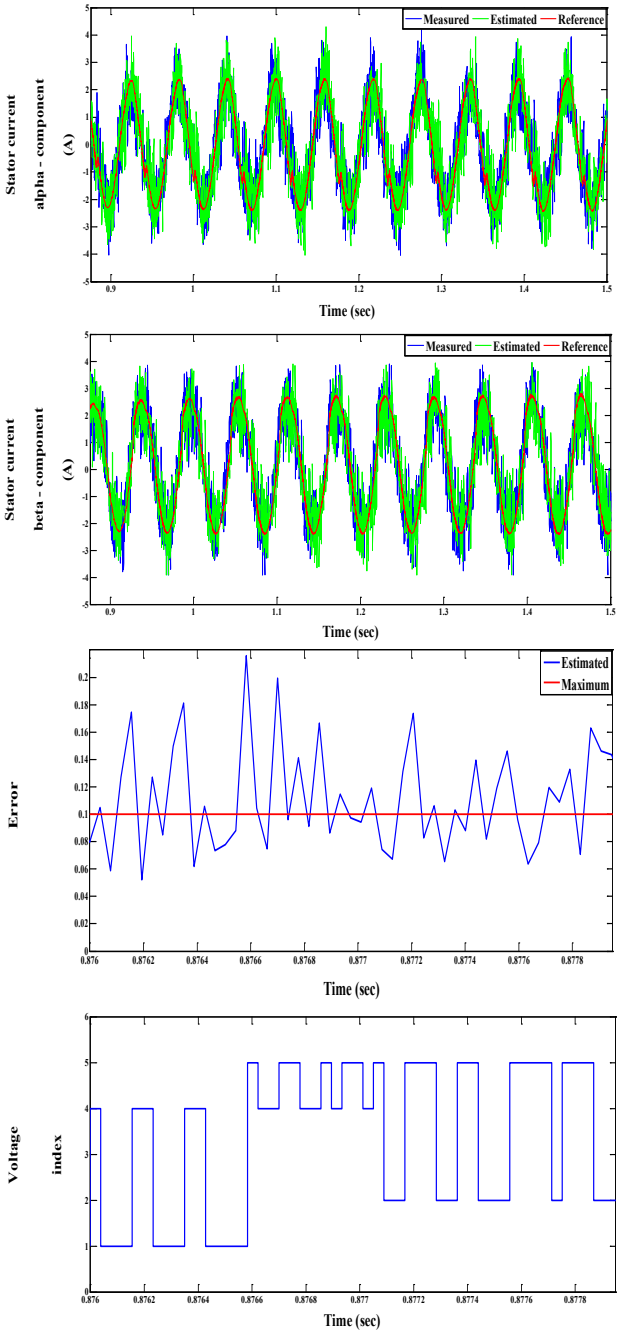

Figure 5.9: Current profiles and control response

The effectiveness of proposed sensorless procedure is also assured through the rotor position profile shown in Figure 5.10. The profiles of estimated rotor flux, load torque and stator current confirm the viability of the proposed control approach, while Figure 5.9 gives a detailed view for the action taken by the controller at each sampling instant.

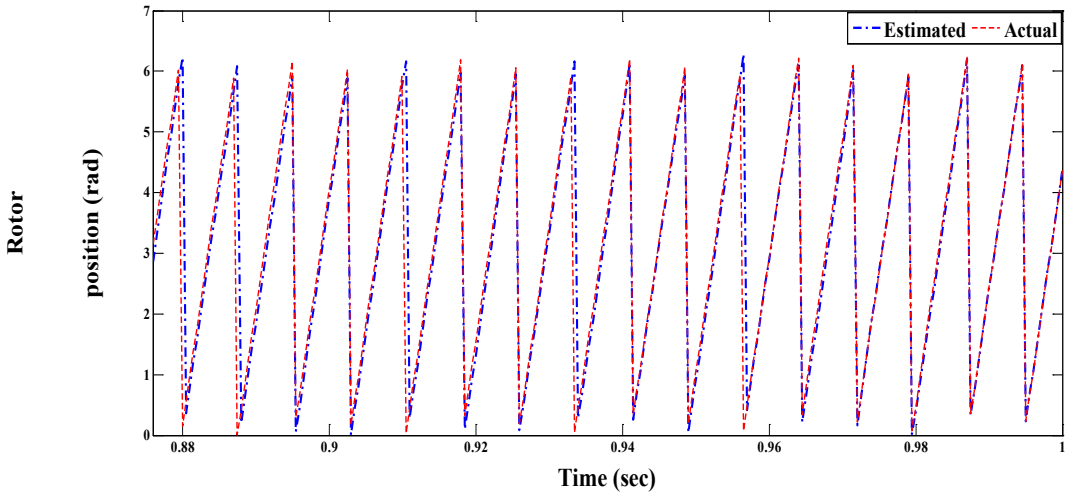

Figure 5.10: Rotor position (experimental)

Chapter 6

Model Predictive Direct Torque Control, Doubly Fed Induction Motor as a Case Study

6.1 Introduction

The doubly fed induction machine (DFIM) presents various advantages in large-power industrial drive applications such as marine propulsion, railway traction, hydroelectric power stations, and metallurgy. It allows a stable operation of the drive both at low speed and at high-speed with sufficient energy efficiency, as well as a rated power of the rotor inverter lower than the rated power of the machine, if starting phase is managed appropriately [90]. DFIM is used because it offers the chance to adapt the power pass into and out of the rotor terminals to acquire a variable speed drive [91, 92]. The DFIM can be controlled from the stator or rotor by different control topologies; field orientation control method can be used to convert the nonlinear and coupled DFIM-mathematical model to a linear model resulting in one definite solution as well as under generating or motoring modes [91-98].

Various techniques of DTC for doubly fed induction machines have been adopted [99, 100, 101, 102, and 103]. Some of them have introduced the principles of the topic; the majority of the others are concerned with implementation variants, dedicated to solve specific problems, and mainly based on the transposition of the DTC applied to squirrel cage IMs. In addition, effects of digital implementation are not always deeply investigated and well managed.

For this purpose, this chapter concerns with a doubly fed induction motor (DFIM) as a case study for implementing an extended topology for the proposed MP DTC presented in Sect. 3.2 . The control topology considers its digital implementation and exploits the finite set of voltages delivered by an inverter thus avoiding the need of a PWM switching control. An effective sensorless procedure is also presented to get a robust drive performance for a wide range of speed change. The striking advantage of the proposed sensorless algorithm is that there is no need for computing or estimating the flux directly or indirectly, as reported by several studies earlier.

6.2 Complete system configuration

Figure 6.1 shows a basic layout of the proposed MP DTC control scheme for the DFIM drive. The machine may be modelled as an induction machine having a 3-phase constant-voltage, constant-frequency supply on the stator

and three-phase voltage source inverter (VSI) supplying the rotor. The rotor circuit is connected by slip rings to the rotor VSI, while stator terminals are fed directly from the power grid. The rotor VSI is controlled according to the proposed MP DTC formulation for tracking the demanded torque and rotor flux level. The reference value of rotor flux is derived in a systematic manner to achieve an optimal exploitation of the machine capabilities, and it will be presented in Sect. 6.5.

The rotor side acts as the power-managing unit, adjusting the power flow through the system [104]. For example, when the machine is rotating at a speed below the synchronous speed, a small part of power is taken from the system through the rotor terminals so that the power enters the system via the stator terminals is stabilized by the power extracted from both mechanical shaft and rotor circuit. In the same manner, when the speed rises above the synchronous speed, a small part of power is inserted to the system through the rotor terminals.

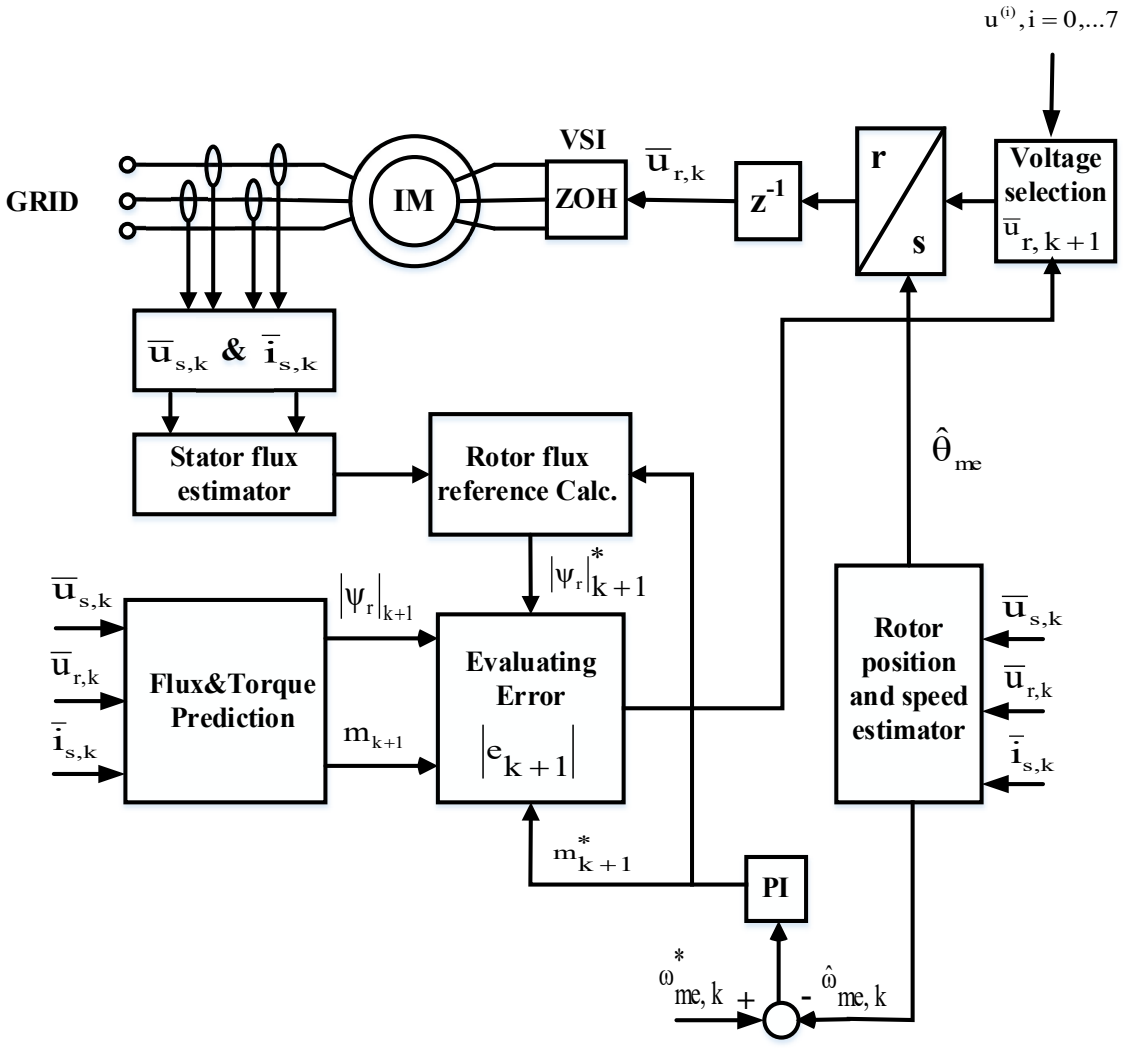

Figure 6.1: Complete System Configuration for proposed MP DTC for DFIM drive

6.3 Theoretical approach

The proposed model predictive direct torque control (MP DTC) is described in a discrete time form. It performs the control of the torque m_k and the rotor flux vector module $|\psi_{r,k}|$ of the machine. According to the analysis of control procedure presented in Sect. 3.2 , when the absolute error goes outside the predefined hysteresis limit, the way to reduce it is to choose a voltage vector that causes a negative derivative of the error amplitude as:

$$\frac{d|\bar{e}_k|}{dt} = \frac{d\sqrt{e_{m,k}^2 + (w_f'')^2\, e_{|\psi r|,k}^2}}{dt} = \frac{e_{m,k}\left(\frac{de_m}{dt}\right)_k + w_f'''\, e_{|\psi r|,k}\left(\frac{de_{|\psi r|}}{dt}\right)_k}{|\bar{e}_k|} < 0 \tag{6.1}$$

The cost function to be utilized by the control system is one of the following two formulations that have been derived from (6.1) as :

$$\Lambda_k = e_m\left(\frac{de_m}{dt}\right)_k + w_f''' w_f e_{|\psi r|,k}\left(\frac{de_{|\psi r|}}{dt}\right)_k \tag{6.2}$$

, and

$$\Lambda_k = -e_{m,k}\left(\frac{d(m/M_n)}{dt}\right)_k - w_f''' e_{|\psi r|,k}\left(\frac{d(|\psi_r|/\Psi_{rn})}{dt}\right)_k < 0 \tag{6.3}$$

In the proposed MP DTC scheme shown in Figure 6.1, the second formulation is used. The control procedure selects the voltage vector that will produce torque and rotor flux variations that reduce $|\bar{e}_k|$, anytime it exceeds the limit. More than one voltage vector may fulfill the cost function (convergence condition), and therefore a criterion of selection will be given in the following sections.

6.4 Mathematical Model of DFIM

In order to apply the proposed control algorithm, an appropriate DFIM discrete model can be carried out. The five parameter equivalent circuit of DFIM shown in Figure 6.2 is used in which all parameters are referred to the stator side. Voltage and current space vectors with superscript ‘’s’’ are defined in the stationary α-β stator reference frame while superscript ‘’r’’ is for those defined in the rotor reference frame.

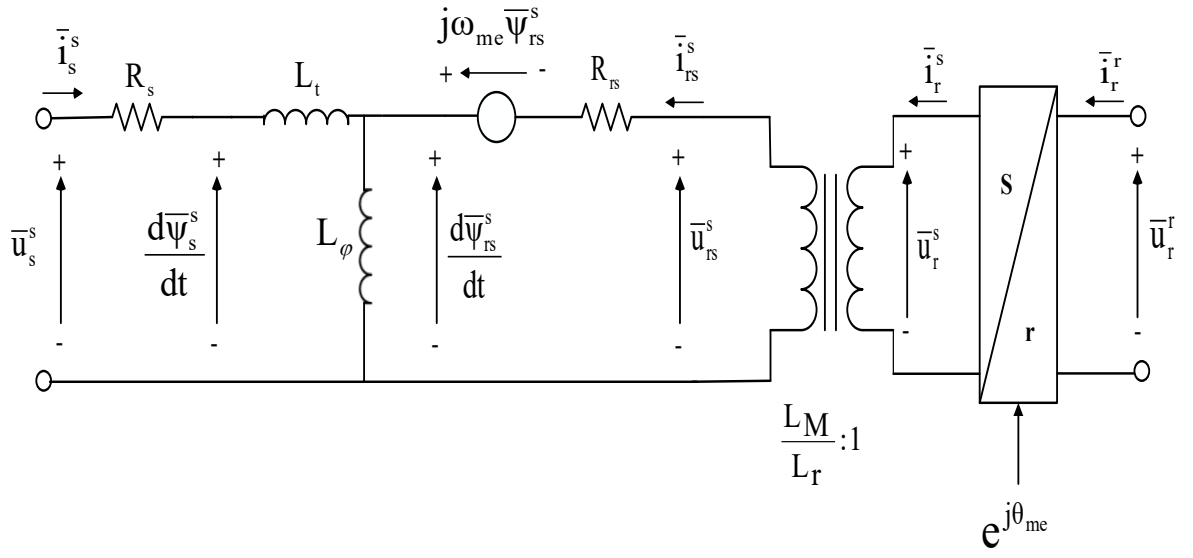

Figure 6.2: Space vector equivalent circuit of DFIM in stationary reference frame

One can realize from Figure 6.2 that, from the electrical point of view, the DFIM is a two state system. Stator and rotor fluxes are adopted hereafter as state variables and then from Figure 6.2 the state equations in the sampling time kT_s can be written as

$$\left(\frac{d\bar{\psi}^s_s}{dt}\right)_k = \bar{u}^s_{s,k} - R_s\bar{i}^s_{s,k} \tag{6.4}$$

$$\left(\frac{d\bar{\psi}^s_{rs}}{dt}\right)_k = \bar{u}^s_{rs,k} - R_{rs}\bar{i}^s_{rs,k} + j\omega_{me,k}\bar{\psi}^s_{rs,k} \tag{6.5}$$

Where

$$\bar{i}^s_{rs,k} = \bar{i}^s_{r,k}(L_r/L_M) \tag{6.6.a}$$

$$\bar{\psi}^s_{rs,k} = \bar{\psi}^s_{r,k}(L_M/L_r) \tag{6.6.b}$$

$$\bar{u}^s_{rs,k} = \bar{u}^s_{r,k}(L_M/L_r) \tag{6.6.c}$$

, and voltage

$$\bar{u}^s_{r,k} = \bar{u}^r_{r,k}e^{j\theta_{me}} \tag{6.6.d}$$

in which $\bar{u}^r_{r,k}$ is the output voltage of the rotor's inverter.
In the Figure 6.2 , the parameters R_{rs}, L_φ, L_t are calculated in the same way presented in Sect. 3.3.

The flux-current relationships can be expressed by

$$\bar{\psi}^{s}_{s,k} = (L_t + L_\varphi)\bar{\imath}^{s}_{s,k} + L_\varphi \bar{\imath}^{s}_{rs,k} = \bar{\psi}^{s}_{rs,k} + L_t \bar{\imath}^{s}_{s,k} \tag{6.7}$$

$$\bar{\psi}^{s}_{rs,k} = L_\varphi \, (\bar{\imath}^{s}_{s,k} + \bar{\imath}^{s}_{rs,k}) \tag{6.8}$$

From (6.5) and (6.8), and after some manipulations (6.5) can be replaced with the following equation,

$$\left(\frac{d\bar{\psi}^{s}_{rs}}{dt}\right)_k = \bar{u}^{s}_{rs,k} + R_{rs}\bar{\imath}^{s}_{s,k} - \frac{R_{rs}}{L_\varphi}\bar{\psi}^{s}_{rs,k} + j\omega_{me,k}\bar{\psi}^{s}_{rs,k} \tag{6.9}$$

Equations (6.4) and (6.9) constitute the state space model that describes the dynamic operation of the motor. Control variables are the stator and rotor voltages, while stator current is a measurable quantity, related to the states by (6.7) and (6.8).
Subsequently motor torque can be then calculated by

$$m_k = 1.5\, p \frac{1}{L_t} \operatorname{Im}\left(\breve{\psi}^{s}_{rs,k}\, \bar{\psi}^{s}_{s,k}\right) \tag{6.10}$$

From (6.10) the derivative for the torque results as

$$\left(\frac{dm}{dt}\right)_k = 1.5\, p \, \frac{1}{L_t} \operatorname{Im}\left(\frac{d\breve{\psi}^{s}_{rs,k}}{dt}\bar{\psi}^{s}_{s,k} + \breve{\psi}^{s}_{rs,k}\frac{d\bar{\psi}^{s}_{s,k}}{dt}\right) \tag{6.11}$$

Similarly, from (6.5) the derivative for the rotor flux module can be expressed by:

$$\left(\frac{d|\bar{\psi}^{s}_{rs}|}{dt}\right)_k = \frac{1}{|\bar{\psi}^{s}_{rs,k}|}\left(\psi^{s}_{\alpha rs,k}\frac{d\psi^{s}_{\alpha rs,k}}{dt} + \psi^{s}_{\beta rs,k}\frac{d\psi^{s}_{\beta rs,k}}{dt}\right) \tag{6.12}$$

where derivatives in (6.11) and (6.12) are given in terms of spatial voltage vectors by (6.4) and (6.9).
At this stage, all derivatives terms of torque and rotor flux consequent of each possible spatial inverter voltage vector can be evaluated and then applied to evaluate the cost function (6.3).

6.5 Implementation steps

To describe the control procedure, let's suppose that the drive is running in interval k-th from sampling time kT_s to time $(k+1)T_s$, fed by voltages $\bar{u}_{s,k}$ and $\bar{u}_{r,k}$ as shown in Figure 6.3.

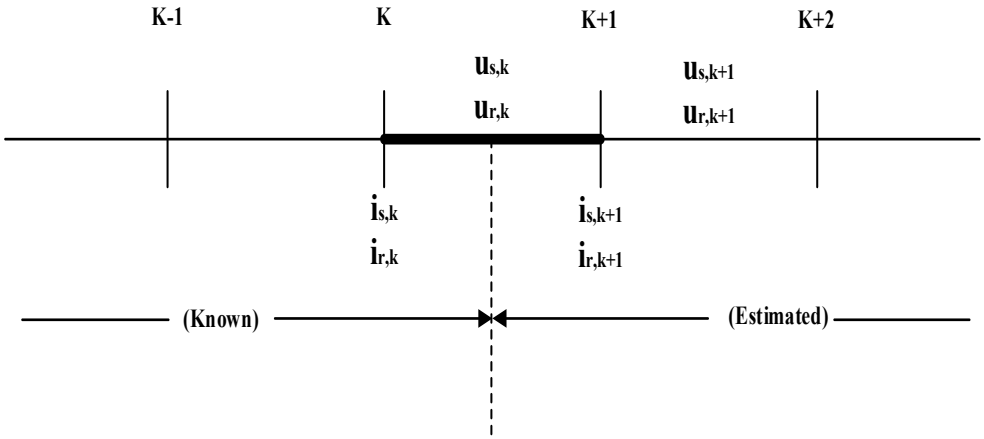

Figure 6.3: Control variables at different sampling intervals

In a systematic manner, the implementation is divided to steps, the first in which the predicted values at instant (k+1) of the stator and rotor fluxes can be derived by applying (6.4) and (6.9) resulting in:

$$\tilde{\bar{\psi}}^{s}_{s,k+1} = \bar{\psi}^{s}_{s,k} + T_s\left(\frac{d\bar{\psi}^{s}_{s}}{dt}\right)_k \tag{6.13}$$

$$\tilde{\bar{\psi}}^{s}_{rs,k+1} = \bar{\psi}^{s}_{rs,k} + T_s\left(\frac{d\bar{\psi}^{s}_{rs}}{dt}\right)_k \tag{6.14}$$

where accent ~ is for predicted vectors.

In (6.14) the stator flux in kT_s comes from the previous prediction step. For the sake of reliability of the control algorithm, a low-pass filter can be used instead of the pure integration process given by the first of (6.14), taking advantage from the fixed frequency of the integrated (grid) quantities.

Instead, the rotor flux in kT_s comes from the second equality in (6.7) and then it is partially related to the measured motor quantities.

Using (6.10) and (6.11), the torque at instant (k+1) is also predicted, and then the error is calculated and finally (6.1) can be utilized.

The next step in implementation is the voltage vectors selection, in this stage the algorithm predicts the value of Λ_{k+1} utilizing (6.3) (where the derivatives are obtained applying (6.4), (6.9), (6.11) and (6.12) in (k+1)) for each of the base spatial vectors provided by the rotor inverter:

$$\tilde{\Lambda}^{i}_{k+1} = \left[\tilde{e}_{m,k+1}\left(\frac{\widetilde{de_m}}{dt}\right)_{k+1} + w_f'''\tilde{e}_{|\psi_r|,k+1}\left(\frac{\widetilde{de_{|\psi|}}}{dt}\right)_{r,k+1}\right]^{i} \tag{6.15}$$

where i=0,…,7 refers to the voltage vector index.

The control system will select the appropriate voltage vector that minimizes the value of convergence condition $\widetilde{\Lambda}^{i}_{k+1}$, (higher negative value), and will apply this vector to the rotor terminals of the machine in the next control interval.

In spite of its denomination, a DFIM is really a synchronous machine in which synchronization of the rotor poles with those of the stator is obtained by coordinating rotor current phase angle with rotor position. Therefore, rotor position is required for a tight control of the machine as can be realized by Figure 6.2 where rotor position appears in the rotor side equivalent circuit. The knowledge of the speed is also required for the speed loop and for the MP DTC procedure within the calculation steps of prediction and voltage selection. A solution for estimating the rotor speed (for speed loop) and position is proposed in the following section. As far as DTC is concerned, it has been found that accuracy of the estimated speed is adequate for the prediction step too, while voltage selection step can be rearranged to be performed without speed information and this is proofed analytically in Sect. 6.6.

6.6 Sensorless algorithm

The stator current $\bar{\imath}_{s,k}$, the rotor current $\bar{\imath}_{r,k}$ and the stator voltage $\bar{u}_{s,k}$, are used for the estimation of rotor position and speed. The spatial distribution of the rotor current vector in different frames of reference is shown in Figure 6.4.

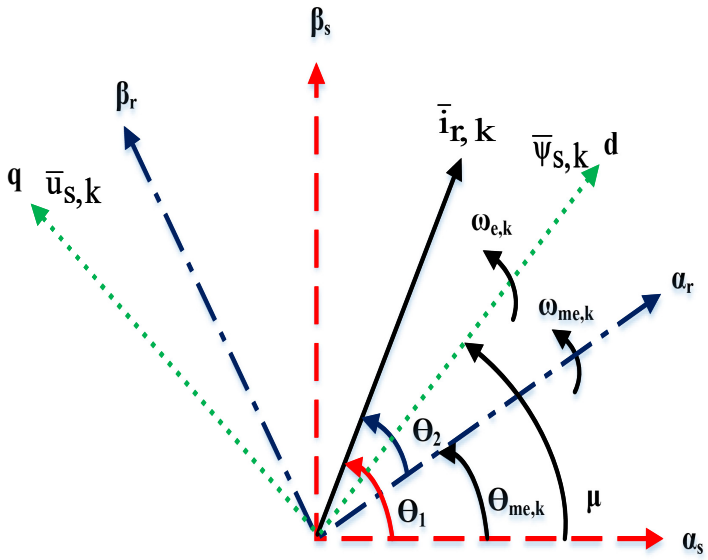

Figure 6.4: Spatial distribution of rotor current vector in different reference frames

The total stator voltage vector $\bar{u}_{s,k}$ is chosen to be aligned with the q-axis in the synchronous reference frame (i.e. $u_{qs,k} = \bar{u}_{s,k}$ and $u_{ds,k} = 0$). This implies further that the stator magnetizing flux can be considered to be

aligned with d-axis (in quadrature with $\bar{u}_{s,k}$ vector), assuming the stator resistance drop to be negligible. In addition, the reference axes for the rotor reference frame are as indicated in Figure 6.4.

The rotor current space vector $\bar{\imath}_{r,k}$ makes an angle θ_1 with respect to the α_s- axis of stator reference frame and an angle θ_2 with respect to the α_r- axis of rotor reference frame. Hence, the difference of angles θ_1 and θ_2 gives the required rotor position $\theta_{me,k}$ information. The estimation algorithm is explained in a systematic manner as follows:

6.6.1 Step 1 (in rotor reference frame)

Since the rotor winding currents can be measured, the (α_r_β_r) components of rotor current $\bar{\imath}^r_{r,k}$ in rotor reference frame can be computed using the abc to (α _ β) transformation. From these, $\sin\theta_2$ and $\cos\theta_2$ can be computed as:

$$\sin\theta_2 = \frac{i^r_{\alpha r,k}}{|\bar{\imath}^r_{r,k}|} \tag{6.16}$$

$$\cos\theta_2 = \frac{i^r_{\beta r,k}}{|\bar{\imath}^r_{r,k}|} \tag{6.17}$$

6.6.2 Step 2 (in stationary reference frame)

The rotor current co-ordinates in the stationary reference frame $i^s_{\alpha r,k}$ and $i^s_{\beta r,k}$ can be computed in an implicit manner without the need for stator flux estimation. The procedure is based on analytical substitutions for the resolved flux components in terms of measureable stator and rotor quantities. Thus, the scheme eliminates the need for computing or estimating the stator flux.

The rotor current components in the stationary reference frame can be computed by

$$i^s_{\alpha r,k} = \frac{\psi^s_{\alpha s,k} - L_s i^s_{\alpha s,k}}{L_M} \tag{6.18}$$

$$i^s_{\beta r,k} = \frac{\psi^s_{\beta s,k} - L_s i^s_{\beta s,k}}{L_M} \tag{6.19}$$

At this stage, the resolved components of the stator flux can be written in terms of other known variables. From the machine basics, the stator voltage components in the stationary reference frame can be expressed as

$$u^s_{(\alpha,\beta)s,k} = R_s i^s_{(\alpha,\beta)s,k} + \frac{d\psi^s_{(\alpha,\beta)s,k}}{dt} \tag{6.20}$$

Since the total stator magnetizing flux is along the d-axis in the synchronous reference frame, the components of stator flux in the stationary reference frame can be expressed as

$$\psi^{s}_{\alpha s,k} = \left|\bar{\psi}^{s}_{s,k}\right| \sin\mu \tag{6.21}$$

$$\psi^{s}_{\beta s,k} = \left|\bar{\psi}^{s}_{s,k}\right| \cos\mu \tag{6.22}$$

Since the stator flux and the angle μ are function of time 't ', differentiating the stator flux components (6.21) and (6.22) with respect to time gives

$$\frac{d\psi^{s}_{\alpha s,k}}{dt} = \frac{d|\bar{\psi}^{s}_{s,k}|}{dt}\sin\mu + \left|\bar{\psi}^{s}_{s,k}\right|\cos\mu\frac{d\mu}{dt} = \frac{d|\bar{\psi}^{s}_{s,k}|}{dt}\sin\mu + \psi^{s}_{\beta s,k}\omega_{e,k} \tag{6.23}$$

$$\frac{d\psi^{s}_{\beta s,k}}{dt} = \frac{d|\bar{\psi}^{s}_{s,k}|}{dt}\cos\mu + \left|\bar{\psi}^{s}_{s,k}\right|(-\sin\mu)\frac{d\mu}{dt} = \frac{d|\bar{\psi}^{s}_{s,k}|}{dt}\cos\mu - \psi^{s}_{\alpha s,k}\omega_{e,k} \tag{6.24}$$

where $\omega_{e,k}$ is the angular velocity of the stator magnetizing flux. In (6.23) and (6.24) above, the first term involving the time derivative of the stator flux magnitude can be considered negligible under normal grid conditions.

Considering the stator flux variation, time derivative of the stator flux magnitude in the first term in (6.23) and (6.24) can be written as

$$\frac{d|\bar{\psi}^{s}_{s,k}|}{dt} = \frac{d}{dt}\left|L_s\bar{i}^{s}_{s,k} + L_M\bar{i}^{s}_{r,k}\right| = L_s\frac{d|\bar{i}^{s}_{s,k}|}{dt} + L_M\frac{d|\bar{i}^{s}_{r,k}|}{dt} \tag{6.25}$$

Since the magnitudes of both stator and rotor current are known (measurable), the time derivatives of the stator flux components $\psi^{s}_{\alpha s,k}$ and $\psi^{s}_{\beta s,k}$ as in (6.23) and (6.24) can be precisely computed. Thus, the proposed estimation algorithm allows for the stator flux variation also.

Using the result of (6.23) and (6.24) in (6.20) gives

$$u^{s}_{\alpha s,k} = R_s i^{s}_{\alpha s,k} + \omega_{e,k}L_s i^{s}_{\beta s,k} + \omega_{e,k}L_M i^{s}_{\beta r,k} \tag{6.26}$$

$$u^{s}_{\beta s,k} = R_s i^{s}_{\beta s,k} - \omega_{e,k}L_s i^{s}_{\alpha s,k} - \omega_{e,k}L_M i^{s}_{\alpha r,k} \tag{6.27}$$

By rearranging the terms in (6.26) and (6.27), we obtain

$$i^{s}_{\alpha r,k} = \frac{-u^{s}_{\beta s,k} + R_s i^{s}_{\beta s,k} - \omega_{e,k}L_s i^{s}_{\alpha s,k}}{\omega_{e,k}L_M} \tag{6.28}$$

$$i^{s}_{\beta r,k} = \frac{u^{s}_{\alpha s,k} - R_s i^{s}_{\alpha s,k} - \omega_{e,k}L_s i^{s}_{\beta s,k}}{\omega_{e,k}L_M} \tag{6.29}$$

As against (6.18) and (6.19), the (6.28) to (6.29) are seemed to be free of the stator flux terms and contain only the stator voltage and current components in the stationary reference frame which are measureable.

The only other unknown term in (6.28) and (6.29) is the angular velocity of the stator magnetizing flux $\omega_{e,k}$ which can be computed from the measured supply voltage $\bar{u}^s_{s,k}$ as follows:

$$\sin\mu = \frac{u^s_{\alpha s,k}}{|\bar{u}^s_{s,k}|} \tag{6.30}$$

$$\cos\mu = \frac{u^s_{\beta s,k}}{|\bar{u}^s_{s,k}|} \tag{6.31}$$

Hence,
$$\omega_{e,k} = \cos\mu \frac{d\sin\mu}{dt} - \sin\mu \frac{d\cos\mu}{dt} \tag{6.32}$$

From (6.28) and (6.29), the position of rotor current vector in the stationary reference frame can be computed as

$$\sin\theta_1 = \frac{i^s_{\alpha r,k}}{|\bar{i}^s_{r,k}|} \tag{6.33}$$

$$\cos\theta_1 = \frac{i^s_{\beta r,k}}{|\bar{i}^s_{r,k}|} \tag{6.34}$$

6.6.3 Step 3 (estimation of rotor position)

From Sects. 6.6.1 and 6.6.2 , the rotor position ($\hat{\theta}_{me,k} = \theta_1 - \theta_2$) can be obtained in terms of sine and cosine. Knowing the unit vectors $\sin\theta_2$, $\cos\theta_2$, $\sin\theta_1$ and $\cos\theta_1$, the rotor position unit vectors $\sin\hat{\theta}_{me,k}$ and $\cos\hat{\theta}_{me,k}$ can be expressed as

$$\sin\hat{\theta}_{me,k} = \sin\theta_1\cos\theta_2 - \cos\theta_1\sin\theta_2 \tag{6.35}$$

$$\cos\hat{\theta}_{me,k} = \cos\theta_1\cos\theta_2 + \sin\theta_1\sin\theta_2 \tag{6.36}$$

Subsequently, the rotor speed $\hat{\omega}_{me,k}$ can be estimated by using the following formulation

$$\hat{\omega}_{me,k} = \cos\hat{\theta}_{me,k} \frac{d\sin\hat{\theta}_{me,k}}{dt} - \sin\hat{\theta}_{me,k} \frac{d\cos\hat{\theta}_{me,k}}{dt} \tag{6.37}$$

The differential terms in (6.37), which contribute to some noise, can be eliminated by employing a first-order low-pass filter.

6.6.4 Sensitivity to parameters variation

To check the parameter sensitivity of the proposed rotor position estimator, the machine parameters employed in the estimator such as the stator resistance, the stator self-inductance or the magnetizing inductance are varied from their original values. As explained in the previous section, the estimator makes use of the measured rotor current in the rotor reference frame $\vec{i}^{r}_{r,k}$ and the estimated rotor current in the stator reference frame $\vec{i}^{s}_{r,k}$. Thus, the effect of any mismatch in the machine parameters in the estimator has no effect on the measured rotor current but can lead to an error in the estimated rotor current and subsequently to an error in the estimated rotor position. These errors can be evaluated considering a mismatch in the stator resistance R_s and the magnetizing inductance L_M considering one at a time.

Considering the mismatch in stator resistance R_s alone, the change in estimated rotor current $\vec{i}^{s}_{r,k}$ can be written by utilizing (6.28) and (6.29) as follows,

$$\Delta i^{s}_{\alpha r,k} = \left(\frac{\Delta R_s}{\omega_{e,k} L_M}\right) i^{s}_{\beta s,k} \tag{6.38}$$

$$\Delta i^{s}_{\beta r,k} = \left(\frac{-\Delta R_s}{\omega_{e,k} L_M}\right) i^{s}_{\alpha s,k} \tag{6.39}$$

Similarly, considering the mismatch in magnetizing inductance L_M alone, the change in the estimated rotor current can be written as

$$\Delta i^{s}_{\alpha r,k} = \left(\frac{-R_s \Delta L_M}{\omega_{e,k} L_M^2}\right) i^{s}_{\beta s,k} + \left(\frac{\Delta L_M}{\omega_{e,k} L_M^2}\right) u^{s}_{\beta s,k} + \left(\frac{L_{ls} \Delta L_M}{L_M^2}\right) i^{s}_{\alpha s,k} \tag{6.40}$$

$$\Delta i^{s}_{\beta r,k} = \left(\frac{-\Delta L_M}{\omega_{e,k} L_M^2}\right) u^{s}_{\alpha s,k} + \left(\frac{R_s \Delta L_M}{\omega_{e,k} L_M^2}\right) i^{s}_{\alpha s,k} + \left(\frac{L_{ls} \Delta L_M}{L_M^2}\right) i^{s}_{\beta s,k} \tag{6.41}$$

From (6.38) to (6.41), since the multiplier term in the numerator (ΔR_s or ΔL_M) is much smaller compared with the denominator ($\omega_{e,k} L_M$ or $\omega_{e,k} L_M^2$), thus the current variations $\Delta i^{s}_{\alpha r,k}$ and $\Delta i^{s}_{\beta r,k}$ can be regarded as small. Further, the new angle θ_1 is calculated as

$$\theta_1 = \tan^{-1}\left(\frac{i^{s}_{\alpha r,k} + \Delta i^{s}_{\alpha r,k}}{i^{s}_{\beta r,k} + \Delta i^{s}_{\beta r,k}}\right) \cong \tan^{-1}\left(\frac{i^{s}_{\alpha r,k}}{i^{s}_{\beta r,k}}\right) \tag{6.42}$$

Thus, the deviation in the calculation of angle θ_1 is negligible even though there is a small mismatch in the machine parameters in the estimator. Hence, the deviation in the estimated rotor position, which is the difference between angles θ_1 and θ_2, is small. For validation, numerical simulations using Matlab/Simulink and experimental tests are carried out to verify the effect of machine parameter variations in the estimation algorithm in the following sections.

6.7 Optimum flux reference

The torque of DFIM can be given as a function of the angle φ between the stator and rotor fluxes space vectors as follows:

$$m_k = 1.5\ p\ \frac{L_M}{б}\left|\bar{\psi}^s_{r,k}\right|\left|\bar{\psi}^s_{s,k}\right| \sin\varphi \tag{6.43}$$

where $б = (L_s L_r - L_M^2)$. From (6.43), we note that the torque control can be achieved by regulating the rotor flux vector which major part comes from the stator side through mutual coupling. By rearranging the torque equation, taking into account the relationship between stator and rotor fluxes of the machine given by the second equality term of (6.7) and illustrated as shown in Figure 6.5, neglecting the voltage drop through stator resistance.

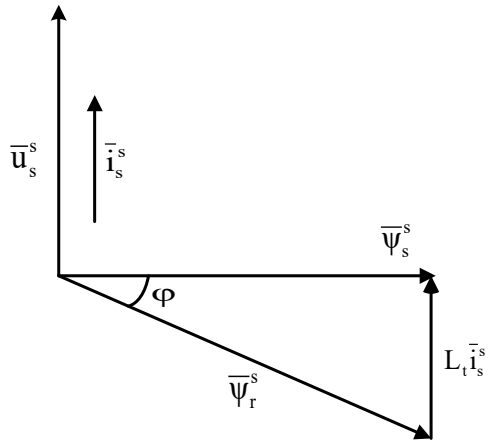

Figure 6.5: Spatial distribution of stator and rotor fluxes in stationary reference frame

Then the reference value of rotor flux to be used by the control system in Figure 6.1 for a given torque reference becomes:

$$\left|\psi^s_{r,k+1}\right|^* = \left|\psi^s_{s,k+1}\right|\sqrt{\left(1+\left(\frac{m^*_{k+1}}{1.5\ p\ \frac{L_M}{б}\left|\bar{\psi}^s_{s,k+1}\right|^2}\right)^2\right)} \tag{6.44}$$

where $\left|\psi^s_{s,k+1}\right| = \left|\psi^s_{s,k}\right|$ is assumed in the calculation of (6.44).

6.8 Speed impacts during implementation

As mentioned previously, theoretically, the speed sample $\omega_{me,k}$ is required for the speed loop and also involved in prediction stage which is then utilized in voltage selection step, but a deep investigation on the speed effect in both steps can be analyzed as following.

6.8.1 During prediction

Speed sample $\omega_{me,k}$ is required (in general) for prediction as both of the derivatives of rotor flux and torque contain a part dependent on the speed as follows:

$$\left(\frac{d\bar{\psi}^s_{rs}}{dt}\right)_{k+1} = \bar{u}^s_{rs,k+1} - R_{rs}\bar{i}^s_{rs,k+1} + j\omega_{me,k+1}\bar{\psi}^s_{rs,k+1} \tag{6.45}$$

$$\left(\frac{dm}{dt}\right)_{k+1} = 1.5\,p\,\frac{1}{L_t}\mathrm{Im}((\check{u}^s_{rs,k+1} - R_{rs}\check{i}^s_{rs,k+1} - j\omega_{me,k+1}\check{\psi}^s_{rs,k+1})\bar{\psi}^s_{s,k+1} + \check{\psi}^s_{rs,k+1}(\bar{u}^s_{s,k+1} - R_s\bar{i}^s_{s,k+1})) \tag{6.46}$$

Prediction step goal is deciding whether the predicted next error amplitude exceed error limit or not. Accuracy of the prediction is important but not crucial and therefore speed estimation by the previous proposed sensorless method is appropriated as well as simple solution.

6.8.2 During voltage vectors selection

The aim of the MP DTC technique is not to calculate an accurate voltage vector, but just to find the best voltage vector that fulfills the condition in the cost function given by (6.15) which can be rewritten as following:

$$e_{m,k+1}\left(\frac{dm}{dt}\right)_{k+1} + \rho' e_{|\psi|}\left(\frac{d|\psi_r|}{dt}\right)_{k+1} > 0 \tag{6.47}$$

where $\rho' = \frac{w''_f}{(1.5p)^2}\frac{M_n^2}{\psi_n^2}$.

The torque derivative given by (6.46) constitutes of two parts, one of which independent of the speed but depends on the voltage as following

$$A(\bar{u}^s_s, \bar{u}^s_{rs}) = 1.5p\frac{1}{L_t}\mathrm{Im}\left[\check{u}^s_{rs,k+1}\bar{\psi}^s_{s,k+1} - R_{rs}\check{i}^s_{rs,k+1}\bar{\psi}^s_{s,k+1} + \check{\psi}^s_{rs,k+1}(\bar{u}^s_{s,k+1} - R_s\bar{i}^s_{s,k+1})\right] \tag{6.48}$$

On the other hand, the second part depends on the speed as

$$B(\omega_{me}) = 1.5p\frac{1}{L_t}Im\left[-j\omega_{me,k+1}\tilde{\Psi}^{s}_{rs,k+1}\bar{\Psi}^{s}_{s,k+1}\right] \tag{6.49}$$

In the same manner the two parts that constitute the rotor flux derivative are given by

$$C(\bar{u}^{s}_{rs}) = \left[\bar{u}^{s}_{rs,k+1} - R_{rs}\bar{i}^{s}_{rs,k+1}\right] \tag{6.50}$$

, and

$$D(\omega_{me}) = \left[j\omega_{me,k+1}\bar{\Psi}^{s}_{rs,k+1}\right] \tag{6.51}$$

By substituting all of these parts in (6.47), the following convergence condition is obtained

$$e_{m,k+1}A(\bar{u}^{s}_{s}, \bar{u}^{s}_{rs}) + \frac{\rho' e_{|\psi_{rs,k+1}|}}{|\psi_{rs,k+1}|}C(\bar{u}^{s}_{rs}) > -\left(e_{m,k+1}B(\omega_{me}) + \frac{\rho' e_{|\psi_{rs,k+1}|}}{|\psi_{rs,k+1}|}D(\omega_{me})\right) \tag{6.52}$$

So if more than one voltage vector $\bar{u}^{s}_{rs}$ fulfills (6.52), then $\bar{u}^{s}_{rs,optimal}$ is the first voltage vector that meets at the largest extend the convergence condition maximizing the left term in (6.52). Since A and C do not depend on speed, it results that optimal voltage vector does not depend on ω_{me}. Then the speed does not affect the voltage selection based on the minimization of $\tilde{\Lambda}^{i}_{k+1}$ and can be neglected. The complete implementation procedure is shown in Figure 6.6, through which it can be noticed that the proposed control procedure fulfils the following five steps:

- **Step 1**: Measuring of input stator voltage $\bar{u}_{s,k}$, stator current $\bar{i}_{s,k}$, and rotor current $\bar{i}_{r,k}$, then estimating the speed sample $\hat{\omega}_{me,k}$ and rotor position $\hat{\theta}_{me,k}$.
- **Step 2**: Prediction of the torque and rotor flux for all possible voltage vectors (i=0…..7).
- **Step 3**: Calculation of rotor flux reference value using (6.44).
- **Step 4**: Checking the predicted values of torque and rotor flux in the cost function given by (6.15).
- **Step 5**: The switching states correspond to the minimum value of cost function are selected in the next sampling time interval to actuate the voltage source inverter.

.

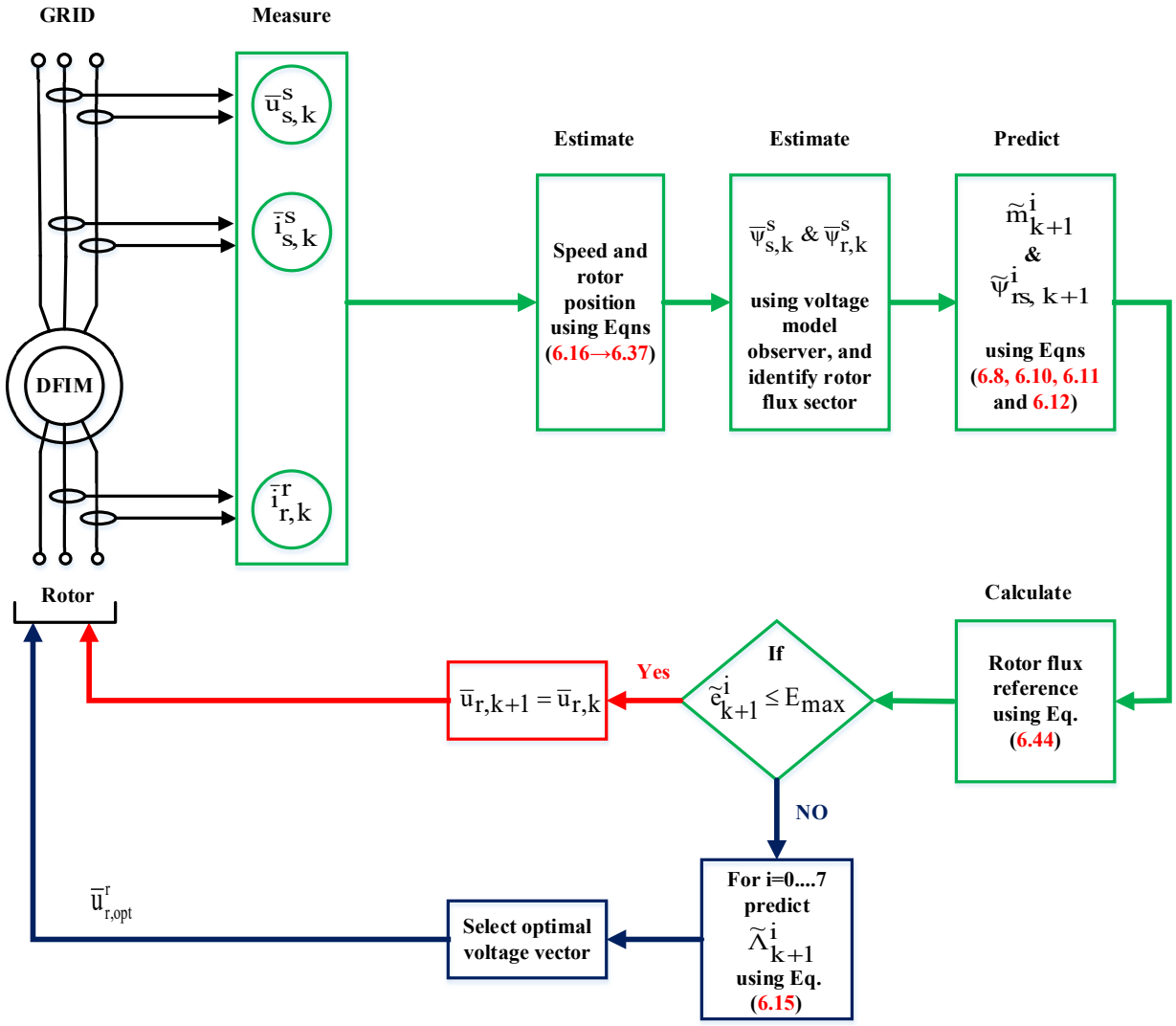

Figure 6.6: Sequence of implementation for proposed MP DTC for DFIM drive

6.9 Simulation validation

Extensive simulations are performed using Matlab Simulink software to validate the proposed MP DTC for DFIM drive; the tests are carried out for a wide range of speed change considering the sub and super synchronous speed modes of operation. In addition, the drive performance is also verified for very low speed ranges and in the following sections, the detailed results are given. It is worth to note that the drive under test is the same machine used before as a single fed wound rotor induction motor in previous chapters, and which all data specifications are given in appendix B. It is also should notice that the control scope here avoided the issue of the ripples contents which is already presented and analyzed indetails in chapter 4 and which can be used for any machine drive working under troque control, and this is to give a more focused view about the operation of the DFIM in different range of speed changes besides introducing an effective sensorless procedure that has the

ability to exhibits high estimation precision for different operating conditions while overcoming previous sensorless approaches used for DFIM drives.

6.9.1 High speed range (sub and super synchronous modes)

The DFIM drive is tested while accelerating from sub-synchronous range to super synchronous range, this is the feature that DFIM can present and manages in achieving it when compared with the squirrel cage induction motor type. For this purpose a speed profile of (2800 → 3200 RPM) at times of (0 → 2 sec), the reference value of rotor flux is derived as given by (6.44). The predefined hysteresis band for absolute error value is set to 0.1. Figures 6.7 show the dynamic response of the drive for the specified speed range from which the feasibility of proposed sensorless control procedure is confirmed, this can be shown though the precise tracking of speed commands while the rotor flux level is tracking its reference value which correspondingly follows the change in the torque. The sensorless procedure confirmed its effectiveness especially near synchronous speed at which classic sensorless schemes, which were dependent on flux estimation via integrator or low pass filters failed in keeping control of the flux. Figure 6.8 shows the stator and rotor currents profiles during switching from sub synchronous to super synchronous mode, while Figure 6.9 illustrates the control action taken at each sampling instant. To show the effect of parameters variation on the precision of estimation of rotor position, Figure 6.10 gives a detailed view for the estimated and actual positions before and after variation of stator resistance and magnetizing inductance each alone. The change in stator resistance is made in the interval from (t=1.98 → 2.155 sec) for +50% error in stator resistance. While the change in magnetizing inductance is applied for a similar interval with a +50% error. The results confirm the null effect of the parameters on the precision of sensorless procedure.

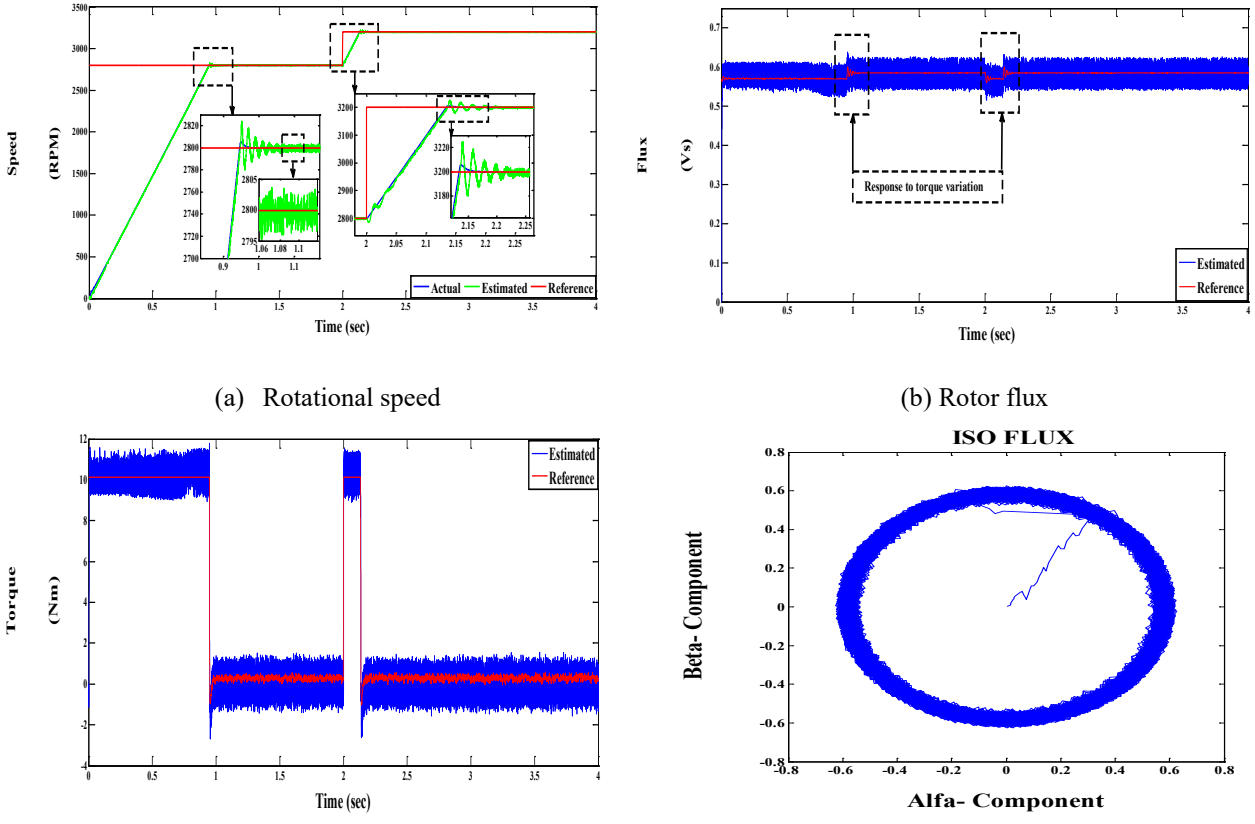

(a) Rotational speed

(b) Rotor flux

(c) Electromagnetic torque

(d) ISO flux

Figure 6.7: Dynamic performance of DFIM drive (Simulation)

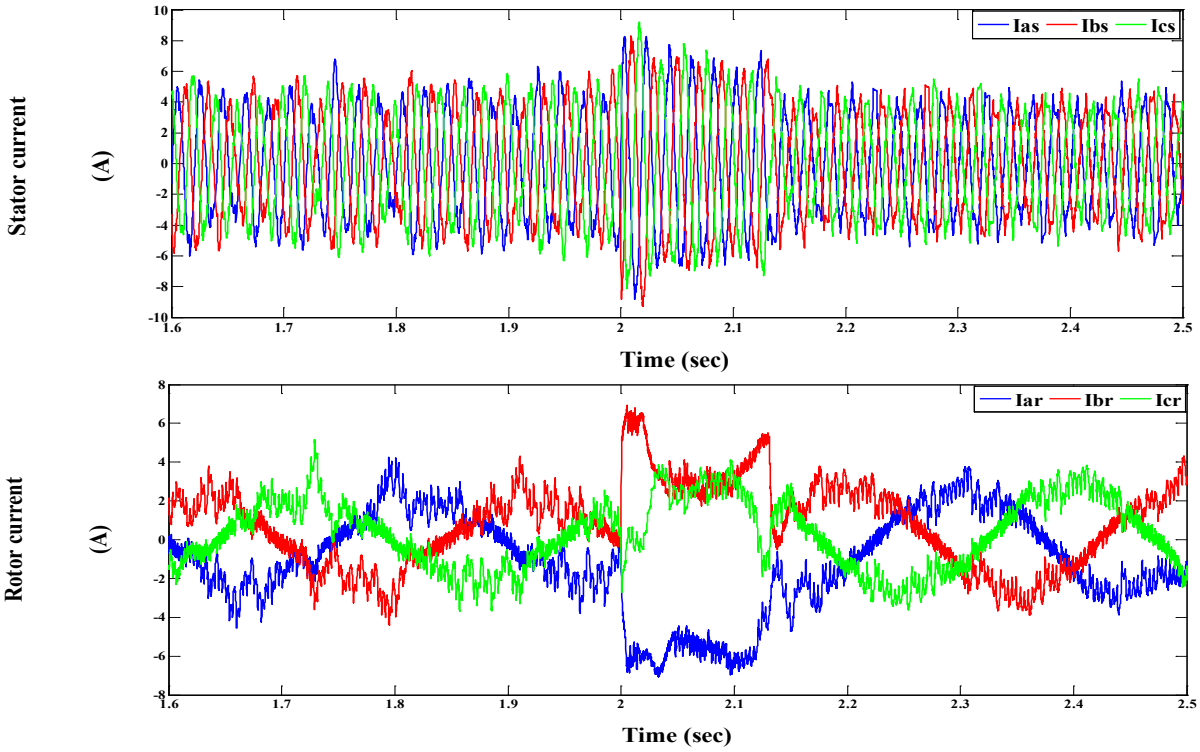

Figure 6.8: Stator and rotor currents waveforms

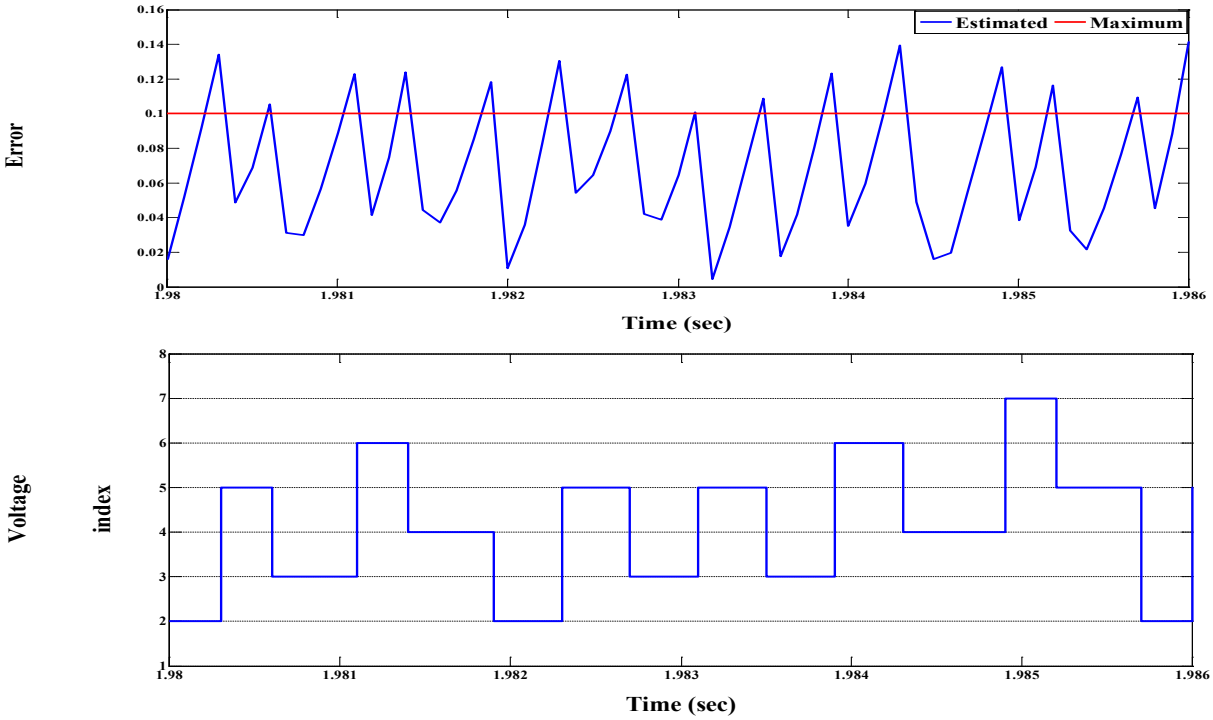

Figure 6.9: Control response to variation in absolute error

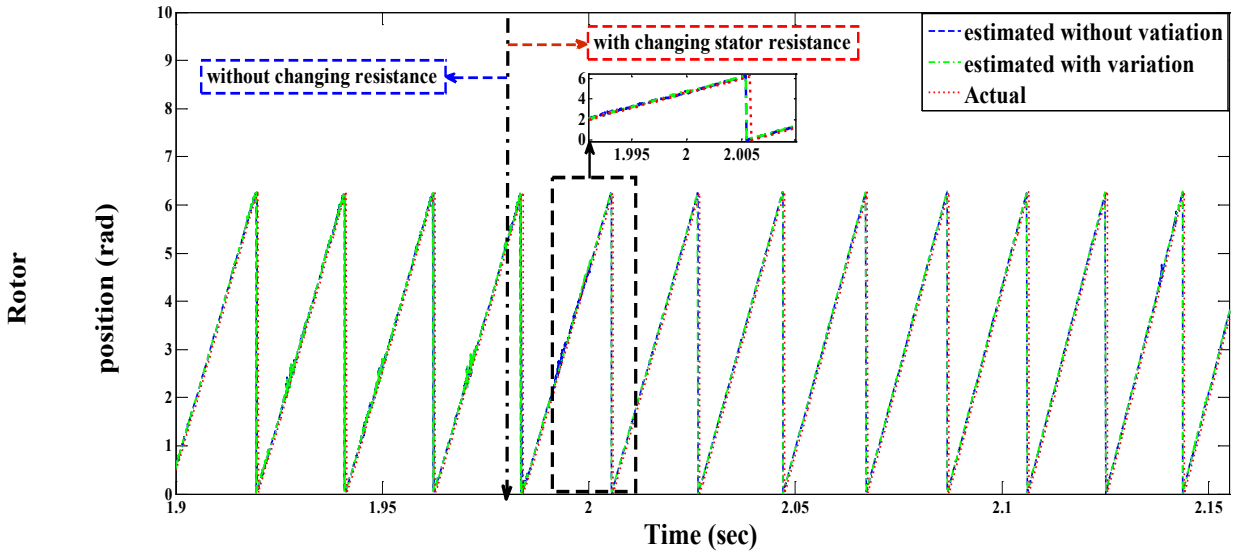

(a) Rotor position with and without variation in stator resistance

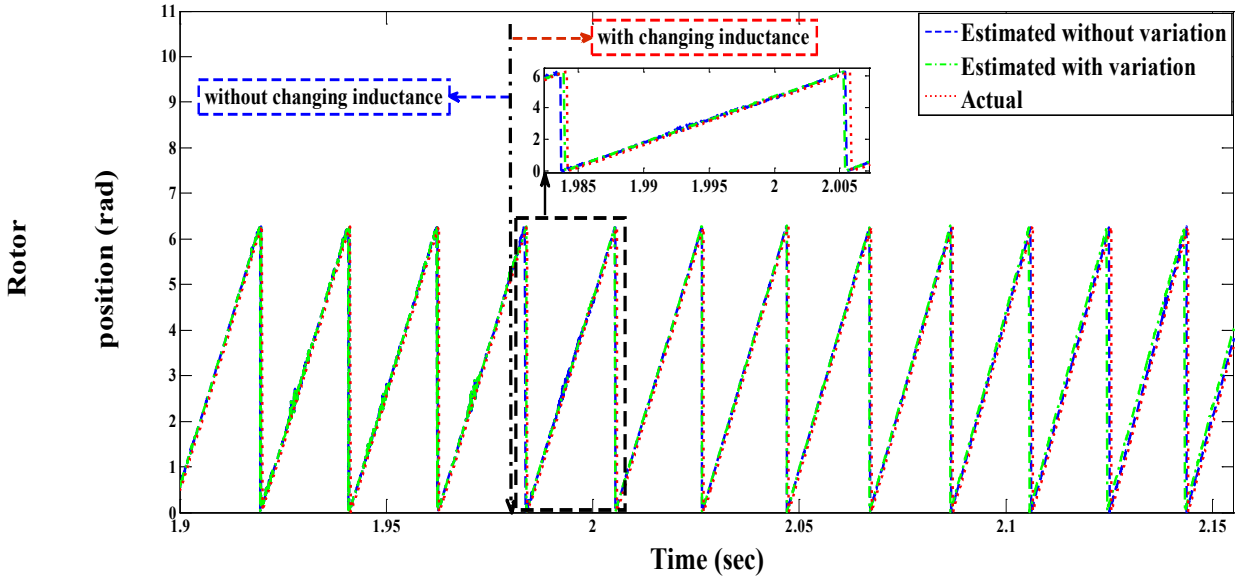

(b) Rotor position with and without variation in magnetizing inductance

Figure 6.10: Rotor position

6.9.2 Low speed range

To investigate the validity of proposed sensorless scheme, the DFIM drive performance is tested at very low speed range about (1 % of rated speed (2830 RPM)). The simulation is performed also in a way that shows the fast transient dynamic performance of the drive, as the speed is shifted from 1200 RPM to 30 RPM. The rotor flux reference is calculated and imposed in the same way used in Sect. 6.9.1. The predefined maximum limit for absolute error is set to 0.1. Obtained results proof and reconfirm the feasibility of proposed control procedure even at very low speed ranges, with precise estimation for speed and rotor position. Figure 6.11 shows the dynamic behavior of the drive (speed, torque, rotor flux and ISO flux), while Figure 6.12 views the stator and rotor currents profiles. Figure 6.13 gives a focused view on the action of the control at each instant happens that absolute error exceeds its limit. Finally, Figure 6.14 illustrates the matching between the estimated and actual rotor position and investigates also what happens in case of changing the values of stator resistance or magnetizing inductance, which they are changed with the same values used in Sect. 6.9.1.

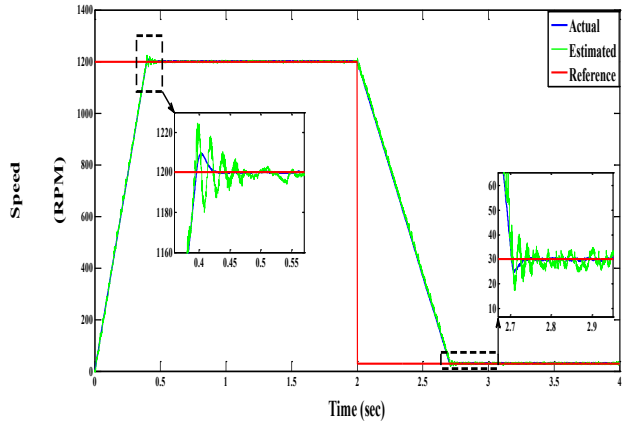

(a) Rotational speed

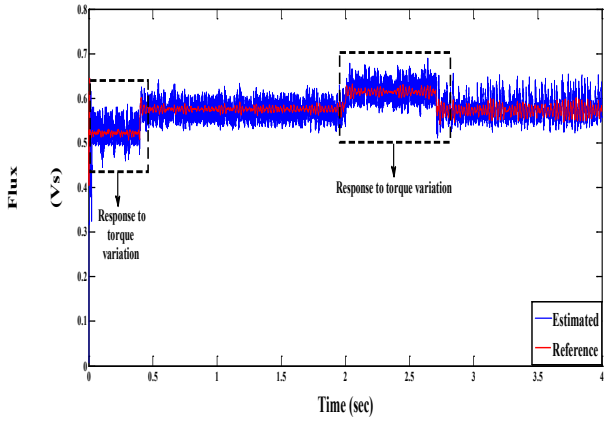

(b) Rotor flux

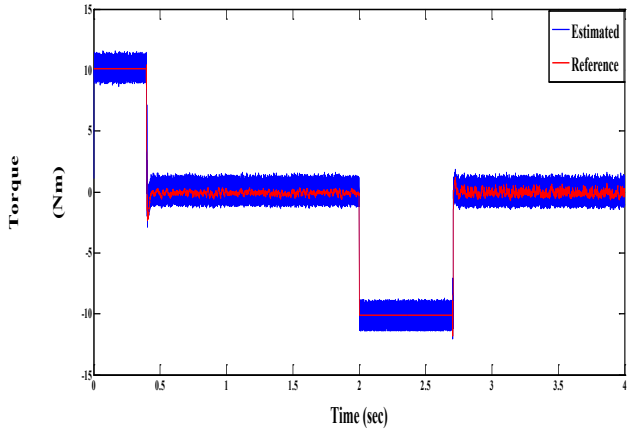

(c) Electromagnetic torque

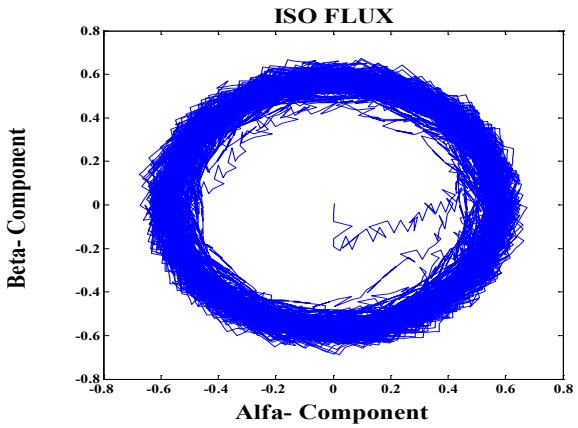

(d) ISO flux

Figure 6.11: Dynamic behavior of DFIM at low speed (Simulation)

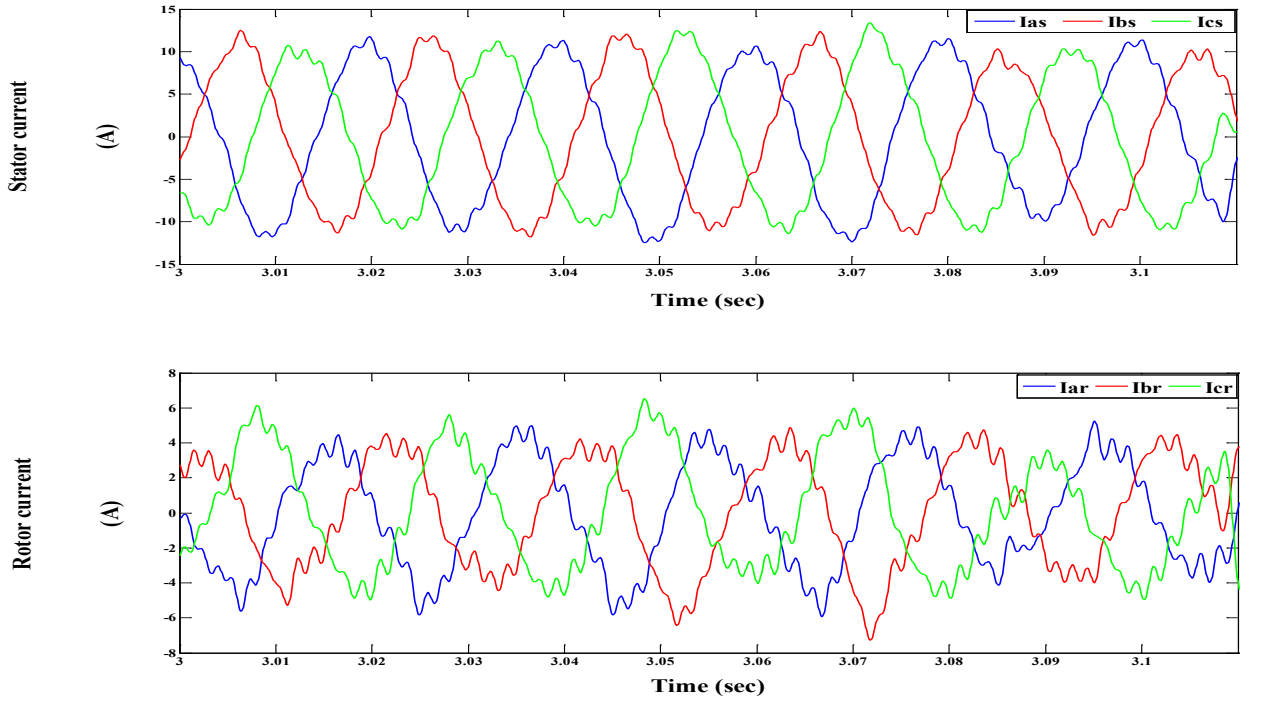

Figure 6.12: Stator and rotor current waveforms

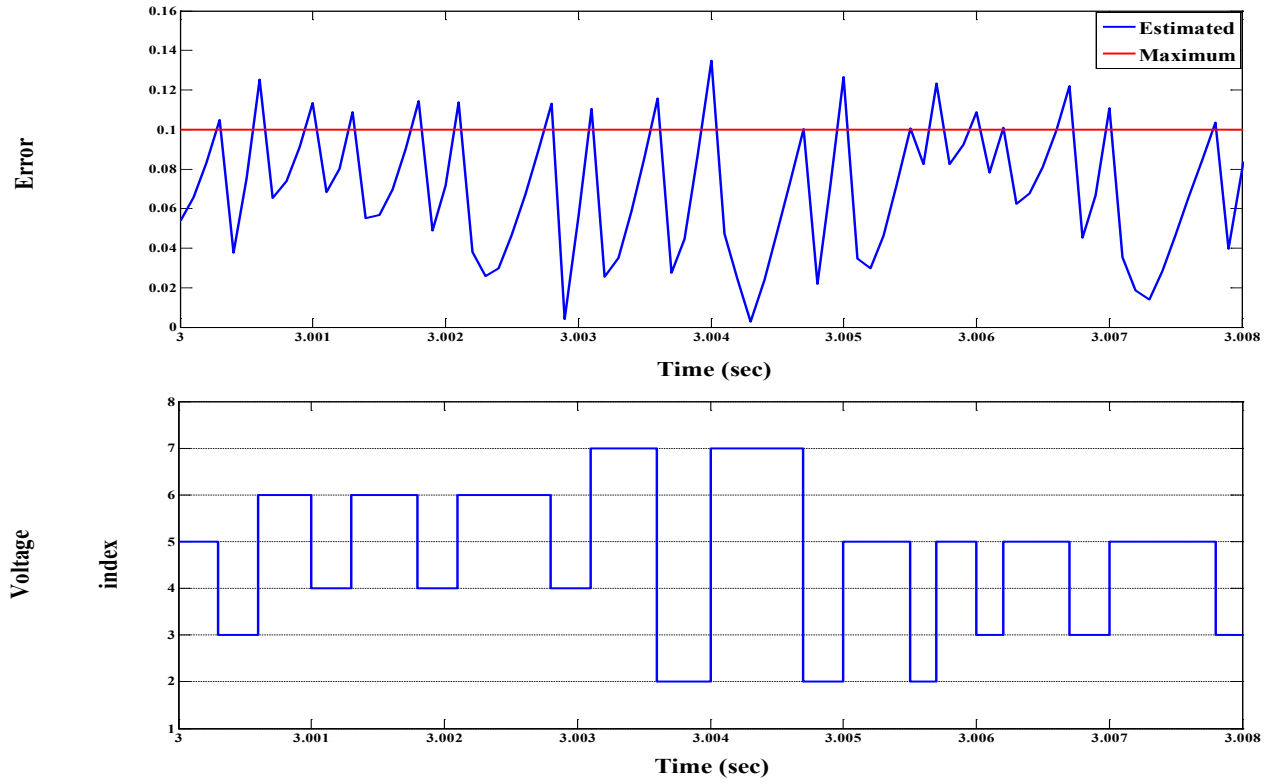

Figure 6.13: Action taken by the control

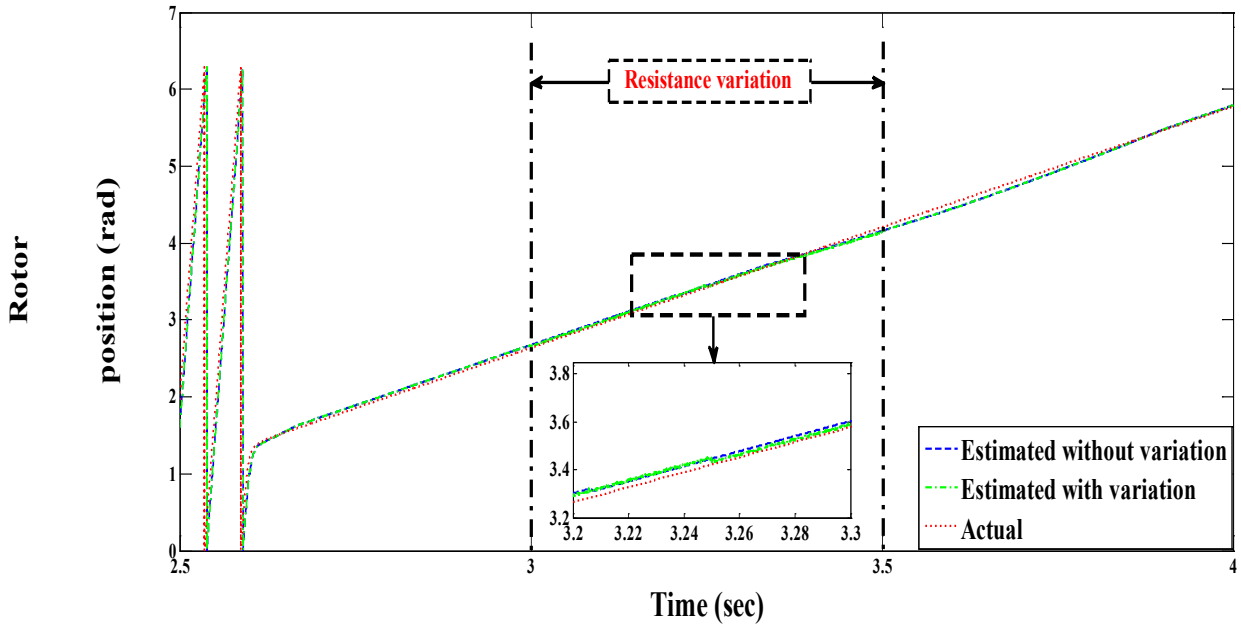

(a) Rotor position with and without variation in stator resistance

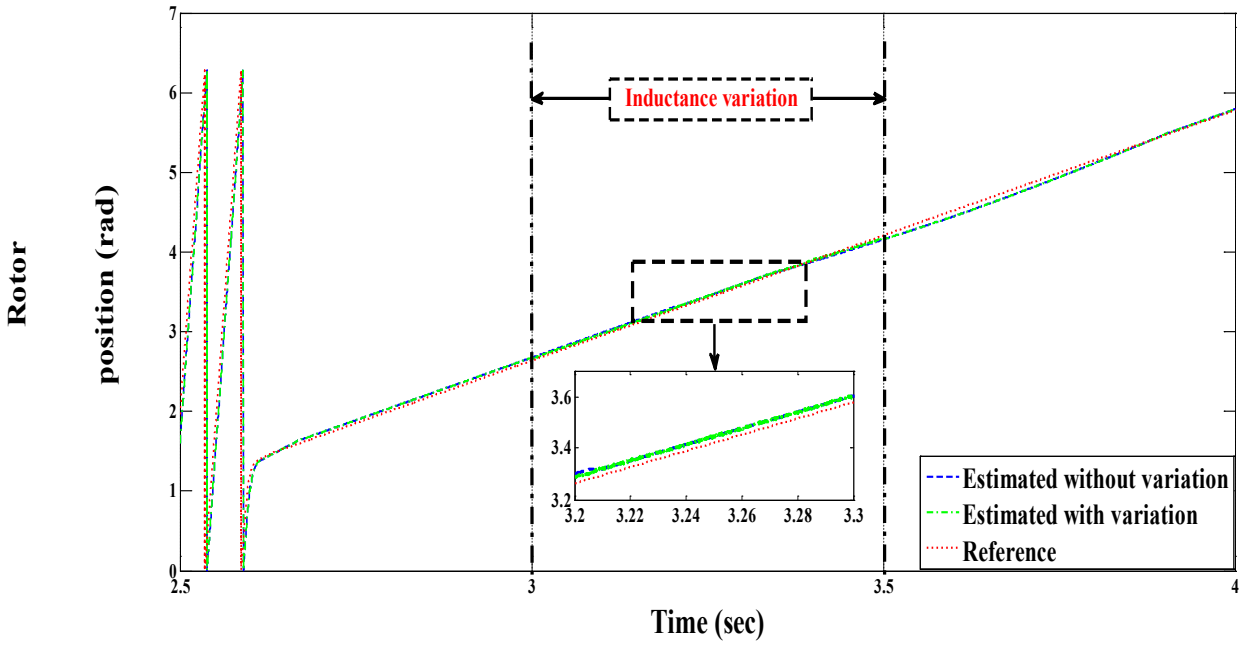

(b) Rotor position with and without variation in magnetizing inductance

Figure 6.14: Rotor position

6.10 Experimental validation

A fast control prototyping dSpace1104 board is used for the purpose of the experimental validation of proposed sensorless MP DTC control procedure. Figure 6.15 sows the experimental bench setup, which consists of a wound rotor induction machine. The stator terminals are connected to a three- phase supply (grid) and its rotor terminals are connected to the inverter's output. It can be noticed also that the stator voltages and currents are acquired through external sensors, while the rotor current is sensed through an embedded sensor inside the rotor's inverter itself. A static load unit is used to apply variable loads to the motor. The tests are also performed for a wide speed range similar to the simulation tests.

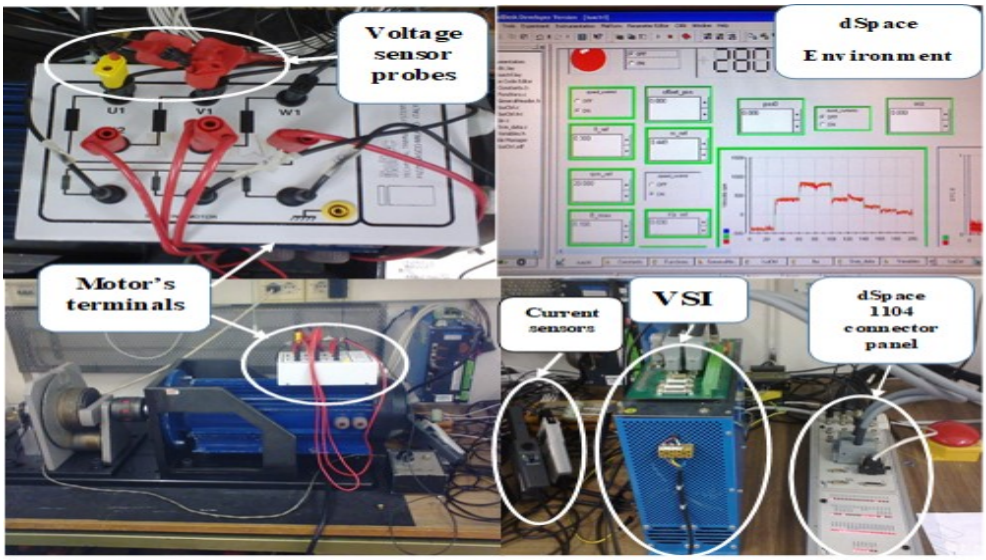

Figure 6.15: Test bench layout

6.10.1 High speed range (sub and super synchronous modes)

The DFIM is tested for the same speed profile given in Sect. 6.9.1. The rotor flux reference also generated using (6.44). The maximum limit for absolute error is kept at 0.1. Through obtained results, the effectiveness of proposed control approach is confirmed and became feasible, this can be viewed through Figure 6.16 in which the speed, torque, flux and ISO flux are shown respectively. The proposed sensorless technique exhibits high performance in tracking precisely the speed while the rotor flux level inside the machine is well managed during the transition period from sub-synchronous to super- synchronous speed range. Figure 6.17 illustrates the stator and rotor current waveforms during the transition period, while Figure 6.18 views the transition from one

voltage index to another based on the instantaneous value of estimated absolute error. Figure 6.19 gives an information about the estimation process of rotor position while changing stator resistance and magnetizing inductance, each alone. The parameters are changed by the same rate used in simulation for a time interval from (1.98 → 2.3 sec) to cover the transition period. From Figure 6.19 it can be confirmed that the change in parameters does not have a remarkable effect on the estimation process and this is confirming what is reported in Sect. 6.6.4.

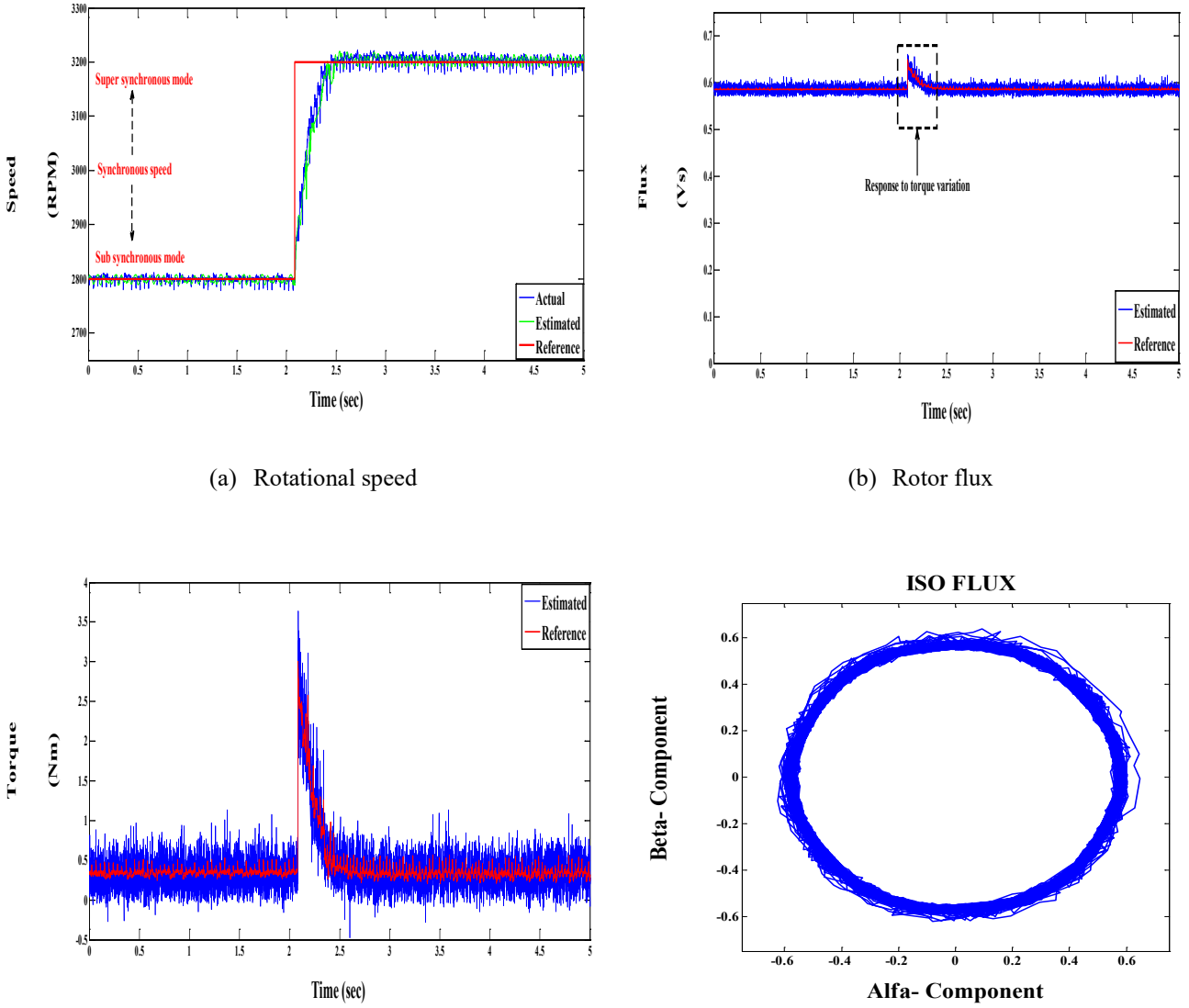

(a) Rotational speed

(b) Rotor flux

(c) Electromagnetic torque

(d) ISO flux

Figure 6.16: Dynamic behavior of DFIM at high speed (Experimental)

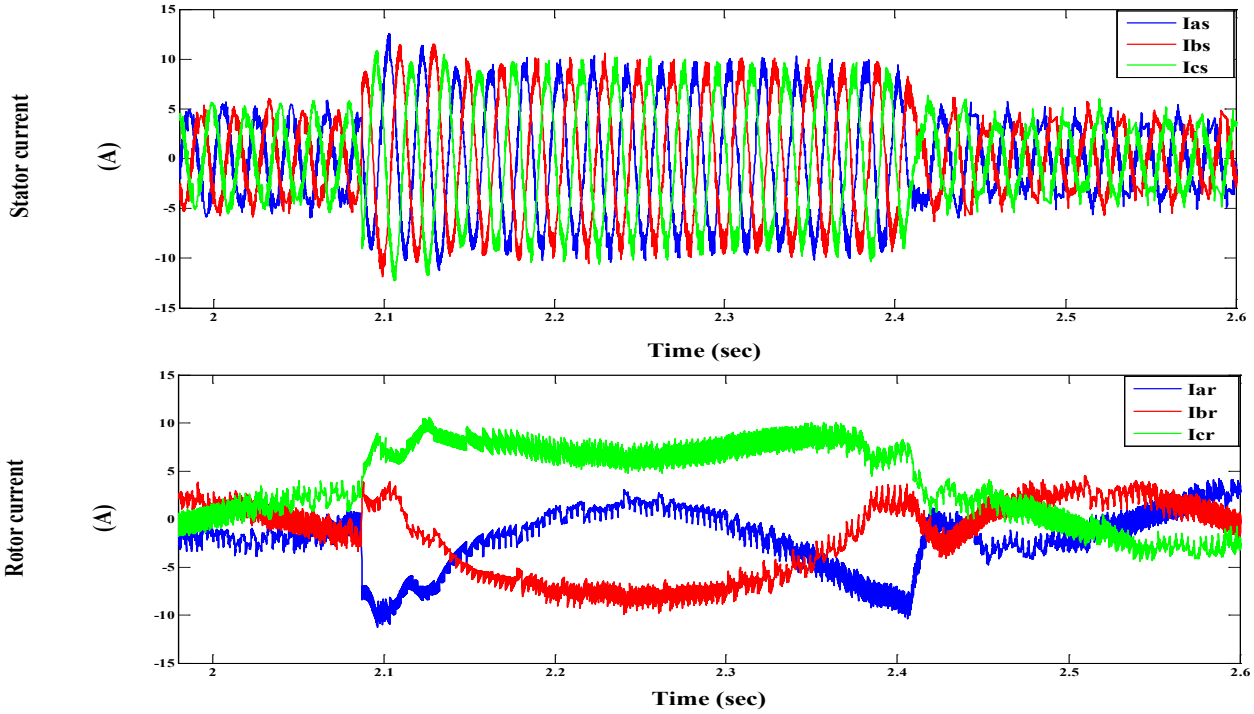

Figure 6.17: Stator and rotor current waveforms

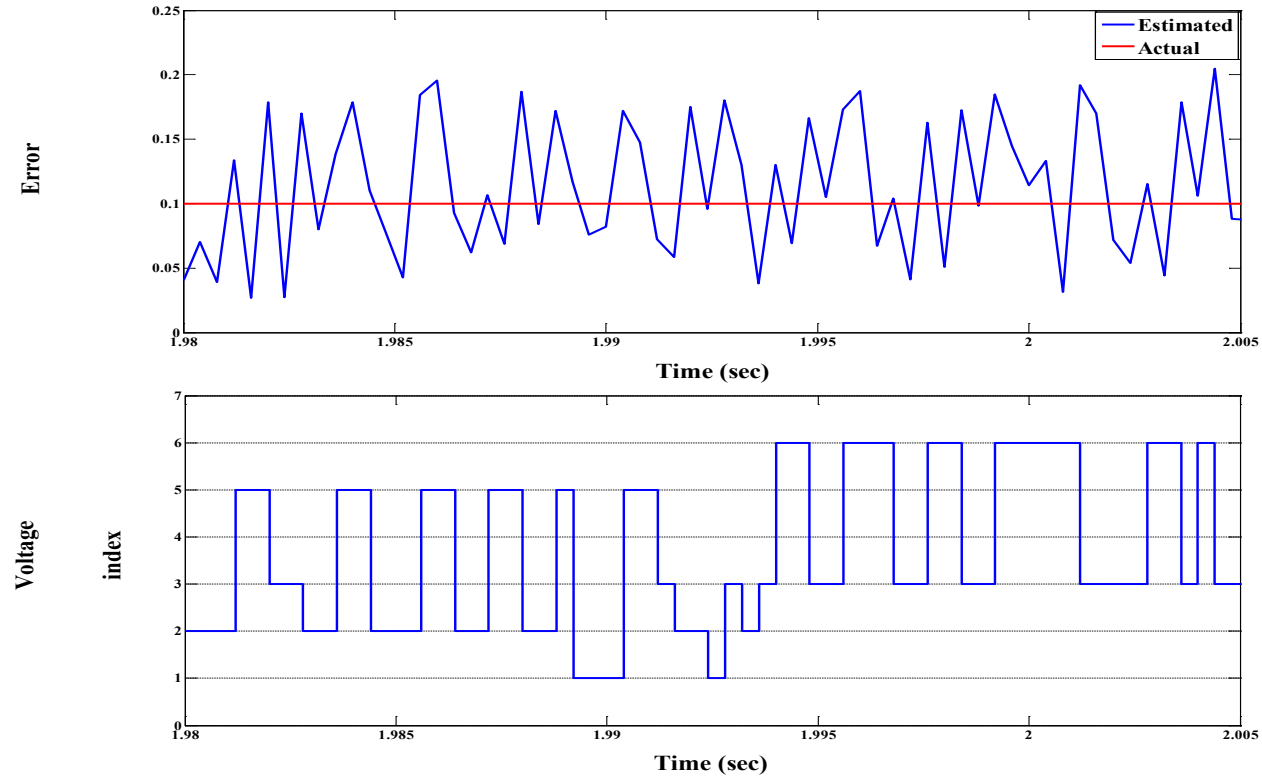

Figure 6.18: Control response to variation in absolute error

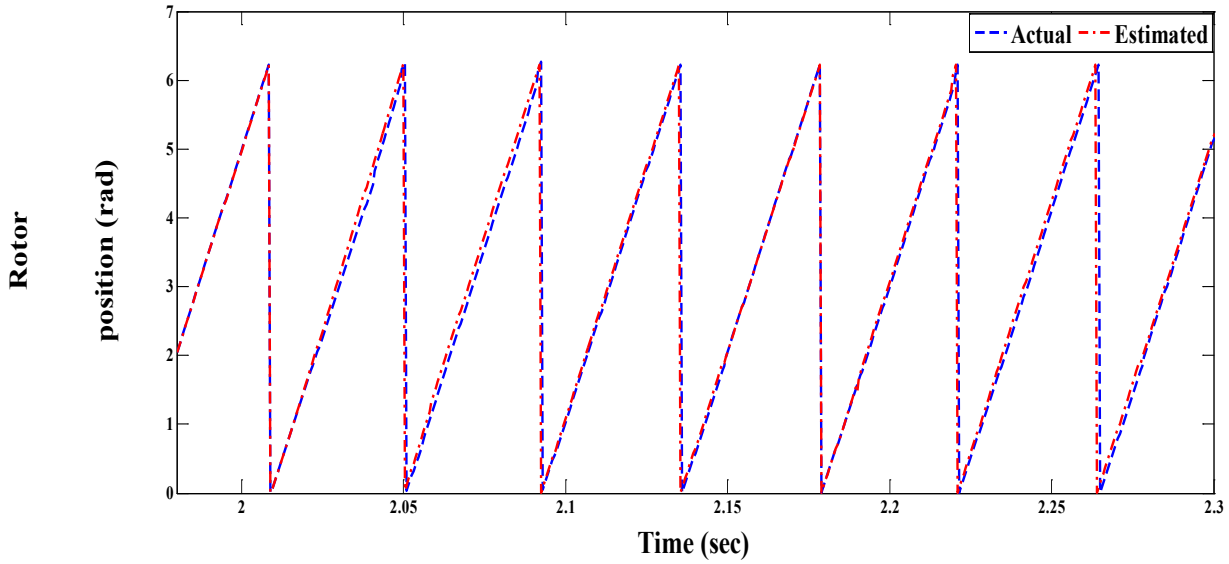

(a) Rotor position with variation in stator resistance

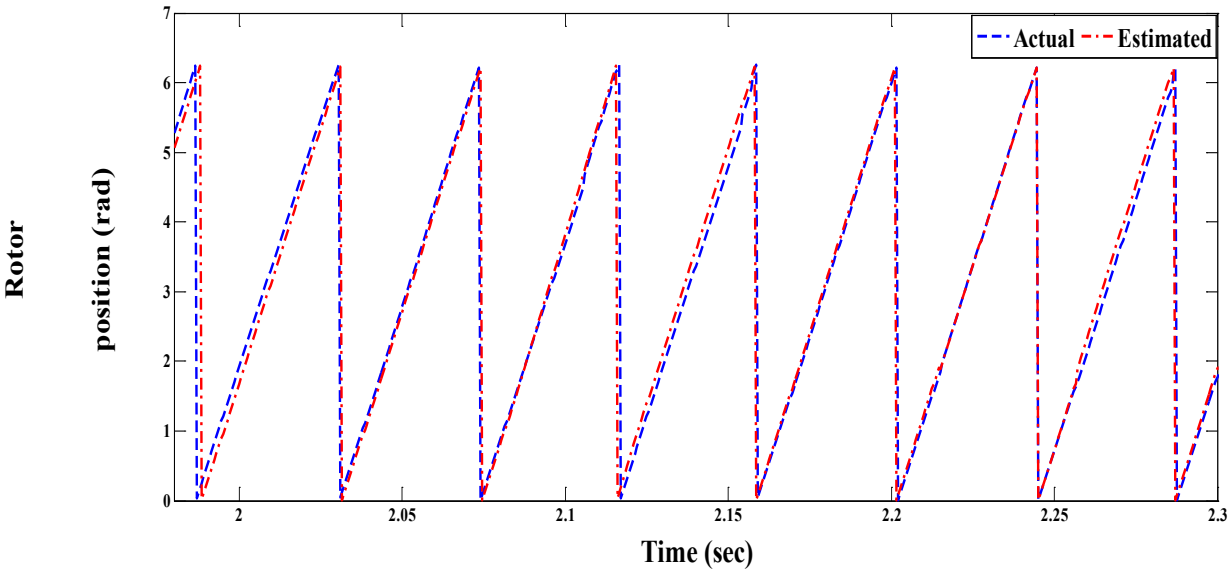

(b) Rotor position with variation in magnetizing inductance

Figure 6.19: Rotor position

6.10.2 Low speed range

The experimental test is carried out also for a low speed range. In addition, the speed is transited from a high speed (1200 RPM) to the specified low speed (30 RPM). More over a load torque of two Nm is applied to the motor since starting. The rotor flux reference is set in the same way as used in previous tests (simulation and results), while the maximum error limit is kept at 0.1. Acquired results are showing a high performance for the drive at low speed while loading. Figure 6.20 gives the speed, torque, rotor flux and ISO flux profiles, respectively. From which it can be noticed that the sensorless procedure succeeded in achieving precise tracking for the speed, while the flux is well established and regulated. Figure 6.21 presents the stator and rotor currents waveforms, while Figure 6.22 shows a specified range for the changing of voltage index with changing the error. Finally, Figure 6.23 illustrates the estimated rotor position while changing separately the stator resistance and magnetizing inductance. From this figure, it can be confirmed that variation in those parameters has no effect in the estimation process and can neglected.

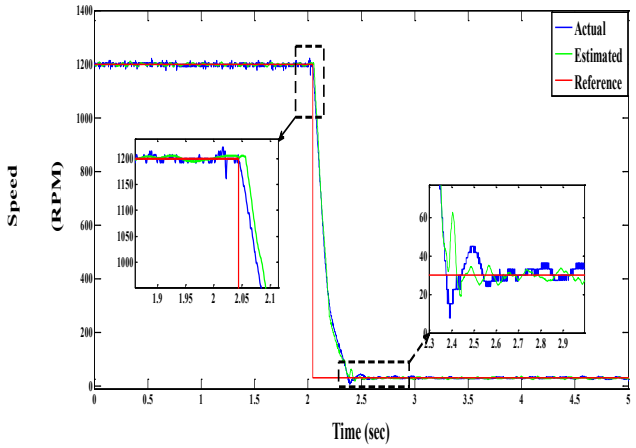

(a) Rotational speed

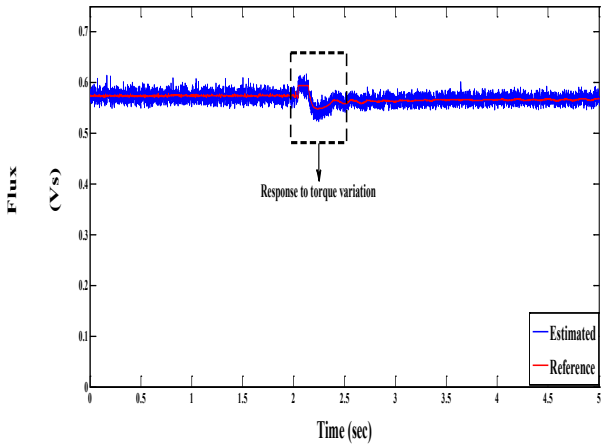

(b) Rotor flux

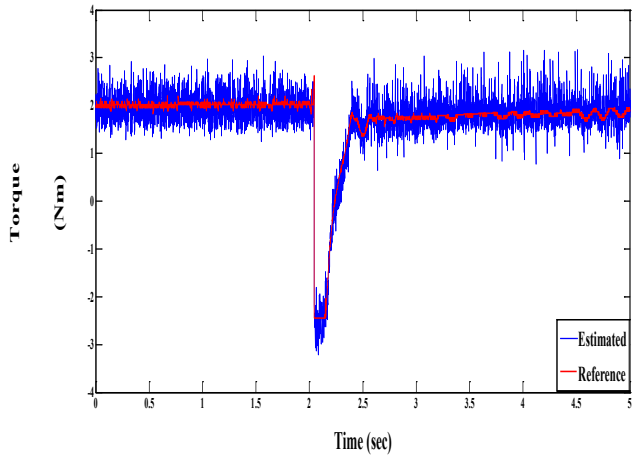

(b) Electromagnetic torque

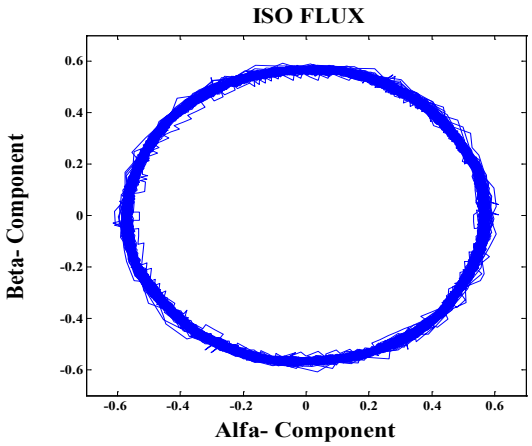

(d) ISO flux

Figure 6.20: Performance of DFIM drive at low speed (Experimental)

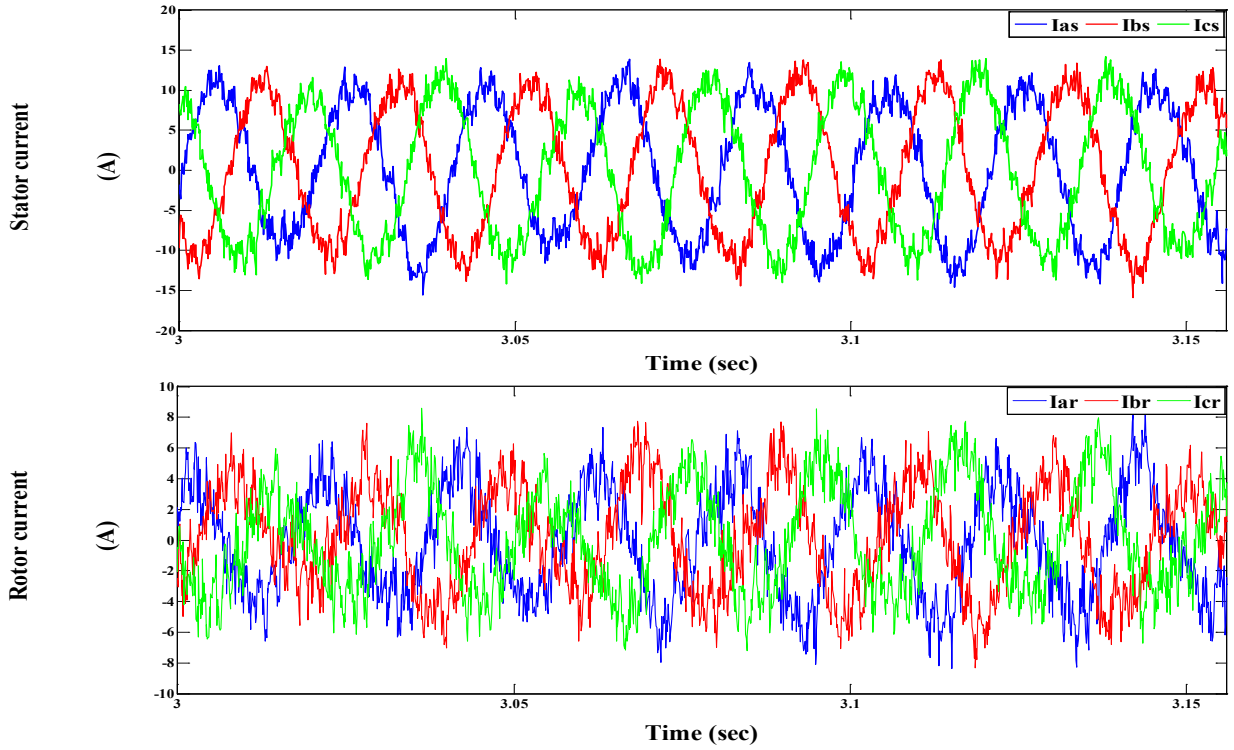

Figure 6.21: Stator and rotor current waveforms

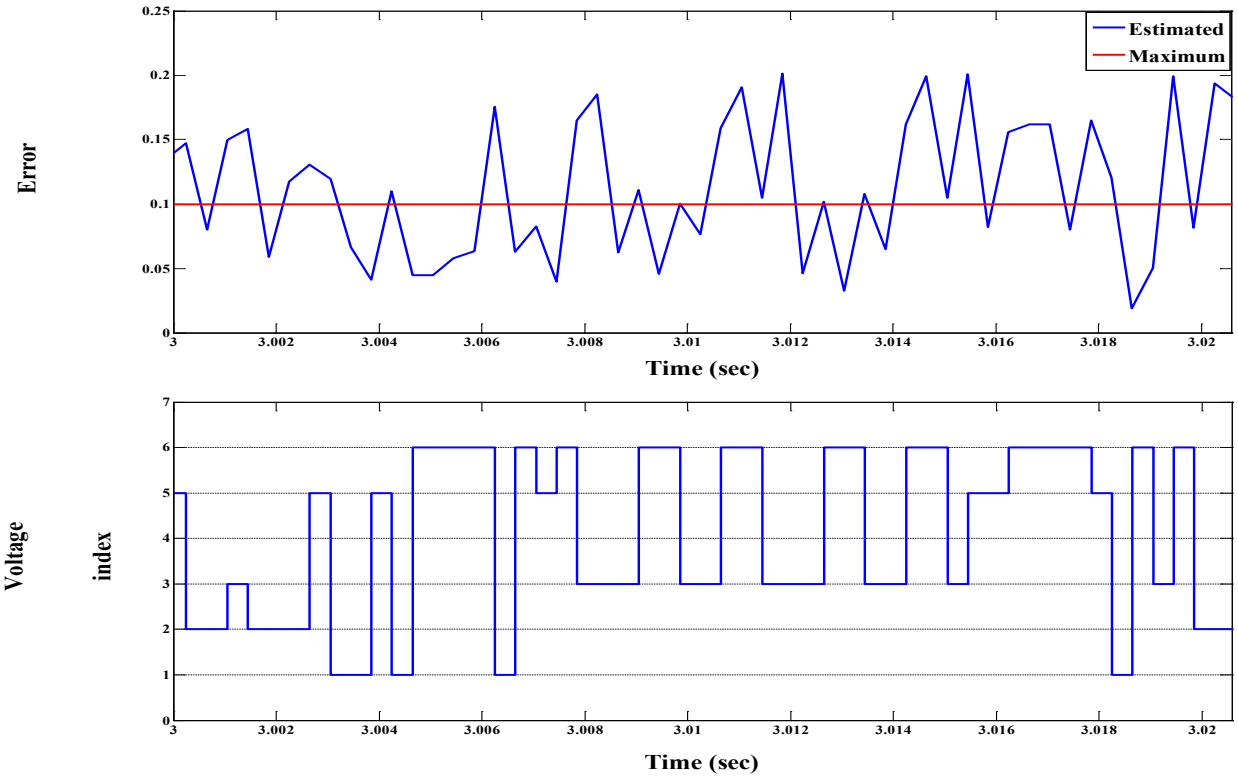

Figure 6.22: Control response to variation in absolute error

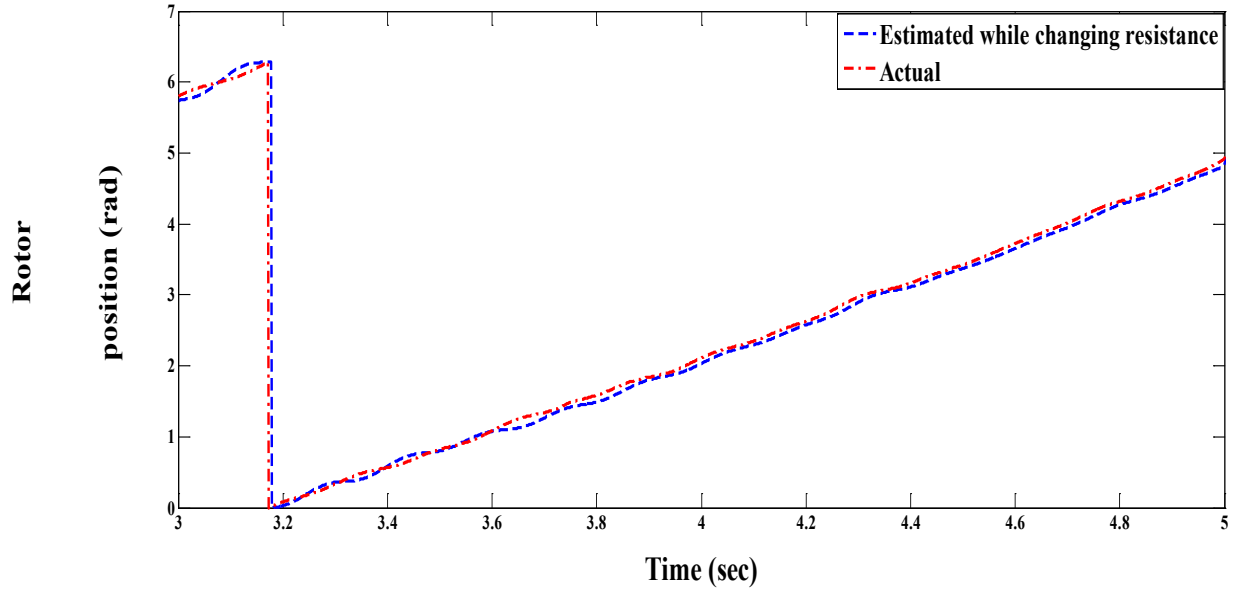

(a) Rotor position with variation in stator resistance

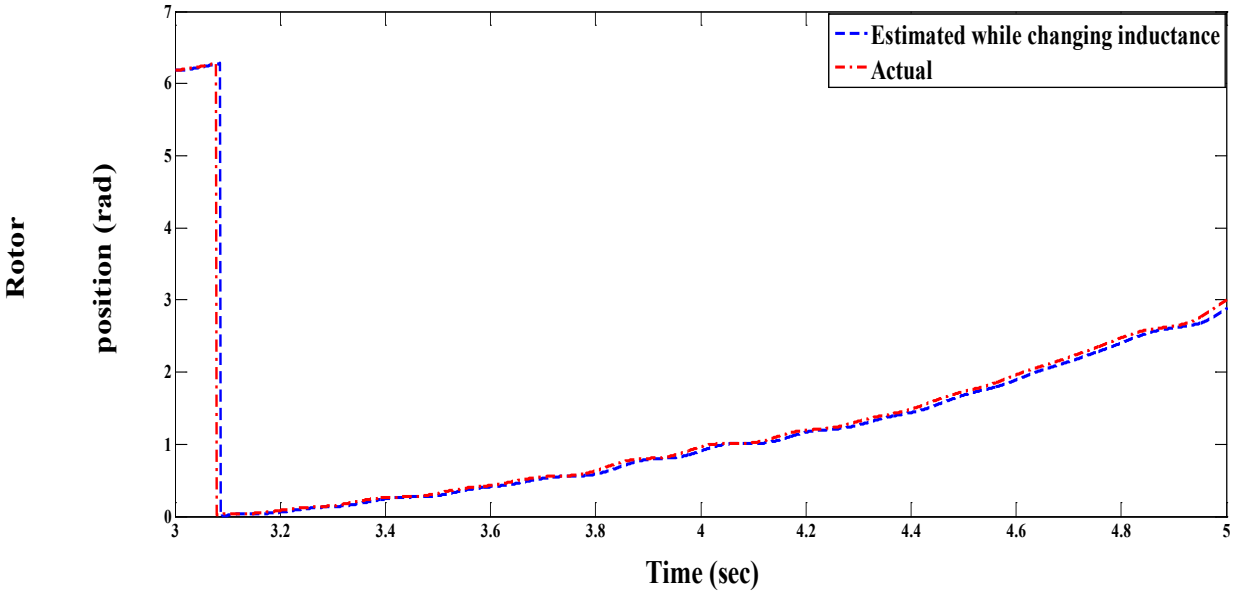

(b) Rotor position with variation in magnetizing inductance

Figure 6.23: Rotor position

Chapter 7

High Performance Direct Power Control for a Doubly Fed Induction Generator Based on Model Prediction

7.1 Introduction

The doubly fed induction generators (DFIGs) have been introduced as a worthy choice for wind generation systems that use variable speed wind turbines. The control of DFIGs has been the issue of several studies during the last decades. In comparison to the fixed speed wind driven induction generators, the wind turbines that use DFIG have the merits of variable-speed operation and active and reactive power flow abilities in four-quadrant, in addition to reduced power losses and converter cost [105, 106, 107]. The dynamic performance of DFIG driven by a wind turbine system during steady state and transient conditions is now well known. The direct power control (DPC) strategy was proposed and introduced by T. Noguchi in 1998 [8, 108] and applied to DFIG in 2006 by L. Xu [109]. DPC has the advantages of fast and precise dynamic response, simple implementation, it is insensitive to parameter variations and it does not involve any current control loop. In the DPC strategies cited above, active and reactive powers are controlled with hysteresis logic blocks and using lookup tables [108-114] similar to those utilized by a direct torque control (DTC) applied to induction motors.

Various methodologies of DPC for a doubly fed induction generator have been adopted [109-116]. Some of them have introduced the principles of the topic; the majority of the others are concerned with implementation variants, dedicated to solve specific problems, and mainly based on the transposition of the DTC applied to squirrel cage IMs. In addition, effects of digital implementation are not always deeply investigated and well managed. A contribution in such a sense is given in [116, 117, 118, and 119] in which however, a PWM voltage control is used.

In order to cover these gaps, this chapter is concerned with presenting an effective new formulation of direct power control (DPC) topology for a doubly fed induction generator (DFIG). It fully considers its digital implementation and it exploits the finite set of voltages delivered by an inverter thus avoiding the need of a PWM switching control as well as the need of speed or position transducers. As a solution for the speed and rotor position estimation purposes, a model reference adaptive system (MRAS) observer is utilized. The chapter starts with a theoretical study of the DPC technique. This theoretical analysis is essential to understand the basics of the DPC strategy and provides the necessary clearance to understand the parallelism between the DTC for DFIM introduced in chapter 6 in which the DFIM was under speed control mode and the DPC control introduced here in which the machine is under power control mode.

7.2 Theoretical analysis of the direct power control (DPC)

As stated before, DPC is defined as the control technique for a three-phase two level voltage source inverter which feeds the DFIG drive , in which the inverter's voltage vectors are identified " directly" according to the active and reactive powers errors without interposing any current control loop. The stator active and the reactive power of the machine can be calculated directly from the stator voltage and currents as follows:

$$P_{s,k} = 1.5\ \mathrm{Re}\left(\bar{u}^{s}_{s,k}\check{i}^{s}_{s,k}\right) \tag{7.1}$$

$$Q_{s,k} = 1.5\ \mathrm{Im}\left(\bar{u}^{s}_{s,k}\check{i}^{s}_{s,k}\right) \tag{7.2}$$

These last two expressions do not provide the required information to analyze the direct power control, so in the following subsections equivalent modified expressions will be derived.

7.2.1 Dependency of active and reactive powers on fluxes

The relation of the stator active and reactive powers with stator and rotor fluxes can be derived as following: From Figure 6.2, the stator voltage vector in stationary reference frame can be given by

$$\bar{u}^{s}_{s,k} = R_s\bar{i}^{s}_{s,k} + \left(\frac{d\bar{\psi}^{s}_{s}}{dt}\right)_k \tag{7.3}$$

while the stator current can be given in terms of stator and rotor fluxes as follows

$$\bar{i}^{s}_{s,k} = \frac{1}{\sigma L_s}\bar{\psi}^{s}_{s,k} - \frac{L_M}{\sigma L_s L_r}\bar{\psi}^{s}_{r,k} \tag{7.4}$$

From Figure 6.2, the active and reactive powers in the circuit can be calculated by

$$P_{s,k} = 1.5\left(\bar{u}^{s}_{s,k}\cdot\bar{i}^{s}_{s,k}\right) \tag{7.5}$$

, and

$$Q_{s,k} = 1.5\left(\bar{u}^{s}_{s,k}\times\bar{i}^{s}_{s,k}\right) \tag{7.6}$$

where $(\cdot)$ and $(\times)$ denote to dot and cross product, respectively.

The relationship between the stator and rotor flux in the stationary (α_s_β_s) and rotor (α_r_β_r) reference frames is shown in Figure 7.1.

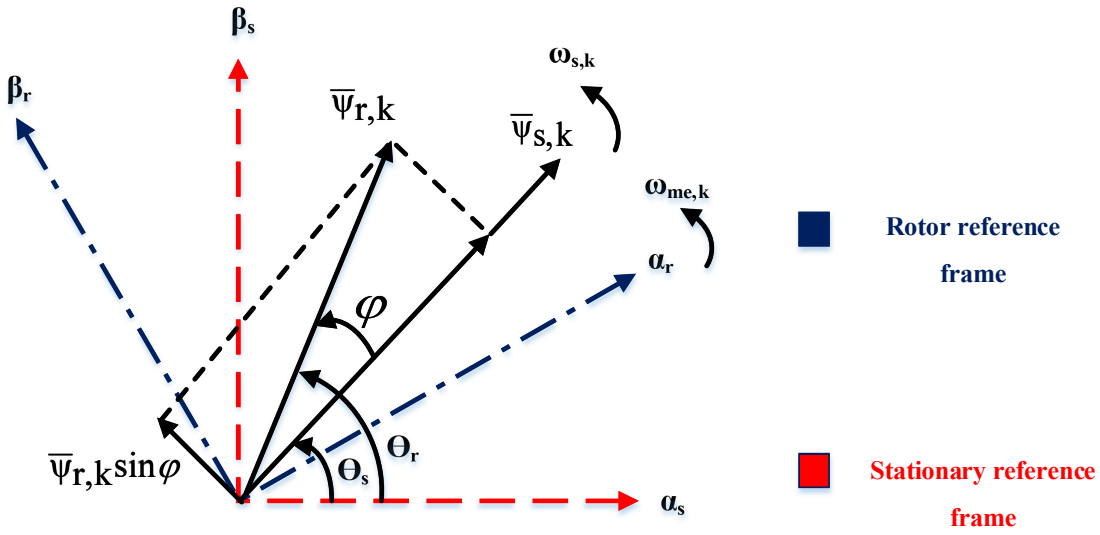

Figure 7.1: Relation of stator and rotor flux linkage vectors in stationary and rotor reference frames

From Figure 7.1, the stator flux in the stationary (α_s_β_s) frame can be expressed as

$$\bar{\psi}^{s}_{s,k} = \left|\bar{\psi}^{s}_{s,k}\right|.\, e^{j\theta_s} \tag{7.7}$$

where θ_s is the stator flux angle in stationary reference frame.

Neglecting the voltage drop due to stator resistance in (7.3) and assuming that the ac network (grid) connected to the stator is well balanced and the rotor speed does not change within the sampling period T_s which is usually true due to the relatively large inertia of the wind turbine, then from (7.3) and (7.7) the following relationships are derived.

$$\bar{u}^{s}_{s,k} \cong \left(\frac{d\bar{\psi}^{s}_{s}}{dt}\right)_k \tag{7.8}$$

, and

$$\left(\frac{d\bar{\psi}^{s}_{s}}{dt}\right)_k = \left|\bar{\psi}^{s}_{s,k}\right|.\, j\dot{\theta}_s.\, e^{j\theta_s} = j\dot{\theta}_s.\, \bar{\psi}^{s}_{s,k} = j\omega_{s,k}.\, \bar{\psi}^{s}_{s,k} \tag{7.9}$$

where $\omega_{s,k}$ is the stator angular frequency.

Then, by substituting from (7.4), (7.) and (7.) into (7.5) and (7.6), the following formulations are obtained:

$$P_{s,k} = 1.5\left(\left(\frac{d\bar{\psi}_s^s}{dt}\right)_k \cdot \left(\frac{1}{\sigma L_s}\bar{\psi}_{s,k}^s - \frac{L_M}{\sigma L_s L_r}\bar{\psi}_{r,k}^s\right)\right) = 1.5\left(j\omega_{s,k}\bar{\psi}_{s,k}^s \cdot \left(\frac{1}{\sigma L_s}\bar{\psi}_{s,k}^s - \frac{L_M}{\sigma L_s L_r}\bar{\psi}_{r,k}^s\right)\right) \quad (7.10)$$

Then, from (7.) and from Figure 7.1, it can be deduced that the active power is calculated in terms of stator and rotor fluxes and the phase angle between the two vectors φ as follows:

$$P_{s,k} = 1.5\left(j\omega_{s,k}\bar{\psi}_{s,k}^s\left(-\frac{L_M}{\sigma L_s L_r}\bar{\psi}_{r,k}^s\right)\right) = 1.5\frac{L_M}{\sigma L_s L_r}\omega_{s,k}\left|\bar{\psi}_{s,k}^s\right|\left|\bar{\psi}_{r,k}^s\right|\sin\varphi \quad (7.11)$$

In the same manner, the reactive power can be calculated as

$$Q_{s,k} = 1.5\left(\left(\frac{d\bar{\psi}_s^s}{dt}\right)_k \times \left(\frac{1}{\sigma L_s}\bar{\psi}_{s,k}^s - \frac{L_M}{\sigma L_s L_r}\bar{\psi}_{r,k}^s\right)\right) = 1.5\left(j\omega_{s,k} \times \left(\frac{1}{\sigma L_s}\bar{\psi}_{s,k}^s - \frac{L_M}{\sigma L_s L_r}\bar{\psi}_{r,k}^s\right)\right) \quad (7.12)$$

Then,
$$Q_{s,k} = 1.5\frac{\omega_{s,k}}{\sigma L_s}\left|\bar{\psi}_{s,k}^s\right|\left(\left|\bar{\psi}_{s,k}^s\right| - \frac{L_M}{L_r}\left|\bar{\psi}_{r,k}^s\right|\cos\varphi\right) \quad (7.13)$$

Thus from (7.11) and (7.13), it can be deduced that the active and reactive powers for the DFIG can be controlled by controlling the phase angle φ between the two flux vectors and their amplitudes. Consequently, the effect of the voltage vectors on the two flux vectors can be analyzed in a systematic manner as following.

7.2.2 Analysis of voltage vectors effect on the fluxes

The equivalent circuit of DFIG in rotor reference frame can be represented as shown in Figure 7.2, in which the stator and rotor voltage equations can be expressed by

$$\bar{u}_{s,k}^r = R_s\bar{i}_{s,k}^r + \frac{d\bar{\psi}_{s,k}^r}{dt} + j\omega_{me,k}\bar{\psi}_{s,k}^r \quad (7.14)$$

$$\bar{u}_{r,k}^r = R_r\bar{i}_{r,k}^r + \frac{d\bar{\psi}_{r,k}^r}{dt} \quad (7.15)$$

Then from (7.15), by neglecting the voltage drop due to rotor resistance, the rotor flux vector can be estimated and predicted at instant $(k+1)T_s$ as

$$\bar{\psi}_{r,k+1}^r = \bar{\psi}_{r,k}^r + \int_0^{T_s}\bar{u}_{r,k}^r\,dt \quad (7.16)$$

By considering that the voltage vector is constant during the entire sampling interval, this results in

$$\bar{\psi}_{r,k+1}^r = \bar{\psi}_{r,k}^r + \bar{u}_{r,k}^r T_s \quad (7.17)$$

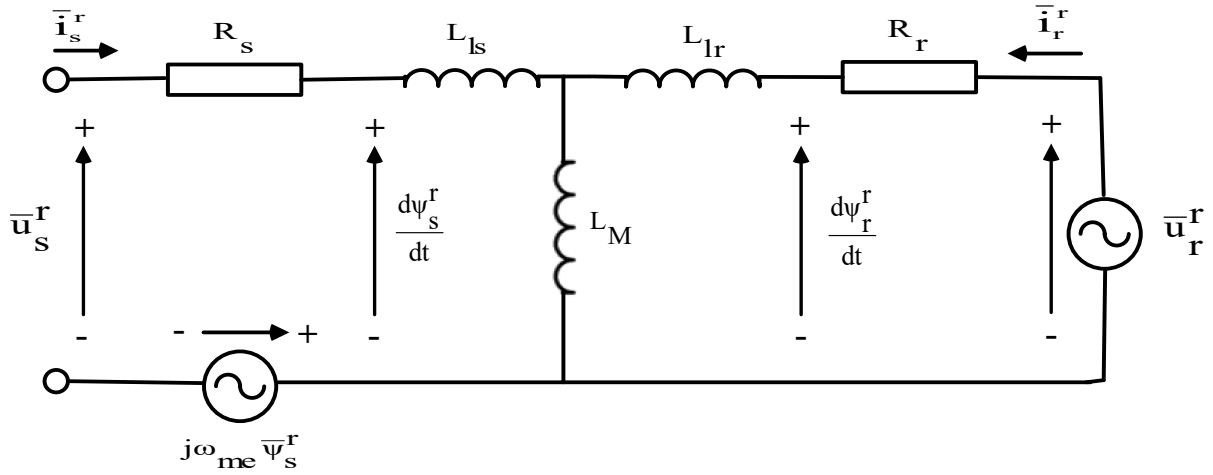

Figure 7.2: Equivalent circuit of DFIG in rotor reference frame

As the stator is directly connected to the grid, then the stator flux vector is assumed to be with constant amplitude and constant speed of $\omega_{s,k}$ in the stationary reference frame, and speed $\omega_{r,k}$ in the rotor reference frame.

These facts are illustrated in Figure 7.3, from which it can be noticed that the application of a sufficiently large constant voltage vector in the rotor, results in a simultaneously increase of φ and the rotor flux space vector amplitudes.

Thus, the value of phase angle φ and amplitude of rotor flux vector can be regulated by controlling the applied rotor voltage vector.

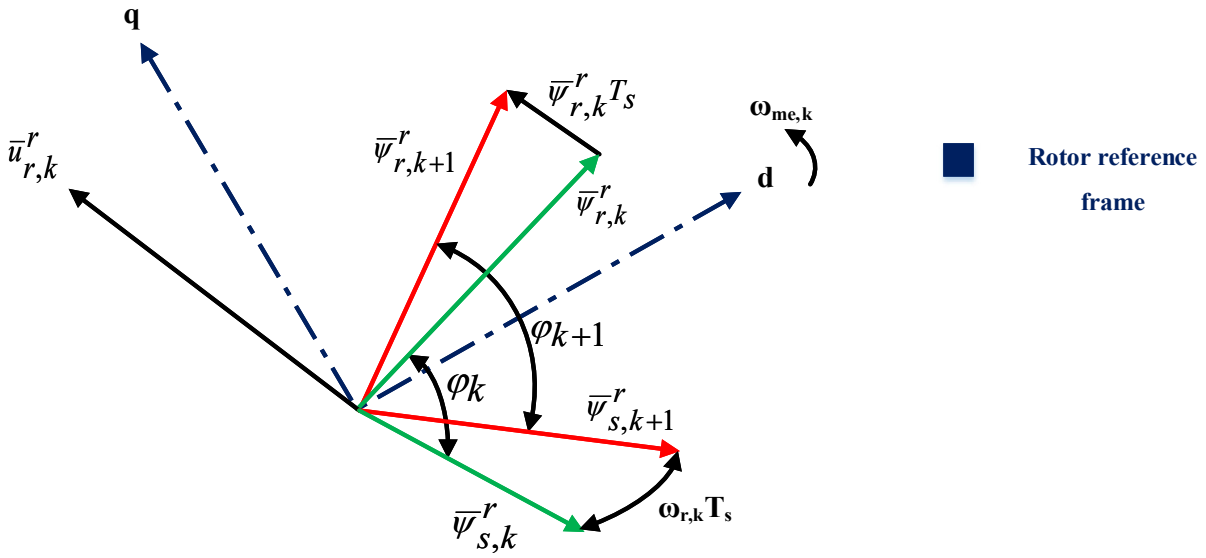

Figure 7.3: Stator and rotor voltage vector effects on the stator and rotor fluxes

7.2.3 Analysis of rotor voltage vector effect on the active and reactive powers

As the effect of rotor voltage vector on the fluxes variation is studied in previous section. Then expressions (7.11) and (7.13) can provide sufficient information about the effect of rotor voltage vector on the variation of active and reactive powers. As the stator flux vector is assumed to have constant amplitude, then any of the eight possible rotor voltage vectors supplied from a three phase two level converter, will make a change in the phase angle φ . Thus, any variation in the active and reactive powers can be investigated by checking the terms $|\bar{\psi}^{r}_{r,k}| \sin\varphi$ and $|\bar{\psi}^{r}_{r,k}| \cos\varphi$ defined in rotor reference frame, respectively.

From Figure 7.4, it can be noticed that both terms $|\bar{\psi}^{r}_{r,k}| \sin\varphi$ and $|\bar{\psi}^{r}_{r,k}| \cos\varphi$ are increasing due to the effect of the active rotor voltage vector $U^{6}_{r,k}$, and consequently this increase causes an increase in active power and a decrease in reactive power, respectively. This is happened when the DFIM is running at sub synchronous speed in motor mode.

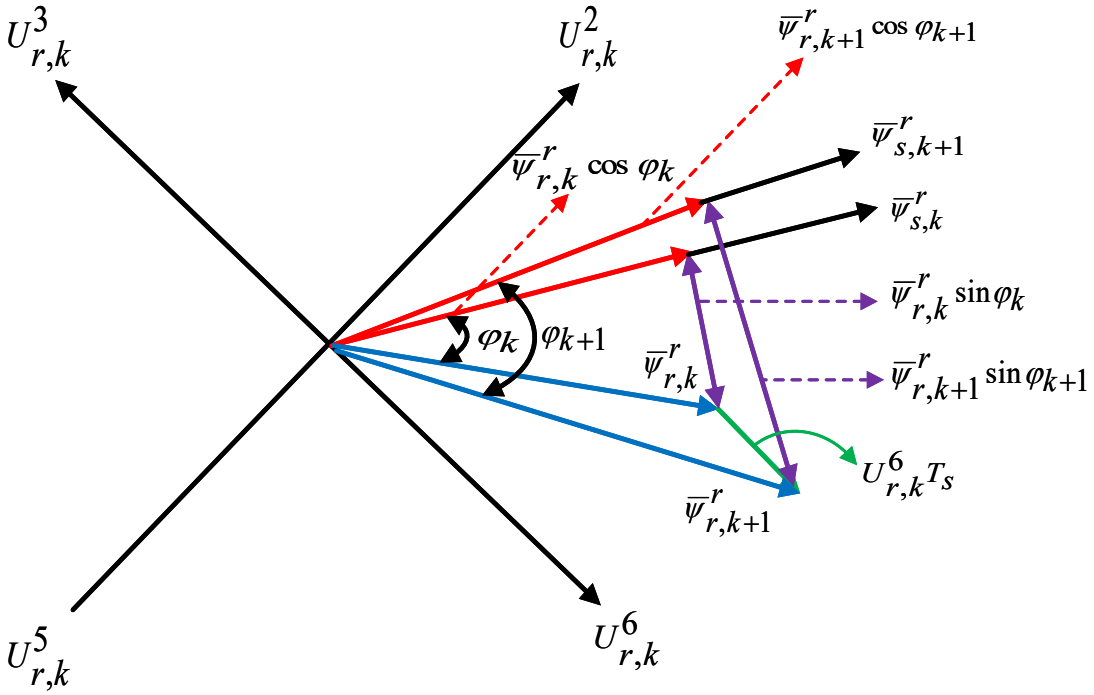

Figure 7.4: Effect of $U^{6}_{r,k}$ voltage vector, on the active and reactive powers

It can be shown also in Figure 7.4, that according to the position of the rotor flux space vector in the plane, the same voltage vector can produce different effect on the active and reactive powers. Thus, with this geometrical analysis, the parallelism between the DPC and the DTC basic principles can be investigated.

Both control methods are based on a direct control of a pair of magnitudes, torque and rotor flux in the DTC and stator active and reactive powers in the DPC. These magnitudes are controlled by providing rotor voltage

vectors that produce variations in the rotor flux space vector amplitude ant its relative distance with the stator flux space vector.

It should be noted that, although the DPC algorithm does not impose a direct rotor flux control, indirectly by controlling the stator active and reactive powers, it is imposing an amplitude for the rotor flux space vector and its rotation to a distance φ from the stator flux space vector (see (7.11) and (7.13)). This is mandatory to ensure that the DFIM reaches a stable steady state operation point, because as shown before, the proper creation and rotation of the stator flux space vector is already guaranteed by feeding the stator terminals of the DFIM from the grid.

The previous sections give the relation between the applied rotor voltage space vector and the variation in the active and reactive powers, in a graphical form. The following section presents this analysis in an analytical form.

7.2.4 Analytical investigation of rotor voltage vector effect on the active and reactive powers

To explain briefly the effect of rotor voltage vector in a mathematical way, it is preferred to introduce and consider the following space vectors represented in rotor reference frame as following:

$$\bar{\psi}^{r}_{r,k} = \left|\bar{\psi}^{r}_{r,k}\right| e^{-j\omega_{r,k}t} \tag{7.18}$$

$$\bar{\psi}^{r}_{s,k} = \left|\bar{\psi}^{r}_{s,k}\right| e^{-j(\omega_{r,k}t+\varphi)} \tag{7.19}$$

$$\bar{u}^{r}_{s,k} = \left|\bar{u}^{r}_{s,k}\right| e^{-j\left(\omega_{r,k}t+\varphi+\frac{\pi}{2}\right)} \tag{7.20}$$

$$\bar{u}^{r}_{r,k} = \frac{2}{3} U_{dc} e^{-j\frac{\pi}{3}(i-1)} \tag{7.21}$$

where U_{dc} is the dc link voltage, and (^{i}) refers to the voltage index (0……7).
From equations (7.1) and (7.2), the stator active and reactive power derivatives can be calculated in coordinates referenced to the rotor reference frame by

$$\frac{dP_{s,k}}{dt} = 1.5\left(\frac{du^{r}_{ds,k}}{dt} i^{r}_{ds,k} + \frac{di^{r}_{ds,k}}{dt} u^{r}_{ds,k} + \frac{du^{r}_{qs,k}}{dt} i^{r}_{qs,k} + \frac{di^{r}_{qs,k}}{dt} u^{r}_{qs,k}\right) \tag{7.22}$$

$$\frac{dQ_{s,k}}{dt} = 1.5\left(\frac{du^{r}_{qs,k}}{dt} i^{r}_{ds,k} + \frac{di^{r}_{ds,k}}{dt} u^{r}_{qs,k} - \frac{du^{r}_{ds,k}}{dt} i^{r}_{qs,k} - \frac{di^{r}_{qs,k}}{dt} u^{r}_{ds,k}\right) \tag{7.23}$$

Then by substituting from (7.14) and from (7.18) to (7.21) into (7.22) and (7.23), considering that the amplitude of the stator flux is constant, thus the active and reactive power derivatives can be represented by

$$\frac{dP_{s,k}}{dt} = -P_{s,k}\left(\frac{R_s}{\sigma L_s} + \frac{R_r}{\sigma L_r}\right) - \omega_{r,k}Q_{s,k} + 1.5\omega_{r,k}\frac{\left|\bar{u}^r_{s,k}\right|^2}{\sigma L_s \omega_{s,k}} + \frac{L_M}{\sigma L_s L_r}U_{dc}\left|\bar{u}^r_{s,k}\right|\sin\left(\omega_{r,k}t + \varphi - \frac{\pi}{3}(i-1)\right) \quad (7.24)$$

$$\frac{dQ_{s,k}}{dt} = -Q_{s,k}\left(\frac{R_s}{\sigma L_s} + \frac{R_r}{\sigma L_r}\right) + \omega_{r,k}P_{s,k} + 1.5\frac{R_r\left|\bar{u}^r_{s,k}\right|^2}{\sigma L_s L_r \omega_{s,k}} - \frac{L_M}{\sigma L_s L_r}U_{dc}\left|\bar{u}^r_{s,k}\right|\cos\left(\omega_{r,k}t + \varphi - \frac{\pi}{3}(i-1)\right) \quad (7.25)$$

As can be noticed from (7.24) and (7.25), the derivatives are consisted of three constant terms and other one term that is defined as sin or cos function, with an angular frequency $\left(\omega_{r,k} = \omega_{s,k} - \omega_{me,k}\right)$ and amplitude dependent on the DC bus voltage. The zero voltage vector produces a null effect on the active and reactive powers, because the sin and cosine terms in (7.24) and (7.25) are only valid for the six active vectors.
Figure 7.5 shows a graphical illustration for the active and reactive powers derivatives for the DFIG under study. These waveforms are obtained at steady-state operation for the eight possible rotor voltage vectors.

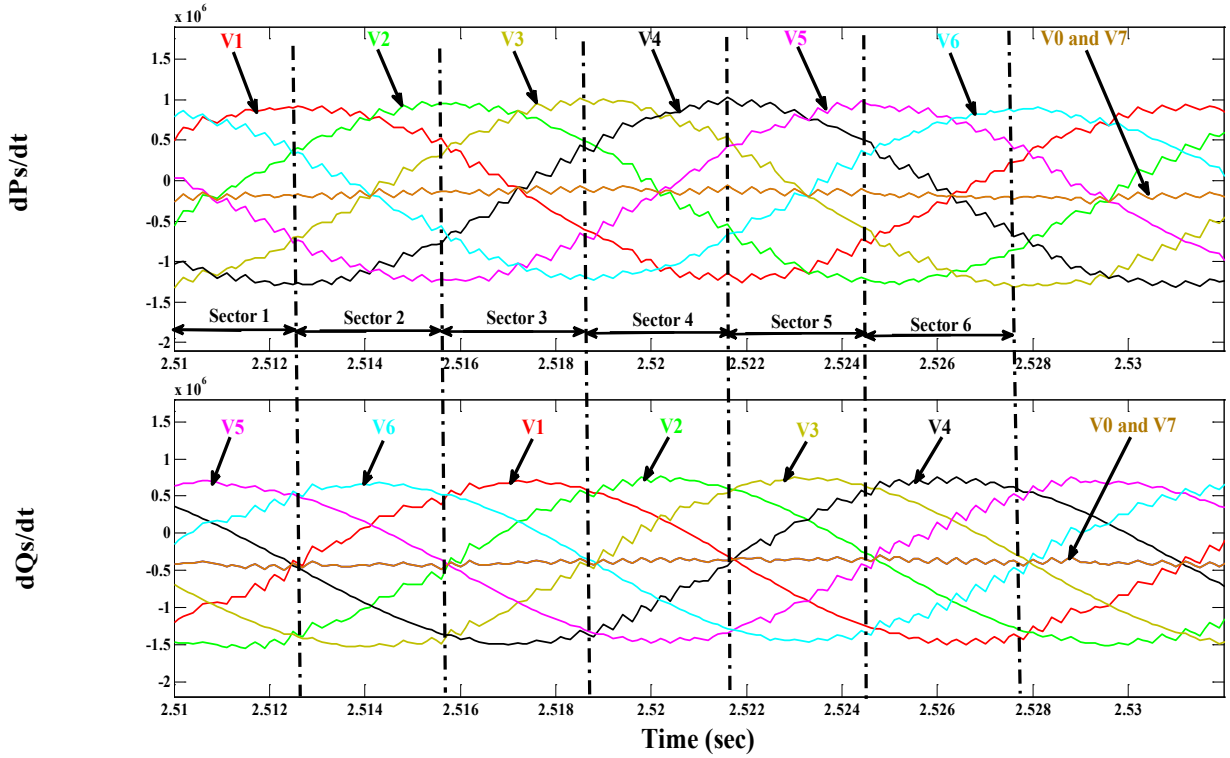

Figure 7.5: Active and reactive power slopes as a function for each rotor voltage vector

From Figure 7.5, it can be noticed that the chosen interval for representing the power derivatives waveforms are divided into six sectors and the limit between a given sector and the other is specified with reactive power derivative crossing zero.

7.3 Theoretical approach for the proposed MP DPC strategy

As stated before, there is a parallelism between the DTC and DPC control strategies, and based on this, the proposed MP DPC procedure is introduced in a discrete time form, which aims to control the active and reactive powers for DFIG instead of controlling the torque and rotor flux as introduced in chapter 6.
To describe DPC, it is proper to present a new complex variable $\bar{\delta}$ given by

$$\bar{\delta}_k = \frac{P_{s,k}}{S_n} + jw_f^{iv}\frac{Q_{s,k}}{S_n} \tag{7.26}$$

where S_n is the nominal apparent power of the machine, and w_f^{iv} is a weighting factor used for balancing the weight of reactive power with respect to the active power. The two components of $\bar{\delta}$ are normalized in order to allow (7.26) to be applied to machines of any power sizes.

For a reference vector given at instant kT_s by

$$\bar{\delta}_k^* = \frac{P_{s,k}^*}{S_n} + jw_f^{iv}\frac{Q_{s,k}^*}{S_n} \tag{7.27}$$

It is likely to express, at the same sampling instant, the error $\bar{e}_k$ as

$$\bar{e}_k = \bar{\delta}_k^* - \bar{\delta}_k = \frac{P_{s,k}^* - P_{s,k}}{S_n} + jw_f^{iv}\frac{Q_{s,k}^* - Q_{s,k}}{S_n} = e_{P_{s,k}} + jw_f^{iv}e_{Q_{s,k}} \tag{7.28}$$

Objective of the control is to keep at any sampling instant the actual vector $\bar{\delta}_k$ as near to the target $\bar{\delta}_k^*$ as possible that is $|\bar{e}_k|$ almost near to zero. In other words, the following condition has to be fulfilled:

$$|\bar{e}_k| = \sqrt{\left(e_{P_{s,k}}\right)^2 + \left(w_f^{iv}\right)^2\left(e_{Q_{s,k}}\right)^2} \leq E_{max} \tag{7.29}$$

at a given sampling instant kT_s, where E_{max} is a predefined value larger than zero used for limiting switching frequency . When $|\bar{e}_k|$ touches or exceed the boundary E_{max} an action has to be taken to bring it again inside the borders in order to fulfill again condition (7.29) by $|\bar{e}_{k+1}|$, choosing the most proper voltage vector to be applied to the rotor side of the machine, so as to return the working point back again inside the boundary circle. Figure 7.6 shows the vectors $\bar{e}_k$ in the (P_s - Q_s) plain after two different control responses.

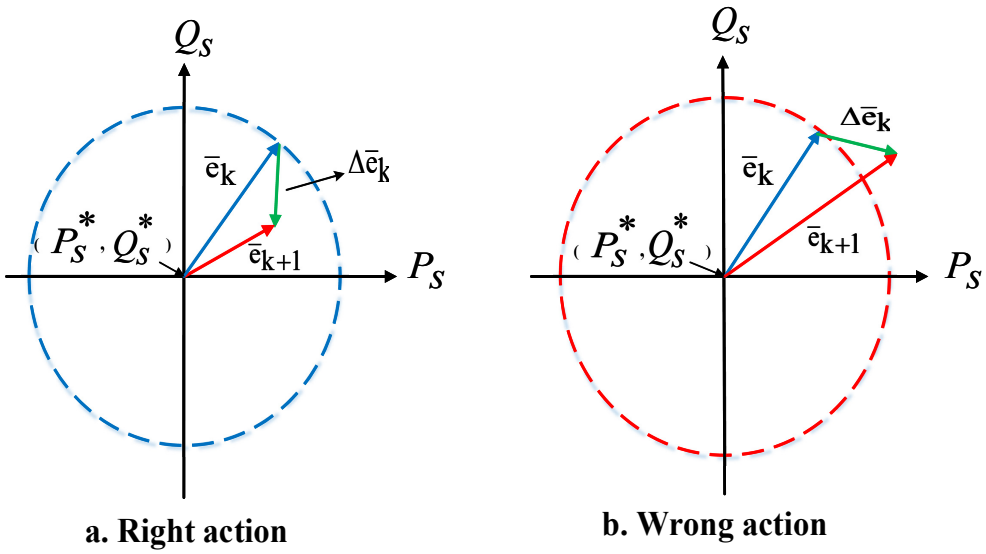

Figure 7.6: States for the presence of DPC in the error plain

Condition (7.29) is assured if the working point (P_s, Q_s) is within the horizon of radius E_{max} center in ($P^*_{s,k}$, $Q^*_{s,k}$). In the state of Figure 7.6 (a) the control response at instant kTs (at which (7.29) is just missed) is right as the condition is accomplished at instant (k+1)T_s. The action viewed in Figure 7.6 (b) is incorrect as the working point at (k+1)T_s is out of the boundary loop and then $|\bar{e}_{k+1}| > E_{max}$.

So, in case of that the error exceeds the boundaries, the right way to bring it again inside the limit circle is to select a voltage vector resulting in a negative derivative of the error vector as:

$$\frac{d|\bar{e}_k|}{dt} = \frac{d\sqrt{e^2_{P_{s,k}} + (w_f^{iv})^2 e^2_{Q_{s,k}}}}{dt} = \frac{e_{P_{s,k}} \frac{de_{P_{s,k}}}{dt} + w_f^{iv} e_{Q_{s,k}} \frac{de_{Q_{s,k}}}{dt}}{|\bar{e}|} \leq 0 \tag{7.30}$$

Then convergence condition (cost function), equal to (7.30) at a sampling instant kT_s can be one of the following conditions:

$$\Lambda_k = e_{P_{s,k}} \left(\frac{de_{P_s}}{dt}\right)_k + w_f^{iv}\, e_{Q_{s,k}} \left(\frac{de_{Q_s}}{dt}\right)_k \leq 0 \tag{7.31.a}$$

$$\Lambda_k = -e_{P_{s,k}} \left(\frac{d(P_s/S_n)}{dt}\right)_k - w_f^{iv} e_{Q_{s,k}} \left(\frac{d(Q_s/S_n)}{dt}\right)_k \leq 0 \tag{7.31.b}$$

Condition (7.31.b) is utilized here by the control algorithm.

7.4 Procedure of Implementation

To explain the steps followed to implement the proposed MP DPC, the mathematical modeling of DFIG is introduced in a discrete form in stationary reference frame, this frame is used for simplifying the calculations and implementation. Thus, the discrete model introduced in chapter 6, and described in detail in Sect. 6.3 is utilized for this purpose.
As given in Sect. 6.3, the voltage balance in DFIG equivalent circuit as shown in Figure 6.2 can be written as:

$$\left(\frac{d\bar{\psi}_s^s}{dt}\right)_k = \bar{u}_{s,k}^s - R_s\bar{i}_{s,k}^s \tag{7.32}$$

$$\left(\frac{d\bar{\psi}_{rs}^s}{dt}\right)_k = \bar{u}_{rs,k}^s - R_{rs}\bar{i}_{rs,k}^s + j\omega_{me,k}\bar{\psi}_{rs,k}^s \tag{7.33}$$

After some alterations and substitutions utilizing the flux- current relationships introduced by (6.7) and (6.8), thus (7.33) can be replaced by the following equation that gives the derivative of the stator current as:

$$\left(\frac{d\bar{i}_s^s}{dt}\right)_k = \frac{1}{L_t}\left[\bar{u}_{s,k}^s - \frac{L_\varphi L_r}{L_M^2}\bar{u}_{rs,k}^s - \left(R_s + R_{rs}\frac{L_t+L_\varphi}{L_\varphi}\right)\bar{i}_{s,k}^s + \frac{R_{rs}}{L_\varphi}\bar{\psi}_{s,k}^s - j\omega_{me,k}(\bar{\psi}_{s,k}^s - L_t\bar{i}_{s,k}^s)\right] \tag{7.34}$$

Equations (7.32) and (7.34) compose the state model that explains the electrical dynamics of the generator.

It is noticeable that the derivative of the stator current given in (7.34) is consisted of two terms, the first term of which

$$\left(\frac{d\bar{i}_s^s}{dt}\right)_k^{(u)} = \frac{1}{L_t}\left[\bar{u}_{s,k}^s - \frac{L_\varphi L_r}{L_M^2}\bar{u}_{rs,k}^s - \left(R_s + R_{rs}\frac{L_t+L_\varphi}{L_\varphi}\right)\bar{i}_{s,k}^s + \frac{R_{rs}}{L_\varphi}\bar{\psi}_{s,k}^s\right] \tag{7.35}$$

relies on the control voltages at instant k-th but it is not affected by the speed, whereas the second term

$$\left(\frac{d\bar{i}_s^s}{dt}\right)_k^{(\omega)} = -\frac{1}{L_t}\left[j\omega_{me,k}(\bar{\psi}_{s,k}^s - L_t\bar{i}_{s,k}^s)\right] \tag{7.36}$$

contains the speed but not the control voltages.

Stator active and reactive powers can be then given by

$$P_{s,k} = 1.5\ \mathrm{Re}\left(\bar{u}_{s,k}^s\check{i}_{s,k}^s\right) \tag{7.37}$$

$$Q_{s,k} = 1.5\ \mathrm{Im}\left(\bar{u}_{s,k}^s\check{i}_{s,k}^s\right) \tag{7.38}$$

From (7.37) and (7.38), the derivative for the active and reactive powers results as

$$\left(\frac{dP_s}{dt}\right)_k = 1.5\ \mathrm{Re}\left(\bar{u}^s_{s,k}\frac{d\check{i}^s_{s,k}}{dt} + \check{i}^s_{s,k}\frac{d\bar{u}^s_{s,k}}{dt}\right) \tag{7.39}$$

$$\left(\frac{dQ_s}{dt}\right)_k = 1.5\ \mathrm{Im}\left(\bar{u}^s_{s,k}\frac{d\check{i}^s_{s,k}}{dt} + \check{i}^s_{s,k}\frac{d\bar{u}^s_{s,k}}{dt}\right) \tag{7.40}$$

At this moment, all derivatives terms for stator active and reactive powers respecting each possible spatial voltage vectors can be evaluated and then applied in terms of the cost function (7.31.b).

7.4.1 Steps of implementation

The implementation procedure consists of two stages; the first is the prediction stage, which can be explained as following:
The predicted values at instant (k+1) of the stator active and reactive powers can be derived by utilizing (7.39) and (7.40) resulting in:

$$\tilde{P}_{s,k+1} = P_{s,k} + T_s\left(\frac{dP_s}{dt}\right)_k \tag{7.41}$$

$$\tilde{Q}_{s,k+1} = Q_{s,k} + T_s\left(\frac{dQ_s}{dt}\right)_k \tag{7.42}$$

Then the error is also calculated by (7.28) at instant (k+1) and eventually (7.31.b) can be applied.
The second stage is the voltage selection stage, in which the control detects if the predicted error $|\bar{e}_{k+1}|$ exceeds the maximum limit E_{max} or not, and if it exceeds the limits, the control predict the cost function at instant (k+1) for all possible voltage vectors as

$$\tilde{\Lambda}^i_{k+1} = \left[\tilde{e}_{P_{s,k+1}}\left(\frac{\widetilde{de_{P_s}}}{dt}\right)_{k+1} + w_f^{iv}\tilde{e}_{Q_{s,k+1}}\left(\frac{\widetilde{de_{Q_s}}}{dt}\right)_{k+1}\right]^i \tag{7.43}$$

Then, the control specifies the voltage vector that minimizes (7.43) at this instant and apply this voltage vector to the machine in the next control step.

7.5 Sensorless procedure

The speed is required for the DPC algorithm within the implementation steps (prediction and voltage selection). As far as DPC is concerned, it has been found that accuracy of the estimated speed is appropriate for the prediction step too, while voltage selection step can be performed without speed information, which was analyzed previously in Sect. 6.8.

For acquiring information about speed $\omega_{me,k}$ (and rotor position θ_{me}), a MRAS observer is intended. In such observer, rotor flux vector is evaluated using two separate models, the first model named as ''reference model'' and it does not require the knowledge of speed, while the second is called ''adaptive model'' in which speed information is used as a parameter. Both models (reference $^{(1)}$ and adaptive $^{(2)}$) are acquired by rearranging the equations given in Sect. 7.4. Then the difference between the two evaluated rotor flux vectors is used as an input to a PI controller that eventually gives the required speed and rotor position information as shown in Figure 7.7.

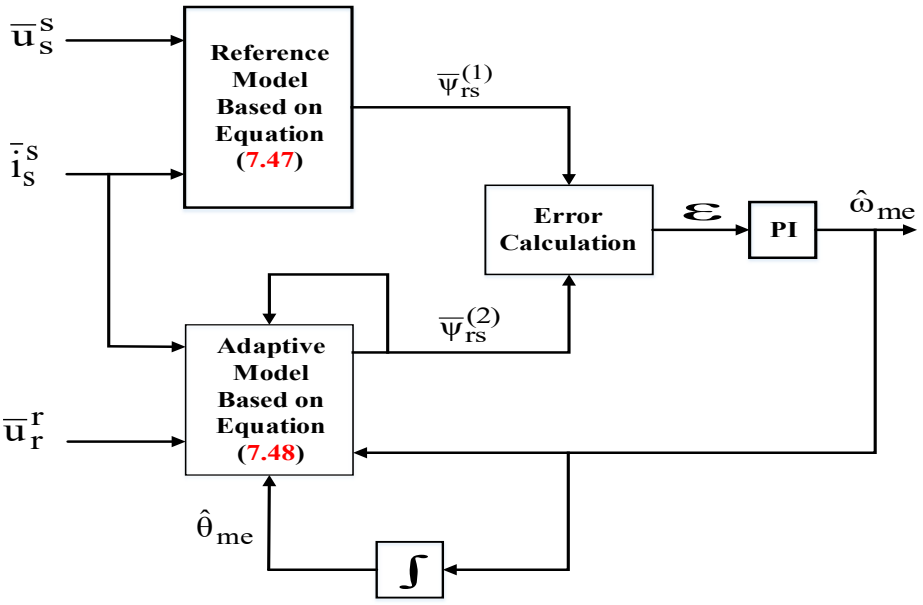

Figure 7.7: Block diagram of MRAS observer

The adaptation technique of MRAS observer here use a PI controller as described by the following equations:

$$\tilde{\omega}_{me,k} = k_{PP}\varepsilon + k_{II}\int \varepsilon dt \tag{7.44}$$

Consequently, the rotor position can be estimated by

$$\tilde{\theta}_{me,k} = \int \tilde{\omega}_{me,k} dt \tag{7.45}$$

where the error (ε) calculation is performed as following:

$$\varepsilon = \psi_{\beta rs,k}^{(1)}\psi_{\alpha rs,k}^{(2)} - \psi_{\alpha rs,k}^{(1)}\psi_{\beta rs,k}^{(2)} \tag{7.46}$$

Reference model is described by the following equation:

$$\frac{d\bar{\psi}_{rs,k}^{(1)}}{dt} = \frac{L_r}{L_M}\left[\bar{u}_{s,k}^{s} - (R_s\bar{i}_{s,k}^{s} + \sigma L_s\frac{d\bar{i}_{s,k}^{s}}{dt})\right] \tag{7.47}$$

whereas that defining the adaptive model is given as

$$\frac{d\bar{\psi}_{rs,k}^{(2)}}{dt} = \bar{u}_{r,k}^{r}e^{j\theta_{me,k}} - \frac{R_r}{L_r}\bar{\psi}_{rs,k}^{(2)} + j\omega_{me,k}\bar{\psi}_{rs,k}^{(2)} + \frac{L_M R_r}{L_r}\bar{i}_{s,k}^{s} \tag{7.48}$$

Now after the estimation of rotor position and speed required by the proposed control procedure to transform from stationary to rotor reference frame and vice versa, the overall layout of the control scheme can be shown through Figure 7.8, in which a squirrel cage induction motor that emulates the task of wind turbine is used to drive the DFIG. The stator terminals of the DFIG are connected to the grid. A digital Phase Locked Loop (PLL) is used to provide an accurate and stable information on the phase of stator voltage, which is required for the purpose of transformation from three phase to (d-q) components. The detailed explanation for the theory of operation of PLL is presented in appendix C. The same wound rotor type induction machine, which previously tested as a motor in chapter 6 is used here as the test unit. The rotor terminals are connected to the rotor side converter, which is controlled by the proposed control algorithm. In addition, the complete scheme that illustrates the sequence of implementation for the proposed MP DPC is shown through Figure 7.9.

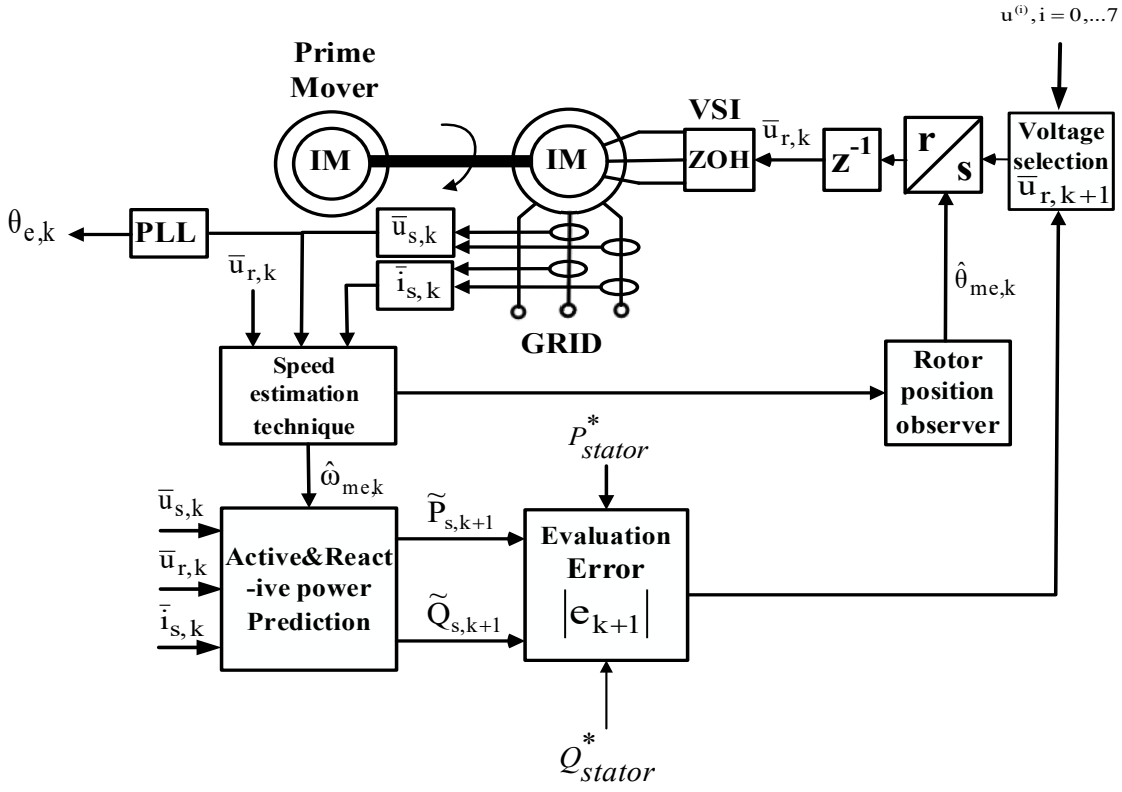

Figure 7.8: Layout for the proposed MP DPC for DFIG

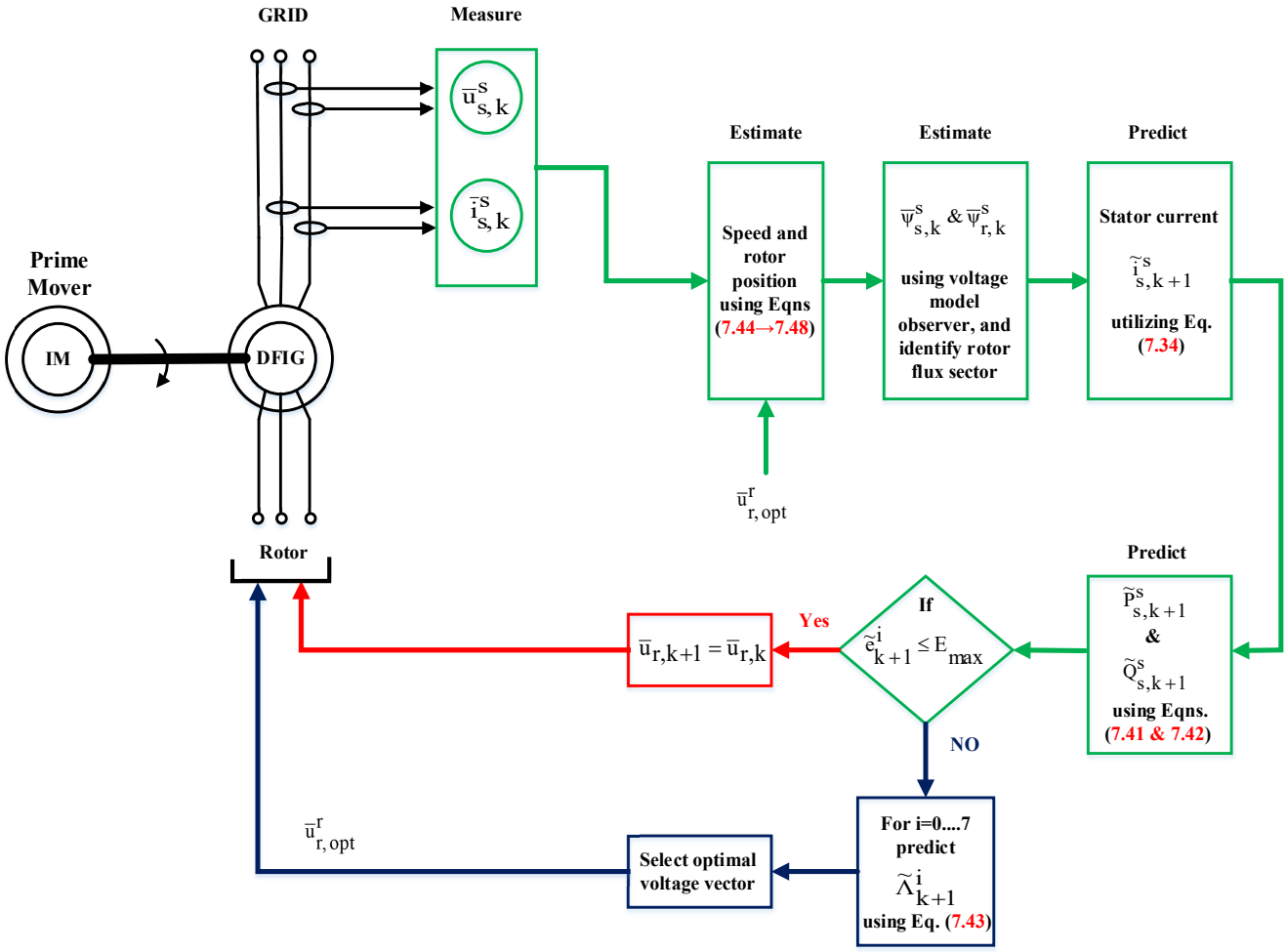

Figure 7.9: Sequence of implementation for proposed MP DPC

The proposed control procedure based on Figure 7.9 fulfils the following four steps:

- **Step 1**: Measuring the stator voltage $\bar{u}_{s,k}$, the stator current $\bar{i}_{s,k}$ through low pass filters with dc offset compensation to improve the measured signals, and by utilizing the rotor voltage control commands $\bar{u}_{r,opt}$, then the speed sample $\hat{\omega}_{me,k}$ and rotor position $\hat{\theta}_{me,k}$ can be estimated using the proposed sensorless procedure.
- **Step 2**: Prediction of the active and reactive powers for all possible voltage vectors (i=0…..7).
- **Step 3**: Checking the predicted values of active and reactive powers in the cost function given by (7.43).
- **Step 4**: The switching states correspond to the minimum value of cost function are selected in the next sampling time interval to actuate the voltage source inverter.

7.6 Simulation validation

Matlab/Simulink software is firstly used to validate the proposed MP DPC, the tests are carried out for an active power commands of (1000 → 2500 → 1500 Watts) at times of (0 → 1 → 2 sec), the reactive power reference value is kept at zero Var. The DFIG is driven at a constant speed of 2800 RPM, using a squirrel cage induction motor drive. It is worth to notice that the DFIG are under power control mode, thus the speed of the prime mover is not changed. The operation of the DFIM under speed control mode was presented in details in chapter 6. The values of estimated active and reactive powers are normalized respecting to the nominal apparent power of the machine. The maximum error limit E_{max} is set to 0.03. Obtained results confirm the effectiveness of proposed MP DPC approach which accompanied by fast and precise transient response for changing in the power commands. This can be shown via Figure 7.10 in which it can be noticed that the estimated values of active and reactive powers tracks their commands and achieved fast dynamic response. While Figure 7.11 illustrates the stator and rotor currents, and stator voltage waveforms. The stator terminals are connected to a 50 Hz, 380 V supply. Figure 7.12 illustrates the control response for each instant at which the value of absolute error exceeds its permissible limit according to the detection of minimum value for a cost function. Figure 7.13 views also the coincidence between the estimated and actual speed and rotor position profiles, which confirm the validity of proposed MRAS observer for the estimation purpose.

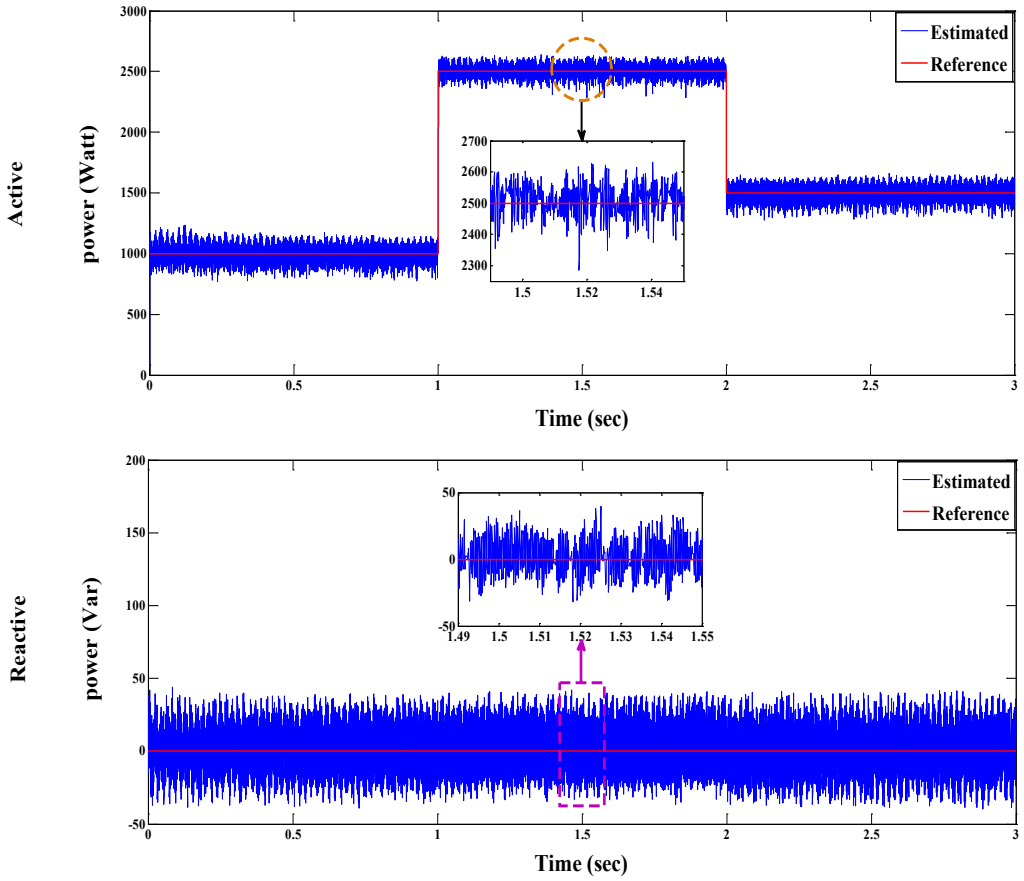

Figure 7.10: Active and reactive powers waveforms (simulation)

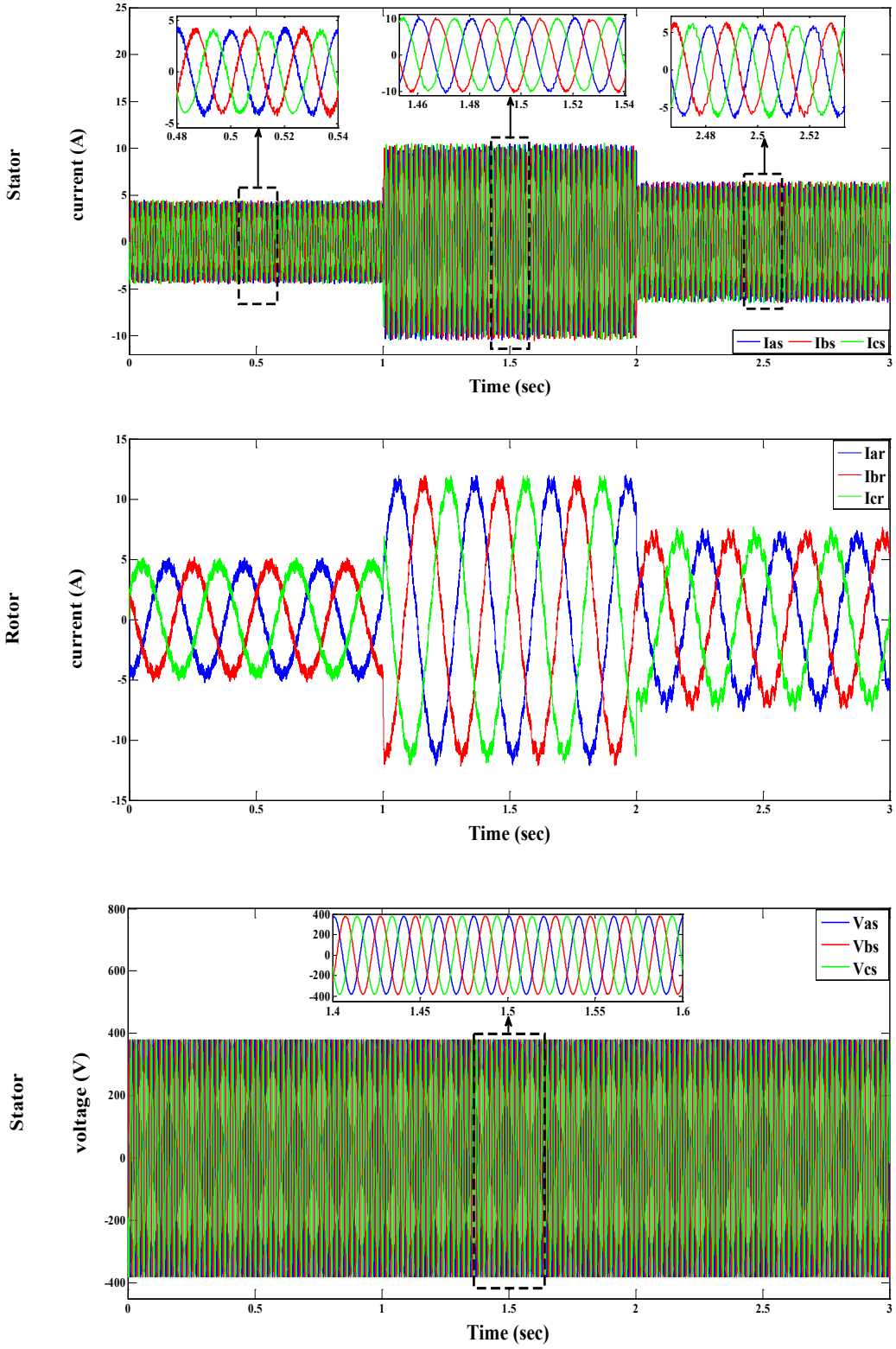

Figure 7.11: Stator and rotor currents and stator voltage waveforms

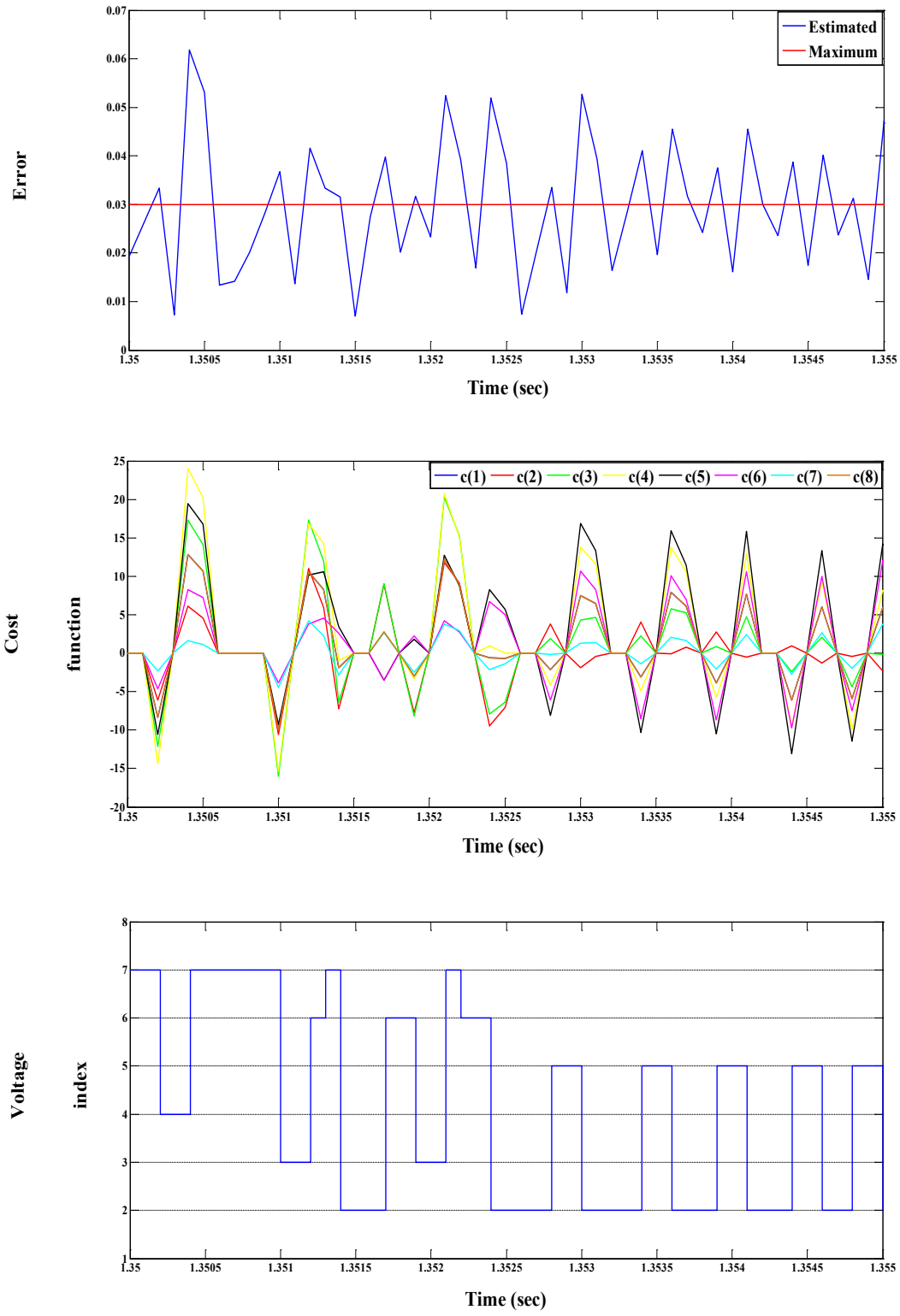

Figure 7.12: Control response and rotor position waveforms

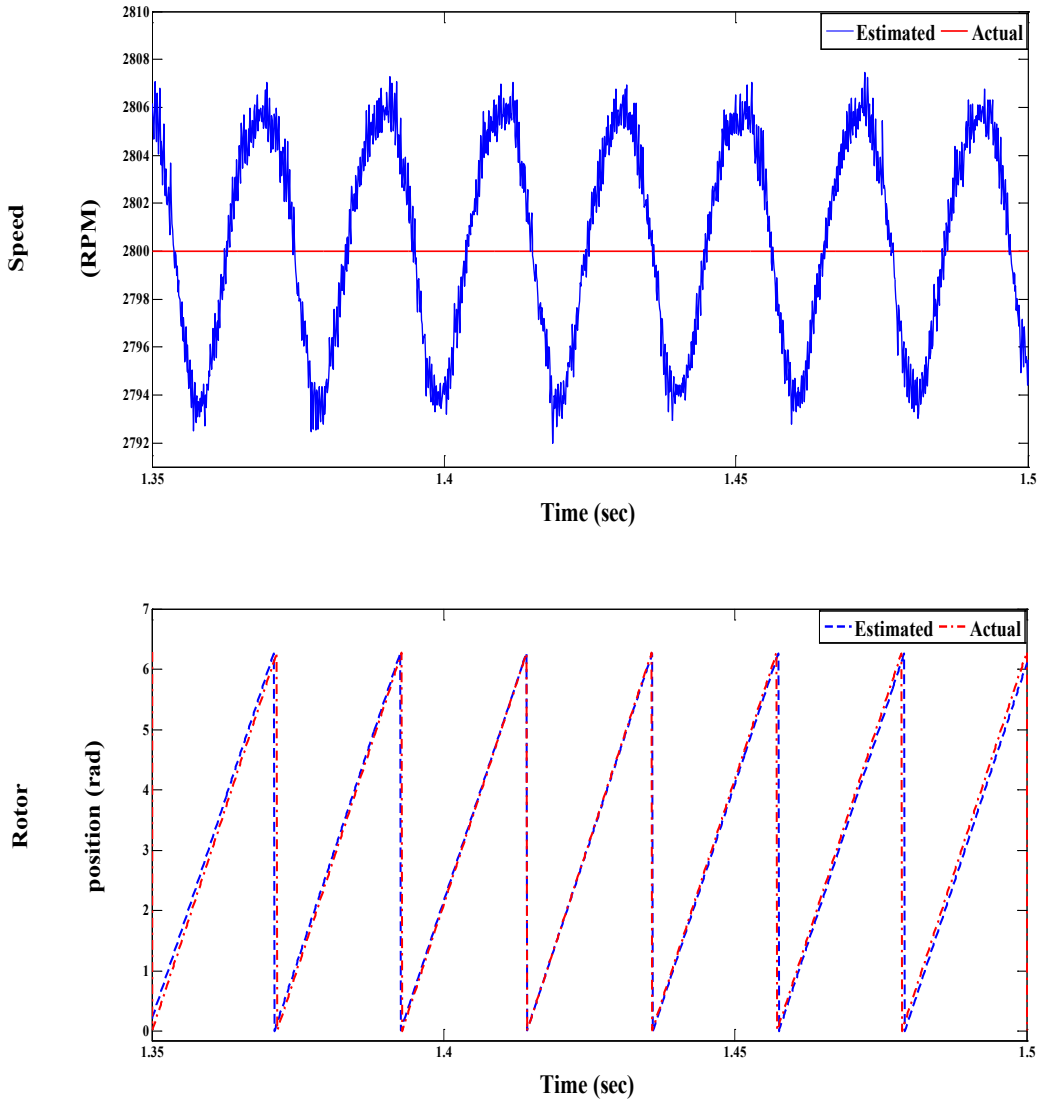

Figure 7.13: Speed and rotor position profiles

7.7 Experimental validation

A dSpace1104 prototyping control board is utilized to implement experimentally the proposed MP DPC, the overall layout of test rig is shown through Figure 7.14 , from which it can be noticed that the DFIG is driven by a squirrel cage induction motor drive at a speed of 2800 RPM, the rotor terminals are connected to the output of the rotor side inverter which in terms is connected to the dSpace 1104 control panel, which receives the control commands from the dSpace control desk on the computer. The stator terminals are connected to the AC supply, which provides a three phase 380 V, 50 Hz voltage waveform. The MRAS observer provides the information for the speed and rotor position for the DFIG.

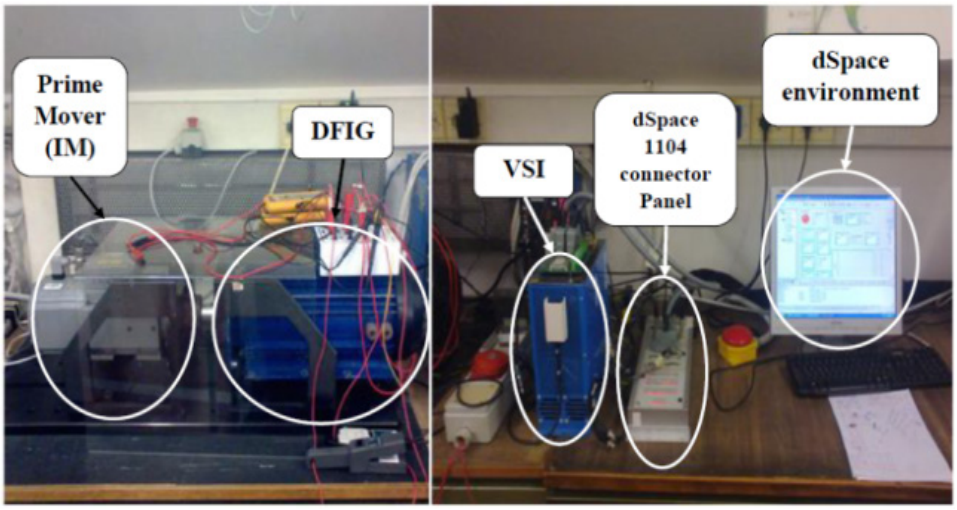

Figure 7.14: Test bench layout

The tests are carried out for a given active power commands of (1000 → 2500 → 1500 Watts) at times of (0 → 1.5 → 3 sec), while the reactive power reference is set to zero value. The maximum error limit used to limit switching frequency is held to 0.03. Obtained results confirm and assure the feasibility of proposed MP DPC control procedure, the results are also with high coincidence of results obtained via simulation. Figure 7.15 presents the profiles for active and reactive powers that they are tracking accurately their references. While Figure 7.16 gives an information about the profiles of stator and rotor currents and stator voltages. It can be noticed from Figure 7.16 that the currents waveforms track the variation in the active power, while the stator voltage is holding its value very near to the supply voltages. Figure 7.17 shows a detailed analysis of the action taken at each sampling instant corresponding to the value of estimated absolute error. Finally, Figure 7.18 illustrates the relationships between the estimated and actual speed and rotor position, from which it can be assured that the sensorless proposal is adequate as a selected solution.

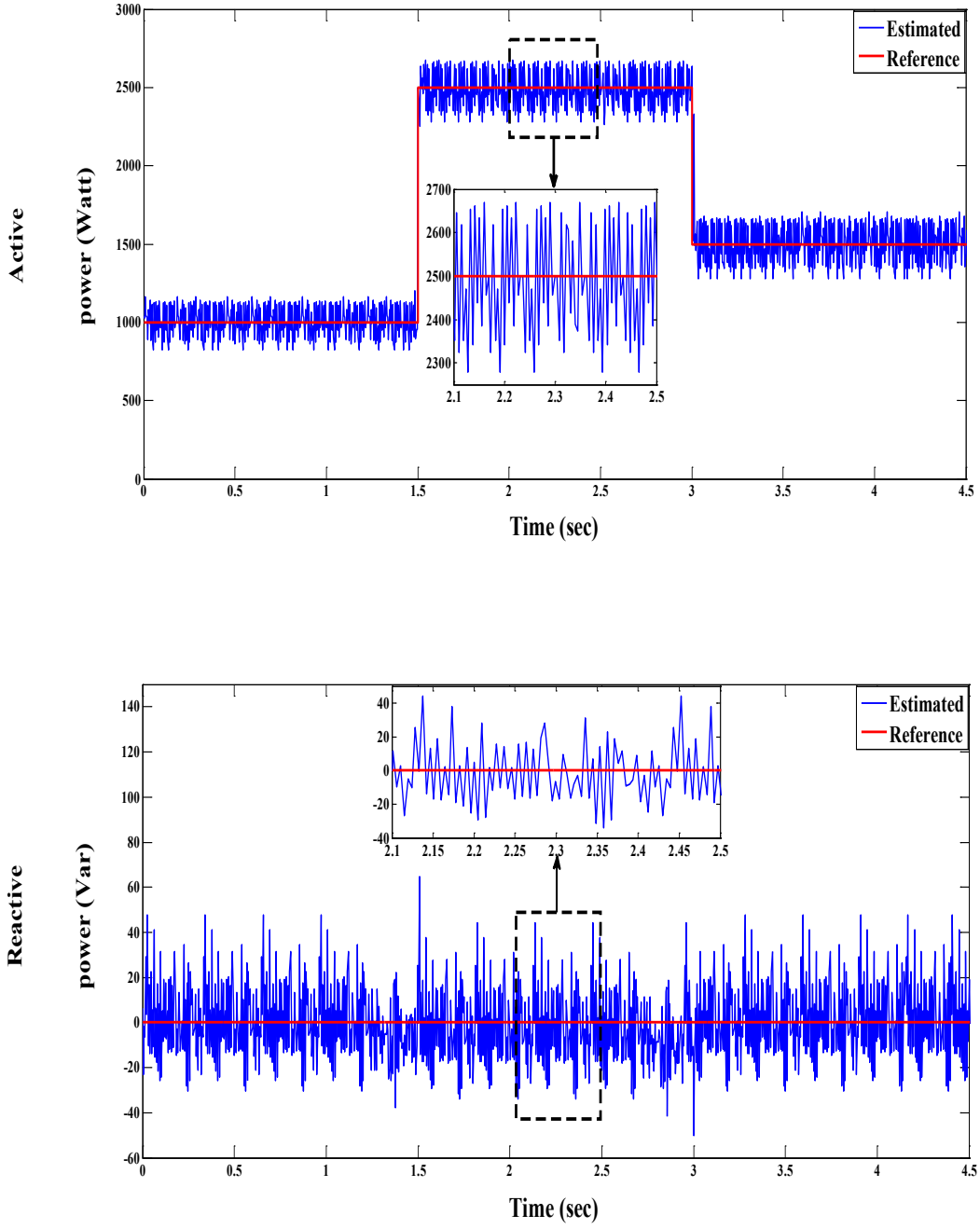

Figure 7.15: Active and reactive powers (experimental)

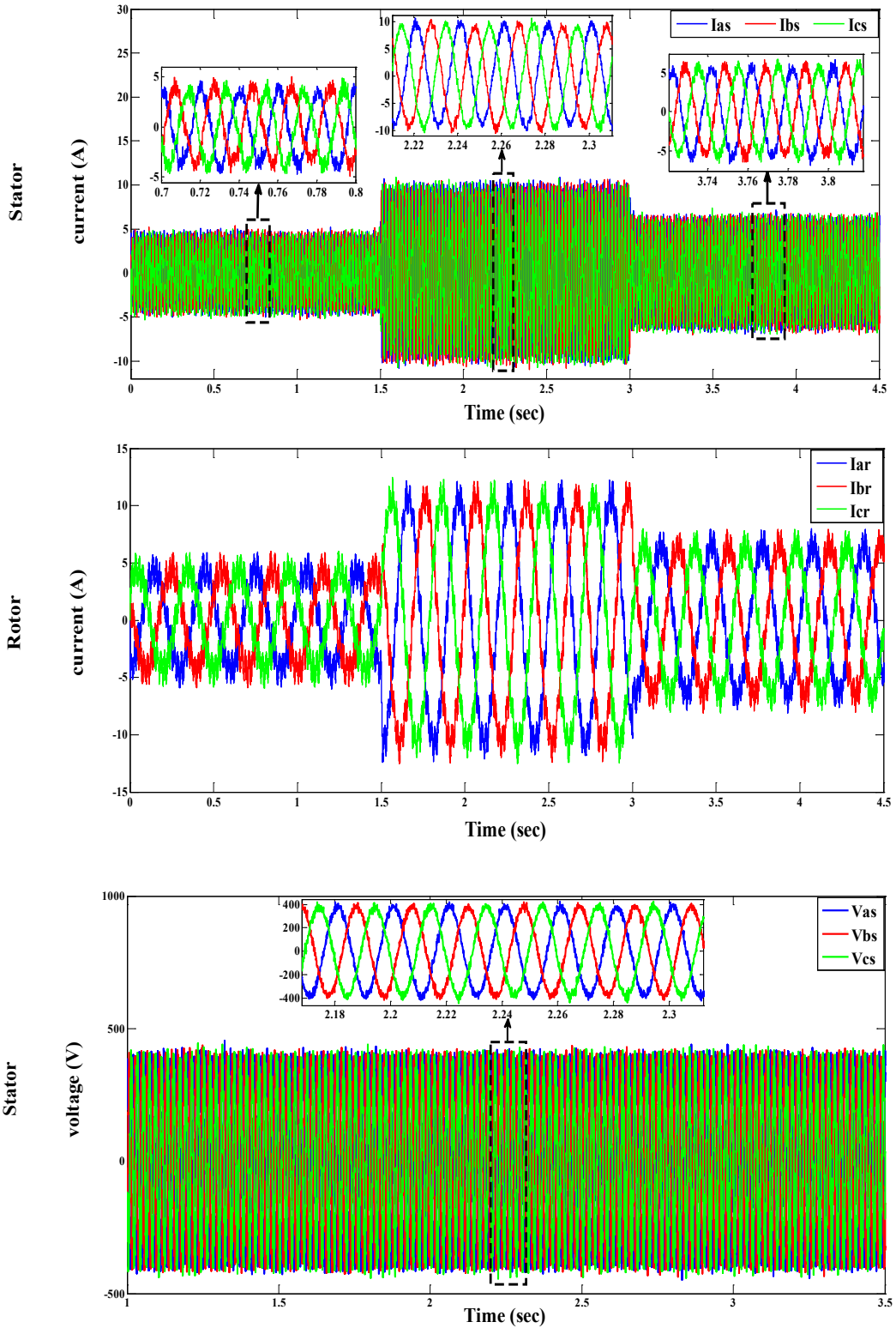

Figure 7.16: Stator and rotor currents and stator voltage waveforms

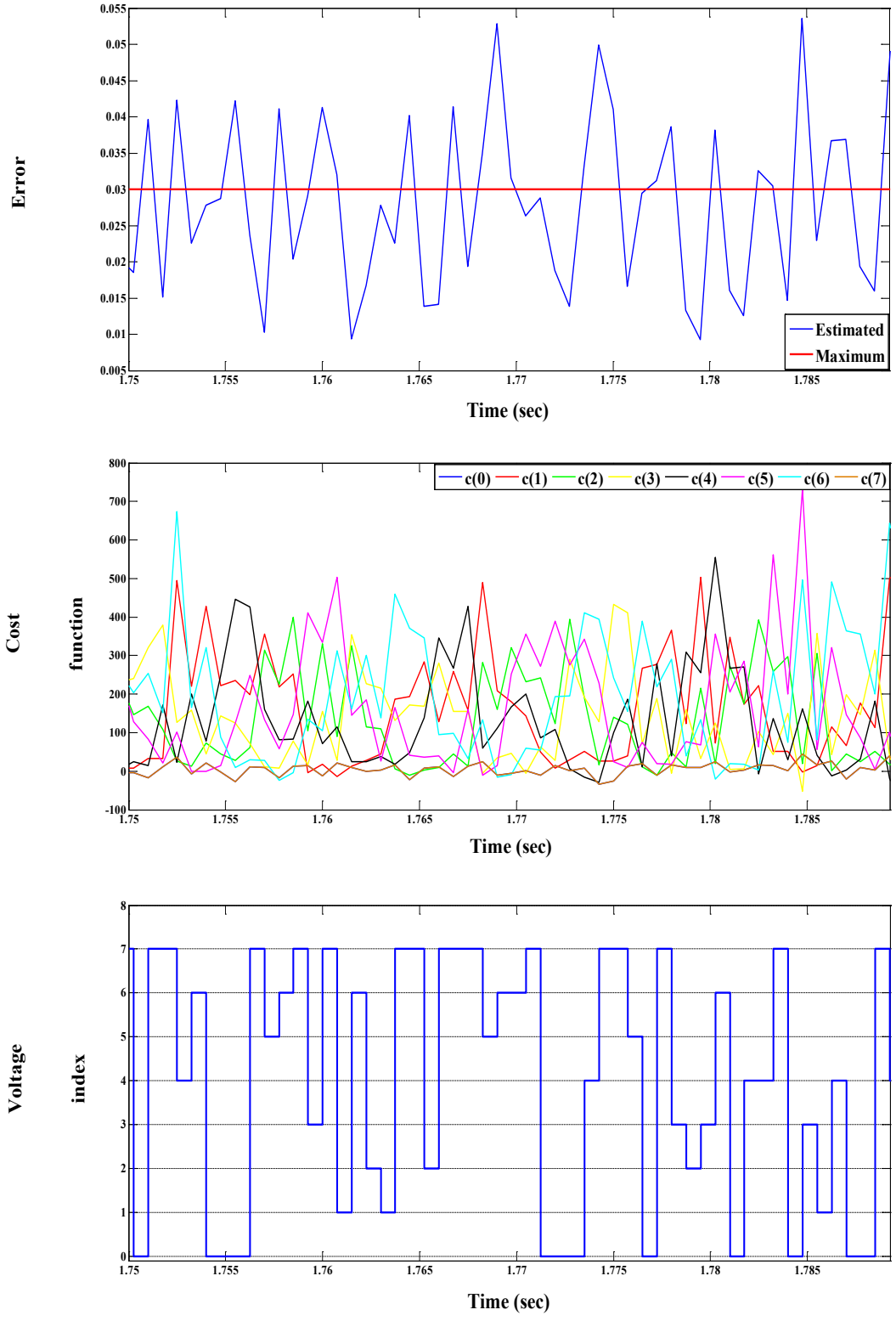

Figure 7.17: Control response

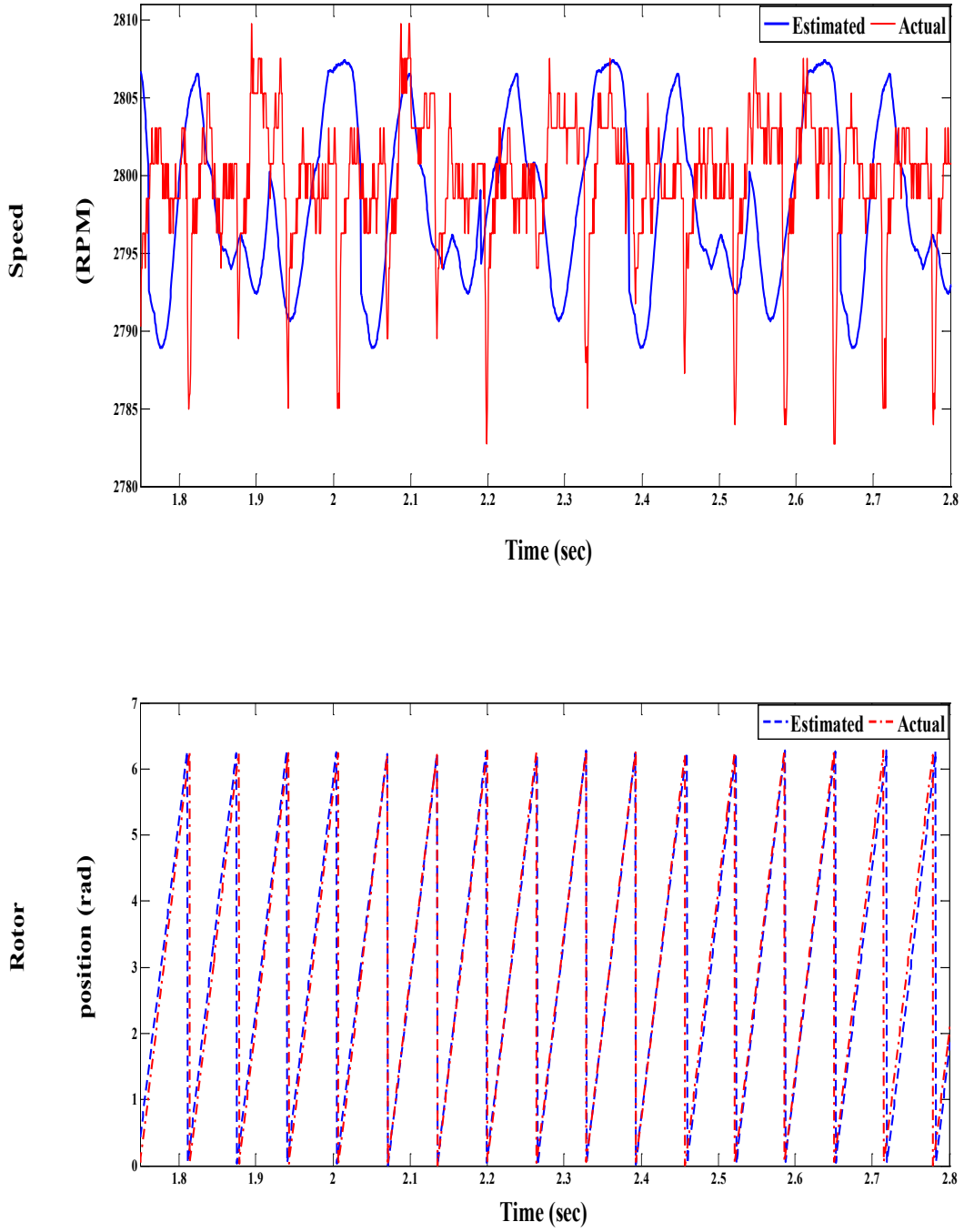

Figure 7.18: Speed and rotor position profiles

Chapter 8

Conclusion

8.1 Contributions

The contributions that are achieved through the presented content of the thesis can be summarized as follows:

- Effective control algorithms for different topologies of asynchronous (induction) machine have been studied and analyzed. The base control principle of the proposed control approaches is the finite control set- model predictive control (FCS-MPC), which proved to be an effective control tool for achieving high dynamic performance for different types of IM drives. In addition to that, for enhancing the robustness of the controlled drives, different effective sensorless techniques are presented and utilized for estimating the speed and rotor position.

- The first case of study is the induction motor (IM) drive that has been controlled by different control approaches based on FCS-MPC control principle, which does not require the usage of PWM for voltage control purposes like classic control techniques. The first control approach is the model predictive direct torque control (MP DTC), in which an effective new formulation of convergence condition is utilized. Through the new formulation, the effect of some control variants (i.e. speed sample) on the overall performance of proposed control procedure has been investigated and well explained. This makes easy the understanding of the real base principle of proposed DTC control approach, as well as why and when it works well.

- Two different sensorless approaches are developed and utilized with the proposed MP DTC for IM drives. The first is a model reference adaptive system (MRAS) observer. The second is an approach, which extracts the speed information from the difference between the predicted values of currents and fluxes and their values at the previous sampling instant, and consequently it utilizes the predictive feature of proposed MP DTC approach. The two sensorless approaches are tested using extensive simulation and experimental tests, from which their effectiveness is confirmed via achieving a precise estimation of mechanical speed and rotor position. The tests are carried out for a wide range of speed variation, from high-speed operation down to very low speed (2% of rated speed).

- The proposed MP DTC scheme for IM drives has been developed assuming torque and rotor flux as references (instead of torque and stator flux). In this way, the highest pullout torque is obtained and it is possible to combine the advantages of rotor flux orientation and stator flux control. The strategy adopted needs neither the rotor resistance of the machine nor the coordinate transformation based on the rotor flux position, leading to a high performance drive using a simple control scheme. The sensorless approach, which utilizes the predictive feature of proposed MP DTC, is used to validate the feasibility

and robustness of the control approach in realizing a precise transient dynamic response for the IM drive.

- The proposed MP DTC scheme for IM drives has been developed also by assuming torque and reactive power as references (instead of torque and stator flux). In this way, the effect of parameters variation (i.e. stator resistance) on the estimated stator flux is eliminated and thus the dynamic performance is improved. This is due the fact that the reactive power is a measured quantity, which can be calculated directly from the measured stator voltages and currents. In addition, the second sensorless approach (utilizes the prediction step feature) is used to enhance the dynamic behavior of IM drive for a wide speed operation range.

- An innovative model predictive instantaneous power control (MP IPC) technique is developed for IM drive, this technique is considered as an effective alternative control approach to classic DTC and FOC techniques, with the advantages of simple implementation procedure and simple configuration. The active and reactive power flow through the IM drive are controlled instead of controlling torque and flux; this is due to the fact that the active power manages the torque, while the reactive power manages the flux inside the machine. The obvious advantage of proposed MP IPC is that it eliminates the effect of parameters variation on the controlled variables, as both active and reactive powers are measured quantities. The dynamic performance of IM drive using the proposed MP IPC is tested in sensorless mode (utilizing the second sensorless approach) via both simulation and experimental tests, and the results validate the feasibility of the technique in achieving high dynamic performance. In addition, the sensorless technique proved its effectiveness in estimating the speed and rotor position.

- An effective ripple reduction procedure has been presented for reducing the ripple contents in the controlled variables (torque and stator flux) of proposed MP DTC. The procedure is based on the derivation and calculation of the optimal value of weighting factor $w_{f,opt}$ that can be used in the cost function during the implementation of MP DTC control approach. The obtained results from simulation and experimental tests confirm the validity of proposed ripple reduction technique compared with the results obtained when using an arbitrary value of weighting factor w_f that is imposed offline. Remarkable reduction in torque, flux and current ripple contents is observed. In addition, the computation process of $w_{f,opt}$ does not increase the overall computational burden of proposed MP DTC by a large amount, and thus the computational time is preserved within the permissible limits. The proposed ripple reduction procedure is tested for a wide speed range with the help of the sensorless approach, which utilizes the prediction step during the implementation of proposed MP DTC.

- An effective new formulation for the model predictive current control (MPCC) for IM drive is introduced. The new proposal gives a way in a systematic manner to investigate and understand the operation principle of MPCC in terms of convergence and stability. The proposed scheme belongs to the class of the hysteresis predictive control (for limiting the switching frequency) as the MPCC is triggered by the exceeding of the error of a given threshold. In addition, a sensorless drive is achieved by including an effective Luenberger observer for precise estimation of rotor flux vector together with stator current, speed and load torque. The gains of the observer are designed in a way that enhances the stability of the observer for a wide speed range; this is confirmed via performing a root locus comparison between the poles of proposed observer and poles of classic observer.

- The second case of study is the doubly fed induction motor (DFIM) drive, which has been controlled based on FCS-MPC control principle. An extended topology of the proposed MP DTC presented and implemented by the IM drive is utilized. The control topology considers its digital implementation and exploits the finite set of voltages delivered by an inverter thus avoiding the need of a PWM switching

control. An effective sensorless procedure is also presented to get a robust drive performance for a wide range of speed change. The striking advantage of the proposed sensorless algorithm is that there is no need for computing or estimating the flux directly or indirectly, as reported by several studies earlier. Extensive simulation and experimental tests are carried out for checking and validating the proposed sensorless MP DTC for the DFIM drive. The obtained results confirm the feasibility of proposed sensorless control technique for a wide range of speed variations (i.e. changing from sub-synchronous to super-synchronous operating mode, and operating at very low speed ranges).

- The performance of the sensorless approach that is used for the DFIM drive approved its robustness against the variation in machine parameters such as stator resistance and magnetizing inductance, this is confirmed through the obtained results from both simulation and experimental tests.

- The third case of study is the doubly fed induction generator (DFIG) drive for which an effective new formulation of direct power control (DPC) topology based on model prediction (MP) is presented. As a solution for the speed and rotor position estimation purposes, a model reference adaptive system (MRAS) observer is utilized, which confirm its validity in the estimation process. A detailed theoretical analysis of the MP DPC technique is presented. This theoretical analysis is essential to understand the basics of the DPC strategy and provides the necessary clearance to understand the parallelism between the MP DTC technique used previously for doubly fed induction motor (DFIM) and the MP DPC control for doubly fed induction generator. A decoupled control between active and reactive powers is achieved and confirmed via the obtained results from both simulation and experimental tests.

8.2 Future Work

The following potential topics are considered appropriate for the future research:

- The proposed control approaches can be applied to other types of electrical machines drives such as synchronous machines.

- The proposed control approaches can be extended to be applied to othe power electronics applications.

- Studying the performance of the induction machines drives when connected to multi-level inverters, such as Matrix converter.

8.3 Publications

- M. A. Mossa and S. Bolognani, "Effective model predictive direct torque control for an induction motor drive," *2016 International Symposium on Power Electronics, Electrical Drives, Automation and Motion (SPEEDAM)*, Anacapri, 2016, pp. 746-754. DOI: 10.1109/SPEEDAM.2016.7525814.

- Mossa, M.A. and Bolognani, S. (2017) 'Effective Model Predictive Instantaneous power Control for a Sensorless Induction Motor Drive'. *Int. J. Industrial Electronics and Drives (IJIED).* (*in press*) [http://www.inderscience.com/info/ingeneral/forthcoming.php?jcode=ijied]

- M. A. Mossa and S. Bolognani, "A Novel sensorless direct torque control for a doubly fed induction machine," *2016 International Conference on Electrical Machines (ICEM)*, Lausanne, 2016, pp. 944-950. DOI: 10.1109/ICELMACH.2016.7732639.

- M. A. Mossa and S. Bolognani, "High performance Direct Power Control for a doubly fed induction generator," *IECON 2016 - 42nd Annual Conference of the IEEE Industrial Electronics Society*, Florence, 2016, pp. 1930-1935. DOI: 10.1109/IECON.2016.7793155.

- M. A. Mossa and S. Bolognani, "Effective sensorless Direct Torque Control for an induction motor drive with reduced ripple contents," *2016 IEEE International Conference on Power Electronics, Drives and Energy Systems (PEDES)*, Trivandrum, 2016, pp. 1-6. DOI: 10.1109/PEDES.2016.7914472.

- M. A. Mossa and S. Bolognani, "Effective Model Predictive Current Control for a Sensorless IM Drive," *2017 IEEE International Symposium on Sensorless Control for Electrical Drives (SLED)*, Catania, Italy, 2017, pp. 37-42. DOI: 10.1109/SLED.2017.8078427.

- M. A. Mossa and S. Bolognani, " A New Formulation of Model Predictive Direct Torque Control for a Sensorless IM Drive," *MEPCON 2017-19th IEEE International Middle East Power Systems Conference*, Cairo (Egypt), (19-21 December 2017). (*Presented*)

- M. A. Mossa and S. Bolognani, "Model Predictive Instantaneous Power Control for a Sensorless IM Drive," *MEPCON 2017-19th IEEE International Middle East Power Systems Conference*, Cairo (Egypt), (19-21 December 2017). (*Presented*)

- M. A. Mossa and S. Bolognani, "Effective Sensorless Model Predictive Direct Torque Control for a Doubly Fed Induction Machine," *MEPCON 2017-19th IEEE International Middle East Power Systems Conference*, Cairo (Egypt), (19-21 December 2017). (*Presented*)

Appendix

A. Equivalent circuit of IM in stationary reference frame

Corresponding to Figure 3.2, the following description is dedicated to show the theoretical reason for using the resistances and inductances naming, which are as follows:
(R_s) is the stator resistance.
(L_t) is the transient inductance and, as will be clarified, equals to ($L_s - \frac{L_M^2}{L_r}$).
(L_φ) as will be clarified equals to $\left(\frac{L_M^2}{L_r}\right)$.
(R_{rs}) is the rotor resistance referred to stator side and it equals the rotor resistance R_r multiplied by the square of the winding ratio $\left(n = \frac{L_M}{L_r}\right)$, thus $R_{rs} = R_r \left(\frac{L_M}{L_r}\right)^2$.

The proofing of obtaining the equivalent circuit of IM referred to stator side can be then summarized as follows:

From the magnetic point of view, the induction motor has two coupled windings, the stator and rotor, which are separated from each other by the airgap. The single-phase schematic can be shown as in Figure A.1(a), such a configuration can be represented by its equivalent circuit of Figure A.1(b), where the following relations are obtained:

$$L_s = L_1 + L_3 \tag{A.1}$$

$$L_r = L_2 + \frac{L_3}{n^2} \tag{A.2}$$

$$L_M = \frac{L_3}{n} \tag{A.3}$$

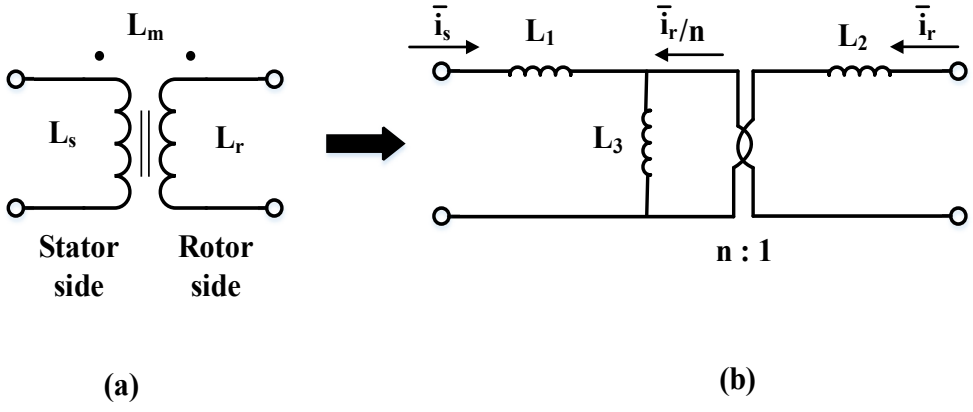

Figure A.1: Magnetic coupling in IM

The relation (A.3) can be realized via the value of rotor flux when the rotor current $\bar{\imath}_r = 0.0$; then the rotor flux from Figure A.1(a) equals $\bar{\psi}_r = L_M \bar{\imath}_s$ and from Figure A.1(b) equals $\bar{\psi}_r = (L_3 \bar{\imath}_s)\frac{1}{n}$.

From (A.1), (A.2), and (A.3), the values of L_1, L_2, and L_3 can be obtained as following:

$$L_1 = L_s - L_M * n \tag{A.4}$$

$$L_2 = L_r - \frac{L_M}{n} \tag{A.5}$$

$$L_3 = L_M * n \tag{A.6}$$

where n can be chosen arbitrarily, for the sake of convenience.

From (A.5) and putting $L_2 = 0.0$, this leads to that $n = \frac{L_M}{L_r}$. Then, by substituting these values in (A.4) and (A.6), the parameters L_1 and L_3, which are the parameters L_t and L_φ of the new equivalent circuit of induction motor, respectively, are calculated as follows:

$$L_1 = L_s - L_M * n = L_s - \frac{L_M^2}{L_r} = L_t \tag{A.7}$$

$$L_3 = L_M * n = \frac{L_M^2}{L_r} = L_\varphi \tag{A.8}$$

Now the 4-parameter equivalent circuit of IM in stationary frame results as shown in Figure A.2.

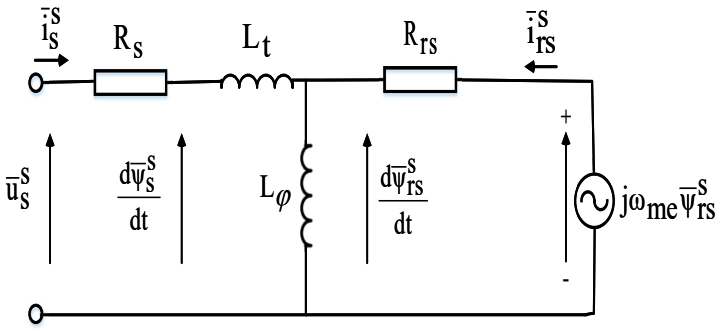

Figure A.2: Space vector equivalent circuit of IM in stationary reference frame

B. Machine Parameters and control data specifications

The parameters of the wound rotor type induction machine and control data specifications are listed in table B.1 as following:

(TABLE B.1)

Parameters and control data specifications of induction machine

Parameters	**Value**
Rated apparent power	3.75 KVAR
Rated power	3.0 KW
Poles pairs	2
Base speed	2830 RPM
R_s	1.50 Ω
L_s	0.1785 H
R_r	0.85 Ω
L_r	0.18451 H
L_M	0.17447 H
Rated Torque	10.125 Nm
Rated flux	1.05 Vs
Nominal current of IM (I_{sn})	6.5 A
ω_n (Natural frequency)	314.16 rad/sec
ξ (Damping ratio)	0.707
J (Moment of inertia)	0.1 Kg.m^2
K_1, K_2 (for Luenberger observer)	50 and 55
K_P (Speed controller) for MRAS observer used by MP DTC approach for IM drive	14.26
K_I (Speed controller) for MRAS observer used by MP DTC approach for IM drive	1263
w_f (Weighting factor) of MP DTC for IM drive	1.15
w_f' (Weighting factor) of MP DTC$^{(\text{reactive power control})}$ for IM drive	1.15
w_f'' (Weighting factor) of MP IPC for IM drive	1.15
w_f''' (Weighting factor) of MP DTC for DFIM drive	1.9
w_f^{iv} (Weighting factor) of MP DPC for DFIG drive	1.9
K_{PP} (Speed controller) for MRAS observer used by MP DPC approach for DFIG drive	1900
K_{II} (Speed controller) for MRAS observer used by MP DPC approach for DFIG drive	25000

C. Phase locked loop (PLL) system

The schematic diagram of the three-phase PLL system can be explained as illustrated in Figure C.1.

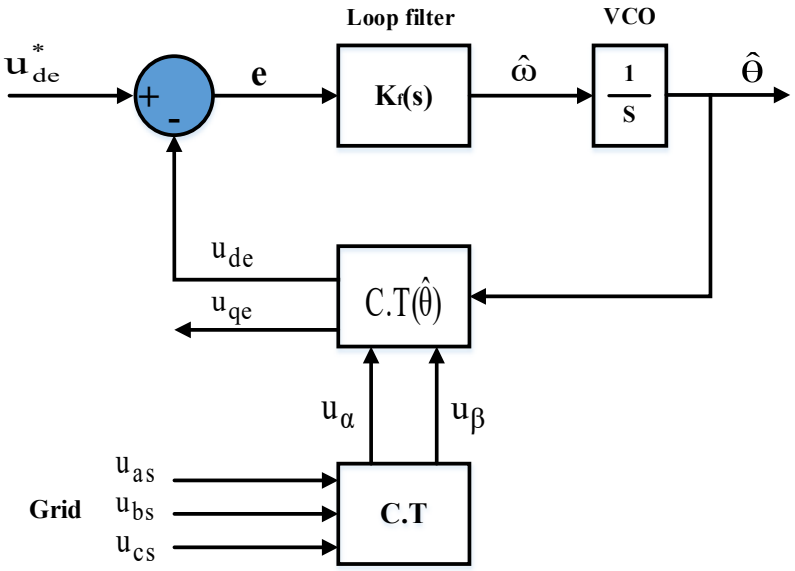

Figure C.1: Block diagram of phase locked loop (PLL) system

In such a system, the three phase grid voltages can be expressed by:

$$u_{abcs} = U_m.\begin{pmatrix} \cos\theta \\ \cos\left(\theta - \frac{2\pi}{3}\right) \\ \cos\left(\theta + \frac{2\pi}{3}\right) \end{pmatrix} \quad (C.1)$$

Where $u_{abcs} = [u_{as}\ u_{bs}\ u_{cs}]^T$. For normal grid conditions, (C.1) can be expressed in stationary reference frame by

$$u_{\alpha\beta} = (C.T).u_{abcs} \quad (C.2)$$

where $u_{\alpha\beta} = [u_\alpha\ u_\beta]^T$, and C. T refers to the transform matrix expressed by

$$C.T = \frac{2}{3} \cdot \begin{pmatrix} 1 & -\frac{1}{2} & -\frac{1}{2} \\ 0 & -\frac{\sqrt{3}}{2} & \frac{\sqrt{3}}{2} \end{pmatrix} \tag{C.3}$$

Now, (C.2) can be rewritten in the synchronous reference frame using the PLL output $\hat{\theta}$ as

$$u_{qde} = C.T(\hat{\theta}).u_{\alpha\beta} \tag{C.4}$$

where $u_{qde} = [u_{qe}\ u_{de}]^T$, and $C.T(\hat{\theta})$ denotes the rotating matrix expressed by

$$C.T(\hat{\theta}) = \begin{pmatrix} \cos\hat{\theta} & -\sin\hat{\theta} \\ \sin\hat{\theta} & \cos\hat{\theta} \end{pmatrix} \tag{C.5}$$

The voltage of interest is the d-axis component and it is derived as

$$u_{de} = E_m \sin\delta = e \tag{C.6}$$

where $E_m = -U_m$, and $\delta = \theta - \hat{\theta}$. The angular frequency of the PLL system can be represented by

$$\hat{\omega} = \frac{d\theta}{dt} = K_f.e \tag{C.7}$$

where K_f refers to the gain of the loop filter. If it is assumed that the phase difference δ is very small, then (C.6) can be linearized as

$$e \cong E_m\delta \tag{C.8}$$

Thus, the PLL frequency $\hat{\omega}$ and phase $\hat{\theta}$ can track the grid frequency ω and phase angle θ, respectively. This can be achieved via the proper design of the loop filter.

The linearized model of the PLL system can be explained as shown in Figure C.2.

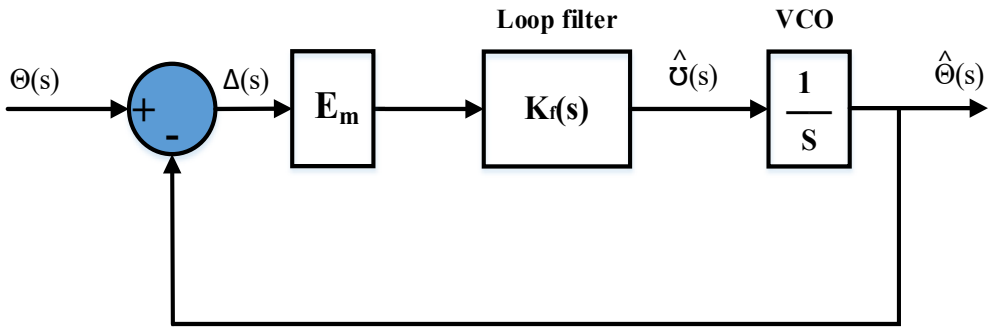

Figure C.2: Linearized model of PLL system

The transfer function of the closed loop system can be represented as

$$H_c(s) = \frac{\widehat{\Theta}(s)}{\Theta(s)} = \frac{K_f(s)E_m}{s+K_f(s)E_m} \tag{C.9}$$

$$H_\delta(s) = \frac{\Delta(s)}{\Theta(s)} = \frac{s}{s+K_f(s)E_m} \tag{C.10}$$

where $\Theta(s)$, $\widehat{\Theta}(s)$ and $\Delta(s)$ denote the Laplace transform of Θ, $\widehat{\Theta}$ and Δ, respectively.

The second order loop method is used for designing the loop filter, in which the PI type filter can be expressed by

$$K_f(s) = K_p.\left(\frac{1+s\tau}{s\tau}\right) \tag{C.11}$$

where K_p and τ denote the gains of the PI type filter. The transfer functions of the closed loop system are rewritten in the general form of the second order loop as

$$H_c(s) = \frac{2\xi\omega_n s+\omega_n^2}{s^2+2\xi\omega_n s+\omega_n^2} \tag{C.12}$$

$$H_\delta(s) = \frac{s^2}{s^2+2\xi\omega_n s+\omega_n^2} \tag{C.13}$$

where $$\omega_n = \sqrt{\frac{K_p E_m}{\tau}}, \quad \text{and} \quad \xi = \frac{K_p E_m}{2\omega_n} = \frac{\sqrt{\tau K_p E_m}}{2} \tag{C.14}$$

where $\omega_{n=}314$ (rad/sec) is the natural frequency, and $\xi = 0.707$ is the damping ratio. Then, the gains of loop filter are calculated through utilizing (C.9), (C.11) and (C.12) for $V_m = \sqrt{2} * 380 = 537$ V, to be as $K_p = 12.85$, and $\tau = 0.000427$.

Bibliography

[1] S. Bennett, *A history of control engineering,* 1930-1955. IET, 1993.

[2] O. Mayr, *The Origins of Feedback Control*, The MIT Press, 1975.

[3] J. Bocker and S. Mathapati, "State of the Art of Induction Motor Control," *IEEE International Electric Machines & Drives Conference*, pp. 1459-1464, Antalya , 2007. DOI: 10.1109/IEMDC.2007.383643.

[4] R.H. Park, "Two-reaction theory of synchronous machines generalized method of analysis-part I," *Transactions of the American Institute of Electrical Engineers*, 48 (3):716–727, 1929. DOI: 10.1109/T-AIEE.1929.5055275.

[5] K. Hasse, "*Zum dynamischen verhalten der asynchronmaschine bei betrieb mit variabler stnder frequenz und stnder spanning*," ("*On the dynamics of speed control of static ac drives with squirrel-cage induction machines*"), Ph.D. dissertation, Darmstadt, ETZ-A, 89:387–391, 1968.

[6] F. Blaschke, "The principle of field orientation applied to the new trans-vector closed-loop control system for rotating field machines," *Siemens Review*, 34:217– 220, 1972.

[7] I. Takahashi and T. Noguchi, "A new quick-response and high-efficiency control strategy of an induction motor," *IEEE Transactions on Industry Applications*, 22 (5):820–827, 1986. DOI: 10.1109/TIA.1986.4504799.

[8] M. Depenbrock, "Direct self-control (DSC) of inverter-fed induction machine," *IEEE Transactions on Power Electronics*, 3(4):420–429, 1988. DOI: 10.1109/63.17963.

[9] W. Zägelein, "*Speed regulation of asynchronous motors using an observer with reduced parameter sensitivity*," Universität Erlangen-Nürnberg, 1984.

[10] P.L. Jansen, R.D. Lorenz, and D.W. Novotny, "Observer-based direct field orientation: analysis and comparison of alternative methods," *IEEE Transactions on Industry Applications*, 30(4):945–953, 1994. DOI: 10.1109/28.297911.

[11] J. Bocker, J. Janning, and K. Anbuhl," Realization of a high-dynamic discrete time controller for PWM inverter-fed induction motor drives," In *Fifth European Conference on Power Electronics and Applications*, volume 4, pages 158–162, 1993.

[12] C. Schauder, "Adaptive speed identification for vector control of induction motors without rotational transducers," *IEEE Transactions on Industry Applications*, 28 (5):1054–1061, 1992. DOI: 10.1109/28.158829.

[13] K. Kubota, K. Matsuse, and T. Nakano, "DSP-based speed adaptive flux observer of induction motor," *IEEE Transactions on Industry Applications*, 29(2):344–348, 1993. DOI: 10.1109/28.216542.

[14] J. Holtz, "Sensorless control of induction machines - with or without signal injection," *IEEE Transactions on Industrial Electronics*, vol. 53, no1, pp. 7–30, Feb. 2006. DOI: 10.1109/TIE.2005.862324.

[15] M. Morari and J.H. Lee, "Model predictive control: Past, present and future," *Computers and Chemical Engineering*, 23(4):667–682, 1999.

[16] J. Richalet, A. Rault, J.L. Testud, and J. Papon, "Model predictive heuristic control: Applications to industrial processes," *Automatica*, 14(5):413 – 428, 1978.

[17] C.R. Cutler and Ramaker B.L, "Dynamic matrix control - a computer control algorithm," In AIChE 86th

National Meeting, Houston, TX, 1979.

[18] D.W. Clarke, C. Mohtadi, and P.S. Tuffs, "Generalized predictive control - part I the basic algorithm," *Automatica*, 23(2):137 – 148, 1987.

[19] D.W. Clarke, C. Mohtadi, and P.S. Tuffs "Generalized predictive control - part II extensions and interpretations," *Automatica*, 23(2):149 – 160, 1987.

[20] H. Kwakernaak and R. Sivan, *Linear optimal control systems*, Wiley, New York, 1972.

[21] C.E. Garcia, "Quadratic dynamic matrix control of non-linear processes. An application to a batch reactor process," *In AIChE Annual Meeting*, San Francisco, 1984.

[22] J. Holtz, S. Stadtfeldt, " A Predictive Controller for the Stator Current Vector of AC-Machines fed from a Switched Voltage Source, " *International Power Electronics Conference IPEC*, Vol. 2, pp. 1665-1675, Tokyo, 1983.

[23] R. Kennel. D. Schroder, "Predictive control strategy for converters," *Third IFAC Symposium* .pp. 415-422, Lausanne, 1983.

[24] S. Vazquez *et al*., "Model Predictive Control: A Review of Its Applications in Power Electronics, " in *IEEE Industrial Electronics Magazine*, vol. 8, no. 1, pp. 16-31, March 2014. DOI: 10.1109/MIE.2013.2290138.

[25] R. Kennel, *Pradiktives Fuhrungsverfahren fur Stromrichter (Predictive Control Strategy for Inverters)*, Dissertation, Kaiserslautern: Kaiserslau-tern University, 1984.

[26] M. Depenbrock, *Direkte Selbstregelung (DSR) fur hochdynamische Dreh-feldantriebe mit Stromrichterspeisung (Direct Self Control for Inverter Supplied High Dynamic AC Drives)*, etzArchiv, Vol. 7, pp. 211–218, 1985.

[27] E. Flach, *Direkte Regelung des Drehmomentmittelwerts einer Induktions maschine (Direct Control of the Mean Torque Value of an Induction Machine*, Dissertation, Darmstadt: Technical University Darmstadt, 1999.

[28] S. V. Emeljanov, *Automatische Regelsysteme mit veranderlicher Struktur (Automatic Control Systems with Variable Structure)*, Munich, Vienna: R. Oldenbourg Verlag, 1969.

[29] M. Aaltonen, P. Tiitinen, J. Lalu, S. Heikkila, *Direkte Drehmomentrege-lung von Drehstromantrieben (Direct Torque Control of Three-Phase Drives)*, ABB Technik, No. 3, 1995, pp. 19–24.

[30] I. Takahashi, T. Noguchi, "A New Quick Response and High Efficiency Control Strategy of an Induction Motor," *IEEE IAS Annual Meeting*, pp. 496–502, Toronto, 1985.

[31] P. Mutschler, *Verfahren zur direkten Regelung der Geschwindigkeit eineselektrischen Antriebs (Principle for Direct Control of the Speed of an Electric Drive)*, German Patent DE 196 35 981 C 2, 1998.

[32] J. B. Rawlings, "Tutorial Overview of Model Predictive Control," *IEEE Control Systems Magazine*, June, pp. 38–52, 2000. DOI: 10.1109/37.845037.

[33] D. W. Clarke, "Adaptive Predictive Control," *Annual Review in Automatic Programming*, Vol. 20, pp. 83–94, 1996.

[34] C. E. Garcıa, D. M. Prett, M. Morari, "Model Predictive Control: Theory and Practice—a Survey," *Automatica*, Vol. 25, No. 3, pp. 335–348, 1989.

[35] D. E. Seborg, "The Prospects for Advanced Process Control," *10th IFAC World Congress*, Munich, 1987.

[36] R. M. C. de Keyser, G. A. van de Velde, F. A. G. Dumortier, " A Comparative Study of Self-adaptive

Long-range Predictive Control Methods, " *Automatica*, Vol. 24, No. 2, pp. 149–163, 1988.

[37] P. Boucher, D. Dumur, P. Raguenaud, C. Rougebief, "Multivariable Generalised Predictive Control for Cognac Distillation," *European Control Conference ECC'99*, Karlsruhe, 1999.

[38] A. Bemporad, M. Morari, V. Dua, E. N. Pistikopoulos, " The Explicit Solution of Model Predictive Control via Multiparametric Quadratic Programming, " *American Control Conference ACC2000*, pp. 872–876,Chicago, 2000.

[39] C. Bordons, E. F. Camacho, " A Generalized Predictive Controller for a Wide Class of Industrial Processes, " *IEEE Transactions on Control Systems Technology*, Vol. 6, No. 3, pp. 372–387, 1998. DOI: 10.1109/87.668038.

[40] J. Rodríguez and P. Cortes, *Predictive Control of Power Converters and Electrical Drives*, 1st ed. New York: Wiley-IEEE Press, 2012.

[41] S. Qin and T. Badgwell, "A survey of industrial model predictive control technology," *Control Eng. Pract*. 11(7), pp. 733–764, July 2003. DOI: 10.1016/S0967-0661(02)00186-7.

[42] P. Cortes, G. Ortiz, J. Yuz, J. Rodríguez, S.Vazquez, and L. Franquelo, "Model predictive control of an inverter with output LC filter for UPS applications," *IEEE Trans. Ind. Electron*., vol. 56, no. 6, pp. 1875–1883, 2009. DOI: 10.1109/TIE.2009.2015750.

[43] C. Xia, M. Wang, Z. Song, and T. Liu, "Robust model predictive current control of three-phase voltage source PWM rectifier with on-line disturbance observation," *IEEE Trans. Ind. Informat.*, vol. 8, no. 3, pp. 459–471, 2012. DOI: 10.1109/TII.2012.2187912.

[44] Z. Song, C. Xia, and T. Liu, "Predictive current control of three-phase grid-connected converters with constant switching frequency for wind energy systems," *IEEE Trans. Ind. Elec-tron* ., vol. 60, no. 6, pp. 2451–2464, 2013. DOI: 10.1109/TIE.2012.2225394.

[45] P. Cortes, J. Rodríguez, D. Quevedo, and C. Silva, "Predictive current control strategy with imposed load current spectrum," *IEEE Trans. Power Electron*., vol. 23, no. 2, pp. 612– 618, 2008. DOI: 10.1109/TPEL.2007.915605.

[46] S. Vazquez, C. Montero, C. Bordons, and L.Franquelo, "Model predictive control of a VSI with long prediction horizon," in *Proc. 2011 IEEE Int. Symp. Industrial Electronics (ISIE)*, 2011, pp. 1805–1810. DOI: 10.1109/ISIE.2011.5984431.

[47] P. Cortes, A. Wilson, S. Kouro, J. Rodríguez, and H. Abu-Rub, "Model predictive control of multilevel cascaded H-bridge inverters," *IEEE Trans. Ind. Electron*., vol. 57, no. 8, pp. 2691–2699, 2010. DOI: 10.1109/TIE.2010.2041733.

[48] S. Vazquez, J. Leon, L. Franquelo, J. Carrasco, O. Martinez, J. Rodríguez, P. Cortes, and S. Kouro, "Model predictive control with constant switching frequency using a discrete space vector modulation with virtual state vectors," in *Proc. IEEE Int. Conf. Industrial Technology (ICIT 2009)*, pp. 1–6. DOI: 10.1109/ICIT.2009.4939728.

[49] P. Cortes, S. Kouro, B. La Rocca, R. Vargas, J. Rodríguez, J. Leon, S. Vazquez, and L. Franque-lo, "Guidelines for weighting factors design in model predictive control of power converters and drives," in *Proc. IEEE Int. Conf. Industrial Technology (ICIT 2009)*, pp. 1–7. DOI: 10.1109/ICIT.2009.4939742.

[50] F. Blaschke, "A New Method for the Estructural Decoupling of AC Induction Machines," *Conf. Rec. IFAC*, Duesseldorf, Germany, pages 1–15, October. 1971.

[51] I. Takahashi, Y. Ohmori, "High-Performance Direct Torque Control of an Induction Motor," *IEEE Trans. on Industrial Applications*, 25(2):257– 264, March/April 1989. DOI: 10.1109/28.25540.

[52] D. Casadei, G. Serra, A. Tani, "Implementation of a Direct Torque Control Algorithm for Induction Motors Based on Discrete Space Vector Modulation," *IEEE Trans. on Power Electronics*, 15(4):769–

777, July 2000. DOI: 10.1109/63.849048.

[53] C. Martins, X. Roboam, T.A. Meynard, A. Carvalho, "Switching Frequency Imposition and Ripple Reduction in DTC Drives by Using a Multilevel Converter," *IEEE Trans. on Power Electronics*, 17(2):286– 297, March 2002. DOI: 10.1109/63.988948.

[54] Zhuohui Tan, Yongdong Li and Min Li, "A direct torque control of induction motor based on three-level NPC inverter," *2001 IEEE 32nd Annual Power Electronics Specialists Conference (IEEE Cat. No.01CH37230)*, Vancouver, BC, 2001, pp. 1435-1439 vol. 3. DOI: 10.1109/PESC.2001.954321.

[55] Dai Nguyen, R. Dutta, and M.F. Rahman, "The preliminary results on direct torque control for a fractional-slot concentrated winding interior permanent magnet synchronous machine," *Proceedings of The 7th International Power Electronics and Motion Control Conference*, Harbin, 2012, pp. 1020-1026. DOI: 10.1109/IPEMC.2012.6258941.

[56] G.S. Buja and M.P. Kazmierkowski, "Direct torque control of pwm inverter-fed ac motors - a survey," *IEEE Transactions on Industrial Electronics*, 51(4):744–757, 2004. DOI: 10.1109/TIE.2004.831717.

[57] Peter Vas, *Sensorless Vector and Direct Torque Control*, Monographs in Electrical and Electronic Engineering. 1998.

[58] Zhanguo Xu, Cheng Shao, Dongju Feng, " An MRAS method for sensorless control of induction motor over a wide speed range," *Journal of Control Theory and Applications*, volume 9, Issue 2, pp 203-209, May 2011. DOI: 10.1007/s11768-011-8202-y.

[59] dSpace GmbH. DS1104 R&D Controller Board – Features. dSpace, Rathenaustrasse 26, 33102 Paderborn – Germany, 2009.

[60] M. Preindl and S. Bolognani, "Model predictive direct speed control with finite control set of pmsm-vsi drive systems," *In Predictive Control of Electrical Drives and Power Electronics (PRECEDE), Workshop* on, pages 17–23, 2011. DOI: 10.1109/PRECEDE.2011.6078682.

[61] D. Casadei, G. Grandi, and G. Serra, "Study and implementation of a simplified and efficient digital vector controller for induction motors," *Conf. Rec. EMD'93*, 196–201, 1993.

[62] D. Casadei, F. Profumo, G. Serra, A. Tani, and L. Zarri, "Performance analysis of a speed-sensorless induction motor drive based on a constant-switching-frequency DTC scheme," *IEEE Transactions on Industry Applications* 39 (2), 476–484, 2003. DOI: 10.1109/TIA.2003.808937.

[63] H. Akagi, Y. Kanazawa, and A. Nabae, "Instantaneous reactive power compensators comprising switching devices without energy storage components," *IEEE Transaction on Industry Applications*, vol. IA-20, pp. 625–630, May/June 1984. DOI: 10.1109/TIA.1984.4504460.

[64] Lee, K. and Blaabjerg, F, "Simple power control for sensorless induction motor drives fed by a matrix converter," *IEEE Trans. Energy Conversion* vol. 23 no. 3 pp. 781-788, 2008. DOI: 10.1109/TEC.2008.921472.

[65] Jianbo, C., Yuwen, H., Wenxin, H., Yong, Li, Jianfei, Y. and Mingjin, W, "Direct active and reactive power control of PMSM," *IEEE 6th International Power Electronics and Motion Control Conference*, Wuhan, pp. 1808-1812, 2009. DOI: 10.1109/IPEMC.2009.5157687.

[66] A. Tripathi, A. M. Khambadkone and S. K. Panda, "Dynamic control of torque in overmodulation and in the field weakening region," in *IEEE Transactions on Power Electronics*, vol. 21, no. 4, pp. 1091-1098, July 2006. DOI: 10.1109/TPEL.2006.876823.

[67] Xinbo Cai, Z. Zhang and R. Kennel, "Deadbeat and Direct Torque-Flux Control of induction motor: A comparison study," *IEEE 8th International Power Electronics and Motion Control Conference (IPEMC-ECCE Asia)*, Hefei, pp. 1909-1914, 2016. DOI: 10.1109/IPEMC.2016.7512587.

[68] J. Beerten, J. Verveckken, and J. Driesen, "Predictive direct torque control for flux and torque ripple

reduction," *IEEE Transactions on Industrial Electronics*, vol. 57, pp. 404-412, 2010. DOI: 10.1109/TIE.2009.2033487.

[69] C. A. Rojas, J. R. Rodriguez, S. Kouro and F. Villarroel, "Multiobjective Fuzzy-Decision-Making Predictive Torque Control for an Induction Motor Drive," in *IEEE Transactions on Power Electronics*, vol. 32, no. 8, pp. 6245-6260, Aug. 2017. DOI: 10.1109/TPEL.2016.2619378.

[70] Y. Zhang, H. Yang and B. Xia, "Model-Predictive Control of Induction Motor Drives: Torque Control Versus Flux Control," in *IEEE Transactions on Industry Applications*, vol. 52, no. 5, pp. 4050-4060, Sept.-Oct. 2016. DOI: 10.1109/TIA.2016.2582796.

[71] Y. Zhang and H. Yang, "Model-Predictive Flux Control of Induction Motor Drives With Switching Instant Optimization," in *IEEE Transactions on Energy Conversion*, vol. 30, no. 3, pp. 1113-1122, Sept. 2015. DOI: 10.1109/TEC.2015.2423692.

[72] C. A. Rojas, J. Rodriguez, F. Villarroel, J. Espinoza and D. A. Khaburi, "Multiobjective Fuzzy Predictive Torque Control of an induction motor drive," *The 6th Power Electronics, Drive Systems & Technologies Conference (PEDSTC2015)*, Tehran, pp. 201-206, 2015. DOI: 10.1109/PEDSTC.2015.7093274.

[73] P. Cortes, S. Kouro, B. La Rocca, R. Vargas, J. Rodriguez, J.I. Leon, S. Vazquez, and L.G. Franquelo, " Guidelines for weighting factors design in model predictive control of power converters and drives," in *Proc. IEEE International Conference on Industrial Technology, ICIT*, Gippsland, VIC, pp. 1-7, 2009. DOI: 10.1109/ICIT.2009.4939742.

[74] J. H. Pujar and S. F. Kodad, "Direct Torque Fuzzy Control of an AC Drive," *International Conference on Advances in Computing, Control, and Telecommunication Technologies*, Trivandrum, Kerala, pp. 275-277, 2009. DOI: 10.1109/ACT.2009.76.

[75] C. Attaianese, V. Nardi and G. Tomasso, "Vectorial torque control of permanent magnet AC (PMAC) machine drives in field weakening region," *7th International Workshop on Advanced Motion Control. Proceedings (Cat. No.02TH8623)*, pp. 257-262, 2002. DOI: 10.1109/AMC.2002.1026927.

[76] M. Azab and A. L. Orille, "Implementation of direct torque control of AC drive with synchronized notched DC link voltage," *Industrial Electronics Society, IECON '01. The 27th Annual Conference of the IEEE, Denver, CO*, pp. 1280-1284 vol.2, 2001. DOI: 10.1109/IECON.2001.975966.

[77] V. Ambrozic, R. Fiser and D. Nedeljkovic, "Direct current control-a new current regulation principle," *IEEE Trans. Power Electronics*, vol 18, no. 1, pp. 485-503, January 2003. DOI: 10.1109/TPEL.2002.807161.

[78] M. Bierhoff and M. Göllner, "A current sensor less speed control algorithm for induction motors," *IECON 2016 - 42nd Annual Conference of the IEEE Industrial Electronics Society, Florence*, pp. 2606-2611, 2016. DOI: 10.1109/IECON.2016.7793049.

[79] J. Rodriguez, J. Pontt, C. Silva, M. Salgado, S. Rees, U. Ammann, P. Lezana, R. Huerta and P. Cortes, "Predictive control of three phase inverter," *IEE Electronic Letters*, vol 40, issue 9, pp. 561- 563, April 2004. DOI: 10.1049/el:20040367.

[80] H. Le-Huy, K. Slimani and P.Viarouge, "Analysis and Implementation of a Real-Time Predictive Current Controller for Permanent-Magnet Synchronous Machine," in *IEEE Transactions on Industrial Electronics*, vol. 41, no. 1, pp. 110-117, Feb 1994. DOI: 10.1109/41.281616.

[81] S. Vazquez *et al*., "Model Predictive Control: A Review of Its Applications in Power Electronics," in *IEEE Industrial Electronics Magazine*, vol. 8, no. 1, pp. 16-31, March 2014. DOI: 10.1109/MIE.2013.2290138.

[82] A. Linder and R. Kennel, "Model Predictive Control for Electrical Drives," *PESC'2005: 36th IEEE Power Electronics Specialists Conference*. pp. 1793 - 1799. Recife (Brazil). June 2005. DOI:

10.1109/PESC.2005.1581874.

[83] A. Linder and R. Kennel, "Direct model predictive control - a new direct predictive control strategy for electrical drives," *EPE 2005: 11th European Conference on Power Electronics and Applications*, Dresden (Germany). September 2005. DOI: 10.1109/EPE.2005.219335.

[84] J. Rodriguez, J. Pontt, C. Silva, P. Correa, P. Lezana, P. Cortes and U. Ammann, "Predictive current control of a voltage source inverter," *IEEE Trans. Ind. Electron*, vol 54, n° 1, pp. 495–503, February 2007. DOI: 10.1109/TIE.2006.888802.

[85] R. Kennel, A. Linder and M. Linke, "Generalized predictive control (GPC)-ready for use in drive applications," *IEEE 32nd Annual Power Electronics Specialists Conference (IEEE Cat. No.01CH37230)*, Vancouver, BC, pp. 1839-1844 vol. 4, 2001. DOI: 10.1109/PESC.2001.954389.

[86] F. Wang, X. Mei, H. Dai, S. Yu and P. He, "Sensorless finite control set predictive current control for an induction machine," *IEEE International Conference on Information and Automation*, Lijiang, pp. 3106-3111, 2015. DOI: 10.1109/ICInfA.2015.7279822.

[87] Bo Wang, Xianle Chen, Yong Yu, Chunying Wang, Binbin Li and Dianguo Xu, "Robust predictive current control for induction motor in synchronous rotating frame," *8th IET International Conference on Power Electronics, Machines and Drives (PEMD 2016)*, Glasgow, pp. 1-5, 2016. DOI: 10.1049/cp.2016.0270.

[88] Xiliang Chen, Wenjie Chen, Yaqiang Han, Yilin Sha, Heyuan Qi and Xu Yang, "Predictive current control method to reduce common-mode interference for three-phase induction motor," *IEEE 8th International Power Electronics and Motion Control Conference (IPEMC-ECCE Asia)*, Hefei, pp. 2859-2862, 2016. DOI: 10.1109/IPEMC.2016.7512751.

[89] H. Kubota, K. Matsuse and T. Nakano, "DSP-based speed adaptive flux observer of induction motor," in *IEEE Transactions on Industry Applications*, vol. 29, no. 2, pp. 344-348, Mar/Apr 1993. DOI: 10.1109/28.216542.

[90] Werner Leonhard, *Control of Electrical Drives*, Springer (3rd edition, 2001), ISBN 3-540-41820-2.

[91] M. Debbou, J. Gillet, T. Achour and M. Pietrzak-David, "Control system for Doubly Fed induction machine in electrical Naval propulsion," *15th European Conference on Power Electronics and Applications (EPE)*, Lille, pp. 1-10, 2013. DOI: 10.1109/EPE.2013.6631879.

[92] P. Han, M. Cheng and Z. Chen, "Single-Electrical-Port Control of Cascaded Doubly-Fed Induction Machine for EV/HEV Applications," in *IEEE Transactions on Power Electronics*, vol. 32, no. 9, pp. 7233-7243, Sept. 2017. DOI: 10.1109/TPEL.2016.2623247.

[93] Y. Bekakra and D. Ben Attous, "A sliding mode speed and flux control of a doubly fed induction machine," *2009 International Conference on Electrical and Electronics Engineering – ELECO 2009*, Bursa, pp. I-174-I-178, 2009. DOI: 10.1109/ELECO.2009.5355328.

[94] S. K. El Khil, I. Slama-Belkhodja, M. Pietrzak-David and B. de Fornel, "Sensorless Field Oriented Control of Doubly Fed Induction Speed Drive," *EUROCON 2007 - The International Conference on "Computer as a Tool"*, Warsaw, pp. 1888-1895, 2007. DOI: 10.1109/EURCON.2007.4400558.

[95] K. Spiteri, C. Spiteri Staines and M. Apap, "Control of doubly fed induction machine using a matrix converter," *Melecon 2010 - 15th IEEE Mediterranean Electrotechnical Conference*, Valletta, pp. 1297-1302, 2010. DOI: 10.1109/MELCON.2010.5475960.

[96] J. K. Lung, Y. Lu, W. L. Hung and W. S. Kao, "Modeling and Dynamic Simulations of Doubly Fed Adjustable-Speed Pumped Storage Units," in *IEEE Transactions on Energy Conversion*, vol. 22, no. 2, pp. 250-258, June 2007. DOI: 10.1109/TEC.2006.875481.

[97] S. Peresada, A. Tilli and A. Tonielli, "Indirect stator flux-oriented output feedback control of a doubly

fed induction machine," in *IEEE Transactions on Control Systems Technology*, vol. 11, no. 6, pp. 875-888, Nov. 2003. DOI: 10.1109/TCST.2003.819590.

[98] A. Chibah, M. Menaa and K. Yazid, "Rotor speed estimation of doubly fed induction motor using high frequency carrier signal injection," *16th International Power Electronics and Motion Control Conference and Exposition*, Antalya, pp. 751-756, 2014. DOI: 10.1109/EPEPEMC.2014.6980587.

[99] M. Aghasi, V. Faraji, D. A. Khaburi and M. Kalantar, "A novel Direct Torque Control for Doubly Fed Induction Machine based on Indirect Matrix Converter," *National Conference on Electrical, Electronics and Computer Engineering*, Bursa, pp. 303-308, 2010. DOI:

[100] G. Abad, M. A. Rodriguez and J. Poza, "Predictive Direct Torque Control of the Doubly Fed Induction Machine with Reduced Torque and Flux Ripples at Low Constant Switching Frequency," *IECON 2006 - 32nd Annual Conference on IEEE Industrial Electronics*, Paris, pp. 1000-1005, 2006. DOI: 10.1109/IECON.2006.347349.

[101] M. Abdellatif, M. Debbou, I. S. Belkhodja, M.P. David," Simple Low-Speed Sensorless Dual DTC for Double Fed Induction Machine Drive," *IEEE Transactions on Industrial Electronics*, Vol. 61, No. 8.p.3915-3922, August 2014. DOI: 10.1109/TIE.2013.2288190.

[102] Ding Xiying and Wang Jian, "A new control strategy of Doubly-fed Induction Machine for Hybrid Electric Vehicle," *2010 International Conference on Computer, Mechatronics, Control and Electronic Engineering*, Changchun, pp. 60-63, 2010. DOI: 10.1109/CMCE.2010.5610211.

[103] Gonzalo Abad; Jesus Lopez; Miguel Rodriguez; Luis Marroyo; Grzegorz Iwanski, "Direct Control of the Doubly Fed Induction Machine," in Doubly Fed Induction Machine: Modeling and Control for Wind Energy Generation Applications , 1, *Wiley-IEEE Press*, pp.363-477, 2011. DOI: 10.1002/9781118104965.

[104] H. Chaal and M. Jovanovic, "Toward a Generic Torque and Reactive Power Controller for Doubly Fed Machines," in *IEEE Transactions on Power Electronics*, vol. 27, no. 1, pp. 113-121, Jan. 2012. DOI: 10.1109/TPEL.2011.2160731.

[105] Petersson, A., Thiringer, T., Harnefors, L., and Petru, T., "Modeling and experimental verification of grid interaction of a DFIG wind turbine," *IEEE Trans. Energy Convers.*, Vol. 20,No. 4, p. 878–886, December 2005. DOI: 10.1109/TEC.2005.853750.

[106] Lopez, J., Gubia, E., Sanchis, P., Roboam, X., and Marroyo , L., "Wind turbines based on doubly fed induction generator under asymmetrical voltage dips," *IEEE Trans. Energy Convers*.,Vol. 23, No. 3, p. 321–330, March 2008. DOI: 10.1109/TEC.2007.914317.

[107] Petersson, A, "*Analysis, modeling and control of doubly fed induction generators for wind turbines*", PhD Thesis, Champers University of Technology, Sweden, 2005.

[108] Noguchi, T., Tomiki, H., Kondo, S., Takahashi, I, "Direct power control of PWM converter without power-source voltage sensors," *IEEE Trans. Ind. Applications,* 34, p. 473- 479, May/June 1998. DOI: 10.1109/28.673716.

[109] Xu, L., Cartwright, P, "Direct active and reactive power control of DFIG for wind energy generation," *IEEE Trans. Energy Conversion,* 21, No.3, p. 750-758, September 2006. DOI: 10.1109/TEC.2006.875472.

[110] Datta, R., Ranganathan, V.T," Direct power control of grid- connected wound rotor induction machine without rotor position sensors," *IEEE Trans. Power Electron,* 16, No.3, p. 390-399, May 2001. DOI: 10.1109/63.923772.

[111] A. Mehdi, A. Reama, H. E. Medouce, S. E. Rezgui and H. Benalla, "Direct active and reactive power control of DFIG based wind energy conversion system," *Int. Symposium on Power Electronics, Electrical Drives, Automation and Motion (SPEEDAM)*, Ischia, pp. 1128-1133, 2014. DOI:

10.1109/SPEEDAM.2014.6872091.

[112] F. Senani, A. Rahab, F. Louar, F. Bourourou and H. Benalla, "Active and reactive power control of DFIG using PI and DPC controllers," *4th International Conference on Electrical Engineering (ICEE)*, Boumerdes, pp. 1-6, 2015. DOI: 10.1109/INTEE.2015.7416841.

[113] A. Hemdani, M. J. B. Ghorbal, M. W. Naouar and I. Slama- Belkhodja, "Design of a switching table for direct power control of a DFIG using sliding mode theory," *Systems, Signals and Devices (SSD), 8th Int. Multi-Conf. on*, Sousse, pp. 1-7, 2011. DOI: 10.1109/SSD.2011.5767487.

[114] A. Mehdi, A. Reama and H. Benalla, "MRAS observer for sensorless direct active and reactive power control of DFIG based WECS with constant switching frequency," *Eleventh International Conference on Ecological Vehicles and Renewable Energies (EVER)*, Monte Carlo, pp. 1-7, 2016. DOI: 10.1109/EVER.2016.7476349.

[115] E. Bogalecka, "Power control of a double fed induction generator without speed or position sensor," in *Conf. Rec. EPE*, vol. 377, pp. 224–228, ch. 50, 1993.

[116] D.Zhi, L.Xu, and B.W. Williams, "Model-Based Predictive Direct Power Control of Doubly Fed Induction Generators," *IEEE Trans. Power Elect.*,vol. 25, no. 2,pp.341-351, Feb 2010. DOI: 10.1109/TPEL.2009.2028139.

[117] Fei Guo, Tao Zheng and Zengping Wang, "Comparative study of direct power control with vector control for rotor side converter of DFIG," *9th IET International Conference on Advances in Power System Control, Operation and Management (APSCOM 2012)*, Hong Kong, pp. 1-6, 2012. DOI: 10.1049/cp.2012.2126.

[118] K. Mahapatra and P. K. Dash, "A model predictive control technique for VSC HVDC converters linking onshore wind farms to synchronous generator based AC network," *IEEE Power, Communication and Information Technology Conference (PCITC)*, Bhubaneswar, pp. 743-749, 2015. DOI: 10.1109/PCITC.2015.7438095.

[119] Y. Zhang, J. Zhu and J. Hu, "Model predictive direct torque control for grid synchronization of doubly fed induction generator," *IEEE International Electric Machines & Drives Conference (IEMDC)*, Niagara Falls, ON, pp. 765-770, 2011. DOI: 10.1109/IEMDC.2011.5994908.